CONSTRUCTION AND DISULFIDE CROSSLINKING OF CHIMERIC *b* SUBUNITS IN THE PERIPHERAL STALK OF F1FO ATP SYNTHASE FROM *Escherichia coli*

By

SHANE B. CLAGGETT

A DISSERTATION PRESENTED TO THE GRADUATE SCHOOL
OF THE UNIVERSITY OF FLORIDA IN PARTIAL FULFILLMENT
OF THE REQUIREMENTS FOR THE DEGREE OF
DOCTOR OF PHILOSOPHY

UNIVERSITY OF FLORIDA

2008

To the highest benefit of all beings.

ACKNOWLEDGMENTS

I thank my parents for the gift of life and the desire to learn and grow, and I thank all of my teachers for the knowledge they have so diligently acquired and patiently passed on. I especially thank my professor, Dr. Brian Cain, and the members of my committee for their support and guidance.

TABLE OF CONTENTS

page

LIST OF TABLES

LIST OF FIGURES

Abstract of Dissertation Presented to the Graduate School
of the University of Florida in Partial Fulfillment of the
Requirements for the Degree of Doctor of Philosophy

CONSTRUCTION AND DISULFIDE CROSSLINKING OF CHIMERIC *b* SUBUNITS IN THE PERIPHERAL STALK OF F1FO ATP SYNTHASE FROM *Escherichia coli*

By

Shane B. Claggett

December 2008

Chair: James Flanegan
Major: Medical Sciences–Biochemistry and Molecular Biology

F1FO ATP synthases produce the majority of ATP consumed by living organisms by harnessing the energy from oxidative phosphorylation and photosynthesis. These enzymes consist of two sections, a membrane bound FO portion which houses a proton or sodium channel and a soluble FO portion which contains the catalytic sites. Two stalks connect F1 to FO–a central stalk which rotates during catalysis and a peripheral stalk which holds the two halves of the enzyme together against the rotation of the central stalk. The F1FO ATP synthase of *Escherichia coli* has been used here as a model system to investigate the role of the peripheral stalk. This peripheral stalk consists of a dimer of identical *b* subunits. Chimeric peripheral stalks were generated by substituting sequence from the peripheral stalk of *Thermosynechococcus elongatus* into the *E. coli b* subunit. *Thermosynechococcus elongatus* has a chloroplast-like peripheral stalk that is composed of two different subunits, *b* and *b'*. The most functional chimeric constructs contained *T. elongatus* sequence for residues E39-I86, abbreviated *Tb* and *Tb'*. These subunits readily formed heterodimeric peripheral stalks that were incorporated into functional F1FO complexes.

Disulfide crosslink formation was used to probe the structure of the *Tb*/*Tb'* peripheral stalks. Cysteine residues were substituted individually at residues *b*(A83) and *b*(A90), positions

chosen based on crosslinking studies done in the lab of our collaborator, Dr. Stanley Dunn (University of Western Ontario). Crosslinking analysis demonstrated a staggered arrangement between the chimeric *b* subunits in this region. Rapid crosslink formation was observed in complexes containing *Tb*(A83C)/*Tb'*(A90C) peripheral stalks at low concentrations of oxidizing agent, results that indicate a close proximity of these two residues. Similar experiments carried out in the homodimeric peripheral stalk of *E. coli* produced results in agreement with those obtained in the chimeric constructs, indicating that the staggered arrangement likely exists in the wild-type enzyme. An effect of high substrate concentrations on crosslink formation was observed, but could not be attributed to catalytic activity.

The interactions of the individual *b* subunits with the single delta subunit of F1 were investigated by disulfide crosslink formation. The truncation of the four C-terminal residues from both *b* subunits disrupts the ability to form the proper interactions with the delta subunit. Data presented here demonstrates that a single full-length *b* subunit is sufficient to form the necessary interactions with the lone delta subunit. The staggered offset of the chimeric peripheral stalk was used to demonstrate that the C-terminally recessed *b* subunit could be truncated and complex formation would not be disrupted. This result indicates that the C-terminally extended *b* subunit is the one that makes the critical interactions with the delta subunit.

CHAPTER 1
INTRODUCTION

Overview of F_1F_O ATP Synthase

ATP hydrolases, or ATPases, are a class of enzymes that catalyze the dephosporylation of adenosine triphosphate (ATP) into adenosine diphosphate (ADP) and free phosphate ion (P_i). The energy released by this reaction can be harnessed to do work, driving chemical reactions and other energetically expensive processes. ATPases are classified into several groups based on homology and function. The F-type ATPases, also known as F_1F_O ATP synthases, are enzymes capable of both hydrolyzing ATP to pump protons (H^+) or sodium ions (Na^+) across a membrane, as well as capturing the energy of H^+ or Na^+ flowing down a concentration gradient and utilizing that energy to synthesize ATP from ADP and P_i. The V-type ATPases are found in intracellular vacuoles where they use the energy obtained from ATP hydrolysis to pump H^+ into the vacuoles in order to acidify these compartments. These ATPases are also found in some epithelia where they function to move H^+ across the membrane. A third type of ATPase is the A-type, found in Archaea and closely related to the V-type ATPases. The P-type ATPases, also known as E_1E_2-ATPases, function to transport a variety of different ions across membranes. Finally, the E-type ATPases are cell-surface enzymes that hydrolyze a range of nucleotides, including extracellular ATP.

The focus of our study was the F_1F_O ATP synthases. These enzymes are found in the cytoplasmic membrane of bacteria, the inner membrane of mitochondria and the thylakoid membrane of chloroplasts [1-3]. As noted above, F_1F_O ATP synthases perform two related functions: the energy of an electrochemical gradient of H^+ or Na^+ can be used to synthesize ATP from ADP and P_i, or ATP can be hydrolyzed to generate a gradient of H^+ or Na^+ ions. ATP synthases are the main producers of ATP in living systems, and they convert the energy obtained

from both oxidative phosphorylation and photosynthesis into a useful chemical form. All ATP synthases share mechanistic and structural properties. Each is composed of two different components that are structurally and functionally distinct: a membrane embedded F_O component and a peripheral, water-soluble F_1 component.

The simplest and most intensely studied F_1F_O ATP synthase is that of *Escherichia coli* (Figure 1-1). It is composed of eight different types of subunits, five in F_1 with a stoichiometry of $\alpha_3\beta_3\gamma\delta\varepsilon$ and three in F_O with a stoichiometry of ab_2c_{10}. The total mass of F_1 is about 400 kDa while that of F_O is approximately 150 kDa. The F_1 and F_O components are both molecular motors, each powered by a different fuel source: F_1 uses ATP as a substrate while F_O uses H^+. The rotor shafts of these two motors are connected to one another, forming the $c_{10}\varepsilon\gamma$ rotor stalk, also known as the central stalk. This central stalk rotates relative to the bodies of the two motors while the peripheral stalk $b_2\delta$ connects the motor bodies to one another and allows an efficient transfer of energy. The energy source that drives F_1F_O ATP synthase depends on which source is stronger. In the presence of a strong electrochemical gradient, the energy released by H^+ flowing down this gradient will be captured by F_O and used to power ATP synthesis in F_1. In the absence of a strong gradient and the presence of ATP, the F_1 component will drive the enzyme, pumping H^+ across the membrane to generate an electrochemical gradient that can be used by other proteins to do work.

Although much is known about the structure and function of F_1F_O ATP synthase, the enzyme is still not fully understood. High-resolution structures of F_1 have been obtained from several species in the presence of different substrates and inhibitors. These structures show F_1 to be asymmetric, containing three catalytic sites whose conformations alternate as the rotor stalk turns and ATP is either hydrolyzed or synthesized. F_O is less well defined, with a high-

resolution structure available only for the *c* subunit. Our current understanding of the structure and function of F_O is based on extensive biochemical experiments.

Crosslinking as a Probe for Molecular Structure

The formation of crosslinks has been used extensively as a probe for molecular structure. Crosslinking is the process of chemically joining two molecules by a covalent bond. Many reagents used for crosslinking contain two reactive ends that target specific functional groups on proteins and are known as bifunctional crosslinking reagents. These reagents usually insert themselves between the two reactive groups and have a fixed "reach," or crosslinking span. Bifunctional crosslinkers are further divided into two groups: homobifunctional and heterobifunctional. Homobifunctional crosslinkers have two identical reactive groups and couple like functional groups — typically two thiols, two amines, two acids or two alcohols. These reagents are predominantly used to form intramolecular crosslinks in a one-step chemical crosslinking procedure. Heterobifunctional crosslinkers possess reactive groups with dissimilar chemistry that allow for the formation of crosslinks between unlike functional groups. These reagents can still form multiple intermolecular crosslinks to yield high molecular weight aggregates, but the crosslinking chemistry of these reagents can be more easily controlled to minimize undesirable polymerization or self-conjugation. A special subset of the heterobifunctional crosslinking reagents are the photoreactive crosslinking reagents in which the activation of the second functional group is accomplished by illumination with ultraviolet light. These reagents react with nucleophiles or form C-H insertion products.

One of the drawbacks of most bifunctional crosslinking reagents is the uncertainty created by the crosslinking span. Reactive groups can typically be 5-15 Å apart from one another and still crosslink, depending on the particular crosslinking reagent used. One technique to overcome this issue is to use oxidizing reagents such as Cu^{2+} to generate disulfide bonds between

adjacent cysteine residues. Cu^{2+} is known as a "zero-length" crosslinking reagent because it is able to form a chemical bond between two groups without incorporating itself into the product. The average length of a disulfide bond is 2.0 Å, and the sulfur atoms can be separated by no more than 2.2 Å in order for the disulfide bond to form [4]. Disulfide bonds between cysteine residues naturally occur in proteins that are secreted in the extracellular medium, where the formation of these bonds plays an important role in protein stability. Two factors make the formation of disulfide bonds an excellent probe for molecular structure *in vitro*. First, only the relatively infrequent amino acid cysteine is capable of forming disulfide bonds, limiting the number of possible crosslinks that can be formed in a given protein. Second, both cysteine residues must be in close spatial proximity and in an appropriate geometry for crosslink formation.

Disulfide crosslink formation has been used to probe the molecular structure of many proteins and complexes, including the aspartate receptor [5, 6], acetylcholine receptor [7-9], Tat receptor [10, 11], glycine receptor [12], Na^+/Ca^{2+} exchanger (NCX1) [13], Na^+/H^+ antiporter (NhaA) [14], Na^+/K^+ ATPase [15], rhodopsin [16], transducin [17], cAMP-dependent protein kinase II [18], troponin [19] and gamma delta resolvase [20], to name a few. This technique has even been used to investigate the kinetics of protein folding [21-25].

Crosslink formation has been used extensively in the investigation of ATP synthase structure and function. Both bifunctional and disulfide crosslinking reagents have provided information about spatial proximity between and within subunits, as well as providing functional information by covalently linking residues to one another. Table 1-1 lists the crosslinking reagents that will be discussed in the following pages, along with their abbreviations and crosslinking spans.

Table 1-1. Crosslinking reagents

Crosslink reagent	Abbreviation	Span (Å)
Zero-length crosslinking reagents		
$CuCl_2$	Cu^{2+}	0
Cu(II)-(1,10-phenanthroline)$_2$	CuP	0
5,5'-dithio-bis(2-nitro-benzoic acid)	DTNB	0
I_2		0
1-ethyl-3-[(3-dimethylamino) propyl]-carbodiimide	EDC	0
Other crosslinking reagents		
p-azidophenacyl bromide	APB	9
benzophenone-4-maleimide	BPM	10
N-[4-(3-(trifluoromethyl)-3H-diazirin-3-yl)benzyl]maleimide	Dia-18	10-15
3-maleimidopropionic acid, 4-[3-(trifluoromethyl)-3H-diazirin-3-yl]benzyl ester	Dia-19	15-20
dithiobis(succinimidyl propionate)	DSP	12
dimethy 3,3'-dithiobispropionimidate	DTBP	12
1,2-ethanediyl bis-methanethiosulfonate	M2M	5.2
1,4-butanediyl bis-methanethiosulfonate	M4M	11
N-(4-azido-2,3,5,6-tetrafluorobenzyl)-3-maleimidopropionamide	TFPAM-3	10-15
N-(4-azido-2,3,5,6,-tetrafluorobenzyl)-6-6-maleimidyl hexanamide	TFPAM-6	20-25

Mechanism of Action of ATP Synthase

Overview: F_1F_O ATP synthase is known to function by a rotary mechanism first proposed by Boyer [26] in the late 1970s. This "binding change mechanism" model was constructed based on the observations "that energy input was involved principally in change in the binding of reactants at catalytic sites by indirect coupling" [27]. It was thus hypothesized that the three catalytic sites in F_1 would pass sequentially through three different conformations, or "binding changes", linked to subunit rotation. This model required mechanistic asymmetry in the enzyme so at any given moment a different step of the mechanism would be occurring at each site. For ATP synthesis this would entail binding of the substrates $ADP{\cdot}Mg^{2+}$ and P_i, synthesis of ATP, and release of ATP. It was proposed that the binding of substrates and release of product were steps that required energy input, while the synthesis of ATP was thought to occur without free

energy change. Not long after the binding change mechanism was proposed, evidence was found that supported the model of alternating participation of catalytic sites in the synthesis reaction [28] and the hydrolysis reaction [29], where the release of products at one site was found to be triggered by the binding of ATP to another. The real confirmation of the proposal that rotation is linked to catalytic activity was the direct visualization of movement in the rotor stalk relative to the rest of the complex, as described below [30].

As F_1 contains three catalytic sites, there are three possible modes of operation: unisite, with only one site filled with substrate at any given time; bisite, with two sites filled and one site empty; and trisite, in which all three catalytic sites are filled with substrate [31]. Unisite catalysis does occur and has been studied extensively, although unisite ATP hydrolysis is not mechanistically coupled to F_O and hence does not pump H^+ [32]. Although the original binding change mechanism proposed bisite catalysis, sufficient evidence has been obtained to determine that bisite catalysis is not the normal mechanism for F_1F_O function. ATP synthase molecules with only two sites filled show negligible activity [32-34], and writing a bisite mechanism with the available data is problematic [35]. Only an F_1F_O complex in which all three sites are filled can rotate, indicating that trisite catalysis is the normal function of ATP synthase [36, 37]. Trisite catalysis exhibits a large degree of catalytic cooperativity between the sites and current models are described below.

At substiochiometric concentrations of $ATP{\cdot}Mg^{2+}$ only a single site operates at a time, termed unisite catalysis [38]. Analysis of unisite catalysis by Mechaelis-Menten kinetics gives a K_m value for $ATP{\cdot}Mg^{2+}$ of 0.2 nM with a very fast binding of ATP and slow hydrolyzing to ADP and P_i. The equilibrium constant for this reaction is close to unity and can be reversed, even in soluble F_1. Four reversible steps occur in unisite catalysis: ATP binding and release, ATP

hydrolysis and resynthesis, P_i release and binding, and ADP release and binding. Release of the product is $k_{off} \leq 10^{-3}$ s^{-1}. Rate constants for all steps except P_i binding have been measured by several labs and are in general agreement [39-46]. It has also been shown that soluble and membrane bound forms of F_1 behave in a similar fashion with regards to unisite catalysis [44, 47].

Trisite catalysis involves all three catalytic sites and can also be analyzed using Michaelis-Menten kinetics. For ATP hydrolysis this produces a single K_m for ATP·Mg^{2+} of 100 μM [48], while for ATP synthesis K_m values for ADP and P_i are 27 μM and 0.7 mM, respectively [49]. There is a high degree of positive catalytic cooperativity during trisite catalysis in which ATP hydrolysis at the highest affinity site is favored upon binding of ATP to the other catalytic sites [31]. The highly cooperative nature of the enzyme becomes apparent when comparing the trisite parameters to the unisite, with the rate of ATP hydrolysis being five times greater during trisite catalysis than unisite [38]. The substrates also bind with greater affinity, with the K_d of ATP·Mg^{2+} three to five orders of magnitude greater during trisite catalysis. Each of the three catalytic sites can bind nucleotide, but with widely different affinities [32]. Dissociation constant values for ATP·Mg^{2+} for the high, medium and low affinity sites are around 1 nM, 1 μM, and 30 μM, respectively. An open site conformation is unoccupied by definition, with a K_d for ATP·Mg^{2+} greater than 10 mM, preventing binding of nucleotide under effectively all physiological conditions. The affinity of each site for nucleotide is determined by the position of the γ subunit, as demonstrated by crosslinking studies [50].

Rotation Steps: Significant advances in the understanding of the mechanism of F_1F_O ATP synthase have been made due the ability to resolve single molecule rotation. A sample diagram

of the relationship between rotation angle and the catalytic mechanism is shown in Figure 1-2 [51].

Initial experiments visualizing the rotation of the γ subunit attached to an actin filament found that the rotor advanced in 120° steps, with pauses evident at low substrate concentrations [52, 53]. Each step was driven by the hydrolysis of a single ATP molecule and the pauses were an indication of time spent waiting for the next productive collision with substrate. This stepping behavior of the γ subunit was soon confirmed by another group using FRET [54]. The next step was the replacement of the actin filament with gold beads having a diameter of 40 nm which produced less drag and allowed a major improvement in time resolution [55]. This increase in resolution allowed the visualization of two substeps within the 120° step, a 90° step that occurs within 0.25 ms upon binding of $ATP \cdot Mg^{2+}$, a stationary interval of about 2 ms, and a second 30° step which also occurs within 0.25 ms. Subsequence studies refined the sizes of these substeps to 80° and 40° [56-58], although the experimental precision is still insufficient for absolute distinction and the possibility remains that there may be a small third substep between the two [59]. The 80° step is driven by the binding of $ATP \cdot Mg^{2+}$ and the 40° step by release of ADP or P_i [55]. Two reactions occur during the ~2 ms pause at the 80 step, each ~1 ms long. The first reaction is ATP hydrolysis of the ATP that was bound 200° prior [57, 58]. Likewise, the ATP that bound at 0° will be hydrolyzed after γ rotates 120° + 80°. The second reaction is P_i release, with this release driving the last 40° step [51]. ADP is released at 240° after binding as ATP at 0°, as determined by direct observation using a fluorescent ATP analog [60]. One detail still left unresolved by current experimental data is exactly when P_i is released. The P_i bound at 0° as ATP could be released at 80° as shown in Figure 1-2, or could be delayed until 200° in an

alternate mechanism. Recently, Yoshida suggested that the latter is in fact the case (EBEC 2008).

Energetics: The energetics of ATP synthase have been investigated experimentally and it has been determined that for ATP synthesis, binding of P_i and release $ATP{\cdot}Mg^{2+}$ are the major energy-requiring steps, while $ADP{\cdot}Mg^{2+}$ binding occurs spontaneously [32]. Surprisingly, it has also been demonstrated that the actual synthesis of ATP is not an energy requiring step [27, 61, 62]. The catalytic sites have a high affinity for ATP over that of ADP and P_i and are capable of forming ATP from ADP and P_i without the input of energy. This high affinity is generated by numerous side chain interactions with ATP which facilitate the appropriate location, orientation and polarization [42, 63, 64]. Energy input is required to release the tightly bound ATP from the catalytic site. The Boyer lab used ^{18}O exchange reactions to demonstrate the reversible nature of the synthesis and hydrolysis reactions occurring during unisite catalysis. The equilibrium between ADP + P_i and ATP was close to unity, indicating that this chemistry step did not require energy.

The torque generated by ATP hydrolysis is in the range of 40-50 pN·nm, an efficiency of close to 100% [53, 65]. It is known for most organisms that a nonintegral number of protons translocate through F_O per ATP synthesized in F_1. The high efficiency and constant output torque imply a soft elastic power transmission between F_1 and F_O. Models have been proposed in which energy is stored in the deformation of the central γ subunit and the stretching of the peripheral stalk in order to facilitate efficient energy transfer between F_O and F_1 [66-68]. Details of power transmission still need to be addressed, but there is little doubt that F_1F_O ATP synthase is a highly efficient molecular motor [69].

Escherichia coli as a Model System of F_1F_O ATP Synthase

As mentioned above, the F_1F_O ATP synthase from *E. coli* is the simplest known ATP synthase and also the most extensively studied. Since all known ATP synthases function by a similar mechanism, information obtained by studying *E. coli* is also applicable to other organisms. The ease of working with bacteria make this an ideal system to elucidate structural and functional details. The eight subunits of F_1F_O ATP synthase from *E. coli* will be grouped into four functional categories below and the current knowledge about the structure and function of each subunit will be discussed. These four categories are: subunits involved in proton translocation through F_O (*a* and *c*); subunits that compose the rotor stalk (γ and ε); catalytic subunits of F_1 (α and β); and subunits that make up the peripheral stalk (δ and *b*).

Proton Translocating Subunits in F_O

Subunit *a*

Overview: Subunit *a* is a membrane spanning component of F_O located on the periphery of the *c* subunit ring (Figure 1-3). The *a* subunit is 271 amino acids long with a mass of 30.3 kDa, making it the largest of the F_O subunits [70]. There is one *a* subunit per ATP synthase complex and this subunit is essential for proton translocation through F_O [71]. Subunit *a* cannot be excessively overproduced [72, 73] and cannot be found in the membranes unless both *b* and *c* subunits are present [74]. It was demonstrated that subunit *a* is a substrate for the FtsH protease [75], so it is probably turned over rapidly if it is not incorporated properly into a complex. Like most membrane proteins, this subunit is extremely hydrophobic. It is currently thought to span the membrane five times with the N-terminus in the periplasm and the C-terminus in the cytoplasm [76, 77]. No high-resolution structure of subunit *a* is currently available, but structural and functional information have been obtained by analyzing mutants, crosslinking results and the accessibility of specific residues to labeling reagents. All known F_1F_O ATP

synthases contain a protein with primary sequence homology to the *a* subunit, and comparison of these sequences from various organisms has directed research by identifying highly conserved and potentially important residues. This sequence homology is the highest in the fourth and fifth transmembrane domains where many functionally important residues reside [78].

The *a* subunit is directly involved in F_O-mediated proton translocation. The first indication of this role for subunit *a* was presented in 1986 [79]. Since then more than 100 mutants have been constructed by site-directed mutagenesis to map out the proton channel in the *a* subunit [80]. Present models propose that the *a* subunit contributes two half channels to provide access to the critical c_{D61} residues that are protonated and deprotonated [81, 82]. A schematic diagram of these residues and the two half-channels is shown in Figure 1-4.

The models cited above propose that two c_{D61} residues are transiently deprotonated in the same moment at the interface between the *a* and *c* subunits. One of these deprotonated c_{D61} residues interacts with a_{R210} and can be protonated from the periplasm via an access channel through subunit *a*. Once protonation occurs, this now neutralized c_{D61} residue can enter the lipid phase as the entire ring of *c* subunits rotates relative to subunit *a*. This rotation brings the next unprotonated c_{D61} towards a_{R210} and a protonated c_{D61} into the interface with subunit *a*. The protonated c_{D61} residue is deprotonated through a second access channel into the cytoplasm. Similar models have been developed and analyzed by others [83-85]. These models are based on experimental evidence that led to our current understanding of the topology and function of subunit *a*, described in more detail below.

Topology: The topological model of subunit *a* is based largely on the accessibility of individually substituted cysteine residues to labeling reagents [76, 77, 86]. The five membrane model is shown schematically in Figure 1-5.

Subunit *a* has two large loops in the cytoplasm in addition to the C-terminus [87]. The first loop, L12, consists of residues $a_{A64\text{-}L100}$ [88]. The accessibility of these residues was investigated by Long *et al.* by individually engineering cysteines at 37 positions between $a_{F60\text{-}P103}$. Inverted membrane vesicles were prepared and the ability of each individual cysteine to react with 3-(N-maleimidylpropionyl) biotcytin (MPB) was investigated. The investigators found that all of the tested residues in the $a_{A64\text{-}K74}$ and $a_{V90\text{-}P103}$ regions could be labeled, while about half of the residues in the $a_{F75\text{-}S89}$ region were resistant to labeling. The residues in the middle region were somehow shielded from the labeling reagent, but the presence of multiple polar residues in this area makes lipid shielding unlikely. The authors discovered that cysteine residues introduced individually at a_{K74} and a_{K91} could be crosslinked to the *b* subunit with TFPAM-3. This crosslink did not affect ATP-driven proton pumping, providing concrete evidence that the *a* and *b* subunits do not need to dissociate for proper enzyme function. These results also indicate that the first loop of the *a* subunit may be in contact with one or both of the *b* subunits.

The second cytoplasmic loop, L34, consists of residues $a_{K169\text{-}L200}$ [89]. The accessibility of the residues in this loop was investigated by Zhang and Vik by individually engineering 41 residues in the $a_{L160\text{-}S206}$ region. Once again, inverted membrane vesicles were prepared and the ability to label the cysteines with MPB was investigated. All residues tested in the $a_{M168\text{-}F174}$ region labeled readily with the exception of a_{T179C}. This region of subunit *a* is known to be in proximity to the *c* subunits because the individually engineered cysteines a_{S165C}, a_{M169C}, a_{G173C}, a_{F174C}, a_{E177C}, a_{L178C}, a_{P182C}, a_{F183C} and a_{N184C} were all able to be crosslinked with TFPAM-3 to the *c* subunit ring. In contrast, all of the residues tested in the $a_{H185\text{-}S206}$ region were resistant to labeling with MPB. Earlier studies have shown that substitutions at a_{E196} [82] and a_{N192} [90]

diminished the rates of proton translocation, indicating that residues in this region may be involved in protein-protein interactions with other regions of the enzyme.

The C-terminal eleven residues are also located in the cytoplasm. Several of these residues could be labeled from the cytoplasmic side with MPB [76, 77]. Many bacterial homologs contain E and H residues at their C-terminal ends, such as –EEH in *E. coli*, so the effects of truncating these residues was investigated [91]. It was shown that the truncation of four residues had no effect at 37 °C and the deletion of nine residue was tolerated at 25 °C, indicating that these residues were nonessential for function but may be important for overall complex stability.

Subunit *a* contains two loops in the periplasm in addition to the N-terminus. The N-terminal end is about 37 residues long and is the largest segment of the *a* subunit exposed to the periplasm. It was shown that seven out of the eight residues tested in this N-terminal end could be labeled with MPB in [76, 77, 92]. Similar results were obtained in labeling studies carried out in whole cells permeabilized with polymyxin B nonapeptide (PMBN), an antibiotic derivative that partially permeabilizes the outer membrane of *E. coli* [77]. Two studies which contradict these results used antibodies against the N-terminus and located it in the cytoplasm [93, 94], but the majority of the experimental evidence supports the previous model. Both models are essentially the same from residue a_{K65} onwards, so there is no difference between the two when discussing the functionally important residues.

The first loop in the periplasm, L23, consists of residues $a_{I123\text{-}D146}$ [89]. Twenty-one residues in the $a_{D119\text{-}D146}$ region were individually changed to cysteine and labeled with MPB in whole cells. About half of them could be labeled, with no significant segment shielded. The second loop, L45, consists of residues $a_{G227\text{-}W235}$. The residues in this region are partially

shielded, with residues $a_{P230\text{-}W232}$ exhibiting modest levels of labeling while four other residues in L45 were found to be resistant [77].

Rastogi and Girvin [95] have attempted to model the last four transmembrane helices of the *a* subunit, shown below in Figure 1-6. Their model contains twelve copies of the *c* subunit and residues $a_{H95\text{-}S265}$ without cytoplasmic loop L34. This model was built based on the known biochemical information available for the *a* subunit. Notice that all of the residues labeled in Figure 1-4 are spacefill rendered below.

Mutagenic analysis: Many missense mutations have been constructed and analyzed beyond the cysteine substitutions described above. These experiments have provided critical evidence of the importance of certain residues for proper *a* subunit function.

Residue a_{R210}: a_{R210} is an essential residue for enzyme function and is strictly conserved, even in mitochondria and chloroplasts [80]. All single amino acid substitutions that have been tried resulted in nonfunctional ATP synthase complexes. Residues tested at this position include A, Q, K, I, V and E [96-100]. This lack of enzyme function was not due to an assembly failure, as F_1F_O complexes could be purified to homogeneity [101]. With the exception of the a_{R210A} substitution, all passive F_O-mediated proton conduction was blocked by substitutions of this residue. The a_{R210A} subunit left the proton channel open such that limited passive proton conduction was possible through F_O, producing a rare condition where F_1 was fully functional and F_O was semi-functional, with the two halves of the enzyme were uncoupled [99]. A second site suppressor of the a_{R210Q} mutation, a_{Q252R}, was capable of growth on succinate. This result indicated that the fifth transmembrane helix containing a_{Q252R} may be located close enough to the fourth transmembrane helix containing a_{R210Q} to contribute the essential R residue, a "horizontal" repositioning of these residues [97]. Recent attempts at "vertical" repositioning in the $a_{R210A,}$

$_{N214R}$ subunit resulted in a nonfunctional F_1F_O complex [102]. The double substitution $a_{R210Q,}$ $_{Q252K}$ was recently shown to result in a functional enzyme, making it the first known instance of an ATP synthase complex that functions without the critical R residue in the *a* subunit [103]. It is thought that a_{R210} is directly involved in mediating protonation of the essential c_{D61} residues on the *c* subunit ring.

Residue a_{E196}: The codon for a_{E196} has been extensively mutagenized [87]. Nine substitutions were initially tried: K, P, A, S, H, Q, D, N and T [104, 105]. This residue was not as sensitive to substitution as a_{R120} because only the K and P substitutions producing seriously defective F_1F_O complexes. Interestingly, the passive permeability to protons and the rate of proton translocation was depended on the substitution: E > D > Q = S = H > N > A > K. These results suggest that a_{E196} is not required for proton translocation, but it may reside near the proton pathway.

Residue a_{E219}, a_{H245}: Residue a_{E219} is located on the fourth transmembrane span and a_{H245} on the fifth (Figure 1-4). Substitutions at either site had a significant effect on F_O proton translocation, but neither residue is essential for enzyme activity because replacement with several different amino acids resulted in functional enzyme [78, 96, 106]. The substitutions for a_{E219} that have been tried are Q, H, D, L, K, G and C [99, 100, 105-107]. Substitution with either D, K or G resulted in functional F_1F_O, while substitution with H produced complexes exhibiting slight activity. Residue a_{H245} was changed to Y, L, E, C, S and G [79, 82, 98-100, 107]. Only substitutions with E and G showed any functional activity. These results shown that protonation or deprotonation of either a_{E219} or a_{H245} is not obligatory for proper enzyme function.

Second site suppressors have been found for both residues. The mutation a_{A145E} was found to suppress the a_{E219C} mutation [86], indicating a relationship between these residues. The same

authors found a second site suppressor for the a_{H245C} mutation, a_{D119H}. This second mutation indicated that the imidazole chain can be provided by another transmembrane span and was also shown to improve the growth properties of a_{H245S} on acetate.

It has been proposed that residues a_{E219} and a_{H245} may interact because they are conserved in mitochondria, but their positions are swapped [107]. The double substitution $a_{E219H, H245E}$ was constructed to test this possibility and was found to be slightly functional. There also exists evidence of a potential interaction between a_{G218} and a_{H245}, originally discovered by the observation that many species do not have an H residue in the corresponding location to *E. coli's* a_{H245}, but rather a G or E [78]. Species that contain G at the equivalent 245 position have either K or D at the equivalent a_{G218} position, while those with a E at 245 have a G at a_{G218}. The *E. coli* sequence has a_{H245} and a_{G218}. This observation led to the discovery of two interesting second site suppressor for the a_{H245G} mutation, a_{G218D} or a_{G218K}. These results support a close spatial arrangement between residues a_{G218}/a_{E219} and a_{H245}, but this could not be demonstrated with certainty without a high resolution structure of the *a* subunit.

Residue a_{A217}: The residue a_{A217} is important but nonessential for enzyme function [96]. The mutation a_{A217R} is the most fully characterized single mutation in F_O [80]. This mutation inhibited enzyme activity and eliminated passive proton permeability. Proteolysis and crosslinking of the ε subunit demonstrated that the effects of this substitution were propagated into the ε subunit [101], while measurement of rate constants for unisite catalysis revealed that a_{A217R} had no effect on the F_1 catalytic sites [108]. The a_{A217R} substitution most likely impairs rotation of the central stalk as opposed to causing a change in the catalytic properties of F_1.

Others: There are other strongly conserved amino acids in the *a* subunit that have been investigated by mutagenesis. The substitutions a_{D44N}, a_{D124N} or a_{R140Q} blocked the proton

channel, indicating these residues influence the function of the *a* subunit in some fashion [109]. The effects of substitutions at residues a_{N214} [90, 96], a_{Q252} [81, 100, 110] and a_{Y263} [91, 100] have also been investigated. These conserved residues were found to accommodate a range of substitutions, with positive amino acid substitutions generally having the most significant effect on enzyme function [87].

Insertions and deletions: Site-directed insertions and deletions have been used to probe subunit *a* for functional information. A series of deletions were constructed and analyzed for growth on minimal media [111]. The N-terminal region was shown to be essential for incorporation of the *a* subunit into the membrane. Deletion of regions $a_{K91\text{-}K99}$, $a_{G163\text{-}I171}$ or $a_{K167\text{-}E177}$ still allowed some enzyme function, while the deletion $a_{L120\text{-}D124}$ resulted in subunit *a* in the membrane but a nonfunctional ATP synthase.

Later experiments took advantage of the knowledge that single amino acid insertions of A or G are generally well-tolerated in globular proteins unless they occur near an active site [112, 113]. Insertions of A were constructed at 13 locations in the $a_{A187\text{-}H245}$ region [82, 114]. It was found that an insertion near a_{E196} had no effect, while an insertion after a_{F212}, near a_{R210}, caused a total loss of ATP-driven proton pumping. Interestingly, an insertion after a_{A217} was not as detrimental but an insertion after a_{F222} also destroyed enzyme function. Likewise, insertions after residues a_{N238} and a_{I243} caused total loss of function. Insertions after residues a_{I225}, a_{L229}, a_{S233} and a_{H245} had only small effects on function. The exact influence these insertions and deletions have on the structure of subunit *a* is not fully understood, but they may move critical residue out of alignment or disrupt helix-helix interactions.

A series of mutants were generated which contained deletions in the first cytoplasmic loop of subunit *a* (Cain lab, unpublished data). Surprisingly, large deletions in this region had no

detectable effect on enzyme viability. The strain expressing the mutant $a_{\Delta(K66\text{-}S98)}$ subunit was capable of growth on succinate and appeared normal in assays for ATP hydrolysis and ATP-driven proton pumping. Likewise, the deletion of residues A67-G73 had no detectable effect, while the deletion of residues F75-V90 resulted in a viable strain that demonstrated reduced proton pumping activity. The exact function of the first cytoplasmic loop of subunit *a* is unknown, but it is likely that this region has some purpose due to its retention in the gene over time.

Crosslinking analysis: Disulfide crosslinking experiments have been used to investigate the topology of subunit *a*. Cysteines were substituted into two transmembrane helices and their propensity to form disulfide crosslinks when treated with either CuP or I_2 was investigated [115]. The authors found bond formation between helices in the $a_{L120C,\ S144C}$, $a_{L120C,\ G218C}$, $a_{L120C,\ H245C}$, $a_{L120C,\ I246C}$, $a_{N148C,\ E219C}$, $a_{N148C,\ H245C}$, $a_{G218C,\ I248C}$, and $a_{D119C,\ G218C}$ mutants. These results suggest that transmembrane helices two, three, four and five form a four helix bundle. The aqueous access channel that allows protons to reach c_{D61} from the periplasmic side is thought to be in the center of this four helix bundle based on the reactivity of residues to water soluble labeling reagents [116]. The key a_{R210} residue of helix four would be located at the periphery in this model, facing out towards subunit *c*. A more recent study [117] provided more evidence of an interaction between transmembrane helices three and four. The mutants $a_{L160C/K203C}$, $a_{L160C/V205C}$, $a_{I161C/S202C}$, $a_{I161C/K203C}$, $a_{I161C/V205C}$ and $a_{S165C/S202C}$ formed crosslinked when incubated with M2M, while the mutant $a_{V157C/K203C}$ could also be crosslinked with M4M. The same study also demonstrated a spatial relationship between L12 and L34. The reagent M2M was capable of forming crosslinks in the mutants $a_{V86C/L195C}$ and $a_{M93C/L195C}$, indicating that loops

L12 and L34 may make protein-protein contacts with one another on the cytoplasm side of subunit *a*.

A similar approach has been used to investigate the spatial arrangements between the *a* and *c* subunits [118]. The investigators introduced cysteine pairs in the fourth transmembrane helix of subunit *a* and the second transmembrane helix of subunit *c* and determined if CuP could catalyze the formation of an *a*-*c* dimer. Seven of the 65 double mutants showed crosslink formation at 0, 10 and 20 °C: a_{S207C}/c_{I55C}, a_{N214C}/c_{A62C}, a_{N214C}/c_{M65C}, a_{I221C}/c_{G69C}, a_{I223C}/c_{L72C}, a_{L224C}/c_{Y73C}, and a_{I225C}/c_{Y73C}. Nine other double mutants showed lesser dimer formation at 20 °C. These results provide direct crosslinking evidence that these two helices are closely associated with one another in the membrane.

Subunit *c*

Overview: The *c* subunit is a member of the F_O proton channel that exists as an oligomeric ring structure in the membrane (Figure 1-7). Each individual *c* subunit is 79 amino acids long and forms a hairpin structure with two antiparallel α helical transmembrane segments connected by a short, structured loop [70, 119, 120]. Both ends of the *c* subunit are located at the periplasmic side of the membrane as demonstrated by the reactivity of residues c_{Y10} and c_{Y73} to tetranitromethane [121]. The existence of two transmembrane domains was initially predicted based on analysis of the *c* subunit primary sequence. This prediction was supported by labeling experiments using 3-(trifluoromethyl)-3-(m-[^{125}I]iodophenyl)diazirine ([^{125}I]TID), a photoactivatable carbene precursor that selectively labels proteins in the hydrophobic core of membranes [122]. The regions $c_{L4–L19}$ and $c_{F53–F76}$ were found to label with TID, indicating these regions were located in the membrane.

The suspected topology of the *c* subunit was confirmed when NMR analysis was used to solve the structure of the monomeric *c* subunit in chloroform/methanol/water (4:4:1) [119]. This NMR structure showed two antiparallel helices packed closely to one another, extending over 40 residues for the first transmembrane helix and 30 residues for the second (Figure 1-8). It was already known from previous NMR work [123-125] that the structure of the *c* subunit in solution resembled that of the folded protein incorporated into an F_O complex. Data supporting this conclusion include ^{1}H NMR resonance assignments of unmodified and nitroxide-derivatized c_{D61}, as well as spin label difference 2-D NMR of a c_{A67C} mutant that had been modified with a maleimido spin label. More recently, the structure of a peptide modeling the loop region $c_{G32\text{-}Q52}$ bound to dodecylphosphocholine micelles was solved by NMR [120]. The $c_{R41\text{-}P47}$ region was found to form a well ordered structure similar to what was observed in the entire subunit, flanked by short α helical segments. This suggests that the polar loop is rigid and contributes significantly to the stability of the hairpin formed by the two helices of the *c* subunit.

The conserved carboxyl group c_{D61} is located at a slight break in the middle of the second transmembrane helix in the NMR structure described above. This residue plays a crucial role in ion translocation. Proton translocation and ATP synthesis were completely abolished if this residue was modified by dicyclohexylcarbodiimide (DCCD) or replaced with G or N [126]. This essential carboxyl group can be moved from the second transmembrane helix to the first in the $c_{D61G/A24D}$ double mutant and still retain enzyme function, providing evidence of a close interaction between the two helices in the context of the holoenzyme [127]. A number of third-site mutations have been identified which optimize the function of the $c_{D61G/A24D}$ double mutant–c_{F53C}, c_{F53L}, c_{M57V}, c_{M57I}, c_{M65V}, c_{G71V} and c_{M75I} [128]. All of these substitutions are

present at the interface between the two transmembrane helices, providing further evidence of helix-helix interaction.

The polar loop region between the two transmembrane helices of subunit *c* is exposed to the cytoplasmic side of the membrane as initially determined with antibodies specific to this hydrophilic loop [129, 130]. These antibodies would only bind to F_1-stripped, everted membrane vesicles. Residues c_{A40}, c_{R41}, c_{Q42}, and c_{P43} of the polar loop are highly conserved in bacteria, mitochondria, and chloroplasts. These residues are located at the top the polar loop in the NMR structure shown above [119]. Although all four residues are conserved, only residue c_{R41} is absolutely necessary for enzyme function [131, 132]. It has recently been shown that the positive charges on this loop are essential for the proper insertion of the *c* subunit in the membrane by YidC [133-135].

Structure of *c* subunit ring: The *c* subunits exist as a multimeric ring in the membrane. This arrangement was initially suspected based on the stoichiometry of subunits of F_O and supported by evidence obtained using electron and atomic force microscopy [136-138]. The exact number of *c* subunit in the ring has long been a matter of debate, but evidence indicates the preferred number for *E. coli* is ten [139]. The number of *c* subunits varies between organisms, with some organisms having rings of up to 15 subunits [140-143]. The existence of a multimeric ring of *c* subunit was supported by the formation of disulfide crosslinks between adjacent *c* subunits, forming a "ladder" on an SDS-PAGE gel extended up to c_{10}-oligomers. This was first demonstrated by individually crosslinking the $c_{A14C, M16C}$, $c_{M16C, G18C}$, $c_{A21C, G23C}$, $c_{L70C, L72C}$, $c_{A14C, L72C}$, $c_{A21C, M65C}$, and $c_{A20C, I66C}$ mutants with CuP [144]. These results were recently confirmed and extended with the observation that crosslinking of both $c_{A21C, M65C}$ and $c_{A21C, I66C}$ mutants resulted in oligomeric structures from c_2 to c_{10} [145]. The crystallization of the *c* subunit rings

from three other species, *Saccharomyces cerevisiae* [146], *Ilyobacter tartaricus* [147] and *Enterococcus hirae* [148] makes the existence of a *c* subunit ring in *E. coli* almost certain. These *c* subunit rings are shown in Figure 1-9, panels A, B and C, respectively. Researchers have generated models of the *E. coli* ring as shown in Figure 1-9D using the structure of the monomeric *c* subunit, known biochemical data and the *c* subunit rings from other organisms, but a complete structure of the *c* subunit ring has yet to be obtained [95, 149].

It has long been hypothesized that the *c* subunit ring interacts with the γ and ε subunits to form the stator component of the F_1F_O ATP synthase complex. However, only in the last decade has this been conclusively proven. Direct observation of the rotating *c* subunit ring was first obtained by Sambongi *et al.* [150]. These researchers immobilized F_1F_O on a Nickel nitrilotriacetic (Ni-NTA) coated glass slide by engineering a histidine tag on the N-terminus of each α subunit. The c_{E2C} subunit was expressed and the native cysteine in γ was mutated, resulting in only a single cysteine in the rotor subunits. This engineered cysteine was biotinylated to allow binding of streptavidin and a fluorescently labeled actin filament. It had previously been demonstrated that the γ and ε subunits rotated relative to the $\alpha_3\beta_3$ hexamer upon the addition of ATP by a similar technique [30, 151]. The study done by Sambongi *et al.* clearly showed that the actin filament rotated for up to 2 min upon the addition of ATP, proving that the *c* subunit ring was part of the rotor. This important experiment was reproduced and the results confirmed by two other labs [152, 153]. However, Tsunoda *et al.* [153] expressed concern that the enzyme had lost sensitivity to DCCD in all three studies, raising questions about the validity of the results. A loss of sensitivity to DCCD indicates a possible uncoupling in the enzyme such as a disruption of the interactions between the *c* subunit ring and the *a* subunit against which it must rotate to drive proton translocation. This concern was partially alleviated by the

demonstration that covalently crosslinking the γ, ε and *c* subunits together to form a single unit still allowed the enzyme to function [154], providing more evidence that the *c* subunit ring did indeed rotate along with γε. Conditions were eventually discovered that allowed a setup similar to that used by Sambongi *et al.* which resulted in F_1F_O complexes that were DCCD sensitive [155]. The authors were able to measure enzyme activity under a range of different substrate concentrations and inhibitors, clearly proving rotation of the *c* subunit ring is driven by ATP hydrolysis in F_1.

Subunit interactions: The *c* subunit interacts with both the *a* and *b* subunits in F_O. The structure of F_O has been investigated by several groups using microscopy [136-138]. Electron microscopy studies of F_O revealed a 75 Å wide structure which is consistent with a ring of *c* subunits flanked by the *a* and *b* subunits [136]. Atomic force microscopy was also used to examine the structure of the F_O sector [138]. Two different structures were observed, probably corresponding to different orientation of F_O in the membrane. One structure exhibited a central mass and the other a central hollow, both with an asymmetric width of about 130 Å, large enough to accommodate the *a* and *b* subunits as well as the *c* subunit ring. Finally, scanning force microscopy was also used to investigate the structure of membrane-bound F_O [137]. The images obtained show a ring structure with a central dimple and an asymmetric mass to one side. This mass decreased when the membranes were treated with trypsin, probably due to degradation of the *b* subunits, and disappeared completely when examining pure *c* subunit oligomers.

The interaction of the *c* subunits with the *a* and *b* subunits is extremely efficient–single molecule studies reveal the protein-protein interaction to be almost frictionless during rotation [155], while the large output torque of the ATP synthase complex indicates an absence of slipping in the rotor/stator interface in F_O [156]. Crosslinking results, described below,

demonstrate an intimate interaction between the *a* and *c* subunits in which the *a* subunit is thought to provide two proton half-channels to allow access to the essential c_{D61} residue (Figure 1-4). New evidence supporting this model was recently obtained by probing the accessibility of the second transmembrane helix of subunit *c* by engineering cysteines and testing for their reactivity to membrane-impermeable compounds [157]. Residues in the membrane-embedded pocket surrounding c_{D61} were reactive to NEM and methanethiosulfonate, especially c_{G58C}. This reactivity was only observed in the presence of subunit *a*, indicating this subunit is required to form the aqueous channel to the *c* subunit. The interactions between the *a* and *c* subunit are such that modification of even a single c_{D61} residue with DCCD is sufficient for complete inactivation of F_O [158, 159].

The *c* subunit ring also interacts with the ε and γ subunits to bind F_1 and F_O. Mutations in the loop region are known to disrupt this binding [131, 132, 160-163]. For example, the c_{Q42E} mutation in the loop region disrupts complex formation, but suppressor mutations ε_{E31G}, ε_{E31V}, and ε_{E31K} in F_1 restore function [164]. This interaction between the *c* subunit and F_1 was investigated by individually generating the c_{A39C}, c_{A40C}, c_{Q42C}, c_{P43C} and c_{D44C} mutants and testing for the ability to react with NEM [165]. It was found that mutants c_{Q42C}, c_{P43C} and c_{D44C} were able to react with NEM while c_{A39C} and c_{A40C} were not. All c_{P43C} and c_{D44C} residues reacted identically, but two classes of c_{Q42C} residues were observed–about 60% of the residues reacted rapidly while 40% reacted more slowly. It was suggested that the slow reacting residues were involved in interactions with the ε and γ subunits. Crosslinking results also demonstrate an interaction between the *c* subunit and both ε and γ, discussed below.

Crosslinking analysis: Crosslinking analysis indicates a close proximity between the *c* subunits and the *a* and *b* subunits. These crosslinking experiments are described in more detail

in the sections on the *a* subunit and *b* subunits. Briefly, crosslink formation between the fourth transmembrane helix of subunit *a* and the second transmembrane helix of subunit *c* was demonstrated by introducing double cysteine mutants and crosslinking with CuP [118]. It has also been shown that cysteine substitutions individually engineered in the second cytoplasmic loop of the *a* subunit, L34, could be crosslinked to the *c* subunits using the crosslinking agent TFPAM-3 [166]. Likewise, cysteines engineered at the N-terminus of the *b* subunit could be crosslinked with CuP to cysteines introduced at the bottom of the second transmembrane helix of subunit *c* [167]. The formation of this crosslink inhibited enzyme function as would be expected if the *c* subunit ring must rotate relative to the ab_2 subunits.

A close spatial proximity between the polar loop of the *c* subunits and the ε subunit has been demonstrated by the formation of disulfide crosslinks [168]. The individual mutants $c_{A40C}/\varepsilon_{E31C}$, $c_{Q42C}/\varepsilon_{E31C}$, and $c_{P43C}/\varepsilon_{E31C}$ were capable of forming crosslinks when treated with CuP while the mutant $c_{A39C}/\varepsilon_{E31C}$ was not. Interestingly, the formation of the $c_{Q42C}/\varepsilon_{E31C}$ crosslink inhibited ATP-driven proton pumping, possibly as a result of the formation of *c*-*c* dimers rather than a result of a crosslink between the *c* and ε dimer subunits. This was investigated further by crosslinking the ε_{E31C} subunit to the genetically fused cc'_{Q42C} subunit in which a linker region had been introduced between the C- and N-terminal ends of two consecutive *c* subunit monomers [169]. Expression of these genetically fused *c* subunits resulted in a functional ring composed of five dimers instead of ten monomers, each of which had only a single substituted cysteine. The $cc'_{Q42C}/\varepsilon_{E31C}$ mutant did not form *c*-*c* dimers upon treatment with CuP, but the *c*-ε crosslink still formed with high efficiency and had a minimal effect on ATP hydrolysis activity, ATP-driven proton pumping and ATP synthesis. These results were expanded upon with the discovery that cysteines substituted individually at c_{A40C}, c_{Q42C} and c_{D44C}

could be crosslinked to individual cysteines substituted throughout the entire $\varepsilon_{V26\text{-}L33}$ region [170].

Likewise, crosslinking evidence indicates a spatial proximity between the *c* and γ subunits. This was initially demonstrated by the formation of a nonspecific crosslink [171]. A cysteine was engineered in the loop of the c_{Q42C} mutant and crosslinked to any nearby tyrosine or tryptophan residues using Cupric 1,10-phenanthrolinate. Crosslink formation was observed between the c_{Q42C} subunit and the region $\gamma_{K202\text{-}V286}$, likely in the $\gamma_{K202\text{-}Q230}$ segment. The same authors later showed that specific crosslinks could be form using CuP in the double mutants c_{Q42C}/γ_{Y205C}, c_{P43C}/γ_{Y205C} and c_{D44C}/γ_{Y205C} but not c_{A39C}/γ_{Y205C} [172]. These crosslinks, which could also be formed using DTNB, reduced but did not eliminate ATP-driven proton pumping. This reduction in activity may be the result of *c*-*c* dimer formation as described above, since a comparable reduction in activity was also observed in mutants lacking the γ_{Y205C} mutation.

Finally, crosslinking results have also demonstrated that the *c* subunit ring contains lipids. The individual substitutions c_{L4C}, c_{L8C} and c_{M11C} all contained cysteine residues which were oriented towards the inside of the ring [173]. The outer membranes of *E. coli* were permeabilized with PMBN and crosslinking was induced with either Dia-18 or Dia-19. All three mutants crosslinked to lipid when treated with Dia-18, while only c_{L8C} crosslinked to lipid when treated with Dia-19. The most noticeable product had a mass increase of 719 Da, consistent with a crosslinked product between a *c* subunit and phosphatidylethanolamine. This was confirmed by digestion with phospholipase C.

Rotor Stalk Subunits

Subunit ε

Overview: The ε subunit of F_1F_O ATP synthase composes part of the rotor stalk (Figure 1-10). This subunit is 139 amino acids long and is essential for the binding of F_1 to F_O [70, 174, 175]. In the absence of the ε subunit, there was no enzyme assembly or membrane-associated ATP-drive proton pumping activity observed [174, 176, 177]. This subunit interacts with the *c* subunit ring of F_O as well as the α, β and γ subunits of F_1 [164, 168, 178-180]. The folded protein consists of two domains, an N-terminal 10-stranded β-sandwich and two α-helices at the C-terminal end [181, 182]. The N-terminal β-sandwich domain is critically important for complex assembly [183, 184]. One side of this β-sandwich domain interacts with the polar loops of the *c* subunit ring [164, 168] while the other side interacts with the γ subunit [180, 185, 186]. The two C-terminal α-helices interact with α and β subunits of the F_1 [185]. They do not play a role in complex assembly [177, 187-190], but they are important for the efficient coupling between ATP hydrolysis and proton pumping [190, 191]. The ε subunit was shown to rotate along with the γ subunit as observed by video microscopy when F_1 was powered with ATP [151].

Structure: The structure of the ε subunit in solution was first solved in 1995 using two- and three-dimensional heteronuclear (^{13}C, ^{15}N) NMR spectroscopy and found to consist of two distinct domains (Figure 1-11) [181]. The N-terminal domain consisted of 84 residues $\varepsilon_{M3\text{-}R86}$ and formed a 10-stranded β-sandwich with a hydrophobic interior between the two sandwich layers. The C-terminal domain was composed of 48 residues $\varepsilon_{D91\text{-}M138}$ which were arranged as two α-helices running antiparallel to one another in a hairpin structure. A series of alanine residues from each helix formed the central contacting residues between the two helices in a sort

of 'alanine zipper'. The C-terminal hairpin folded back and interacted with one side of the β-sandwich. The same authors published a more detailed analysis of the interactions between the two domains several years later [192]. Strand seven of the β-sandwich was shown to interact hydrophobically with the second α-helix of the hairpin region. An analysis of the dynamics between the two domains revealed a tight association with little or no flexibility relative to one another. The ε subunit has also been crystallized and solved to a resolution of 2.3 Å [193]. The crystal structure and the NMR structure are in excellent agreement.

Both the NMR and crystal structures were obtained with the ε subunit alone, not in the context of F_1F_O. Therefore, there is the question of whether these structures actually represent the conformation the protein takes in the intact complex. Two pieces of evidence indicate that the structure of the ε subunit in the holoenzyme is similar to the one observed. First, both structures put the ε_{M49} residue of the N-terminal domain and the ε_{A126} residue of the C-terminal domain in close proximity, within 5 Å. Cysteine residues engineered at these two positions were able to form a disulfide crosslink in the holoenzyme as described below [194], indicating these two residues are in close spatial proximity. Second, similar protease digestion pattern are observed for subunit ε both in solution and in the intact complex. Six trypsin cleavage sites exist in the ε subunit, after residues ε_{A93}, ε_{A98}, ε_{K99}, ε_{R100}, ε_{A123} and ε_{T135} [185, 195]. Certain trypsin sites in the ε subunit were cleaved very slowly both when it was isolated as well when it was in an intact F_1F_O with ADP bound. However, if the ATP synthase complexes are incubated with the nonhydrolyzable substrate 5′-adenylyl-β-γ-imidodiphosphate (AMP·PNP) and Mg^{2+}, these same sites cut rapidly. This evidence and other experiments indicate that the ε subunit may be able to adopt more than one conformation in the context of F_1F_O depending on whether the enzyme contains ADP or ATP in the active sites.

The ε subunit has also been crystallized at 2.1 Å in the presence of the γ subunit (Figure 1-12) [182]. The ε subunit took a markedly different conformation in this study, with the two C-terminal helices not forming a hairpin, but rather an extended conformation wrapped around the γ subunit. This structure was not in the context of the whole enzyme and the N- and C- terminal regions of γ were truncated, so it is questionable if this conformation actually exists *in vivo*. However, this alternate conformation is consistent with some of the existing crosslinking data as discussed below, and may represent the trypsin-sensitive conformation mentioned above. After the appearance of this new structure, a previous F_1 electron density map at 4.4 Å was re-evaluated and the existence of such an ε conformation in the intact complex was concluded to be a possibility [196, 197].

Investigators have attempted to determine which of these conformations the ε subunit actually takes in the intact enzyme. Two different approaches have demonstrated a nucleotide-dependent shift in the position of the ε subunit similar to what was observed in the trypsin digestion experiment described above. The first study used cryoelectron microscopy to examine F_1 labeled with a gold particle at ε_{H38C} [198]. The gold particle was shown to move from below an α subunit in the presence of ADP to below a β subunit in the presence of an ATP analog, indicating a change in the position of the ε subunit. The second study used disulfide bond formation to demonstrate that the ε subunit was in proximity to the β subunit when the enzyme was incubated with ADP and the α subunit when incubated with an ATP analog [199]. These two studies showed a change in the position of the ε subunit, but not necessarily a change in conformation. A study by Tsunoda *et al.* used crosslink formation to demonstrate that both of the crystallized conformations described above can be observed in the whole enzyme [200]. A recent study probed the conformation of the ε subunit by introducing cysteines and determining

their reactivity to MPB under resting conditions, during ATP hydrolysis and after inhibition with ADP-AlF_3 [201]. Some residues near the ε-γ interface showed significant changes in the extent of MPB labeling depending on the nucleotide present, but the residues in the C-terminal α-helices showed a labeling pattern consistent with a partially open helical hairpin. It is possible that there is inherent flexibility and movement in the hairpin domain during the normal functioning of the enzyme.

Crosslinking the two α-helices of the hairpin together or the second α-helix to the β-sandwich had little effect on enzyme function [202], indicating that flexibility of subunit ε is not essential for enzyme activity. However, a very interesting result was obtained by locking the C-terminal domain in the extended conformation–ATP synthesis was unaffected, but ATP hydrolysis was inhibited, allowing the enzyme to run in one direction only [200]. It was proposed that this function of the ε subunit allows it to act as a ratchet and prevent the unnecessary hydrolysis of ATP. A similar result was observed when studying the ATP synthase of the thermophilic organism *Bacillus PS3* [203]. Locking the C-terminus out in this experiment inhibited ATP hydrolysis by about 80% without having a significant effect on ATP synthesis. The same study found subunit ε to be in the extended state when no nucleotide was present while the addition of ATP induced a transition to the hairpin conformation. This result was further confirmed by the solution of an NMR structure of the *Bacillus PS3* ε subunit that found a previously unrecognized ATP binding motif, I(L)DXXRA, which recognizes ATP together with three R and one E residues [204]. The two C-terminal α-helices were found to fold into a hairpin in the presence of ATP but extend in the absence of ATP, suggesting that the C-terminal domain of ε can undergo an arm-like motion in response to an ATP concentration change and thereby

contribute to regulation of F_1F_O activity. The authors also found that the *E. coli* ε subunit binds ATP in a similar manner as judged by NMR.

Inhibitory effects: One of the functions of the ε subunit is the inhibition of ATPase activity in F_1. This phenomenon has been known in *E. coli* since the 1970s [205-207]. The inhibitory effect is most noticeable when studying the isolated F_1 portion of the enzyme, where the ε subunit causes a five- to seven-fold decrease in the rate of ATP hydrolysis [45, 208]. This inhibition by the ε subunit can be relieved in three different ways. First, the ε subunit can be dissociated from F_1 by either heat treatment [206, 209, 210] or the addition of alcohols [211, 212]. Second, certain detergents can be added that will disturb the inhibitory protein-protein interactions without actually dissociating ε from F_1 [178, 213-216]. Third, the treatment of F_1 with trypsin will cleave the C-terminal domain from ε and relieve the inhibition [195, 217, 218]. The ε subunit also plays an inhibitory role in the context of the entire F_1F_O enzyme. Experimental evidence supporting this conclusion include the enhanced rates of ATP hydrolysis observed in the presence of mutations affecting ε-γ subunit interactions [219], protease removal of part of the C-terminal end of the ε subunit [218], and crosslink formation between the N- and C-terminal domains [194].

This inhibitory effect of the ε subunit is a function of the C-terminal domain. It was initially discovered that up to 60 C-terminal amino acids could be deleted without any other significant effect on enzyme function besides the loss of ATPase inhibition [177]. The deletion of the second α-helix alone does not have a detectable effect on inhibition, rather both α-helices must be deleted [177, 188, 190]. It is also possible to abolish the inhibitory effects of subunit ε by genetically fusing 12-28 kDa proteins to the C-terminus [191]. These large fusion proteins are probably sterically hindered from performing the normal inhibitory role of the ε subunit. The

area of F_1F_O with which the C-terminal domain of the ε subunit is most likely to interact is the $\beta_{381D\text{-}387D}$ region, termed the DELSEED sequence. When the $\beta_{381D\text{-}387D}$ residues were replaced by A, a loss of the inhibitory effects of the ε subunit was observed [220]. Even the replacement of only the first D residue in this region led to a similar increase in ATPase activity [221].

Crosslinking analysis. Crosslink formation has been used extensively to investigate the structure and function of the ε subunit. As mentioned above, crosslinking results have been employed to determine what conformations the ε subunit takes within the intact complex. The first investigators to tackle this question using crosslinking created four cysteine mutants based on the NMR structure [202]. Two of the mutants would lock the β-sandwich domain to the α-helical domain, $\varepsilon_{M49C/A126C}$ and $\varepsilon_{F61C/V130C}$. The other two mutants would lock the two α-helices to one another, $\varepsilon_{A94C/L128C}$ and $\varepsilon_{A101C/L121C}$. The investigators found that all four crosslinks formed efficiently upon treatment with $CuCl_2$ in both the isolated subunit and the intact enzyme, providing evidence that the NMR structure accurately reflected the conformation of ε in the holoenzyme. They also found that ATP hydrolysis activity increased after crosslinking the two domains to one another but not after crosslinking the two α-helices to each other. None of the crosslinks had any negative effect on enzyme function. A contemporary study was published in which the authors also crosslinked the two domains using $CuCl_2$ treatment of the $\varepsilon_{M49C, A126C}$ double mutant [194]. These sites were chosen because they existed very close to one another in the solved structures, within 5 Å. Finally, an experiment was conducted that demonstrated that ε adopted both of the solved structures in the intact complex [200]. The authors were able to efficiently form both the up conformation by crosslinking the $\varepsilon_{S118C}/\gamma_{L99C}$ double mutant as well as the down conformation by crosslinking the $\varepsilon_{A117C}/cc'_{Q42C}$ double mutant using $CuCl_2$. These results demonstrate that the ε subunit must be able to assume two or more conformations.

Crosslink formation between the ε subunit and the other subunits in the complex was first discovered in the 1980s by treating the enzyme with the water-soluble carbodiimide EDC [178]. Among the products formed was an ε-β dimer. A more specific interaction was obtained with the observation that a cysteine engineered at residue ε_{S108C} could be crosslinked with TFPAM-3 to the α subunit [219]. About the same time, a paper was published that investigated the ε-β crosslink formed by treatment with EDC and determined the residues involved to be β_{D381} and ε_{S108} [179]. The β_{D381} residue is the first residue in the conserved DELSEED sequence, mentioned above with regards to the inhibitory function of the ε subunit. The formation of specific disulfide crosslinks involving the residues of the DELSEED sequence was published several years later, along with more evidence of a nucleotide-dependent change in the position of the ε subunit [180].

Crosslink formation was observed in the $\beta_{E381C}/\varepsilon_{S108C}$ and $\beta_{S383C}/\varepsilon_{S108C}$ double mutants upon treatment with $CuCl_2$. It was shown that the yield of the β-ε dimer was nucleotide dependent–highest in the presence of ADP + Mg^{2+} and much lower in the presence of the ATP analog AMP·PNP + Mg^{2+} or when ATP was combined with the inhibitor azide. It was also observed that formation of the β-ε dimer inhibited the ATPase activity of the enzyme in proportion to the yield of the cross-linked product. The same authors published a study the next year investigating this nucleotide-depended change in the position of ε in more detail [199]. The authors engineered the cysteines mutants ε_{S108C}, β_{E381C}, and α_{S411C}. A clear nucleotide-dependence effect on crosslink formation with the ε subunit was observed. For the $\beta_{E381C}/\varepsilon_{S108C}$ double mutant, the β-ε dimer was obtained preferentially in the presence of ADP + Mg^{2+} while for the $\alpha_{S411C}/\varepsilon_{S108C}$ double mutant, the α-ε dimer was strongly favored in the in the presence of

AMP·PNP + Mg^{2+}. In the triple mutant $\alpha_{S411C}/\beta_{E381C}/\varepsilon_{S108C}$, the ε-β dimer formed in the presence of ADP + Mg_{2+} and to the ε-α dimer formed presence of AMP·PNP + Mg^{2+}, indicating a significant movement of the ε subunit. All of these crosslinks led to inhibition of ATP hydrolysis activity. Crosslink formation between the ε and β subunits was used to obtain evidence of ε subunit rotation relative to the $\alpha_3\beta_3$ hexamer during ATP hydrolysis [222]. The authors formed $\beta_{D380C}/\varepsilon_{S108C}$ crosslinks in the context of the intact F_1F_O, separated the subunits, mixed with epitope tagged $\beta_{FLAG,\ D380C}$ subunits and reconstituted the enzyme. They reduced the existing ε-β dimers, powered the enzymes with ATP for a brief period of time and then recrosslinked. They were able to show randomized distribution of the ε_{S108C} subunits with the original β_{D380C} subunits and the epitope tagged $\beta_{FLAG,\ D380C}$ subunits, providing evidence of rotor stalk movement. Finally, crosslink formation has been used to demonstrated that the ADP inhibited state of F_1 exists in such a conformation that the ε subunit is interacting with two different β subunits [192]. This was done by forming a crosslink between ε_{M138C} and one of the β subunits with TFPAM-3 and then crosslinking a different β_{D381} to ε_{S108} using EDC.

A spatial relationship exists between the ε subunit and the ring of *c* subunits as described above. Briefly, disulfide crosslink formation was shown to occur between cysteines engineered at ε_{E31C} and individually at c_{A40C}, c_{Q42C}, and c_{P43C} when treated with CuP. Crosslinking formation led to an inhibition of enzyme function, but this was due to formation of *c*-*c* dimers, not the ε-*c* dimer. This was demonstrated clearly by Schulenberg *et al.* by crosslinking the ε_{E31C} subunit to the genetically duplicated and fused *c* subunit cc'_{Q42C} [169]. These results demonstrated that the *c* subunit ring rotates with the central stalk. It has also since been shown

that cysteines substituted individually in the $\varepsilon_{V26\text{-}L33}$ region could all be crosslinked to c_{A40C}, c_{Q42C} and c_{D44C}, describing the potential binding surface of ε to the *c* subunit ring [170].

Several experiments demonstrated that crosslink products were formed between the ε and γ subunits. Cysteines engineered into the ε_{S10C} mutant could be crosslinked to the γ subunit using TFPAM-3 [219]. Likewise, the mutant ε_{S10C} was able to crosslink to the $\gamma_{R222\text{-}A242}$ region while the ε_{H38C} and ε_{T43C} mutants crosslinked to the $\gamma_{K202\text{-}V286}$ region, both with TFPAM-3 [185].

Subunit γ

Overview: The γ subunit composes part of the rotor stalk (Figure 1-13). This subunit is 286 residues long with a molecular mass of 31.4 kDa [39]. This subunit is essential for enzyme assembly and is required for proper ATPase activity in F_1 [223, 224]. Experimental evidence indicates that the γ subunit makes contacts with the ring of *c* subunits [171, 172], the ε subunit [185, 200, 219] and the β subunits [180, 199, 219]. A structure was obtained in 1994 for most of F_1, which included about half of the γ subunit [225]. This structure greatly increased the understanding in the field of the structure and function of the γ subunit. The rotation of the γ subunit inside the $\alpha_3\beta_3$ hexamer of F_1 has been demonstrated by several methods [54, 226-230], most convincingly by direct observation using video microscopy [30].

Structure: The structure of the γ subunit was originally obtained at 2.8 Å along with the $\alpha_3\beta_3$ hexamer isolated from bovine mitochondria (Figure 1-14) [225]. Less than half of the γ subunit was resolved in the electron density map, consisting of only three α-helical sections. These helices were the N-terminal 45 residues, $\gamma_{M1\text{-}T45}$, a short segment from the middle of the subunit, $\gamma_{S73\text{-}K90}$, and the C-terminal 64 residues, $\gamma_{I209\text{-}L272}$ (mitochondria residue numbering). The N- and C-terminal α-helices of the γ subunit formed an antiparallel coiled coil structure 90 Å

in length which filled the central cavity of the $\alpha_3\beta_3$ hexamer and extended below to form part of the central stalk. There are minimal interactions between the γ subunit and the $\alpha_3\beta_3$ hexamer as revealed by the crystal structure. The C-terminus region $\gamma_{S265\text{-}L272}$ passes through a hydrophobic sleeve near the top of F_1 formed by six proline-ring loops, three from the $\alpha_{Y287\text{-}C294}$ region and three from the $\beta_{E274\text{-}R281}$ region. Abrahams *et al.* described this region as a "molecular bearing, lubricated by a hydrophobic interface." The γ subunit interacts with F_1 in two other regions, described as "catches" by Abrahams *et al*. The first catch is a salt bridge formed between residue γ_{R252} and α_{D233} of an "empty" site, a designation used to describe the α/β pair which did not contain nucleotide. The second catch was formed between γ_{K87}, γ_{K90} and γ_{A80}, all located in close proximity in a short helical region, and β_{D394} and β_{E398}, both in the DELSEED region of a "tight" site, described in more detail below.

A partial structure of the γ subunit from *E. coli* was solved at 2.1 Å in the presence of the ε subunit as described above, consisting of the region $\gamma_{I11\text{-}I258}$ [182]. The central portion of the γ subunit formed a helix-sheet-helix domain, featuring a five-stranded β-sheet wedged between the two α-helices $\gamma_{L91–D108}$ and $\gamma_{I150–D161}$. The first four strands, $\gamma_{K74–V80}$, $\gamma_{V111–M117}$, $\gamma_{A135–T138}$ and $\gamma_{D166–K174}$ are in a parallel conformation, while the fifth strand, residues $\gamma_{M179–P183}$ runs antiparallel to the fourth. A short α-helix, $\gamma_{S120–V124}$, connects the second and third β-strands. There are 53 Cα atoms shared between the *E. coli* and mitochondrial structures, all of which align relatively well with an RMS deviation of 1.4 Å (Figure 1-14). This close alignment implies that the structure of γ in the ε-γ dimer may be similar to the structure found in the intact complex.

Subunit movement: Two types of movement of the γ subunit relative to the rest of F_1 have been demonstrated: movement associated with nucleotide binding, and full rotation during

catalysis. The movement in γ observed upon ligand binding is similar to that described for the ε subunit, with the same mechanism potentially responsible for both. It was first noticed in the 1980s that the trypsin digestion of γ is retarded in the presence of $ATP \cdot Mg^{2+}$, an effect potentially attributed to a conformational change as a result of ligand binding [231]. This was further investigated by Turina and Capaldi by covalently binding the fluorescent probe coumarin maleimide (CM) to the individual mutants γ_{R8C} and γ_{W106C} in F_1 [43]. The authors were able to detect changes in the steady-state fluorescence of the probe upon binding of ATP and its noncleavable analog AMP·PNP, but not upon binding of ADP. A cyclical increasing and decreasing of the probe at γ_{W106C} was noticed during unisite ATP hydrolysis. The investigators were able to show that the increase in fluorescence was associated ATP binding and the decrease with ATP hydrolysis, indicating a nucleotide-specific change in the structure of the γ subunit.

The second type of movement is the full rotation of the γ subunit relative to the $\alpha_3\beta_3$ hexamer during catalysis. The crystallographic structure described above strongly implied that the γ subunit could carry out this role [225]. The rotation of γ has been demonstrated by a number of groups using a variety of techniques [30, 54, 226-230], clearly establishing that the rotation of γ occurs during enzyme activity. The first group to provide evidence of rotation used a disulfide crosslink that could be formed between γ_{C87} and a cysteine engineered in the DELSEED region of the β subunit, β_{D380C} [226]. Formation of this crosslink inactivated F_1, while reduction restored full activity. The authors were able to crosslink γ_{C87} to β_{D380C}, separate the subunits of F_1, reassemble with radiolabeled β_{D380C} and reduce the crosslink. If ATP was added to power enzyme activity prior to reforming the crosslink, a mixture of radiolabeled and nonradiolabeled β_{D380C} subunits were crosslinked to γ_{C87}. This experiment demonstrated that catalytic activity was associated with a movement of the γ subunit relative the $\alpha_3\beta_3$ hexamer, the

first real evidence of rotation. The same group soon published another study in which they performed a similar experiment in intact ATP synthase complexes, demonstrating that rotation of γ also occurs when F_1 is properly coupled to F_O [232]. Around the same time, another group published a study in which they were able to immobilize F_1 and observe rotation of eosin-labeled γ subunit by applying polarized absorption relaxation after photobleaching [227]. This rotation was not observed if the non-hydrolysable ATP analogue AMP·PNP was used as a substrate. The most convincing evidence of rotation was obtained by Noji *et al.* by direct observation using videomicroscopy [30]. The authors employed a setup in which F_1 was immobilized on a glass coverslip and a fluorescent actin filament was bound to the γ subunit and observed rotating upon the addition of ATP. Experimental designs similar to this one were later used to demonstrate rotation of the ε subunit [151] and *c* subunit ring [150, 152, 153, 155] as described above. Investigators have since use polarized confocal fluorometry [228] and FRET [54, 229, 230] to further investigate the mechanism of γ subunit rotation.

Mutagenic analysis: Limited analysis of the γ subunit has been done using mutagenesis. One line of investigation that has been revealing involves substitutions of the conserved residue γ_{M23K}. The γ_{M23K} substitution resulted in a temperature sensitive loss of coupling efficiency, observed both in ATP-driven proton pumping as well as during ATP synthesis [233, 234]. Several second site suppressors of this substitution were isolated in which the individual mutants γ_{R242C}, γ_{Q269R}, γ_{A270V}, γ_{I272T}, γ_{T273S}, γ_{E278G}, γ_{I279T}, and γ_{V280A} were able to suppress γ_{M23K}, indicating a potential spatial proximity between the N- and C- terminal regions [234]. Additional second site suppressors for the γ_{M23K} substitution were found in the β subunit: β_{E381A}, β_{E381D}, and β_{E381Q} [235]. The crystal structure described above revealed that the positively charged K replacement of γ_{M23} could form an extra hydrogen bond with the β_{E381} residue of the DELSEED sequence.

Truncation of the last ten residues of the γ subunit resulted in reduced growth characteristics but not a complete loss of activity, indicating that these residues are not essential for function [236]. However, truncation of 18 C-terminal residues abolished all enzyme activity, potentially due to a failure of the γ subunit to be able to reach into the "molecular bearing" formed by the $\alpha_3\beta_3$ hexamer. Another group has more recently investigated the extent of C-terminal truncation that could be tolerated and found that genetic deletions of 3, 6, 9 and 12 residues still allowed the formation of a functional complex, while deletions of 15 or 18 residues were not tolerated [237]. Interestingly, the average torque generated by a single molecule of F_1 when loaded by a fluorescent actin filament was unaffected by deletions of up to 12 residues, as was their rotational behavior, demonstrating that an intact C-terminal region of γ is not required for rotary action under load.

Mutagenesis has been used to demonstrate that the conserved residues in the $\gamma_{Q269\text{-}L276}$ region are important but not essential for activity, as substitutions at γ_{Q269}, γ_{T273} and γ_{E275} resulted in F_1F_O that exhibited a significant decrease in activity but still functioned to some extent [236]. A recent paper confirmed these findings with an investigation into the effects of substitutions in region of γ that interacts with the first "catch" loop in the β subunits, $\beta_{Y297\text{-}D305}$ [238]. Again, residues γ_{Q269} and γ_{R268} were found to be sensitive to substitution, with deleterious effects on both ATP hydrolysis and the ability to grow by oxidative phosphorylation. On the N-terminal end of subunit γ, it was found that most substitutions in the regions $\gamma_{I19\text{-}K33}$ and $\gamma_{D83\text{-}C87}$ had little effect on enzyme function, and neither did substitutions at residue γ_{D165} [233]. Another study demonstrated a functional interaction between the N- and C-terminal end of the γ subunit [239]. These authors engineered individually the above-mentioned γ_{Q269E} and γ_{T273V} mutations and looked for second site suppressors. Suppressors were found at residues γ_{Q18}, γ_{K34}, γ_{S35}, γ_{L236},

γ_{S238}, γ_{A242}, and γ_{A246}, leading the authors to hypothesize that the three γ subunit segments $\gamma_{Q18\text{-}S35}$, $\gamma_{L236\text{-}A246}$ and $\gamma_{R269\text{-}I280}$ constitute a domain that is critical for both catalytic function and energy coupling.

Crosslinking analysis: Multiple experiments have investigated crosslink formation between the γ and β subunits. It was first shown in the early 1990s that a crosslink could be formed between the substitution γ_{S8C} and one of the β subunit upon treatment with TFPAMs [219]. The formation of this crosslink was found to be dependent on nucleotide concentrations, with different product obtained when the enzyme was incubated with ATP + EDTA compared with ATP + Mg^{2+} or ATP + Mg^{2+} + P_i. The formation of this γ-β crosslinking inhibited ATPase activity in proportion to the yield of crosslinked product. The same authors found that γ_{V286C} crosslinked to the α subunit in a nucleotide-independent manner upon treatment with TFPAMs, and the formation of this crosslink also resulted in inhibition of ATPase activity. More specific disulfide crosslinks were formed by engineering cysteines into the γ and β subunits after the publication of the high-resolution structure of F_1 [225]. It was demonstrated that disulfide crosslinks could be formed between the $\gamma_{C87}/\beta_{E381C}$ subunits and the $\gamma_{C87}/\beta_{S383C}$ subunits by incubating with $CuCl_2$ [180]. Again, the yield of γ-β dimer was shown to be nucleotide dependent and highest in the presence of ATP and much lower in the presence of ADP. Cross and coworkers formed a similar disulfide crosslink between $\gamma_{C87}/\beta_{D380C}$ using $CuCl_2$. They showed that this crosslink formation inhibited ATPase activity and were able to demonstrate rotation of the γ subunit relative to the β_{D380C} subunits by mixing with radiolabeled β_{D380C} as described above [226]. They repeated this experiment in intact F_1F_O with both radiolabeled β_{D380C} subunit [232] and FLAG tagged β_{D380C} subunit [240]. A nucleotide-dependent effect was shown once more by crosslinking γ_{S8C} to the β subunit using TFPAM-6, forming a crosslink

product in the presence of ATP + Mg^{2+} which was different from that obtained when ATP hydrolysis was inhibited [241]. All of the above crosslinking experiments resulted in an inhibition of enzyme activity as would be expected if the γ subunit must rotate relative to the $\alpha_3\beta_3$ hexamer.

An interesting result has been obtain by Gumbiowski *et al.* [242]. These investigators engineered cysteine residues into positions located roughly at the "top," "center," and "bottom" portions of the γ coiled-coil along with suitable residues on α or β and demonstrated disulfide bridge formation by SDS-PAGE and immunoblotting. The ATPase activities were fully inhibited upon formation of the $\gamma_{L262C}/\alpha_{A334C}$ crosslink at the center and the $\gamma_{C87}/\beta_{D380C}$ crosslink at the bottom, as expected. Surprisingly, formation of a disulfide crosslink between $\gamma_{A285C}/\alpha_{P280C}$ at the top impaired neither ATP hydrolysis nor full rotation of the γ subunit. The authors concluded that the amino acids at the C-terminal portion of γ were rotating around their dihedral angles, much like a cardan shaft or universal joint. These results were confirmed by the same group later in a further investigation of the phenomenon [243].

Crosslinking experiments have demonstrated a spatial proximity between the γ subunit and both the *c* and ε subunit as discussed above. Briefly, a crosslink can be formed between γ_{Y205C} and the polar loop region of the *c* subunit ring [171, 172]. The substitution ε_{S10C} was able to crosslink to the $\gamma_{R222\text{-}A242}$ region while ε_{H38C} and ε_{T43C} crosslinked to the $\gamma_{K202\text{-}V286}$ region, both using TFPAM-3 [185, 219]. A disulfide crosslink in the double substitution $\varepsilon_{S118C}/\gamma_{L99C}$ was formed using $CuCl_2$ to probe the conformation of the ε subunit [200]. Crosslinking of the γ subunit to either the ε subunit or the *c* subunit ring did not disrupt enzyme function, indicating that these subunit move together as a unit.

Catalytic Subunits of F_1

Overview: Three copies of each α and β subunit compose most of the mass of F_1 (Figure 1-15). The α and β subunits are 513 and 460 amino acids long, respectively. Both subunits are strongly conserved among various species and share a high degree of homology to one another with 24% identity and 51% similarity and nearly identical folds [32, 244]. These two subunits make up most of the mass of F_1 and are arranged as a hexamer of alternating α and β subunits [225]. Each α and β subunit contains a nucleotide binding domain, but neither subunit alone has detectable ATPase activity, while the $\alpha_3\beta_3$ hexamer in the absence of γ exhibits only a small amount [245]. The γ subunit must be included in order to hydrolyze ATP at a physiological rate, making the $\alpha_3\beta_3\gamma$ complex the minimum required for full catalytic ATPase activity [223, 224].

Structure: The first high-resolution crystal structure of F_1 was obtained by the Walker lab in 1994 (Figure 1-16) [225]. This structure showed that F_1 was arranged as a hexamer of alternating α and β subunits surrounding a central cavity which contained the N- and C-terminal helices of the γ subunit. The α and β subunits were arranged like slices of an orange taking the shape of a flattened sphere 80 Å high and 100 Å across. Both subunits folded in an almost identical manner with each consisting of three domains as shown in Figure 1-16C: an N-terminal six stranded β-barrel ($\alpha_{19\text{-}95}$, $\beta_{9\text{-}82}$), a central domain with alternating α-helices and β-strands typical of a nucleotide binding site ($\alpha_{96\text{-}379}$, $\beta_{83\text{-}363}$) and a C-terminal bundle of seven or six α-helices ($\alpha_{380\text{-}510}$ and $\beta_{364\text{-}474}$, respectively). The six N-terminal β-barrels of α and β are linked to form a crown at the top of F_1. This crown and the nucleotide binding domains of each subunit are separated, whereas the helical domains interdigitate with the crown to some extent. The crystal structure showed all six nucleotide binding sites in detail, three on the α subunits and three on the β, described below. All three α subunits contained the non-hydrolysable ATP

analog, AMP·PNP, and took similar conformations. The β subunits were in three distinct states with different ligands bound to each–a tight (β_T) conformation, containing AMP·PNP; a loose (β_L) conformation, containing ADP; and an empty and open (β_E) conformation, with no substrate bound. The β_T and β_L subunit conformations were quite similar with less than 1 Å root-mean-square separation between Cα atoms. They were only distinguished by the presence of different nucleotides in the catalytic sites. The β_E subunit, however, was clearly in a different conformation–the lower segment, the region closest to the membrane, was rotated about 30° with the residues displaced up to 20 Å. This hinge motion around residue β_{208} of its C-terminal domain separated the two halves of the nucleotide binding domain such that the residues necessary for binding nucleotide were no longer in the appropriate arrangement.

A total of 18 additional structures of F_1 have been published since the 1994 structure. These structures show F_1 complexes from various organisms and in the presence of different substrates and inhibitors. Most of the structures thus far are of bovine F_1, which has been crystallized in the presence of the inhibitors efrapeptin [246], aurovertin B [247], 4-chloro-7-nitrobenzofurazan (NBD-Cl) [248], DCCD [249], the regulatory protein IF1 [250, 251], and phytopolyphenol, resveratrol, and the related polyphenols quercetin and piceatannol [252]. Crystals have also been obtained for bovine F_1 grown in high concentrations of nucleotides. These also showed two sites occupied and one empty, with F_1 in the ground state [253, 254]. Several structures have also been solved containing the transition state mimics ADP·Mg^{2+} and aluminum fluoride [255, 256], as well as ADP and beryllium fluoride [257]. F_1 from three other sources has also been obtained–*Bacillus PS3* [258, 259], spinach chloroplast [260, 261] and rat liver [262, 263]. All these crystals show similar structures for the F_1. The only significant

difference between these structures is the conformation of the β subunits which correlates with the ligand bound in the nucleotide binding site.

Nucleotide binding sites: The six nucleotide binding sites are found at the α/β interfaces of F_1 and all share a similar structure as a result of the high degree of homology between the α and β subunits. There are three catalytic sites predominantly in the β subunits with a few residues contributed by the α subunits. Conversely, there are three noncatalytic sites predominantly in the α subunits with a few residues contributed by the β subunits. The determination of which sites were catalytic and which were noncatalytic was based on chemical inactivation experiments with DCCD and NBD-Cl, labeling experiments using nucleotide analogs, and mutagenesis [39, 41]. For example, the mutagenesis of the β_{K155} and β_{D242} residues drastically decreased activity, while modification of the corresponding residues in the α subunits did not [64, 264-266]. Although the noncatalytic sites bind both ADP and ATP with high affinity, they have no known functional or regulatory role [265, 267-269]. Bound [γ-^{32}P]ATP remains unhydrolyzed for long periods of time in the noncatalytic sites [270].

The nucleotide binding domains consist of a nine-stranded β-sheet with nine associated α-helices [225]. The major residues of β involved in nucleotide binding are shown in Figure 1-17 and discussed below. The adenine binding domain of the catalytic site consists of residues around helix three of the C-terminal domain, residues β_{F404}, β_{A407}, β_{F410}, β_{T411}, as well as the aromatic ring of β_{Y331}. Early mutational analysis and use of the fluorescent nucleotide analog *lin*-benzo-ADP identified residue β_{Y331} as adjacent to the bound nucleotide [271]. The crystal structure confirmed these mutational studies by showing that the aromatic ring of β_{Y331} is stacked with the adenine ring of the nucleotide. This residue is important but not required for enzyme

function [271-273]. The phosphates in the catalytic site are bound by the residues of the P-loop, $\beta_{G149\text{-}T156}$ [225]. This region has been the subject of extensive mutagenesis as described below. In addition to this region, the nucleotide phosphates are surrounded by six charged residues, three acidic and three arginines–β_{E181}, β_{E185}, β_{D242} and β_{R182}, β_{R246}, α_{R376}, respectively. It is thought that residues β_{E185} and β_{D242} are involved in binding Mg^{2+} indirectly through water molecules, a view supported by evidence obtained from mutagenesis studies [64, 274]. Residue β_{E181} appears to be aligned such that it could activate a water molecule for an attack on the terminal phosphate of the bound nucleotide [225]. In the mutants β_{E181Q} and β_{E181A} the rate of the hydrolysis step was reduced by two orders of magnitude, highlighting the importance of this residue [46, 64, 275].

Mutagenic analysis: Mutagenesis has been used extensively to investigate the structure and functional characteristics of the α and β subunits. One region of the α and β subunits that has been investigated extensively using mutagenesis is the sequence known as a P-loop or Walker A sequence [264]. This sequence, GXXXXGK(T/S), is conserved in a large and diverse group of nucleotide-binding proteins and interacts with phosphate groups of the bound nucleotide. The actual sequence for $\beta_{G149\text{-}T156}$ is GGAGVGKT. The substitution β_{A151P} was shown to exhibit higher ATP hydrolysis than wild-type, while β_{A151V} retained significant activity, indicating this residue is tolerant of substitutions [276]. The residue β_{K155} was shown to be important for proper enzyme function by affinity labeling with adenosine triphosphopyridoxal [277, 278]. To investigate the sensitivity of this residue, a large number of substitutions covering the β_{K155} and β_{T156} residues were created–β_{K155A}, β_{K155S}, β_{K155T}, β_{T156A}, β_{T156C}, β_{T156D} and β_{T156S} [279]. Only β_{T156S} showed any ATP synthesis activity, while the others were defective, suggesting that the β_{K155} and β_{T156} residues are essential for catalysis. The same group also

attempted to move the side chains around in the $\beta_{K155T, T156K}$ and $\beta_{T156A, V157T}$ double substitutions, but neither supported enzyme function. Another group found that insertion of a G residue between β_{K155} and β_{T156} also resulted in an inactive enzyme [276]. These same investigators replaced the entire Walker A motif with the corresponding region of adenylate kinase (GGPGSGKGT) and p21 ras protein (GAGGVGKS), resulting in a loss of enzyme activity for the former and a retention of significant activity for the latter. The mitochondrial β subunit has a Walker A motif identical to that of the *E. coli* subunit at the corresponding location $\beta_{G190-T197}$. Each residue in the mitochondrial Walker A motif was tested individually for functional replacements [280]. It was found that the residues β_{G149}, β_{G154}, and β_{K155} (*E. coli* numbering) were not tolerant of any substitutions while β_{T156} could only be replaced with S, results that correlate well with the work done in *E. coli*. The most pliable residue was β_{G150}, where ten different substitutions resulted in a functional enzyme.

The α subunit also contains a Walker A motif of GDRQTGKT at residues $\alpha_{G169-T176}$. It was initially discovered that the mutations α_{K175I} and α_{K175E} resulted in a decrease in ATP hydrolysis activity of 2.5 and 3 fold, respectively [265]. This result is surprising, since the noncatalytic sites in the α subunit have no known function. These results were expanded later to demonstrate that single amino acid substitutions at residues α_{K175} and α_{T176} drastically altered enzyme assembly [281]. The substitutions α_{K175F}, α_{K17W}, α_{T176F} and α_{T176Y} completely disrupted enzyme assembly, while α_{K175H}, α_{K175S}, α_{K175G}, α_{Y176S}, α_{T176H}, α_{T176A}, α_{T176C}, α_{T176L}, and α_{Y176V} had effects on enzyme assembly that were less severe. This region is not involved in catalysis, but it appears to be important for proper enzyme assembly.

Mutagenesis has been used to identify other residues in the β subunit that are important for function. For example, the substitution β_{S174F} was discovered in 1980 and found to significantly

affect enzyme function [282]. Four second site suppressors were later found, β_{G149S}, β_{A295T}, β_{A295P} and β_{L400Q} [283]. Since the β_{G149S} substitution was determined to be a second site suppressor, the substitution β_{G150S} was tried and found not to suppress β_{S174F} [284]. A number of different residues were substituted for β_{S174} and a relationship between the size of the side chain and enzyme activity was observed [285]. Whereas β_{S174F} was defective in ATP driven proton pumping, β_{S174L} could pump proton efficiently. Both of these substitutions resulted in essentially the same levels of ATP hydrolysis, indicating that this residue had an effect on F_1 to F_O coupling. A recent publication revisited the individual β_{S174F} and β_{S174L} substitutions and found a slower single revolution time and a 10 fold increase in pause time at each 120° step [286]. As expected, the $\beta_{G149A, S174F}$ and $\beta_{G149A, S174L}$ retained function. Further *in silico* analysis of these substitutions suggested that the β_{S174F} residue is involved with β_{I163} and β_{I166} through hydrophobic interactions [287]. The addition of the β_{I163A} substitutions partially suppressed β_{S174F}, supporting this hypothesis. Finally, the β_{E181} and β_{R182} residues were also found to be sensitive to substitutions, with defects in enzyme function found in β_{E181Q}, β_{E181D}, β_{E181N}, β_{E181T}, β_{E181S}, β_{E181A}, β_{E181K}, β_{R182K}, β_{R182A}, β_{R182E} and β_{R182Q} [46].

A subset of mutations that affect F_1 function appear to inhibit catalytic cooperativity without exhibiting a significant effect on unisite catalysis. Substitutions known to cause such effects in the α subunit are α_{S347F}, α_{G351D}, α_{S373F}, α_{S375F} and α_{R376C} [288-291]. These amino acids are in the α-β interface close to the catalytic site, termed the "α/β signal transmission region" [292]. A similar effect was observed after reaction of the α_{S373C} mutant with NEM, with only a single residue per F_1 required for the deleterious effect [293]. The substitution β_{A151V} exhibited a similar effect on catalytic cooperativity [294], while multiple substitutions at β_{E185}

also had such an effect [274]. Positive catalytic cooperativity was blocked in these mutant enzymes, not nucleotide binding [295]. The modification of the β_{E192} residue with DCCD also inhibited multisite catalysis but not unisite catalysis despite being 16–17 Å away from the γ-phosphate [296, 297].

Several mutagenesis studies have identified residues important in interactions between the α and β subunits and other subunits of F_1. The α_{G29D} substitution was identified by random mutagenesis and found to cause functional defects due to a disruption of the α-δ binding interactions [292]. Likewise, β_{D305V}, β_{D305S} and β_{D305E} exhibited low levels of ATP hydrolysis activity due to a disruption of the β-γ interactions [238]. The individual substitutions β_{D301E}, β_{R323K}, and α_{R282Q} were also found to affect the kinetics of ATP hydrolysis by disrupting hydrogen bonding interactions between the α and β subunits [298].

Crosslinking analysis: Crosslinking has not been used as extensively in the α and β subunits as mutagenesis. The photoactivatable, bifunctional crosslinking reagent 2,8-diazidoadenosine 5'-triphosphate (2,8-DiN3ATP) was used to demonstrate that both the α and β subunit contribute to the catalytic nucleotide binding sites [299]. UV irradiation of F_1 in the presence of 2,8-DiN3ATP caused an inactivation of F_1 and the formation of α-β dimers. Crosslink formation was also used to abolish catalytic cooperativity by crosslinking two β_{I376C} subunits [300]. Two of the β subunits in the $\alpha_3\beta_3\gamma$ complex contact each other with a segment that includes β_{I376} despite the intervening α subunit. The formation of this disulfide crosslink blocks a conformational change involved in the enzyme mechanism and disrupts multisite ATP hydrolysis while still allowing unisite activity.

Peripheral Stalk Subunits

Subunit δ

Overview: The δ subunit is the member of F_1 which composes part of the peripheral stalk (Figure 1-18). This subunit is 177 amino acids long. Evidence indicates it is located at the upper periphery of the $\alpha_3\beta_3$ hexamer [301-303]. There are currently no high-resolution structures of the entire δ subunit, but portions of this subunit have been solved by NMR spectroscopy [304, 305]. The experimental evidence indicates that δ exists as two domains, an N-terminal domain involved in binding to the α subunit of F_1 and a less well-defined C-terminal domain involved in binding to the *b* subunits of F_O.

Structure: The first detailed structure of the δ subunit was obtained using NMR spectroscopy in 1997 [304]. The researchers set out to obtain structural information for full length δ, but the full length protein exhibited a tendency to aggregate during data collection and did not produce sufficient quality data for structural analysis. However, enough data was obtained from the full length protein to demonstrate that the N-terminal region was similar to the protease degradation product $\delta_{M1\text{-}S134}$ which did not aggregate. This $\delta_{M1\text{-}S134}$ protein was determined to be globular and consisted of two domains: an N-terminal domain of residues $\delta_{M1\text{-}A105}$ which was arranged in a compact, globular structure, and a C-terminal domain of residues $\delta_{T106\text{-}S134}$ which was disordered except for a short α-helix. The N-terminal domain folded as a six α-helix bundle with dimensions of approximately 45 x 20 x 30 Å. Helices one ($\delta_{F4\text{-}V20}$), two ($\delta_{S24\text{-}V38}$), five ($\delta_{D70\text{-}A81}$) and six ($\delta_{A88\text{-}E104}$) were arranged as two intercalating V-shaped pairs that formed the core of the structure, while helices three ($\delta_{N41\text{-}L47}$) and four ($\delta_{A53\text{-}V64}$) were packed tightly against the four-helix core. The C-terminal domain was disordered

except for a loop ($\delta_{T106-L117}$) and α-helix seven ($\delta_{S118-M129}$). Helix seven was found to be relatively unstable and solvent exposed, interacting only weakly with the six-helix bundle.

Another NMR structure of the δ subunit was published recently (Figure 1-19) [305]. This structure is a 1:1 complex of the N-terminal domain of the δ subunit and the N-terminal 22 residues of the α subunit. This new structure shows a nearly identical fold for the N-terminal domain of the δ subunit, with α-helices one and five forming the binding surface for the α subunit fragment. Residues α_{I8-Q18} fold as an α-helix when bound to the δ subunit. The authors were able to describe the structural details of the α-δ interaction based on their NMR results.

Subunit interactions: The N-terminal domain for the δ subunit is involved in binding to F_1, as first indicated by proteolysis experiments [306]. This domain alone binds to F_1 with a similar affinity as the entire δ subunit, but does not support binding of F_1 to F_O [302]. The N-terminal 30 residues of the α subunit were implicated in binding of δ by early experiments using proteolysis and mutational analysis [269, 292, 307]. More recent electron microscopy studies of intact F_1F_O complexes decorated with a monoclonal antibody against the δ subunit localized the δ subunit to the top of F_1 in the dimple formed by the N termini of the α and β subunits [303]. Much of the work done on the δ subunit in the last decade has focused on elucidating the details of this δ-α interaction. The binding affinity of a peptide consisting of α_{M1-V22} to the δ subunit was quantified using the fluorescence signal from the natural occurring δ_{W28} as well as the engineered δ_{Y11W} and δ_{V79W} [308, 309]. This N-terminal region of the α subunit binds to δ with high affinity, K_d = 130 nM, while mutations in helices one and five of the δ subunit impair this protein-protein interaction. The same group also analyzed which residues on the N-terminal region of α were most important for proper δ binding and demonstrated that

the most sensitive were the hydrophobic residues located on the nonpolar surface of the predicted α helix, α_{I8}, α_{L11}, α_{I12}, α_{I16}, and α_{F19} [310]. This work was done initially in the $\alpha_{M1\text{-}V22}$ peptide and significant results were confirmed in intact F_1F_O. The NMR structure of the $\alpha_{M1\text{-}V22}$ peptide bound to the N-terminal domain of δ provided a detailed picture of how these two proteins interacted. It was found that residues δ_{Y11}, δ_{A14}, δ_{F18}, δ_{L76} and δ_{V79} form a hydrophobic pocket that bound to the N-terminal region of the α subunit [305]. An interesting detail of the δ-α interaction was provided recently with the observation that the N-terminal region of the isolated α subunit is not susceptible to trypsin cleavage and is probably sequestered until the isolated α subunit forms a complex with the other F_1 subunits [311]. This observation provides a possible explanation for why δ and α monomers have not been seen to dimerize in solution.

Several studies have attempted to quantify the binding energy between the δ subunit and the rest of F_1. The first study labeled the δ subunit with tetramethylrhodamin-5-maleimide (TMR-5-M) and used fluorescence correlation spectroscopy (FCS) to calculate the K_d between monomeric δ and $\alpha_3\beta_3\gamma$ as 0.8 nM or less [312]. This K_d corresponds to a free energy of binding of at least 52 kJ/mol, sufficient to withstand the estimated 50 kJ/mol of elastically stored energy accumulated during enzyme function [65]. The second study used a fluorometric assay based on the δ_{W28} residue to detect binding of the δ subunit to the $\alpha_3\beta_3\gamma\varepsilon$ complex [313]. The second value obtained for K_d of δ binding was 1.4 nM, energetically equivalent to 50.2 kJ/mol, again sufficient to withstand the strain the δ subunit experiences during catalysis. The investigators demonstrated that the $\delta_{M1\text{-}S134}$ fragment bound with the same K_d as the full length δ subunit, providing further evidence that the C-terminal domain of δ contributes no binding energy, at least in the absence of F_O. This study also characterized the effects of two different mutations on

the binding of the δ subunit to the $\alpha_3\beta_3\gamma\varepsilon$ complex. The first mutation, δ_{W28L}, was discovered during the course of this study and increased the K_d to 4.6 nM, equivalent to a loss of 2.9 kJ/mol of binding energy. While this decrease in binding energy was insufficient to cause detectable functional impairment, it did facilitate the preparation of δ-depleted F_1. The second mutation characterized was previously discovered in the 1980's, α_{G29D} [292]. This mutation caused functional impairment, reducing the K_d to 26 nM, equivalent to a loss of 7.2 kJ/mol binding energy.

The interaction of the δ and *b* subunits is essential for the proper association of F_1 and F_O, details of which will be discussed more in the *b* subunit section. Briefly, a number of early experiments demonstrated an interaction between the δ and *b* subunits [314-318]. In particular, it was shown that the deletions of as few as four residues from the C-terminal end of δ prevented binding of F_1 to F_O [314]. Mutagenesis of the $\delta_{K145\text{-}R167}$ region demonstrated that this C-terminal domain was important for the proper function of δ, with the substitutions δ_{A149T} and δ_{G150D} being especially deleterious [319]. Crosslinking experiments also supported the idea of a close spatial proximity between the two subunits.

Crosslinking analysis: Crosslink formation has provided additional information about the spatial proximity of the δ subunit to the rest of the complex. Two native cysteines exist in the δ subunit, δ_{C64} and δ_{C140}, which can readily form an intramolecular disulfide bridge when treated with $CuCl_2$ [320]. The formation of this crosslink demonstrates that the two domains of δ associate closely with one another in the intact complex. It was noticed in the 1980s that oxidizing conditions caused disulfide bond formation between the δ and α subunits in the absence of genetically introduced cysteines [321, 322]. This dimer was only formed in isolated F_1, not F_1F_O, indicating additional structural effects caused by binding to F_O. Residue α_{C90} was

shown to be involved in the formation of this crosslink [320]. The engineered cysteine in α_{Q2C} was shown to crosslink to both δ_{C64} and δ_{C140} upon treatment with $CuCl_2$, with a preference for δ_{C140} [302]. Significantly, the formation of a δ_{C140}-α_{Q2C} crosslink in excess of 90% had no effect on ATP hydrolysis or ATP-driven proton pumping, demonstrating that δ does not need to move relative to the α subunit for proper enzyme function. Crosslinks could also be formed between the δ subunit and the *b* subunit of the peripheral stalk as described in more detail below [323-326]. The formation of a disulfide crosslink between δ_{M158C} and $b_{+G157, +C158}$ did not impair enzyme function, demonstrating that the *b* subunits do not need to move relative to the δ subunit for enzyme activity [325].

Subunit *b*

Overview: The *b* subunit is a member of F_O which composes part of the peripheral stalk (Figure 1-20). The peripheral stalk of the *E. coli* F_1F_O ATP synthase is the simplest peripheral stalk in the ATP synthase family and one of the most completely studied. It is composed of a dimer of identical *b* subunits which are 156 amino acids in length. The *E. coli b* subunit has a topology similar to all other bacterial and photosynthetic ATP synthase peripheral stalks. *In silico* secondary structure analysis predicts an N-terminal membrane spanning domain followed by a long, mostly α helical hydrophilic domain [327-330]. Each *b* subunit crosses the membrane once and then extends from the membrane surface all the way to the δ subunit perched on top of F_1, a distance of about 110 Å [331].

A number of experiments indicate that the peripheral stalk is highly extended and largely α helical. Circular dichroism analysis of the hydrophilic portion of the *b* subunit, residues $b_{V25\text{-}L156}$, showed mostly α helix [318, 332, 333]. Measurement of the molecular weight of $b_{V25\text{-}L156}$ by sedimentation equilibrium gave a value of approximately 31.2 kDa, indicating a dimer of

15.5 kDa $b_{V25\text{-}L156}$ subunits [333]. When the protein was passed through a size exclusion column it eluted with an apparent molecular weight of 80-85 kDa. These results, along with the measured sedimentation coefficient of 1.8 S, are indicative of a highly extended shape. The values obtained from working with just the hydrophilic portion of the *b* subunit were confirmed by circular dichroism experiments conducted on the full length *b* subunit reconstituted into *E. coli* lipid vesicles [334]. This analysis on the full length protein showed the peripheral stalk to be 80% α helix and 14% β turn. A fully extended, completely α helical *b* subunit would be 190 Å long, reaching far beyond the apex of F_1 [335]. This indicates that there is additional structure in the peripheral stalk besides a linear α helix. Indeed, analytical ultracentrifugation of truncated $b_{V25\text{-}L156}$ suggested that the extreme C-terminus is bent back in a hairpin-like fashion [336].

The *b* subunit exists in the intact ATP synthase complex as a dimer. It has been demonstrated that only the dimeric form of the *b* subunit interacts with F_1 [318, 332] and that the formation of the *b* subunit dimer is likely an early step in the assembly of the entire complex [332]. Likewise, the $b_{V25\text{-}L156}$ polypeptide also dimerizes in solution [333]. This $b_{V25\text{-}L156}$ polypeptide has been shown to exist in solution in an equilibrium between the monomeric and dimeric forms. The dimeric form is prevalent at 5 °C and 20 °C while $b_{V25\text{-}L156}$ exists predominantly in the monomeric form at 40 °C [337]. Analytical ultracentrifugation analysis of the $b_{V25\text{-}L156}$ dimer supported the hypothesis that the two proteins may form a coiled coil arrangement [333, 337]. There is uncertainty in the field as to whether this is a right or left handed coiled coil, discussed in more detail below.

The peripheral stalk was conceptually divided into four functional regions by Revington *et al.* [337]. The N-terminal region is the hydrophobic membrane spanning domain which covers residues $b_{M1\text{-}K23}$. The next section is termed the tether domain and extends from the end of the

membrane spanning domain to the beginning of the dimerization domain, residues $b_{Y24\text{-}A59}$. The third region involves residues $b_{S60\text{-}K122}$ and is required and sufficient for the formation of the *b* subunit dimer in the $b_{V25\text{-}L156}$ polypeptide, appropriately termed the dimerization domain [338]. The C-terminal region is the F_1 binding domain. This domain is required for proper interaction of the peripheral stalk with F_1 in the intact complex [339] and covers residues $b_{Q123\text{-}L156}$. These four regions will be discussed in more detail below.

Membrane spanning domain: The membrane spanning domain is the hydrophobic N-terminus of the *b* subunit which includes residues $b_{M1\text{-}K23}$ [337]. This region of the *b* subunits is required and sufficient to interact with the ac_{10} subunits and form the proton channel of F_O [340]. The structure of the monomeric peptide of residues $b_{M1\text{-}E34}$ was solved by NMR in a membrane mimetic solvent composed of chloroform/methanol/H_2O (4:4:1) (Figure 1-21A) [149]. This structure was composed of an α helix for residues $b_{N4\text{-}M22}$ which likely spans the hydrophobic lipid bilayer and anchors the peripheral stalk. There was a rigid bend around residues $b_{K23\text{-}W36}$ and the α helix resumed for the remaining residues $b_{P27\text{-}E34}$ at an angle offset about 20º from the transmembrane helix. Crosslinking experiments discussed in more detail below suggested a structural model in which the *b* subunits associate closely with one another at their N-terminal ends and flare apart as they traverse the membrane in order to accommodate the bends (Figure 1-21B).

There is ample evidence that the membrane spanning domains of the *b* subunits interact with the single *a* subunit. Probably the strongest argument for a tight interaction between these subunits is the fact that the $a_{his}b_2$ complex can withstand affinity purification in different detergents and detergent mixtures [341]. Crosslinks can be formed between the *a* and *b* subunits (see below). Several second site suppressors for the mutation b_{G9D} were found at residue a_{P240}

[342], located in the C-terminus of the five putative transmembrane helices of the *a* subunit [76, 86]. At the time this was considered evidence that the helices of subunits *a* and *b* interacted directly. However, a more recent model proposes that these second site suppressors are transmitted through helix two of the *a* subunit and are not a result of direct interaction [343].

Some evidence exists for an interaction between the *b* and *c* subunits in ATP synthase based on crosslinking results. However, only *ac* or *ab* subcomplexes have been purified, indicating a weak or transient interaction between the *b* and *c* subunits [344-346].

Tether domain: The tether domain is the region between the membrane spanning domain and the dimerization domain which includes residues $b_{Y24\text{-}A59}$ [337, 338]. Analysis of the protein sequence of the tether domain shows a heptad repeat of small hydrophobic amino acids that starts just outside the membrane spanning domain and continues without interruption until b_{A79}, suggesting a coiled coil arrangement [333, 347]. Little is actually known about the structure of the tether domain and there is no published data showing any interaction between the *b* subunits in this region.

A residue found in the tether domain that is highly conserved across species is b_{R36}, positioned approximately two helical turns above the surface of the membrane [80]. A collection of mutants were constructed by Caviston *et al.* to probe the role played by this residue [348]. Many of the amino acid substitutions resulted in intact and functional ATP synthases that were capable of supporting growth on succinate as the sole carbon source. The b_{R36I} substitution resulted in intact but completely inactive F_1F_O. Substitution of a glutamic acid for b_{R36} resulted in an unusual phenotype where proton conduction through F_O was uncoupled from ATP synthesis in F_1. Results obtained in the Cain lab demonstrated that only a single b_{R36} residue was required, since F_1F_O containing heterodimeric b_{R36}/b_{R36E} or b_{R36}/b_{R36I} were functional [349]. A

recent paper attempted to compensate for the defective b_{R36} mutations by engineering additional mutations in the *b* subunit [350]. No suppressor mutations could be found for the b_{R36I} substitution, but the b_{R36E} substitution could be suppressed in $b_{R36E, E39R}$. These results demonstrated that efficient coupling in the enzyme is dependent upon a basic amino acid located at the base of the peripheral stalk. The exact function of this amino acid remains uncertain, but the experimental evidence indicated it affects the proton conduction mechanism, probably in an indirect manner through the *a* subunit.

Early concepts for the function of the *b* subunit dimer proposed it to be a rigid, rod-like feature that prevented F_1 from rotating along with the central stalk, hence the name "stator". This idea was based on both the apparently conserved secondary structure among bacterial *b* subunits and the conserved distance between the $b_{R36\text{-}A79}$ residues [80]. Although there is low conservation in the amino acid sequences between *b* subunits from different organisms, gaps are seldom found in alignments [351, 352]. Work performed in the Cain lab provided evidence that changed the way in which the field viewed the peripheral stalk. A series of deletions and insertions were constructed in the tether domain between residues $b_{R36\text{-}A79}$ to test the hypothesis that the peripheral stalk was a rigid, rod-like structure. It was found that the deletion of seven residues had virtually no effect on enzyme function. Peripheral stalks with up to 11 residues deleted were capable of supporting growth on succinate but exhibited reduced levels of F_1F_O complex assembly [353]. A second paper published by Sorgen *et al.* found that the insertion of seven amino acids in the tether domain resulted in a normal phenotype while insertions of up to 14 amino acids were capable of supporting growth on succinate [354]. The deletion of 11 residues would shorten an α helix about 16 Å while the insertion of 14 residues would lengthen it by about 20 Å. Taken together, these papers changed the perception of the tether domain of

peripheral stalk to one of a flexible, rope-like structure. It appears that the length of the *b* subunit has been conserved to a size optimal for complex assembly but not essential for function of a fully assembled, intact F_1F_O. In fact, it was recently shown that it is possible to form an asymmetric peripheral stalk composed of a subunit containing an internal deletion, $b_{\Delta(L54\text{-}S60)}$, and a subunit containing an internal duplication, $b_{+(L54\text{-}S60)}$, indicating that the individual *b* subunits do not even have to be the same length to form a functional complex [355].

A recent study attempted to investigate the distance between the *b* subunits in the tether domain region using electron paramagnetic resonance (EPR) [356]. The mutant subunits b_{I40C}, b_{H51C}, b_{D53C}, b_{T62C} and b_{Q64C} were expressed individually along with the rest of the ATP synthase subunits and the cysteines were labeled with a nitroxide spin label. All of the residue pairs were found to be in a hydrophilic environment and separated by a distance of 29 Å. These results suggest that the two *b* subunits are either in register and separated by about 19 Å, in close contact and displaced along the helical axis by up to 27 Å, or some combination of the two. Collectively the results indicate that there is little interaction between the *b* subunits in the tether domain region and they may be located a significant distance apart.

Dimerization domain: The dimerization domain is the smallest region capable of dimerizing in a manner similar to the full $b_{V25\text{-}L156}$ polypeptide. The residues involved in dimerization were originally thought to be $b_{D53\text{-}K122}$ due to the fact that truncating the protein to start at b_{K67} or end at b_{K114} resulted in monomeric protein [337, 357]. More recent experiments moved the N-terminus of this domain to at least b_{S60} [337, 338]. Neither the tether domain or the F_1 binding domain contribute significantly to dimer formation in $b_{V25\text{-}L156}$ [336, 357].

Evidence suggests that the dimerization domain exists as a highly extended, largely α helical structure in a coiled coil arrangement. Data supporting this model include the frictional

coefficient obtained from ultracentrifugation experiments and NMR relaxation parameters [337]. The CD spectra of the dimerization domain alone at 5 °C or 20 °C gave results consistent with almost 100% α helix and a coiled coil arrangement [338]. A crystal structure has been obtained for the $b_{T62\text{-}K122}$ fragment, showing a single, linear α helix [358]. Although this crystal structure supports the hypothesis that the dimerization domain is mostly α helical, it provides no information on exactly how the two proteins come together to form a dimer. There is currently a controversy in the field regarding whether the coiled coil is left or right handed. The crystallization paper mentioned above was the first to propose that the dimerization domain forms a unique right handed coiled coil. Three additional papers have been published by the Dunn lab that support the right handed coiled coil model. The 2006 paper by Del Rizzo *et al.* investigated the crosslinking pattern between soluble *b* subunit fragments, in particular looking for the presence of patterns indicative of a right handed coiled coil and investigating if the soluble *b* subunits were staggered relative to one another [359]. The results presented in this paper support the model of a staggered arrangement which possibly exists as a right handed coiled coil. The authors also presented data from thermal denaturation and gel filtration experiments to demonstrate that the staggered *b* subunits were more stable than the *b* subunits in register. The 2007 paper by Woods and Dunn demonstrated that soluble *b* subunits locked in a staggered orientation bound F_1 more tightly than *b* subunits that were in register [326]. The most recent 2008 paper by Bi *et al.* investigated the effects of substituting regions of *E. coli's b* subunit with other sequences that have the potential to form either right or left handed coiled coil arrangements [360]. It was shown that many of the chimeric peripheral stalks containing right handed coiled coil sequences still formed functional complexes, while none of the left handed coiled coil sequences were able to support oxidative phosphorylation. In contrast, two papers

have been published in 2008 by the Vogel lab arguing for a more traditional, left handed coiled coil. The first paper used *in silico* methods to analyze possible packing arrangements for the *b* subunits and concluded that the available structural and biochemical evidence can be accommodated by a left handed coiled coil structure [361]. Their second paper contained sequence analysis showing that all bacterial, cyanobacterial and plant *b* subunit have extensive heptad repeats suggesting these subunits are capable of packing as left handed coiled coils [362]. The authors engineered cysteines at 38 positions in the soluble form of the *b* subunit and measured intersubunit distances with EPR. The distances obtained fit the model for a left handed coiled coil arrangement. Although data has been presented to support both left and right handed models, it is currently difficult to determine which model is correct.

Certain regions of the dimerization domain have been shown to be very sensitive to mutation. It was first observed that the deletion of a single residue, $b_{\Delta K100}$, resulted in the loss of dimerization in the $b_{V25\text{-}L156}$ construct and the failure to support growth on succinate when incorporated into the holoenzyme [338]. A more recent study presented evidence that all single amino acid deletions in the $b_{K100\text{-}A105}$ region allowed complex assembly but failed to support growth on acetate [363]. Interestingly, the deletion of the entire region, $b_{\Delta K100\text{-}Q106}$, resulted in only moderately reduced growth. These results can be interpreted to suggest that the single amino acid deletions disrupted the α helix such that the coiled coil structure could no longer form properly, while removing two full turns of the α helix only slightly affected enzyme functional. Another recent paper showed that many regions of the dimerization domain were relatively insensitive to duplication [330]. Duplication of the $b_{A59\text{-}T62}$, $b_{E73\text{-}I76}$, $b_{A90\text{-}E93}$ and $b_{V102\text{-}A105}$ regions individually had no effect on the ability of the enzyme to support growth on succinate.

Secondary structure predictions indicate a β turn in the dimerization domain around residues $b_{R82\text{-}Q85}$, immediately after the first α helical segment [329, 364]. The majority of bacterial *b* subunits have a highly conserved alanine as the last residue of the first α helical segment, with only one known exception [80]. Mutagenesis experiments showed this alanine residue to be sensitive to substitutions which produced an unstable *b* subunit and an assembly defect in the entire complex [347, 365]. These b_{A79} mutations were reproduced in the $b_{V25\text{-}L156}$ construct and showed a marked decrease in dimer formation along with convincing evidence that dimer formation was an essential step required prior to the binding of $b_{V25\text{-}L156}$ to F_1 [332].

A number of pieces of data demonstrate that interactions exist between the *b* subunit dimerization domain and the α and β subunits of F_1. EPR spectroscopy has been used by the Vogel lab in two different experiments to produce results suggesting significant interactions between the dimerization domain and F_1. The first study demonstrated that the binding of $b_{V25\text{-}L156}$ to spin-labeled F_1 significantly changed the conformation of the catalytic sites in the $\alpha_3\beta_3$ hexamer [366]. The second study introduced spin labels at a number of positions along the *b* subunit and generated data suggesting that the *b* dimer packs tightly to F_1 between residues b_{N80} and the C-terminus with some segments in that region where the packing interactions are quite loose [367]. Finally, electron microscopy visualization of ATP synthase lends support to the idea that the peripheral stalk closely associates with the $\alpha_3\beta_3$ hexamer [368-370].

F_1 binding domain: The F_1 binding domain is the C-terminal end of the *b* subunit which is required for the proper interaction of the peripheral stalk with F_1 in the intact complex [339, 371]. This domain involves residues $b_{Q123\text{-}L156}$ [337]. Little is known about the structure of this region, but evidence suggests a different structure than the straight linear α helix that is believed to dominate the first three domains. A more compact structure is likely based on analytical

ultracentrifugation experiments of truncated $b_{V25\text{-}L156}$ that suggested that the extreme C-terminus is bent back in a hairpin like fashion [336]. Experimental evidence exists for an interaction between the *b* subunits in the F_1 binding domain as well as with the α and δ subunits.

Experiments showed that the substitution b_{A128D} abolished enzyme function, indicating that the proper interaction between the *b* subunits in the F_1 binding domain is critical [372]. Sedimentation equilibrium experiments presented in the same paper indicated that the $b_{V25\text{-}L156,\ A128D}$ subunits were unable to dimerize. This mutation was examined later by the another lab who failed to detect any significant effect on dimerization as measured by sedimentation equilibrium [338]. However, the authors did see evidence of a conformational change in the C-terminus of the $b_{V25\text{-}L156,\ A128D}$ subunits that resulted in an inability to bind F_1. It was proposed that residue b_{A128} may be located on the inner face of an amphipathic helix such that the electrostatic repulsion caused by substituting a D for this residue could push the helices apart and disrupt the F_1 binding domain [338]. It has been recently shown that the entire sequence from $b_{V124\text{-}A130}$, known as the VAILAVA sequence, was sensitive to both deletions and duplications of various sizes [330]. Modifying the *b* subunit in this region destroyed enzyme function, while deletions and duplications in the $b_{A143\text{-}S146}$ region had no effect on the ability of the enzyme to support growth on succinate. The C-terminal region $b_{V153\text{-}L156}$ was also sensitive to both deletions and duplications. Although this region was known to be sensitive to deletions, the effect of duplication was surprising since appending a V5 epitope tag to the C-terminus of the *b* subunit had no significant effect on enzyme activity [355].

Ample evidence exists of a *b*-δ interaction that is essential for enzyme function, but recognition of this interaction took years to develop. Deletion analysis of the δ subunit showed that it was essential for the proper binding of F_1 to F_O, but the role of the *b* subunit in this

interaction was not known [314]. Evidence of a *b*-δ interaction was initially observed in other species. Work with the mitochondrial form of the enzyme using size exclusion chromatography produced evidence of an interaction between the mitochondrial *b* subunit and OSCP, the mitochondrial equivalent of *E. coli*'s δ [315]. A similar experiment carried out with *E. coli* $b_{V25\text{-}L156}$ and δ did not show any complex formation, probably due to the weakness of the interaction, discussed below [316]. An interaction between the *b* and δ proteins *in vivo* was observed using a yeast two hybrid system [317]. The same authors also demonstrated that *b* does not interact with δ-depleted F_1. Additional evidence of a *b*-δ interaction was seen in the NMR structure of ^{15}N-labeled δ when $b_{V25\text{-}L156}$ was added to the solution [318].

The affinity between $b_{V25\text{-}L156}$ and the δ subunit alone is relatively weak – NMR experiments estimated a dissociation constant (K_d) of greater than 2 μM [318]. Two different labs used analytical centrifugation to obtain K_d values of 1.8 μM and 5-10 μM [316, 373]. When the full F_1 component is used with $b_{V25\text{-}L156}$ instead of the δ subunit alone we see a decrease in the K_d to somewhere in the 0.6-14 nM range, depending on the binding model [373]. A recent experiment employing full-length *b* subunit incorporated into proteoliposomes used single-molecule fluorescence resonance energy transfer to measure a K_d of about 10 nM [374]. It has also been shown that Mg^{2+} impacts the binding of the $b_{V25\text{-}L156}$ dimer to F_1. Removal of Mg^{2+} lowers the binding affinity by a factor of 10, explaining why a decrease in Mg^{2+} concentration has long been used as an effective method for dissociating F_1 from F_O [375].

The exact structural interactions of the *b* and δ subunits are unknown, but sedimentation equilibrium analysis of the $b_{V25\text{-}L156}$-δ complex showed a protein even more elongated than the $b_{V25\text{-}L156}$ complex alone [316]. This result is suggestive of an end-to-end interaction rather than a side-by-side arrangement. It has been demonstrated that monomeric *b* subunits have a

significantly lower affinity for the δ subunit than the dimeric form [318]. Reconstitution experiments carried out with a recombinant *b* subunit that exhibited impairment of dimerization confirmed that monomeric *b* has no significant affinity for F_1 [332]. Surprisingly, proteolytic degradation of the C-terminus of δ back to approximately residue δ_{R154} did not prevent the interactions of F_1 and F_O while genetic deletion of the last four residues of δ resulted in a predominately cytoplasmic location of F_1 [306, 314]. The implications these results have on our understanding of the *b*-δ interaction is difficult to interpret.

The last four amino acids of the *b* subunit have been shown to be essential for forming the proper interactions with δ [324]. Removal of one to four amino acids from the C-terminus of the $b_{V25\text{-}L156}$ construct impaired interaction with both F_1 and isolated δ. The last 10 residues of the *b* subunit have the potential to form an amphipathic helix, so the deletion of the last four residues could disrupt the integrity of this region. Indeed, sedimentation analysis of $b_{V25\text{-}L156}$ with the last four amino acids truncated gave results that implied an unfolding of the extreme C-terminal domain [338].

Crosslinking analysis: The formation of crosslinks as a probe for molecular structure has been used extensively in the case of the peripheral stalk due to the lack of complete structural information. Crosslinking has been used to demonstrate spatial proximity between the two *b* subunits of the peripheral stalk and between the peripheral stalk and the other subunits of the ATP synthase complex. Care must be taken to distinguish crosslinking data obtained with the soluble $b_{V25\text{-}L156}$ protein from that obtain with the full-length *b* subunit in the context of the holoenzyme. The additional structural influences from the rest of the complex and the membrane must exert additional constraints on the structure of the peripheral stalk.

A number of crosslinking experiments indicate that the *a* and *b* subunits are in close proximity to one another. Early experiments showed that *a*-*b* complexes could be formed when intact F_1F_O complexes were treated with the crosslinking reagents DSP or DTBP [376]. A contemporary experiment also showed the formation of *a*-*b* and *a*-b_2 complexes when the F_O portion alone was treated with DSP [377]. A more specific crosslink was obtained much later with the discovery that the mutated b_{R36C} residue could be crosslinked to the *a* subunit with the heterobifunctional crosslinker BPM [378]. The removal of the F_1 subunit did not affect formation of this crosslink. In a review by Greie *et al.*, a similar approach found that the b_{A32} residue was capable of crosslinking to the *a* subunit, but the data for formation of this crosslink has never been shown [379]. Additional evidence of an interaction between the *a* and *b* subunits was obtained with the discovery that the a_{K74C} mutation could be crosslinked to the *b* subunit using TFPAM-3 [88]. The formation of this crosslink has no significant effect on ATP driven proton translocation, providing evidence that the association between the *a* and *b* subunits does not need to dissociate in order for the enzyme to function.

Crosslinking evidence also indicates a close spatial relationship between the *b* and *c* subunits. Jones *et al.* engineered cysteine mutations at b_{N2C} and individually at c_{V74C}, c_{V75C} and c_{V78C} [167]. All three *b*-*c* disulfide bonds could be formed using CuP. The authors also demonstrated that the disulfide bond between b_{N2C}-c_{V78C} inhibited enzyme function as would be expected if the *c* subunit ring must rotate relative to the peripheral stalk.

There is evidence of a close spatial relationship between the peripheral stalk and both the α and β subunits. Initial crosslinking experiments detected the formation of a *b*-β crosslink using both DSP and DTBP [376]. More detailed crosslinking results were obtained recently by McLachlin *et al.* [378]. Cysteines were introduced individually in the soluble form of the *b*

subunit to produce $b_{Y24\text{-}L156,\ A92C}$, $b_{Y24\text{-}L156,\ I109C}$ and $b_{Y24\text{-}L156,\ E110C}$ fragments. These soluble subunits were mixed with F_1 and then crosslinked with various photoactivatable crosslinkers. The crosslinks that formed were repeated in the full length *b* subunit to confirm their formation in intact F_1F_O. It was found that crosslinking the b_{A92C} mutant with BPM resulted in the formation of both *b*-α and *b*-β crosslinks. Mass spectrometry was used to determine that $b_{Y24\text{-}L156,\ A92C}$ crosslinked between residues $\alpha_{I464\text{-}M483}$, indicating that the peripheral stalk interacts with the α subunit near a non-catalytic α/β nucleotide binding site. In a similar manner, the b_{I109C} and b_{E110C} subunits crosslinked with APB between $\alpha_{E213\text{-}N220}$, also near a non-catalytic α/β nucleotide binding site. Another lab has found that a disulfide bond can be formed between a cysteine engineered in the b_{L156C} position and the naturally occurring cysteine at α_{C90} [331]. The α_{C90} residue is located near the top of F_1, close to the α/β interface at a catalytic nucleotide binding site. The formation of this crosslink blocked coupling, indicating that some degree of flexibility in these subunits relative to one another is required for proper enzyme function. This blocking is not because the peripheral stalk needs to dissociate from F_1 for proper function of the enzyme as discussed below.

Crosslinking evidence indicated that the *b* and δ subunits are located close to one another. Evidence of a *b*-δ crosslink was first observed between the chloroplast equivalent of the *b* subunit, named subunit I, and δ [323]. This zero-length I-δ crosslink was formed using a mixture of EDC and N-hydroxysulfosuccinimide (sulfo-NHS). A specific interaction between the *E. coli b* and δ subunits was observed when the subunits $b_{Y24\text{-}L156,\ E155C}$ and $b_{Y24\text{-}L156,\ +157G,\ +158C}$ were crosslinked individually to F_1 using BPM [324]. The *b* subunit was shown to be crosslinked to the C-terminus of δ, probably residue δ_{M158}, and this same crosslink could be formed in the holoenzyme. It was later shown that a disulfide crosslink could be formed

between cysteines engineered at $b_{+G157,\ +C158}$ and δ_{M158C} in the entire F_1F_O complex [325]. The formation of this disulfide crosslink had no effect on coupled activity, proving that the *b* and δ subunits did not need to dissociate for proper enzyme function. A recent paper investigated the effects of the *b* subunits individually in their interactions with δ [326]. The authors locked $b_{V25\text{-}L156}$ subunits in a staggered arrangement in which one of the two subunits had the last four amino acids truncated. It was found that truncating the N-terminally shifted *b* subunit significantly affected binding to F_1, while deleting the same amino acids on the C-terminally shifted *b* subunit had only a modest effect.

Many of the experiments that have used crosslink formation to investigate the interactions between the two *b* subunits of the peripheral stalk have been carried out on the hydrophilic domain alone. Cysteines were substituted throughout the $b_{A59\text{-}L65}$ region of the soluble $b_{Y24\text{-}L156}$ fragment and both glutathione and $CuCl_2$ were used to probe for disulfide formation [357]. It was found that both $b_{Y24\text{-}L156,\ A59C}$ and $b_{Y24\text{-}L156,\ S60C}$ were capable of forming disulfide bonds, although crosslink formation was relatively weak. Cysteines were introduced individually at residues $b_{A103\text{-}E110}$ and disulfide bond formation was induced with $CuCl_2$ [337]. Strong bond formation was observed for the $b_{Y24\text{-}L156,\ A105C}$ construct and weak formation for $b_{Y24\text{-}L156,\ I109C}$, possibly suggesting a coiled coil arrangement. The soluble fragments $b_{Y24\text{-}L156,\ V124C}$, $b_{Y24\text{-}L156,\ A128C}$, $b_{Y24\text{-}L156,\ A132C}$ and $b_{Y24\text{-}L156,\ S139C}$ exhibited strong disulfide bond formation with both glutathione and $CuCl_2$ [357], possibly indicating pair of parallel α helices.

A significant amount of crosslinking evidence exists to suggest that the two *b* subunits interact with one another in the context of the holoenzyme. The first evidence of this interaction was obtained by crosslinking the entire F_1F_O complex with either DSP and DTBP [376], as well as crosslinking of F_O alone using DSP [377]. The propensity of cysteine residues introduced

individually at residues $b_{N2\text{-}C21}$ to form disulfide crosslinks was probed by crosslinking with CuP [149]. It was found that cysteines at positions b_{N2C}, b_{T6C} and b_{Q10C} formed crosslinks with the highest levels of efficiency, leading the authors to propose a model in which the *b* subunits associate closely with one another at their N-terminal ends and flare apart as they traverse the membrane (Figure 1-21B). It was reported in a review by Greie *et al.* that an unnamed photoactivatable crosslinker was able to crosslink cysteines substituted individually at b_{Q37C}, b_{G43C} and b_{S60C} in the context of the entire enzyme [379]. The same review also reported disulfide crosslinks formation between cysteines substituted individually at b_{G43C}, b_{A45C}, b_{S60C} and b_{L65C}, again in the context of the entire enzyme. The fact that the data showing these crosslinks has never been published, along with the previously reported inability to form a disulfide crosslink between b_{S60C} subunits in the holoenzyme [318], means these reports must be taken lightly. Two papers from the Capaldi lab have produced convincing data showing crosslink formation between cysteines engineered individually at b_{S84C}, b_{Q104C}, b_{A128C}, b_{G131C}, b_{A144C}, b_{S146C} and b_{L156C}, all in the context of the entire complex [318, 331]. The authors showed that the *b*-*b* crosslink formation had no effect on ATP driven proton pumping for the b_{S84C} and b_{A144C} mutants, while the decrease in activity for the b_{L156C} mutant can likely be attributed to the deleterious *b*-α crosslink [331].

Comparison of The Peripheral Stalks of Different Organisms

All known ATP synthases have a functional requirement for a peripheral stalk and contain specific proteins that fulfill this role. The sequence homology between organisms for the peripheral stalk subunits is quite low despite their conserved function [335]. A schematic representation of the peripheral stalk composition of various organisms is shown in Figure 1-22. These peripheral stalks can be classified into three categories: homodimeric peripheral stalks

expressed by bacteria (Panel A), heterodimeric peripheral stalks expressed by cyanobacteria, photosynthetic eubacteria and chloroplasts (Panels B and C) and the unique peripheral stalk found in the mitochondria of higher organisms (Panel D). The peripheral stalk of *E. coli* has been discussed in detail above. The current knowledge about chloroplast-like and mitochondrial peripheral stalks will be summarized below.

Chloroplast and Chloroplast-like Peripheral Stalks

Organisms that use light energy captured by photosynthesis have genes for two *b*-like subunits. In chloroplasts these subunits are named I and II [380, 381] and are presumed to form a heterodimeric peripheral stalk [382, 383]. Likewise, cyanobacteria and photosynthetic eubacteria also contain two *b* subunits named *b* and *b'* [384, 385]. There exists evidence that the soluble domains of these subunits preferentially form heterodimers in solution [386], and may naturally form a heterodimeric peripheral stalk in the context of the intact complex. Indeed, both polypeptides have been shown to be present in purified ATP synthase from *Aquifex aeolicus* [387]. Both classes of organisms also express a δ subunit which is thought to be functionally comparable to the δ subunit of *E. coli* [383].

The thermophilic cyanobacteria *Thermosynechococcus elongatus* BP-1 contains genes for a chloroplast-like peripheral stalk [388]. This organism has been used mainly in the study of photosynthesis [389] and circadian rhythms [390], with little known about its ATP synthase aside from the primary sequence. Analysis of this primary sequence shows that *T. elongatus* encodes genes for both *b* and *b'* subunits, both of which have a relatively high degree of homology to the *Synechocystis* genes studied by Dunn *et al.* [386]. The peripheral stalk of *T. elongatus* will be used in our study as a model for a chloroplast-like peripheral stalk.

Mitochondrial Peripheral Stalks

The peripheral stalk of the mitochondria is more complex than those described above. The role of the two *b* subunits is performed by three subunits in mitochondria – these subunits are named *b*, *d* and F_6, each present in a single copy [315, 391]. The mitochondrial peripheral stalk also contains a protein named oligomycin-sensitivity conferring protein (OSCP) which is functionally equivalent to the *E. coli* δ subunit. Little homology exists between the bacterial and mitochondrial *b* subunits. The mitochondrial *b* subunit consists of two antiparallel α-helical N-terminal membrane spanning domains followed by an highly charged α-helical region [392]. The δ subunit is predicted to be largely α-helical but lacks a N-terminal membrane spanning domain [393], while there is no homolog for subunit F_6 in bacterial systems. The structure of the mitochondria peripheral stalk is known in more detail than the peripheral stalk of any other organism. A complex consisting of truncated versions of *b*, *d* and F_6 was crystallized recently by the Walker laboratory [394] (Figure 1-23A). This structure docked nicely on the existing structures of mitochondrial F_1 (Figure 1-23B) and a combined F_1-*b*/*d*/F_6 structure was recently obtained (EBEC 2008 presentation, unpublished data).

The structure of the OSCP subunit has been solved by NMR (Figure 1-24) [395]. Only the N-terminal domain was of OSCP was suitable for NMR analysis, a trait also observed with the *E. coli* δ subunit [304]. The two subunits share a significant degree of homology, with 28% of their amino acid sequence being identical [393]. They both consist of two separate domains as determined by proteolysis. The main difference is in the surface charge of the subunits, with OSCP having an overall positive charge and the *E. coli* δ subunit having an overall negative charge [395].

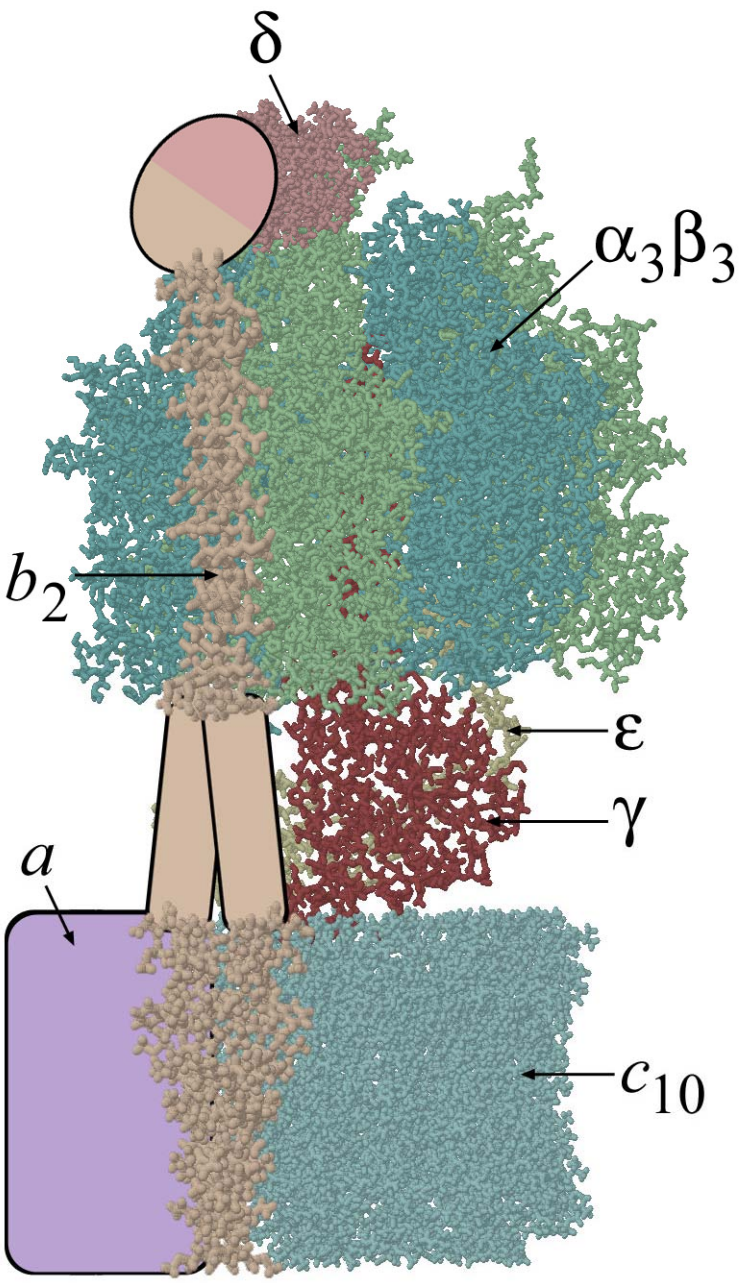

Figure 1-1. Model of F_1F_O ATP Synthase. Image rendered in Rasmol using structure files PDB code 1BMF (subunits α, β and half of γ [225], 1FS0 (ε and half of γ) [182], 1C17 (ring of *c* subunits) [95], 1L2P (*b* subunit dimerization domain) [358], 1B9U (*b* subunit membrane spanning domain) [149] and 2A7U (δ subunit) [305]. Portions of the complex for which no high-resolution structures exist are shown as colored circles.

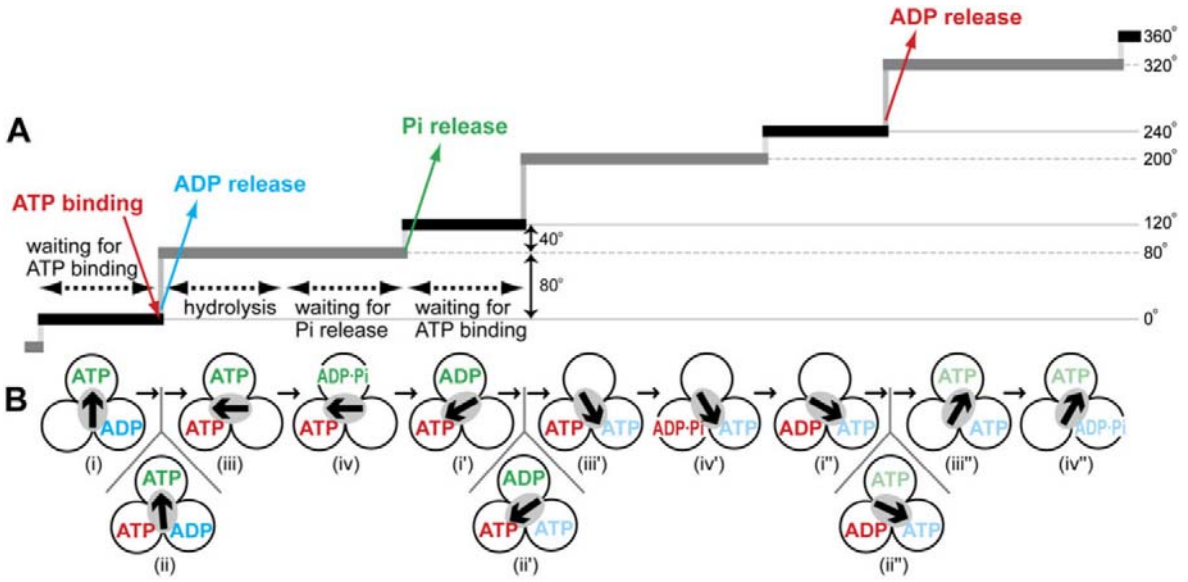

Figure 1-2. Mechanism of ATP hydrolysis. A) Time course of stepping rotation, with the vertical axis representing the rotation angle of γ and the horizontal axis representing time. Events take place in the catalytic sites of the same color in Panel B. B) Corresponding nucleotide states in the three *b* subunits. The central gray shape represents the γ subunit, with the arrow representing the rotation angle. (Figure from [51], used with permission)

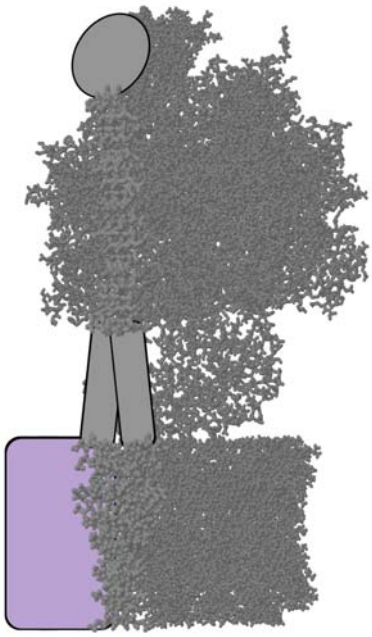

Figure 1-3. Subunit *a* (purple)

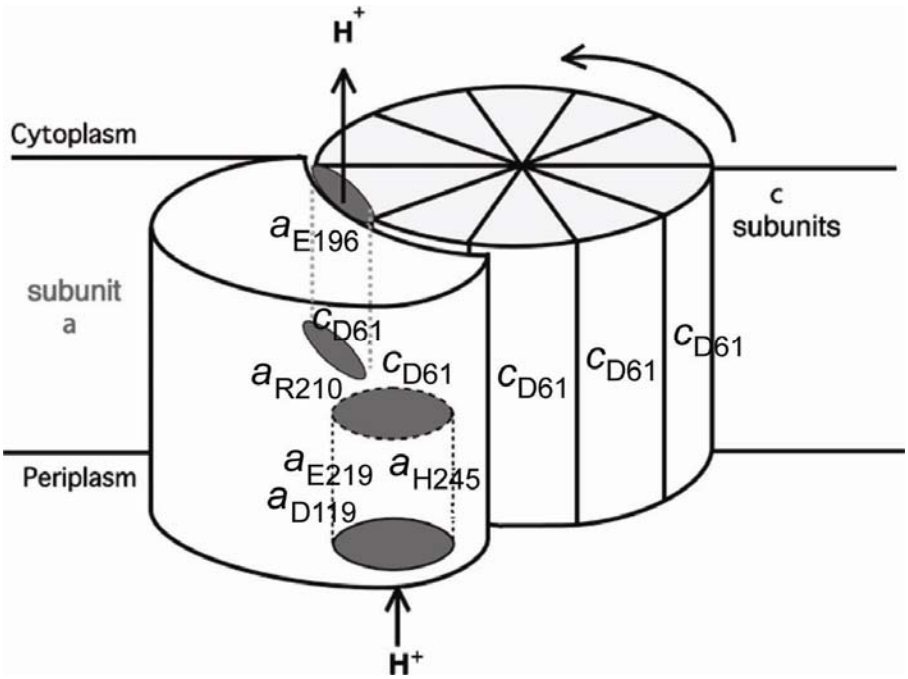

Figure 1-4. Proton channels through the *a* subunit. The two proton half-channels along with the locations of important residues are shown. (Figure from [396], used with permission)

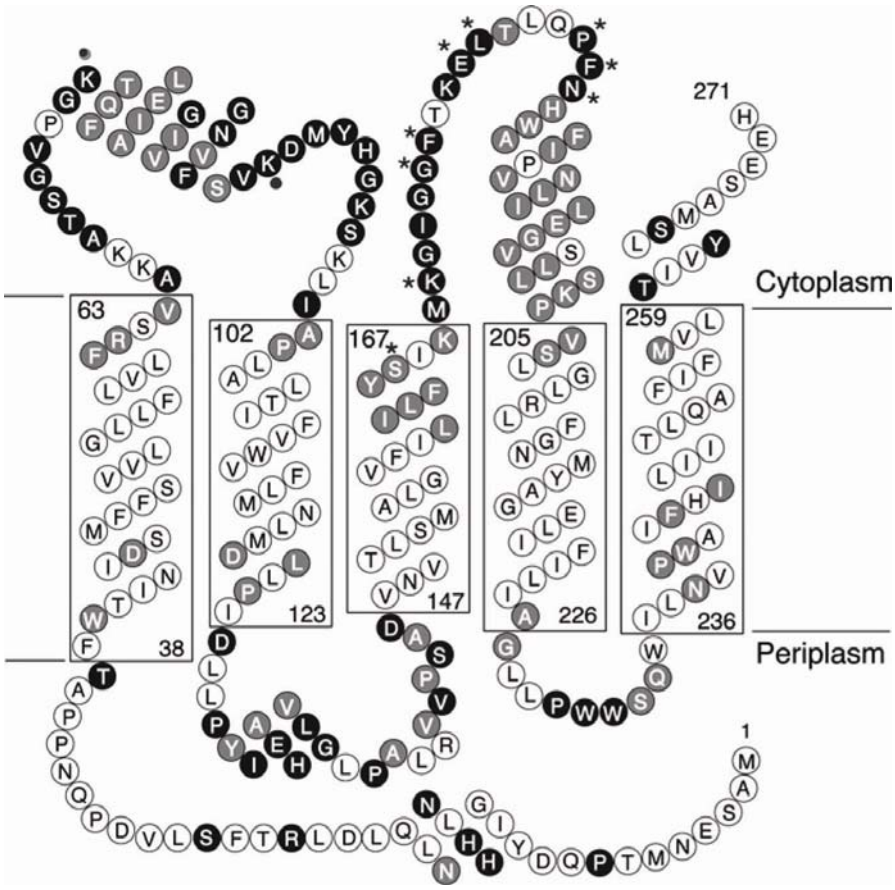

Figure 1-5. Model of the topology of subunit *a*. Residues in black are considered surface accessible while those in gray could not be labeled. Residues marked with a dot (a_{K74} and a_{K91}) could be crosslinked to the *b* subunit and those marked with an asterisk could be crosslinked to the *c* subunits. (Figure from [396], used with permission)

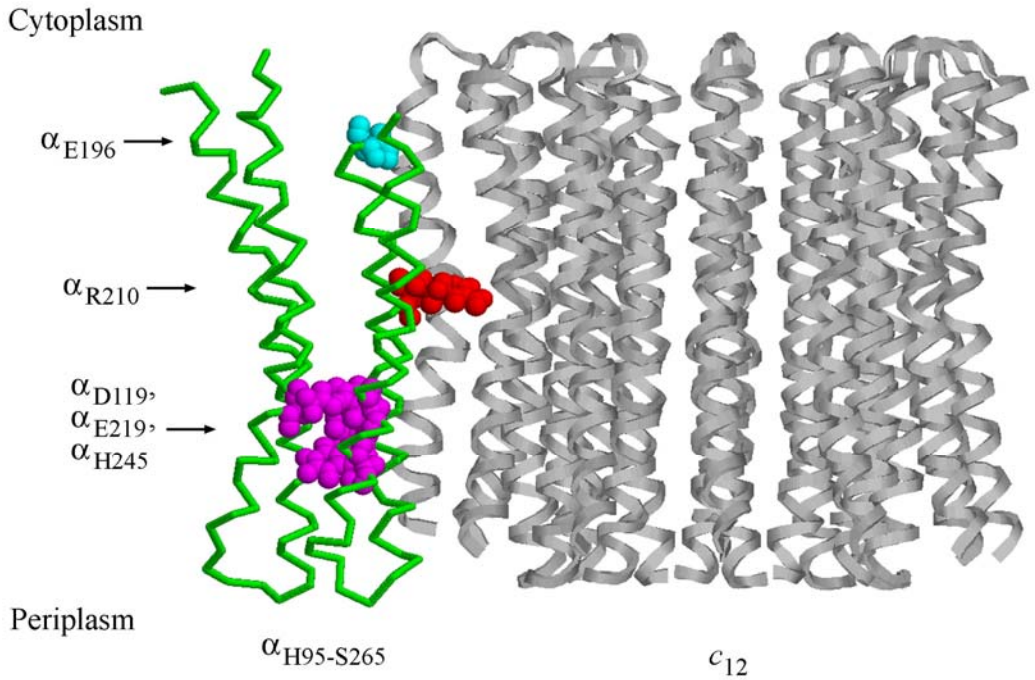

Figure 1-6. Model of the $a_{G170\text{-}S265}c_{12}$ complex. This model was generated by Rastogi and Girvin based on the available biochemical data [95]. The residues labeled in Figure 1-5 are shown here in spacefill rendering. (PDB code 1C17, rendered with RasMol)

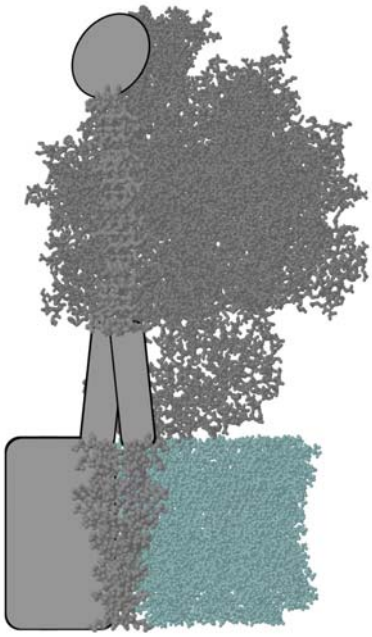

Figure 1-7. Subunit *c* ring (blue)

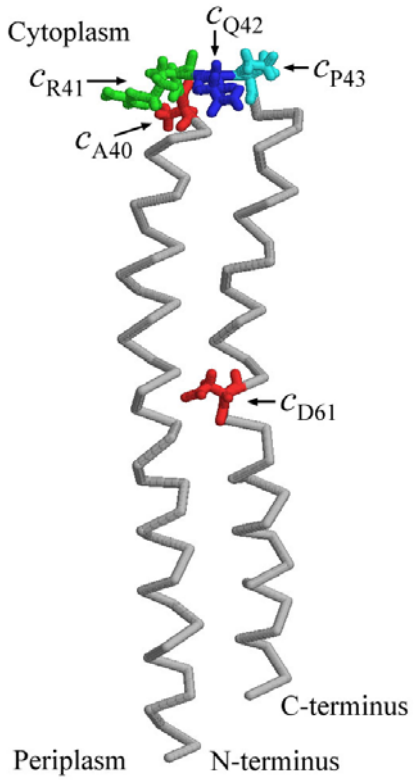

Figure 1-8. Structure of monomeric *c* subunit. The essential residue c_{D61} is shown, as are the residues of the polar loop region $c_{A40\text{-}P43}$ mentioned in the text. NMR structure solved by Girvin *et al.* [119] (PDB code 1A91).

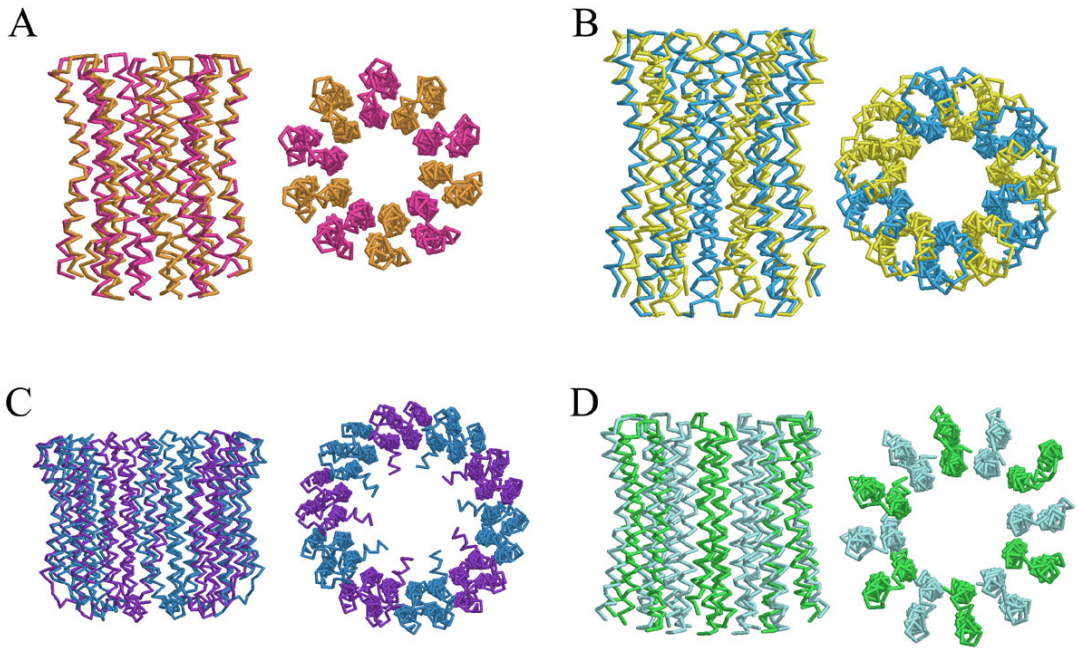

Figure 1-9. Models of *c* subunits rings. A) *Saccharomyces cerevisiae* [146] (PDB code 1QO1). B) *Ilyobacter tartaricus* [147] (PDB code 1YCE). C) *Enterococcus hirae* [148] (PDB code 2BL2). D) Model for *Escherichia coli* [95] (PDB code 1C17).

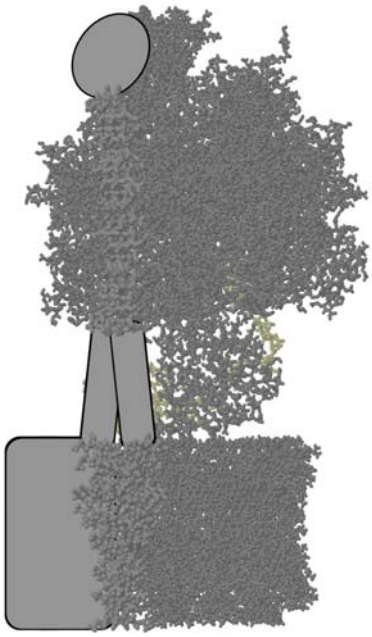

Figure 1-10. Subunit ε (gold, located behind to γ subunit)

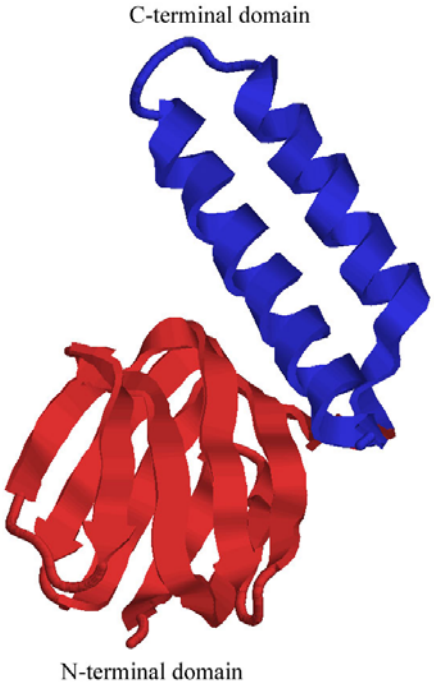

Figure 1-11. Subunit ε structure with closed C-terminal domain. Structure was solved by crystallography [193] (PDB code 1AQT).

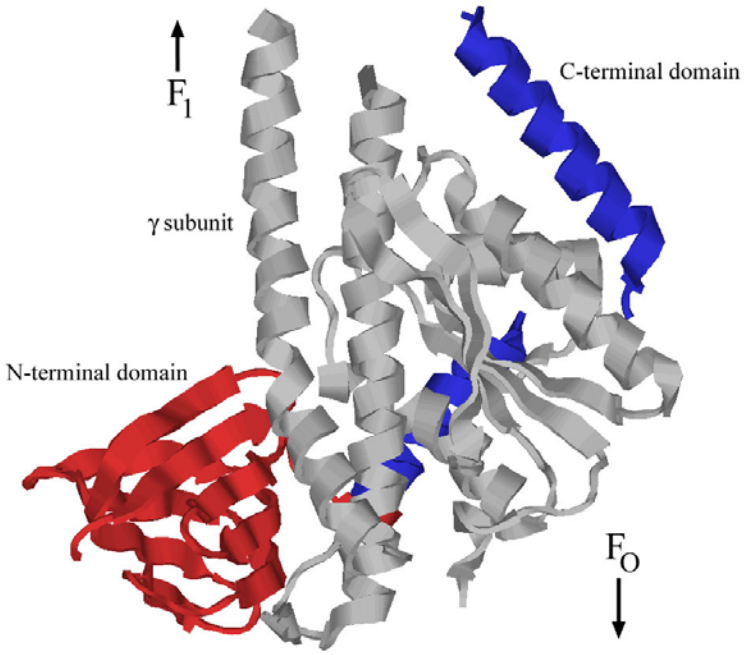

Figure 1-12. Subunit ε structure with open C-terminal domain. Structure was solved by crystallography [182] (PDB code 1FS0).

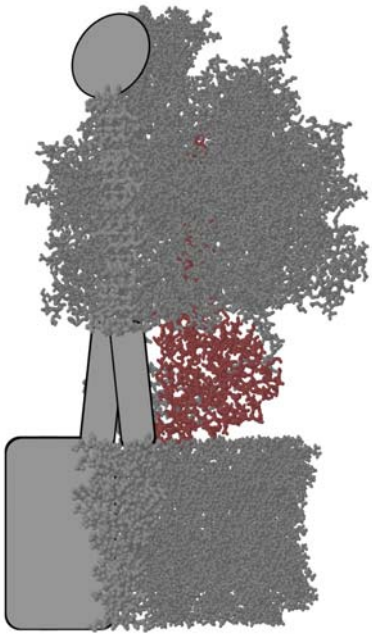

Figure 1-13. Subunit γ (red).

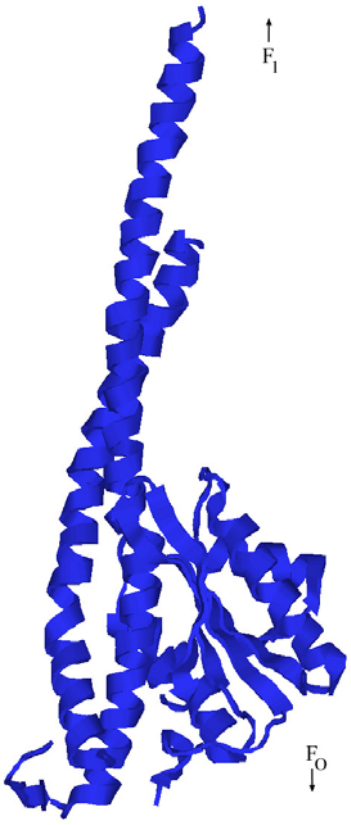

Figure 1-14. Structure of the entire γ subunit generated by combining the upper region as crystallized by Abrahams *et al.* [225] with the lower region obtain by Rodgers and Wilce [182] (PDB code 1BMF and 1FS0, respectively).

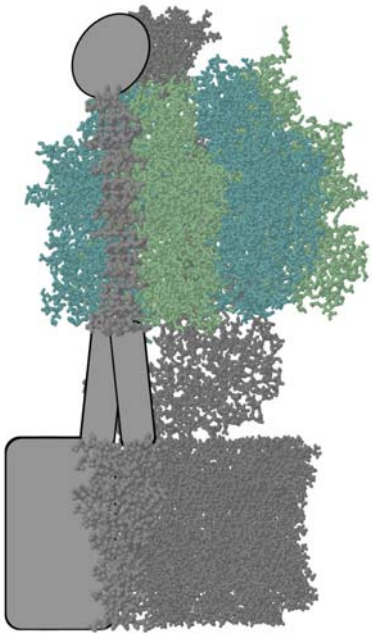

Figure 1-15. Subunits α and β (blue and green, respectively)

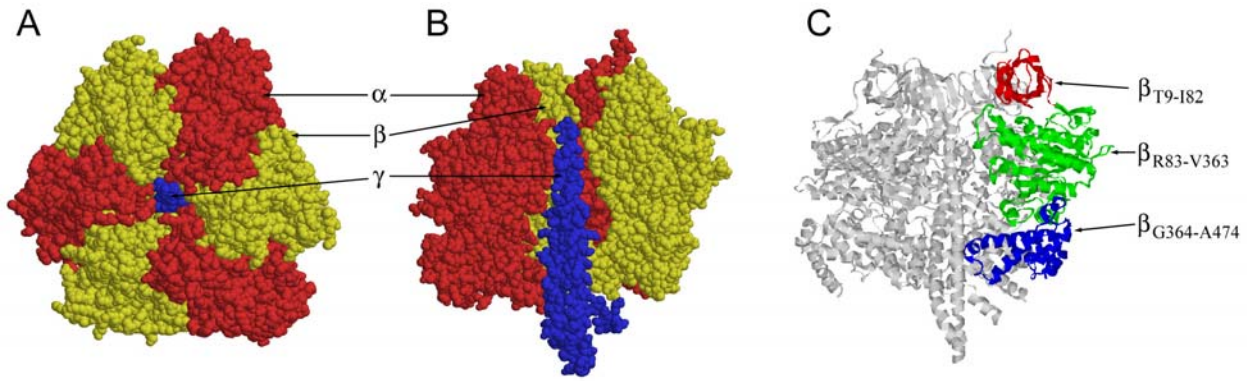

Figure 1-16. High-resolution structure of F_1. A) Top view. B) Side view with one α/β pair removed. C) Side view showing the three domains of a β subunit (PDB code 1BMF).

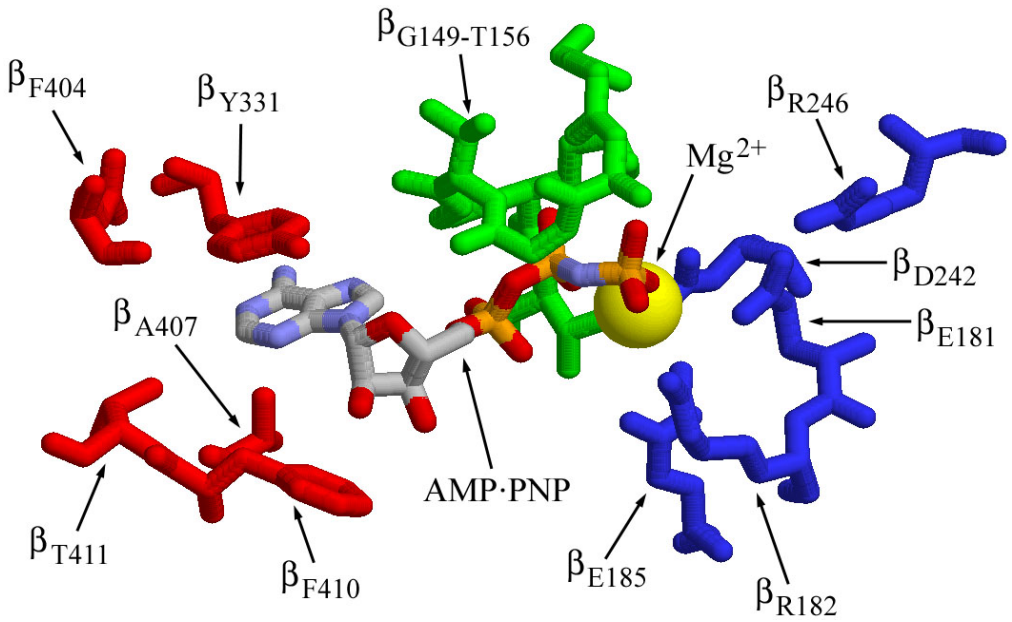

Figure 1-17. Nucleotide binding site of the β subunit. Residues discussed in the text are grouped by color: adenine binding residues are red, Walker A residues are green and additional phosphate binding residues are blue. The structure from bovine mitochondria shows AMP·PNP and Mg^{2+} bound in the catalytic site (*E. coli* numbering).

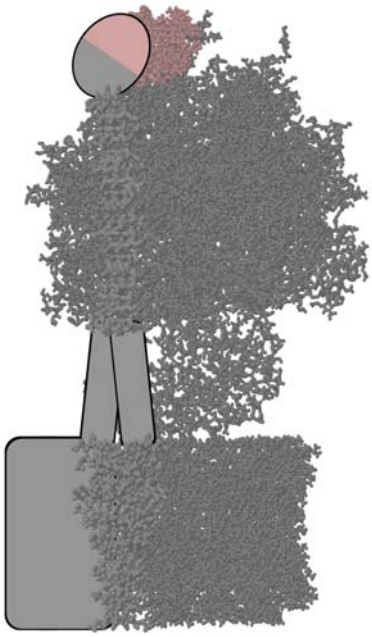

Figure 1-18. Subunit δ (pink)

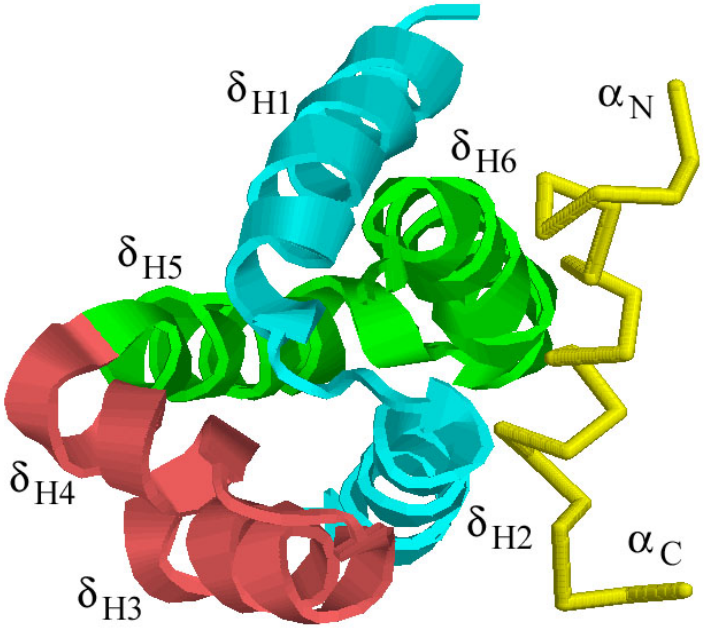

Figure 1-19. Structure of the δ-α complex. Helices 1-2 and 5-6 form an intercalating V-shaped pair which helices 3-4 pack against. A peptide modeling the N-terminal 22 residues of α fits in the grove formed by helices 1 and 5 (PDB code 2A7U).

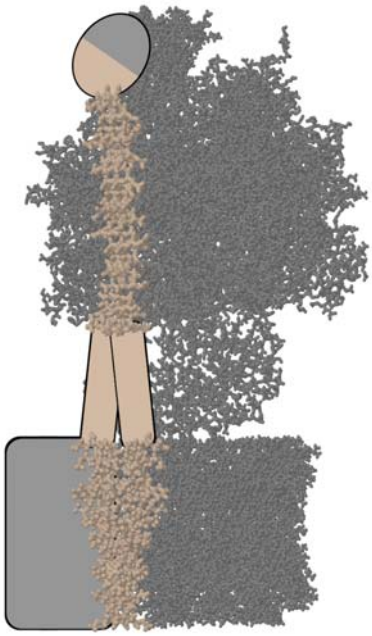

Figure 1-20. Subunit *b* (tan)

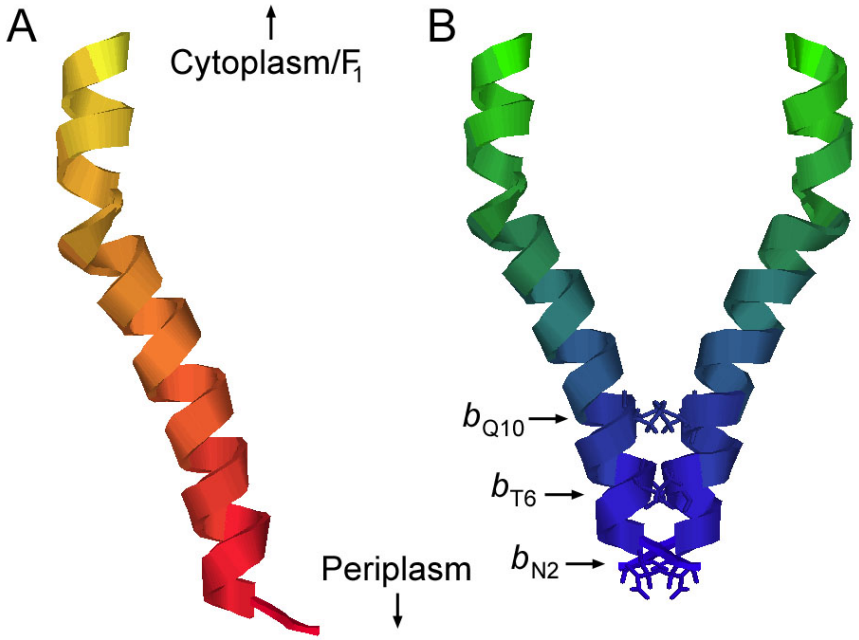

Figure 1-21. Membrane spanning domain of the *b* subunit. A) The structure of a peptide modeling $b_{M1\text{-}E34}$ as solved by NMR [149] (PDB code 1B9U). B) Model of how two membrane spanning domains may interact based on crosslinking analysis.

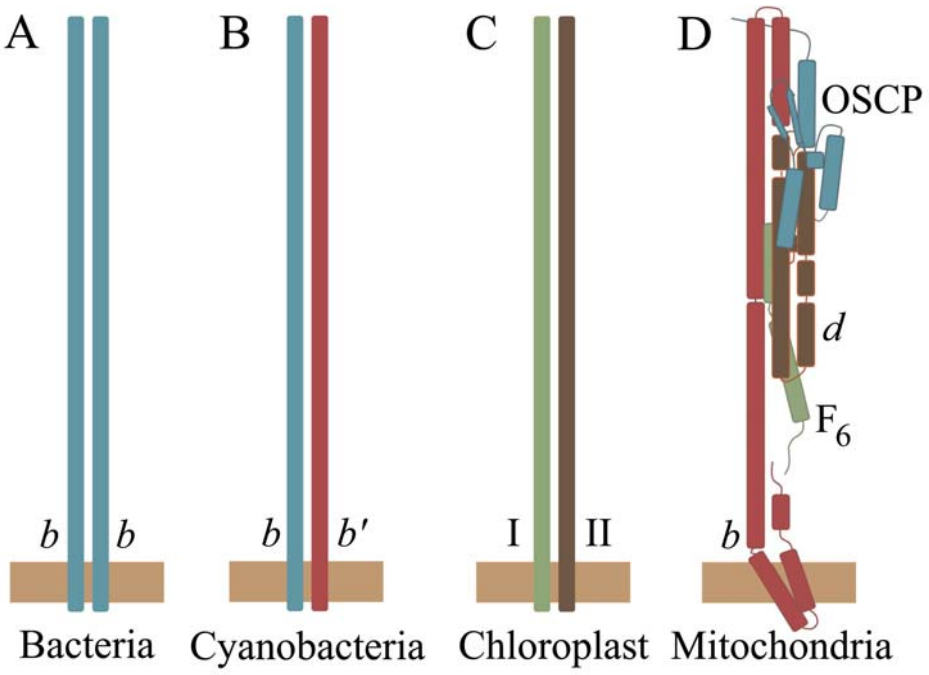

Figure 1-22. Peripheral stalks from different organisms: A) Bacteria, B) Cyanobacteria and photosynthetic eubacteria, C) Chloroplast and D) Mitochondria (Adopted from Walker and Dickson, 2006 [393], used with permission).

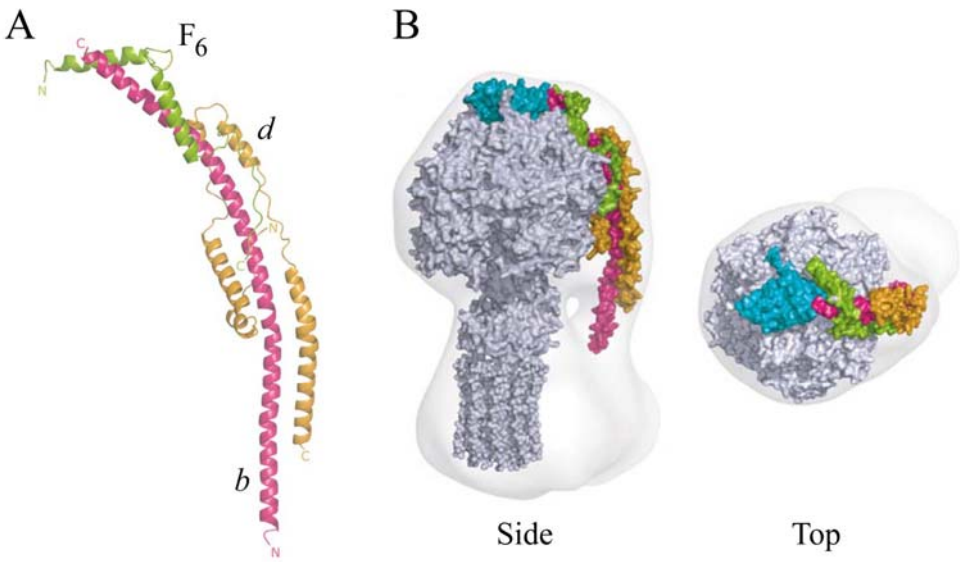

Figure 1-23. Structure of the mitochondrial peripheral stalk. A) The peripheral stalk composed of residues 79-183, 3-123 and 5-70 of subunits *b*, *d* and F6, respectively. B) The peripheral stalk docked on F_1 and the *c* subunit ring inside the shape of F_1F_O obtained using electron microscopy. The OSCP subunit is shown here colored blue. (Figures from Dickson *et al.*, 2006 [394], used with permission).

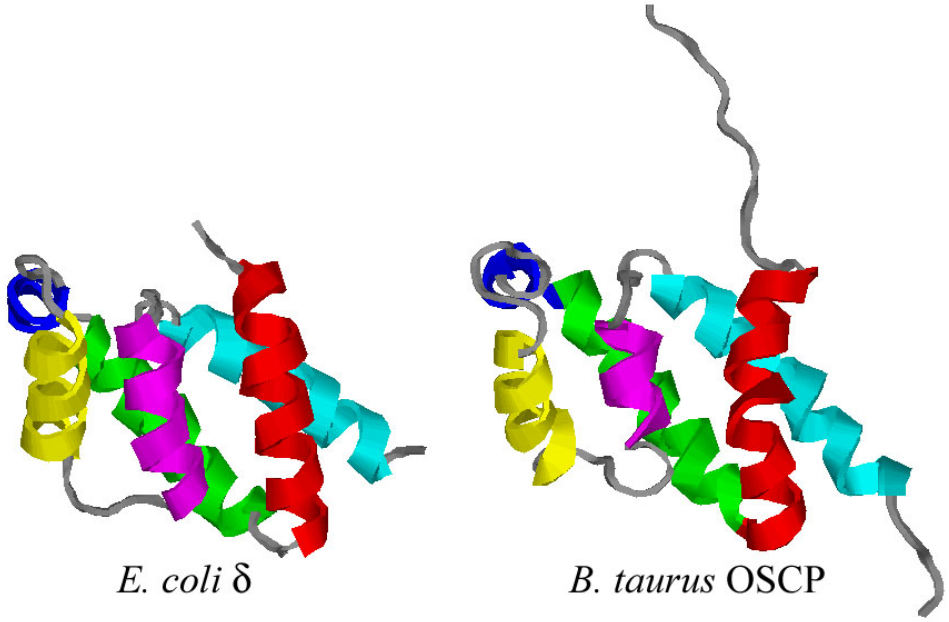

Figure 1-24. Comparison of the δ and OSCP subunits. The δ subunit from *E. coli* (PDB code 1ABV) was solved by Wilkens *et al.* [304] and the OSCP subunit from *B. taurus* mitochondria (PDB code 2BO5) was solved by Carbajo *et al.* [395].

CHAPTER 2
MATERIALS AND METHODS

Bacterial Strains and Growth on Succinate

Escherichia coli strains KM2 (Δb) and 1100 ΔBC (Δ*unc*) carrying chromosomal deletions of the uncF(*b*) gene and the entire *unc* operon, respectively, were used as the host strains [365]. Cells were grown on minimal A media supplemented with succinate (0.2% w/v) to determine enzyme viability. Casamino acids were added to the minimal A media in some cases to a final concentration of 0.2% to encourage growth of particularly F_1F_O-deficient strains. All cells were grown at 37 ºC unless otherwise noted.

Preparation of Membranes

Inverted membrane vesicles containing ATP synthase complexes were prepared using the method of Caviston *et al.* [348]. All reagents and materials were kept at 4 ºC. A 10 mL starter culture of Luria Broth (LB) containing ampicillin (100 μg/ml) and/or chloramphenicol (25 μg/ml) plus 0.2% w/v glucose was inoculated with the desired bacterial strain and grown at 37 ºC overnight with mixing. A 2 L Erlenmeyer flask containing 500 mL of LB was prewarmed to 37 ºC. Glucose and isopropyl-1-thio-β-D-galactopyranoside (IPTG) were added to the Erlenmeyer flask to final concentrations of 0.2% w/v and 40 μg/ml, respectively. The entire 10 mL overnight was used to inoculate the Erlenmeyer flask immediately after the addition of glucose and IPTG. The bacteria were grown at 37 ºC in a New Brunswick Scientific incubator with shaking at 250 rpm and the density was measured periodically using a Klett-Summerson photoelectronic colorimeter. Cells were harvested when they reached approximately 150 Klett units (OD_{600} = 1.0) by centrifuging for 10 minutes at 8,000 x g in a Du Pont Sorvall RC-5B Superspeed Centrifuge with a GSA rotor. The cell pellet was resuspended in 8 mL of TM (50 mM Tris-HCl, pH 7.5, 10 mM $MgSO_4$) buffer and DNaseI (10 mg/mL) was added to a final

concentration of 10 μg/ml. In some cases tris(2-carboxyethyl) phosphine (TCEP, 0.5 M) was added to the TM buffer to a final concentration ranging from 1-5 mM prior to membrane resuspension. The resuspended cells were broken by passing twice through a French Pressure Cell at 14,000 psi. Two sequential centrifugation steps in the same Sorvall centrifuge at 10,000 x g with an SS-34 rotor were done for 10 minutes each to remove unbroken cells and debris. The supernatant was centrifuged in a Beckman-Coulter Optima LE-80K Ultracentrifuge with a 70.1Ti rotor at 150,000 x g for 1.5 hours to recover membrane vesicles. The membranes were resuspended in 9 mL TM buffer using a 10 mL Wheaton tissue grinder and then centrifuging again in the Beckman centrifuge for 1 hour. The purpose of this additional wash step was to remove any ATPases loosely associated with the membrane. The pellet was resuspended once more in 1 mL TM buffer using a 2 mL Wheaton tissue grinder.

Determination of Protein Concentration

The concentration of each membrane sample was determined using the bicinchroninic acid (BCA) assay method [397] in order to normalize the amount of membrane protein used for subsequent assays. All reactions for this assay were done in triplicate in 13x100 mm disposable borosilicate glass tubes, each containing 2 mL of standard working reagent (SWR). The SWR was composed of 50 parts solution A (1% BCA-Na_2, $Na_2CO_3 \cdot H_2O$,0.16% sodium potassium tartrate, 0.95% $NaHCO_3$, pH 11.25 and filtered) to one part solution B (4% $CuSO_4 \cdot 5H_2O$) plus 10% sodium dodecyl sulfate (SDS) to a final concentration of 1%, mixed fresh as needed. The SWR was aliquoted into the glass tubes using a repeat pipetter and the tubes were placed in ice water to prevent the reactions from starting early. A standard curve was generated using bovine serum albumin (BSA) that was made to an initial concentration of 1 mg/mL. The exact concentration of the BSA was determined by measuring the optical density at 280 nm, where the

OD_{280} for 1.0 mg/mL BSA is 0.667. This BSA was aliquoted into the glass tubes containing SWR in volumes of 0, 5, 10, 20, 40, 60, 80 and 100 μL protein (approximately 0-100 μg BSA). The membrane samples were diluted 1:10 in TM buffer and 40 μL of the diluted samples were aliquoted into glass tubes containing SWR. All of the tubes were vortexed briefly after the addition of protein to fully mix. These tubes were removed from the ice bath and incubated in a water bath heated to 37 ºC for 20 minutes, then allowed to cool to room temperature for 10 minutes. The absorbance of each sample at 562 nm was determined using a Varian Cary 50 UV-Vis spectrophotometer. A spreadsheet in Microsoft Excel was used to determined the slope of the standard curve and calculated the concentrations of the membrane samples. Each sample was diluted to a constant concentration to simplify subsequent assays, usually 10-15 mg/mL.

Proton Pumping Assay Driven by ATP

The proton pumping assay measures F_1-driven proton pumping through F_O by detecting membrane vesicle energization via the fluorescence quenching of 9-amino-6-chloro-2-methoxyacridine (ACMA) as previously described [332]. Two different fluorescence spectrometers were used throughout this study, first a Perkin-Elmer LS-3B Fluorescence Spectrometer and later a Photon Technologies International QuantaMaster 4. The output from the Perkin-Elmer spectrometer was recorded with a Perkin-Elmer GP-100 Graphics Printer while the output from the PTI spectrometer was graphed by the Felix32 software provided with the instrument. A total of 500 μg of membrane protein was mixed with 3 mL of assay buffer (50 mM MOPS, 10 mM $MgCl_2$, pH 7.3) in a quartz cuvette. The ACMA was excited at 410 nm and the emission at 490 nm was recorded. A zero baseline was typically recorded for 30 seconds prior to the addition of 0.2 mM ACMA to a final concentration of 1 μM. The sample was recorded for an additional 45 seconds prior to the addition of ATP (0.15 M ATP, 25 mM tris-

HCl, pH 7.5) to a final concentration of 0.75 mM. Fluorescence quenching was recorded for 10 minutes after the addition of ATP. The paper output of the Perken-Elmer Graphics Printer was scanned into a digital form and the traces recorded by PTI's Felix32 software were obtained directly. These digital traces were combined in Adobe Photoshop. A control which was used to verify the integrity of the membrane vesicles was the addition of 5 μL 0.1 mM β-nicotinamide adenine dinucleotide (NADH) instead of ATP. The reaction was recorded long enough to make sure that fluorescence quenching peaked and began to diminish, a sign of intact membrane vesicles.

Measuring the Rate of ATP Hydrolysis

The rate of ATP hydrolysis assay associated with each membrane sample was measured as an indirect indication of the amount of assembled ATP synthase present in each membrane sample. Two different ATP hydrolysis assays were used throughout this study–the acid molybdate method was used initially until it was replaced by the superior MESG method.

Assay Using Acid Molybdate

The acid molybdate assay detects the release of inorganic phosphate (P_i) from ATP as a method of quantifying enzyme activity. Each reaction was carried out in 13x100 mm disposable borosilicate glass tube in a water bath set at 37 ºC as previously described [354]. A total of 4 mL of reaction buffer (50 mM tris-HCl, 1 mM $MgCl_2$) was added to each tube along with 60 μg of membrane protein. Three different reactions buffers were used – pH 9.1, pH 7.5 and pH 7.5 with 0.5% lauryl dimethylamine oxide (LDAO). The pH 9.1 buffer was used to disassociate F_1 from F_O and hence produced higher ATP hydrolysis rates than the pH 7.5 buffer. Likewise, the addition of LDAO to the pH 7.5 buffer releases F_1 from the inhibitory effects of the ε subunit and resulted in an increase in the rate of ATP hydrolysis as previously described [101]. Each

sample was assayed in triplicate. The reactions were started by adding 80 μL of ATP (0.15 M ATP, 25 mM tris-HCl, pH 7.5) to the protein/buffer mixture and vortexing briefly. Data points were taken by removing 435 μL aliquots from the tubes at 0 (before addition of ATP), 2, 5, 7, 10 and 12 minutes. The reaction was stopped by adding these aliquots to disposable glass tubes containing 2 mL of stop buffer (1.3 parts H_2O, 0.6 parts HCl/molybdate [2.5% $NH_4Mo_4O_2 \cdot 4H_2O$, 4.0 N HCl], 0.4 parts 10% SDS) that had been chilled in an ice bath. The stopped mixture was vortexed briefly and the tubes were returned to the ice bath. A standard curve was generated by preparing phosphate standards in triplicate in a total volume of 1 mL of reaction buffer. Solutions of 2 mM or 20 mM KH_2PO_4 were added to final concentrations of 0, 0.02, 0.1, 0.2, 0.4 and 0.6 μmol phosphate. Aliquots of 435 μL of each standard were then transferred to glass tubes containing 2 mL of stop buffer. An additional control used to determine the amount of free P_i in the ATP solution was done by adding 80 μL of ATP to 4 mL of reaction buffer, vortexing briefly and adding 435 μL of that mixture to a glass tube containing 2 mL stop buffer. This last control was also done in triplicate.

After the completion of all of the above time points, standards and controls, the glass tubes containing stop buffer were removed from the ice bath and allowed to warm to room temperature. The amount of P_i was quantified by adding 100 μL of a fresh 1:10 dilution of Eikonogen solution (1 M $NaHSO_3$, 0.1 M Na_2SO_3, 0.01 M 4-amino-3-hydroxyl-1-napthalenesulfonic acid) to each glass tube, shaking briefly by hand and incubating at room temperature for 30 minutes. The stock Eikonogen solution is stable for up to four weeks if kept away from light. The absorbance of each sample at 700 nm was determined using a LKB Biochrom Ultraspec II spectrophotometer. A spreadsheet in Microsoft Excel was used to calculate the standard curve and determine the rate of ATP hydrolysis for each membrane

sample. The final ATP hydrolysis value was reported in units of μmol Pi/min/mg membrane protein.

Assay Using MESG

The MESG assay determines the rate of ATP hydrolysis by measuring the reaction of P_i with 7-methyl-6-thioguanosine (MESG) to form 7-methyl-6-thioguanine as previously described [398]. The enzyme purine nucleotide phosphorylase (PNP) was used to catalyze this reaction and the appearance of product was detected as an increase in absorbance at 360 nm by a Varian Cary 50 UV-Vis spectrophotometer. A PNP stock solution was made by dissolving the solid enzyme in water to a concentration of 0.1 units/μL and stored at 4 °C. An MESG stock solution was made in water to a final concentration of 1 mM and stored in 5 mL aliquots at -20 °C. The MESG solution was thawed prior to use and both MESG and PNP were stored on ice until needed. Each reaction consisted of 10-25 μg of membrane protein, 50 μL of 20x TM buffer (1 M Tris-HCl [pH 7.5], 200 mM $MgSO_4$), 300 μL of MESG, 50 μL of PNP and water to a final volume of 1 mL. The components were combined in a disposable glass tube, vortexed briefly to mix and poured into a cuvette that had been prewarmed to 37 ºC in the spectrophotometer by a circulating water bath. Each reaction was allowed to sit for 1 minute to warm before starting by adding 30 μL of 0.15 M ATP made in TM buffer. Absorbance data points were collected continuously for an additional 5 minutes. The slope of the linear portion of the reaction was determined in units of absorbance per minute using the software associated with the spectrophotometer. LDAO stimulation of ATP hydrolysis was determined by adding LDAO to each reaction to a final concentration of 0.5% as described previously [101]. A standard curve was generated by adding 0, 0.02, 0.04, 0.06, 0.08 or 0.10 μmol P_i to 50 μL 20x TM buffer, 300 μL MESG, 50 μL PNP and water to a final volume of 1 mL in disposable glass tubes, done in

duplicate. These standards were vortexed briefly, incubated at room temperature for 10 minutes and the absorbance at 360 nm was determined. The slope of the standard curve was calculated in units of absorbance per μmol P_i. The combination of this slope and the amount of protein per reaction allowed the rate of each reaction to be calculated into units of μmol P_i/min/mg membrane protein.

Crosslinking Using Cu^{2+}

Disulfide crosslink formation was induced by incubating membrane proteins with $CuCl_2$. Slightly different protocols were developed for the formation of crosslinks between two *b* subunits in the peripheral stalk and between the peripheral stalk and the δ subunits.

Formation of the *b*-*b* Crosslink

Cysteine-cysteine disulfide crosslinks between *b* subunits in the peripheral stalk were formed by incubating membrane samples with either 500 μM Cu^{2+} for 2 minutes or 50 μM Cu^{2+} for 10 minutes. These reactions were carried out with mixing at 300 rpm in open 1.5 mL microcentrifuge tubes in an Eppendorf Thermomixer R heated to 37 ºC. Each reaction was stopped by adding fresh 50 mM NEM to a final concentration of 5 mM, vortexing and placing on ice. Sample that were crosslinked with 500 μM Cu^{2+} were reacted under three different conditions – a zero time point and in the absence and presence of 45 mM ATP. The zero time point samples were obtained by diluting the concentrated membranes in TM buffer to 5 mg/mL and adding NEM to react with free cysteine residues and prevent crosslinking. The reactions were then vortexed and allowed to sit at room temperature for 15 seconds before adding Cu^{2+} and placing on ice. Crosslinking in the absence of ATP was done by diluting membrane samples in TM and warming to 37 ºC in the thermomixer. Pre-warmed Cu^{2+} was added and the samples were allowed to incubate with mixing for 2 minutes before further crosslinking was stopped by

the addition of NEM. Samples crosslinked in the presence of ATP were done in the same manner with the additional step of adding prewarmed 0.15 M ATP made in TM buffer and waiting 15 seconds before starting the crosslinking reaction. Samples that were crosslinked with 50 μM Cu^{2+} for 10 minutes were only reacted under two conditions – a zero time point and in the absence of ATP. These reactions were done exactly as described above except the Cu^{2+} solution was more dilute.

Formation of the *b*-δ Crosslink

Disulfide crosslink formation between the *b* and δ subunits was performed in a manner similar to the method described above. Membranes samples were diluted to 5 mg/mL in TM buffer. These samples were crosslinked under two conditions – a zero time point and a 30 minute time point. The zero time point sample was obtained by adding fresh 50 mM NEM to a final concentration of 1 mM to react with any free cysteine residues, vortexing briefly and incubating at room temperature for 15 seconds. Cu^{2+} was then added to a final concentration of 100 μM and the samples were placed on ice. The 30 minute time point samples were obtained by diluting the membrane proteins to 5 mg/mL with TM buffer and adding Cu^{2+} to a final concentration of 100 μM. These samples were then incubated at room temperature in open microcentrifuge tube with mixing at 300 rpm in an Eppendorf Thermomixer R. NEM was added to a final concentration of 1 mM to quench the crosslinking reaction and the samples were stored on ice.

Nickel Resin Purification

The purification of ATP synthase complexes containing at least one histidine-tagged *b* subunit was done using a High Capacity Nickel Chelate Affinity Matrix (Ni-CAM) as previously described [355]. The purification procedure was previously optimized by Dr. Grabar for the

purification of 0.5 mg aliquots of membrane protein in order to maximize the retention of ATP synthases containing only a single histidine-tagged *b* subunit. The Ni-CAM resin was prepared by putting 75 μL in a microcentrifuge tube and spinning at 5,000 x g for 30 seconds. As much of the liquid as possible was removed by aspiration without disturbing the resin and 0.5 mL of wash buffer (50 mM $NaH_2PO_4 \cdot H_2O$, 300 mM NaCl, 1 mM imidazole, 0.2% tegamineoxide WS-35, pH 8.0) were added. The resin and wash buffer were mixed on a nutator for 1 minute, spun at 5,000 x g for 1 minute and the supernatant was aspirated off. A total of 0.5 mg membrane protein was mixed with 5 M NaCl, 1 M imidazole, 35% tegamineoxide WS-35 and H_2O to 150 μL with final concentration of 400 mM, 10 mM and 0.2%, respectively. This membrane protein mixture was added to the washed Ni-CAM resin and allows to mix on the nutator for 10 minutes. The microcentrifuge tube was spun at 5,000 x g for 1 minute and the supernatant removed by aspiration. The resin was washed five times by adding 0.5 mL of wash buffer to the microcentrifuge tube, mixing on the nutator for 1 minute, spinning at 5,000 x g for 1 minute and carefully aspirating off the supernatant. F_1F_O retained by the Ni-CAM resin were eluted by adding 125 μL of elution buffer (50 mM $NaH_2PO_4 \cdot H_2O$, 300 mM NaCl, 250 mM imidazole, 0.2% tegamineoxide WS-35, pH 8.0) and mixing on a nutator for 10 minutes. The microcentrifuge tube was spun at 5,000 x g for 1 minute and the supernatant was transferred to a fresh microcentrifuge tube. The elution step was repeated once more with another 125 μL of elution buffer and the supernatant from the second elution was pooled with the first. The pooled elutant was spun once more for 1 minute at 5,000 x g to collect any remaining resin at the bottom of the tube. The supernatant was transferred to Millipore Amicon Bioseparations Microcon YM-10 centrifugation filter tube and concentrated from 250 μL to approximately 30-50 μL by centrifugation at 12,500 rpm. The Microcon tube was inverted and placed in a fresh

microcentrifuge tube and centrifuged at 3,300 rpm for 3 minutes. The quantity of retained liquid was estimated by weighing the microcentrifuge tube before and after the 3,300 rpm spin. Additional elution buffer was added to bring the volume of the elutant up to 50 μL.

Trypsin Digestion

Membrane samples were digested with trypsin to determine if the *b* subunits were incorporated into F_1F_O complexes and hence protected as previously described [353]. The reaction was set up by bringing a total of 0.1 mg of membrane protein to 90 μL with TM buffer and adding 10 μL of 2 mg/mL trypsin to start the reaction. Aliquots containing 10 μg (10 μL) of digested protein were removed at 1, 2, 3, 4, 6, 8, and 16 hours and the reaction was stopped by the addition of 2 μL of 10 mg/mL trypsin inhibitor from Glycine max (soybean). For long digestions, additional trypsin was added at 3, 6 and 8 hours to compensate for the estimated activity loss of 25% every 3 hours. The presence of heterodimeric peripheral stalks in intact F_1F_O complexes was examined by the digestion of 0.5 mg membrane protein in a reaction volume of 100 μL. The entire reaction was stopped by the addition of 30 μL of 10 mg/mL trypsin inhibitor and purified over a Ni-CAM resin as described above.

Western Analysis

Western blot analysis was used to probe for the presence of either the *b* subunit or subunits containing a V5 epitope tag, either b_{V5} or δ_{V5}. The first step was the electrophoresis of the protein samples and transfer to a nitrocellulose membrane. The membrane was then incubated with primary and secondary antibodies and visualized on film using chemiluminescence. Densitometry was employed on some films to quantify the intensity of certain bands of interest.

Electrophoresis of Proteins and Transfer to Membrane

Equal amounts by weight of each membrane sample were mixed with 2X Laemmli Sample Buffer (LSB) lacking β-mercaptoethanol (62.5 mM Tris-HCl, pH 6.8, 2% w/v SDS, 20% glycerol, 0.1% Bromophenol blue) and loaded into a precast 15% Tris-HCl Ready Gel purchased from BioRad Laboratories. The amount of protein per lane was generally 10 μg for Western blots that used a primary antibody against the *b* subunit, 1 μg for the anti-V5 antibody, or 10% of the total elutant from the Ni-CAM resin. A Mini-PROTEAN II cell filled with running buffer (25 mM Tris, 192 mM glycine, 0.1% SDS) was run at 50 volts until the samples had cleared the stacking portion of the gel and then at 100 volts until the dye reached the rubber seal at the bottom of the gel. The proteins were then transferred from the gel to a nitrocellulose membrane in transfer buffer (25 mM tris, 192 mM glycine, 20% methanol) at 100 volts for 1 hour with an upper limits of 0.5 amps to prevent overheating.

Antibody Against the *b* Subunit

A polyclonal antibody raised against the *b* subunit was provided to the Cain lab as a gift from Dr. Gabriela Deckers-Hebestreit. This antibody was used as the primary antibody essentially as described previously [355]. A single 250 μL aliquot of this antibody stock was diluted 1:40 in TTBS (tris-buffer saline [TBS, 10 mM tris-HCl, 150 mM NaCl, pH 7.2] supplemented with 0.1% polyoxyethylenesorbitan monolaurate [Tween 20] and 2% BSA) to make 10 mL at the final working concentration.

After electrophoresis and transfer, the nitrocellulose membrane was stained by incubation with fast green stain (50% methanol, 10% glacial acetic acid, 0.01% fast green) at room temperature with gentle shaking on a Bellco Biotechnology Orbital Shaker for 15 minutes. The fast green stain was saved for further use. The membrane was then destained using fast green

destain (50% methanol, 10% glacial acetic acid) three times for 5 minutes each and the destaining solution was disposed of as hazardous waste. TTBS was used to wash the membrane three times for 5 minutes each and the membrane was then blocked to reduce nonspecific binding of the primary antibody. This was done by incubating the membrane with 25 mL TBS supplemented with 5% nonfat dry milk overnight at 4 °C. The membrane was washed 3 times with TTBS for 5 minutes each to remove the blocking solution and then incubated for 1 hour with the primary antibody at room temperature. The three wash steps were repeated to remove any residual primary antibody not bound to the membrane. The membrane was incubated with a horseradish peroxidase-linked donkey anti-rabbit secondary antibody for 1 hour. Three final washings of the membrane removed any residual secondary antibody and enhanced chemiluminescence (ECL) was used to detect the secondary antibody. The ECL was visualized on high performance chemiluminescence film using a Kodak X-Omat.

Antibody Against the V5 Epitope Tag

Probing and visualizing of the nitrocellulose membrane with the anti-V5 antibody was performed essentially as describe above for the anti-*b* subunit antibody. The primary antibody was prepared by diluting 5 μL of anti-V5 antibody (Invitrogen) in 25 mL TTBS. The secondary antibody was a 1:10,000 dilution of horseradish peroxidase-linked sheep anti-mouse antibody. All wash steps and buffers were the same as described for the anti-*b* subunit antibody.

Densitometry Analysis of Western Blots

Western blots suitable for analysis by densitometry were scanned and digitized using the software program UN-SCAN-IT gel 6.1 (Silk Scientific). The average pixel values for bands of interest were analyzed in Microsoft Excel. Variations in film exposure time were corrected for by dividing the average pixel value of each band by the sum total of all the bands on the same Western blot. Results for crosslinked *b* subunit are reported as the fraction of dimer present,

defined as the intensity of the dimer band divided by the sum intensity of the monomer and dimer bands. Multiple repetitions of each experiment were combined to obtain the average fraction dimer and the standard deviation. Experiments involving nickel resin purified samples produced only dimeric bands and are reported in arbitrary band intensity units. Probability values that indicate the likelihood that two data sets are the same were calculated in Excel using a two-tailed Student's t-test.

CHAPTER 3
FUNCTIONAL INCORPORATION OF CHIMERIC *b* SUBUNITS INTO F_1F_O ATP SYNTHASE

Introduction

In *Esherichia coli*, the peripheral stalk is an extended homodimer of two identical *b* subunits [80, 335, 338]. In contrast, the peripheral stalks found in chloroplast F_1F_0 ATP synthase consist of two different *b*-like subunits, named subunits I and II, that form a heterodimer [382]. Some eubacteria, encompassing photosynthetic bacteria but including a few other species, also have genes encoding two *b*-like subunits designated *b* and *b′*. Both proteins have been shown to be present in purified ATP synthase from *Aquifex aeolicus* [387]. The general expectation that *b* and *b′* form a heterodimer has been supported by studies of expressed hydrophilic domains of the subunits from the cyanobacterium *Synechocystis* PCC6803 [386]. Sedimentation analyses showed that the predominant species present in equimolar mixtures of the two polypeptides had a molecular weight expected for the heterodimer, whereas the individual polypeptides gave molecular weights corresponding to monomers. Heterodimer formation was also supported by chemical crosslinking. To our knowledge, however, it has never been demonstrated that only heterodimeric stalks are formed within the enzyme, or alternatively, whether b_2 and b'_2 homodimeric stalks might also exist and support function.

Thermosynechococcus elongatus BP-1 is a thermophilic cyanobacterium whose entire genome has been sequenced [388]. Although little is known about the F_1F_0 ATP synthase of *T. elongatus* other than the sequence information, it has been used as a model organism for the study of photosynthesis [389] and circadian rhythms [390]. *T. elongatus* BP-1 has genes encoding both *b* and *b'* subunits, and these genes share a relatively high degree of sequence identity to the *Synechocystis* genes. There is approximately 50% identity and 70% similarity in the deduced amino acid sequences of both *b* and *b′* genes between the two organisms. Therefore,

it seems reasonable to assume that the *b* and *b'* subunits of *T. elongatus* will preferentially form heterodimeric peripheral stalks.

This chapter involved the construction of chimeric *b* subunits in which segments of the *E. coli uncF*(*b*) subunit gene have been replaced with either *b* or *b'* sequence from the *T. elongatus* genes (Figure 3-1). *T. elongatus* was chosen because it expresses both *b* and *b'* subunits and it is a thermophilic organism which may result in more stable chimeric constructs. The work described in this chapter has been published in a paper titled "Functional incorporation of chimeric *b* subunits into F_1F_O ATP synthase" in the August 2007 issue of the *Journal of Bacteriology* [399] (used with permission). The recombinant subunit genes were expressed alone and in combination in an *E. coli uncF*(*b*) deletion strain. Although some of the chimeric subunits failed to assemble into F_1F_0 ATP synthase complexes, others were incorporated and capable of functional complementation of the deletion strain. Expression of chimeric subunits to form only homodimeric stalks was in some cases sufficient for activity. When expressed together, the *b* and *b'* chimeric subunits readily formed heterodimeric peripheral stalks in F_1F_0 ATP synthase complexes.

Results

Plasmid Construction

A total of ten plasmids were constructed to express chimeric *E. coli/T. elongatus b* and *b'* subunits (Figure 3-2 and Table 3-1). Five of these plasmids express a chimeric *b* subunit with a histidine tag (his_6) on the amino terminus and five express a chimeric *b'* subunit with a V5 tag (GKPIPNPLLGLDST) on the carboxyl terminus. All of the constructions were done in the base plasmid pKAM14 (b_{wt}, Ap^R) [347]. The nucleotide sequence of the *uncF(b)* gene in pKAM14 coding for residues E39-A107 was replaced both in part and in full with the homologous *T. elongatus b* and *b'* sequences. The amino and carboxyl boundaries of the substituted region were

selected to avoid disturbing the environment of the critical residue b_{R36} and to prevent disruption of essential interactions between the peripheral stalk and F_1. The construction was accomplished by consecutive cassette mutagenesis steps in which fragments of pKAM14 were removed using pairs of restriction enzymes and double stranded synthetic oligonucleotides were inserted by ligation (Table 3-2). Four restriction enzyme sites were used for this construction – *SnaB*I which cuts at nucleotide 72 in the *E. coli b* subunit, *PpuM*I at nucleotide 156, *Xba*I at nucleotide 258 and *Sap*I at nucleotide 347. All of the restriction sites exist in the wild-type *uncF(b)* gene except for the engineered *Xba*I site. The *SnaB*I to *PpuM*I region spans 84 nucleotides and was replaced with oligonucleotides TG1/2 for *b* and TG3/4 for *b'*, replacing *E. coli* sequence from E39-K52. The *PpuM*I to *Xba*I region spans 102 nucleotides and was replaced with oligonucleotides TG13/10 for *b* and TG14/12 for *b'*, replacing D53-I86. The *Xba*I to *Sap*I region spans 89 nucleotides and was replaced with oligonucleotides SC39/40 for *b* and SC43/44 for *b'*, replacing L87-A107. An unwanted aspartic acid codon left in the vicinity of the *PpuM*I site was removed by site-directed mutagenesis with oligonucleotides SC59/60 ($b_{\text{-D}}$, +*Sac*II) for *b* and SC61/62 ($b'_{\text{-D}}$, +*Nhe*I) for *b'*. In all ten plasmids the substitution b_{C21S} was introduced using either TB12/13 (b_{C25S}, -*SnaB*I) or SC45/46 (b_{C25S}, +*Afl*III, -*SnaB*I) to facilitate future crosslinking studies. The genes encoding the chimeric *b* and *b'* subunit were then moved from the pKAM14-based plasmids into the expression vectors pTAM37 (b_{his}, Cm^R) and pTAM46 (b_{V5}, Ap^R), respectively [355]. See Appendix A for a detail flowchart of the plasmids construction.

Complementation Analysis

For complementation studies, plasmids pTAM37 (b_{his}, Cm^R) and pTAM46 (b_{V5}, Ap^R) were transformed into deletion strain KM2 (Δ*b*) to serve as the positive controls [355]. The epitope tags on the control *b* subunits had very little effect on enzyme activity as previously observed

[355]. The ten plasmids expressing chimeric *b* subunits were also transformed into KM2 (Δ*b*) both individually and in *b*/*b'* pairs. The ability of these plasmids to complement deletion strain KM2 (Δb) was studied by growth on minimal A media supplemented with succinate (Table 3-3). Plasmids that contained *T. elongatus b* or *b'* sequence between either D54-A107 or E39-A107 were unable to complement strain KM2. Similarly, KM2/pSBC57 ($b'_{\text{E39-D53, V5}}$) failed to grow on succinate media, but a weak positive result was obtained with strain KM2/pSBC56 ($b_{\text{E39-D53, his}}$). Much more impressive complementation was obtained with strain KM2/pSBC76 ($b'_{\text{L54-I86, V5}}$), but KM2/pSBC58 ($b_{\text{L54-I86, his}}$) did not grow. Interestingly, colony formation was in evidence when either chimeric $b_{\text{E39-I86, his}}$ or $b'_{\text{E39-I86, V5}}$ subunits were expressed.

Stability of F_1F_O Complexes

The presence of *b* subunit proteins were studied by Western analysis in order to detect expression of the recombinant *b* subunits and their incorporation into membranes. This analysis was performed on membrane samples prepared from cells expressing chimeric *b* and *b'* subunits either alone or together (Figure 3-3). The Western blots were probed with a polyclonal antibody against the *b* subunit or a monoclonal antibody against the V5 epitope tag.

The *E. coli* anti-*b* subunit antibody recognized the chimeric b_{his} subunits in membranes prepared from KM2 cells expressing the $b_{\text{E39-D53, his}}$, $b_{\text{L54-I86, his}}$ or $b_{\text{E39-I86, his}}$ subunits. Although b'_{V5} subunits appeared to be present at lower levels than the controls, these subunits were detected by the anti-V5 antibody in membranes prepared from cells expressing $b'_{\text{E39-D53, V5}}$, $b'_{\text{L54-I86, V5}}$ or $b'_{\text{E39-I86, V5}}$ subunits. The chimeric *b'* subunits were not detectable with the antibody against the *E. coli b* subunit. The first indication of a likely interaction between chimeric *b* and *b'* subunits within an F_1F_O complex was that the $b'_{\text{E39-D53, V5}}$ subunit seemed to be stabilized in the membrane in the presence of the $b_{\text{E39-D53, his}}$ subunit (Figure 3-3, E39-D53, Lanes

4 and 5). The absence of signals for chimeric *b* or *b'* subunit with *T. elongatus* sequence from D54-A107 or E39-A107 with either antibody suggested that the chimeric segment could not be extended further towards the C-terminus. These proteins apparently failed to be stably incorporated into the membranes and were degraded.

Membrane associated ATP hydrolysis was determined for KM2 cells expressing chimeric *b* and *b'* subunits (Table 3-3). Since the *b* subunit is required for association of the F_1 complex with the F_0 complex, membrane-associated ATPase activity can in some cases be used as an indirect indication of the relative amounts of intact F_1F_0 complexes stably incorporated into the membrane. As expected, only very low levels of ATP hydrolysis were observed in membranes prepared from cells expressing chimeric *b* or *b'* subunits with *T. elongatus* sequence replacing L54-A107 or E39-A107, a result that correlated well with failed complementation tests and negative Western blot results. In contrast, substantial ATP hydrolysis activity was seen with all chimeric *b* subunits with replacements between E39-D53, L54-I86 or E39-I86. Strangely, this was not true of the chimeric *b'* subunits. Membranes prepared from KM2/pSBC57 ($b'_{\text{E39-D53, V5}}$), KM2/pSBC76 ($b'_{\text{L54-I86, V5}}$), and KM2/pSBC98 ($b'_{\text{E39-I86, V5}}$) all had very little membrane associated ATP hydrolysis activity. Given that two of the strains had solidly positive complementation test results, it was necessary to look into this issue further. We successfully reproduced the complementation analysis and then sequenced plasmid DNA prepared from the colonies grown on succinate minimal media. The *uncF*(*b*) genes in these plasmids retained the designed chimeric *b* subunit gene and carried no other mutations. A recent publication suggested that a cold-stabilized form of the complex had a significant lag in ATP hydrolysis activity [400]. Therefore, ATP hydrolysis was carefully reexamined under conditions that would account for a potential lag and results essentially identical to those shown in Table 3-3 were obtained. Another

possibility was that the chimeric *b'* subunits inhibited F_1F_0 ATP hydrolysis. LDAO releases F_1 from the influence of F_0-associated mutations [101] and promotes release of the inhibitory ε subunit [215], so determination of ATP hydrolysis activity in the presence of LDAO yields a value reflecting the total F_1 present in a membrane sample. The amount of LDAO stimulation observed indicated that the KM2/pSBC76 ($b'_{L54\text{-}I86,\ V5}$) and KM2/pSBC98 ($b'_{E39\text{-}I86,\ V5}$) samples had only minimal F_1 bound. Therefore, it seems that although the two strains grew well indicating abundant F_1F_0 ATP synthase function *in vivo*, the F_1F_0 complexes were not stable and were lost during membrane preparation. The reduced levels of b'_{V5} subunits seen during the Western analysis (Figure 3-3) lent further support to this interpretation.

Coupled F_1F_O Activity

ATP-driven proton pumping in membrane vesicles was used to detect coupled activity in F_1F_0 complexes with chimeric peripheral stalks (Figure 3-4). Acidification of inverted membrane vesicles was monitored by fluorescence quenching of ACMA. All membrane samples had strong ACMA quenching upon addition of NADH, confirming the membrane vesicles were intact and closed. KM2/pSBC57 ($b'_{E39\text{-}D53,\ V5}$) membranes showed no proton pumping activity, but strong fluorescence quenching was seen in KM2/pSBC56 ($b_{E39\text{-}D53,\ his}$) membranes (Figure 3-4A, blue traces). KM2/pSBC58 ($b_{L54\text{-}I86,\ his}$) and KM2/pSBC76 ($b'_{L54\text{-}I86,\ V5}$) membranes showed low but detectable levels of ATP-driven proton pumping (Figure 3-4A, red traces). No activity was observed in membranes prepared from either KM2/pSBC94 ($b_{L54\text{-}A107,\ his}$) or KM2/pSBC79 ($b'_{L54\text{-}A107,\ V5}$) (Figure 3-4B, purple traces). Surprisingly, fluorescence quenching was detectable in membranes from KM2/pSBC95 ($b_{E39\text{-}A107,\ his}$) when analyzed on a more sensitive spectrofluorometer (Figure 3-4C). The most interesting results were obtained by looking at the E39-I86 chimeric subunits (Figure 3-4B, green traces). Coexpression of the

chimeric $b_{E39\text{-}I85,\ his}$ and $b'_{E39\text{-}I86,\ V5}$ subunits reproducibly yielded higher proton pumping activity than expression of either of the individual subunits alone. Moreover, the initial rate of fluorescence quenching was substantially higher in the KM2/pSBC97/pSBC98 ($b_{E39\text{-}I86,\ his}/b'_{E39\text{-}I86,\ V5}$) membranes (Table 3-4). These results might have reflected either the additive activity from the $(b_{E39\text{-}I86,\ his})_2$ and $(b'_{E39\text{-}I86,\ V5})_2$ homodimeric complexes, or more likely, the presence of F_1F_0 complexes containing $b_{E39\text{-}I86,\ his}/b'_{E39\text{-}I86,\ V5}$ heterodimeric complexes.

Detection of Heterodimers

In order to detect F_1F_0 complexes with heterodimeric peripheral stalks, a nickel-resin purification procedure developed previously in our lab [355] was used to examine membranes prepared from KM2/pSBC97/pSBC98 ($b_{E39\text{-}I86,\ his}/b'_{E39\text{-}I86,\ V5}$) (Figure 3-5B, Lanes 1-10). Four important controls were included in the experiment. To confirm that the resin was only retaining F_1F_0 complexes containing the chimeric $b_{E39\text{-}I86,\ his}$ subunit, membranes prepared from KM2/pSBC98 ($b'_{E39\text{-}I86,\ V5}$) were processed and no bands were observed using either the anti-*b* or anti-V5 antibodies (lane 6). F_1F_0 complexes from KM2/pSBC97 ($b_{E39\text{-}I86,\ his}$) were purified as a positive control to demonstrate that the resin retained histidine tagged complexes and the anti-V5 antibody detected nothing in samples lacking a V5 epitope tag (lane 7). To address possible aggregation of F_1F_0 complexes during sample preparation, membranes from strains KM2/pSBC97 ($b_{E39\text{-}I86,\ his}$) and KM2/pSBC98 ($b'_{E39\text{-}I86,\ V5}$) were mixed prior to solubilization. As expected, no band was observed using the anti-V5 antibody (lane 8). The positive control was Ni-resin purified F_1F_0 complexes from KM2/pTAM37/pTAM46 (b_{his}/b_{V5}). The presence of complexes containing heterodimeric b_{his}/b_{V5} peripheral stalks was demonstrated by signals from both the anti-*b* and anti-V5 antibodies (lane 10). An essentially identical result was obtained using membranes from KM2/pSBC97/pSBC98 ($b_{E39\text{-}I86,\ his}/b'_{E39\text{-}I86,\ V5}$) (lane 9). The $b'_{E39\text{-}I86,\ V5}$

subunit could only have been retained in the Nickel-resin purified material if it were part of an F_1F_0 complex containing a $b_{E39\text{-}I86,\ his}$ subunit.

Trypsin digestion of membranes samples was used to confirm that the heterodimeric peripheral stalks were incorporated into intact F_1F_0 complexes. A portion of the wild-type b_{V5} subunit remained resistant to degradation during an extended overdigestion with trypsin when expressed in the presence of the other F_1F_0 ATP synthase genes (Figure 3-5A, KM2 digestion). This same subunit was degraded when expressed alone in strain 1100 ΔBC (Δ*unc*), demonstrating that the incorporation of the *b* subunit into an intact F_1F_0 complex protects the peripheral stalk from trypsin digestion. This result is consistent with what has been previously observed [332]. A Western blot using the more sensitive anti-V5 antibody revealed that a small portion of the *b* subunit was resistant to degradation even in the absence of the rest of the F_1F_O subunits (Figure 3-5B). Membrane prepared from the strain KM2/pSBC97/pSBC98 ($b_{E39\text{-}I86,\ his}/b'_{E39\text{-}I86,\ V5}$) showed that a portion of the chimeric subunits were also protected from degradation in the presence of the other subunits. Ni-resin purification of samples digested with trypsin demonstrated that the heterodimeric peripheral stalks were incorporated into intact F_1F_0 complexes (Figure 3-5B, Lanes 11-16). A band was seen using the anti-V5 antibody after 3 hours of trypsin digestion for both the positive control KM2/pTAM37/pTAM46 (b_{his}/b_{V5}) and the chimeric KM2/pSBC97/pSBC98 ($b_{E39\text{-}I86,\ his}/b'_{E39\text{-}I86,\ V5}$) sample, but not for the 1100 ΔBC/pSBC97/pSBC98 ($b_{E39\text{-}I86,\ his}/b'_{E39\text{-}I86,\ V5}$) sample. The $b'_{E39\text{-}I86,\ V5}$ subunit survived trypsin digestion and Ni-resin purification as a component of a heterodimeric F_1F_0 complex containing the $b_{E39\text{-}I86,\ his}$ subunit.

Discussion

A series of plasmids have been constructed that were designed to express chimeric subunits such that portions of the tether and dimerization domains of the *E. coli* F_1F_0 ATP synthase *b* subunit were replaced with homologous sequences from the *b* and *b'* subunits of the thermophilic cyanobacterium *T. elongatus*. The chimeric subunits with the largest successful *T. elongatus* segments had replacements spanning positions E39-I86. The chimeric $b_{E39\text{-}I86}$ and $b'_{E39\text{-}I86}$ subunits each contained a total of 48 replaced amino acids, or almost one-third of the entire *b* subunit. Plasmids expressing either recombinant chimeric subunit were individually capable of genetic complementation of an *uncF*(*b*) deletion strain. In addition to the homodimeric stalks formed by the expression of each subunit alone, co-expression of the $b_{E39\text{-}I86}$ and $b'_{E39\text{-}I86}$ subunits yielded readily detectable F_1F_0 complexes with heterodimeric peripheral stalks. Attempts to extend the *T. elongatus* segment further toward the carboxyl terminus resulted in failure. The most logical interpretation was that critical interactions between the peripheral stalk and F_1 known to occur in this area of the *b* subunit [367, 378] were interrupted, leading to a general defect in assembly of the F_1F_0 complex.

The secondary structure of the *b* subunit throughout the area under study here is thought to be an extended, linear α-helix [335]. This has been confirmed by x-ray crystallography for the section covering amino acids 66-122 [358]. In view of the properties of tether domain insertion and deletion mutants [353-355], one might have expected that any α-helical sequence substituted in the tether domain would be sufficient if the protein-protein contacts within F_0 and F_1 were maintained. However, the $b'_{E39\text{-}D53,\ V5}$ chimeric subunit was fully defective. Extension of the chimeric region in the $b'_{E39\text{-}I86,\ V5}$ subunit resulted in formation of an active F_1F_0 ATP synthase. Therefore, the structural defect induced by the substitutions in $b'_{E39\text{-}D53}$ region was dramatically suppressed within the $b'_{E39\text{-}I86}$ subunit. The phenotype of the defective $b_{L54\text{-}I86,\ his}$ subunit was

suppressed to a lesser degree in the $b_{E39\text{-}I86,\ his}$ subunit. The evidence suggests that there must be determinants throughout the E39-I86 section of the *b* subunit that act together to specify the structure of the peripheral stalk. The obvious interpretation is that multiple protein-protein interactions between the two *b* subunits likely provide these structural determinants. There is ample evidence for direct contacts within the dimerization domain [318, 331]. To date, there is no evidence of intimate interactions between the two *b* subunits within the tether domain between positions K23-D53.

F_1F_0 complexes containing chimeric *b′* subunits were much less stable *in vitro* than complexes with chimeric *b* subunits. Within the E39-I86 segment there are 14 amino acids found in the *E. coli* and *T. elongatus b* subunits that are different in subunit *b′* (Figure 3-1). While it is possible that these specific amino acids have an important influence on F_1F_0 complex stability, it seems more likely that the overall structure of the *b′* subunit does not necessarily favor maintenance of the inter-subunit contacts needed for a stable enzyme in aqueous buffers. This view is supported by the observation that the levels of $b'_{E39\text{-}D53}$, $b'_{L54\text{-}I86}$ and $b'_{E39\text{-}I86}$ were all increased by coexpression with the cognate *b* subunit (Figure 3-3). Therefore, formation of chimeric *b*/*b′* heterodimeric F_1F_0 complexes seems to stabilize the chimeric *b′* subunits *in vitro*.

Table 3-1. Plasmids used in this chapter

Plasmids	Gene product[a]	Antibiotic resistance[b]	Source or reference
pBR322	Δb	Ap	New England Biolabs
pKAM14	b_{wt}	Ap	[365]
pTAM37	b_{his}	Cm	[355]
pTAM46	b_{V5}	Ap	[355]
pSBC56	$b_{C21S,\ E39\text{-}D53,\ his}$	Cm	This study
pSBC57	$b'_{C21S,\ E39\text{-}D53,\ V5}$	Ap	This study
pSBC58	$b_{C21S,\ L54\text{-}I86,\ his}$	Cm	This study
pSBC76	$b'_{C21S,\ L54\text{-}I86,\ V5}$	Ap	This study
pSBC97	$b_{C21S,\ E39\text{-}I86,\ his}$	Cm	This study
pSBC98	$b'_{C21S,\ E39\text{-}I86,\ V5}$	Ap	This study
pSBC94	$b_{C21S,\ L54\text{-}A107,\ his}$	Cm	This study
pSBC79	$b'_{C21S,\ L54\text{-}A107,\ V5}$	Ap	This study
pSBC95	$b_{C21S,\ E39\text{-}A107,\ his}$	Cm	This study
pSBC96	$b'_{C21S,\ E39\text{-}A107,\ V5}$	Ap	This study

[a]his, six-histidine tag at the amino terminus; V5, epitope tag with the sequence GKPIPNPLLGLDS appended to the carboxyl terminus. Replaced regions are designated by the first and last *E. coli* amino acids that were replaced with *T. elongatus* sequence.

[b]Ap, ampicillin; Cm, chloramphenicol.

Table 3-2. Synthetic oligonucleotides used in this chapter

Oligos	Annealed oligonucleotides[a]
TG1/2[b]	TG1 5′-GTATGGCCGCCACTGATGGCAGCCATCGAAAAACGTCAAAAACAGATCGCTACTGCTATCGCTGAAGCTGAAGAACGTCAGAAG-3′
$b_{E39\text{-}D53}$	TG2 3′-CATACCGGCGGTGACTACCGTCGGTAGCTTTTTGCAGTTTTTGTCTAGCGATGACGATAGCGACTTCGACTTCTTGCAGTCTTCCTG-5′
TG3/4	TG3 5′-GTATGGCCGCCACTGATGGCAGCCATCGAAAAACGTCAAAAATACATCCGTACTAACCTGCAGCAGGCTAAAGAACGTCTGCAGCAG-3′
$b'_{E39\text{-}D53}$	TG4 3′-CATACCGGCGGTGACTACCGTCGGTAGCTTTTTGCAGTTTTTATGTAGGCATGATTGGACGTCGTCCGATTTCTTGCAGACGTCGTCCTG-5′
TG13/10[c]	TG13 5′-GACGTTGCTGCTGCTCGTCTGGCTGAAGCTCAGCAGAAACTGACTCAGGCTAAACAGGAGGCTCAGCGTATCCGTGAAGATGCTCTGACTCGTGCTAAAGCTGTT-3′
$b_{L54\text{-}I86}$	TG10 3′-CAACGACGACGAGCAGACCGACTTCGAGTCGTCTTTGACTGAGTCCGATTTGTCCTCCGAGTCGCATAGGCACTTCTACGAGACTGAGCACGATTTCGACAAGATC-5′
TG14/12	TG14 5′-GACGCTACTGAACTGGCTCAGCAGTACGAACAGGAGCTGGCTTCCACTCGTCGTCAGGCTCAGGCTCTGATCGAAGAAGCTCGTGTTGAAGCTCAGAAAATT-3′
$b'_{L54\text{-}I86}$	TG12 3′-CGATGACTTGACCGAGTCGTCATGCTTGTCCTCGACCGAAGGTGAGCAGCAGTCCGAGTCCGAGACTAGCTTCTTCGAGCACAACTTCGAGTCTTTTAAGATC-5′
SC39/40[d]	SC39 5′-CTAGAAGAAATTATTGCTCAGGCTAAACGTGAAATTGAACGTCTGCAGGAGACCGCTAGCCAGGAAATTGAAGCCGAGCGTAAACGTGC-3′
$b_{L87\text{-}A107}$	SC40 3′-TTCTTTAATAACGAGTCCGATTTGCACTTTAACTTGCAGACGTCCTCTGGCGATCGGTCCTTTAACTTCGGCTCGCATTTGCACGGGC-5′
SC43/44	SC43 5′-CTAGATGCGGAAATTGCGGAAGCGCAGCAGGCGGTCCAGGCGGAGCTCTTGAAAATTCAGGCGGAAATTGAAGCCGAGCGTAAACGTGC-3′
$b'_{L87\text{-}A107}$	SC44 3′-TACGCCTTTAACGCCTTCGCGTCGTCCGCCAGGTCCGCCTCGAGAACTTTTAAGTCCGCCTTTAACTTCGGCTCGCATTTGCACGGGC-5′
SC45/46	SC45 5′-CTGTTCGTTCTGTTCTCCATGAAGTACGTGTGGCCGCC-3′
b_{C21S},+*Afl*III	SC46 3′-GACAAGCAAGACAAGAGGTACTTCATGCACACCGGCGG-5′
TB12/13	TB12 5′-CTGTTCGTTCTGTTCTCCATGAAGTACGTTTGGCCGCC-3′
b_{C21S},-*SnaB*I	TB13 3′- GACAAGCAAGACAAGAGGTACTTCATGCAAACCGGCGG-5′
SC59/60[e]	SC59 5′-ACTGCTATCGCTGAAGCTGAAGAACGTCAGAAGGTTGCCGCGGCTCGTCTGGCTGAAGCTCAGCAGAAACTG-3′
b_{-D}, +*Sac*II	SC60 3′-TGACGATAGCGACTTCGACTTCTTGCAGTCTTCCAACGGCGCCGAGCAGACCGACTTCGAGTCGTCTTTGAC-5′
SC61/62	SC61 5′-ACTAACCTGCAGCAGGCTAAAGAACGTCTGCAGCAGGCTACTGAGCTAGCTCAGCAGTACGAACAGGAGCTGGCT-3′
b'_{-D}, +*Nhe*I	SC62 3′-TGATTGGACGTCGTCCGATTTCTTGCAGACGTCGTCCGATGACTCGATCGAGTCGTCATGCTTGTCCTCGACCGA-5′
SC53/54	SC53 5′-GCTGCTAACAGCGACATCGTGGATAAACTAGTCGCTGAACTGTAAGGAGGGAGG-3′
b_{+SpeI}	SC54 3′-CGACGATTGTCGCTGTAGCACCTATTTGATCAGCGACTTGACATTCCTCCCTCC-5′
SC57/58	SC57 5′-CTGTTCGTTCTGTTCTCCATGAAGTACGTATGGCCGCC-3′
b_{+SnaBI}	SC58 3′-GACAAGCAAGACAAGAGGTACTTCATGCATACCGGCGG-5′
TB38/39	TB38 5′-CGTGGATAAACTTGTCGCTGAGCTCGGTAAACCGATCCCGAACCCGCTGCTGGGTCTGGACTCTACCTAAGGAGGGAGGGGCTGATG-3′
b_{+V5}, +*Sac*I	TB39 3′-GCACCTATTTGAACAGCGACTCGAGCCATTTGGCTAGGGCTTGGGCGACGACCCAGACCTGAGATGGATTCCTCCCTCCCCGACTAC-5′

[a]Added restriction sites are underlined.
[b]Oligonucleotides TG1/2 (*b*) and TG3/4 (*b'*) were used to replace DNA between restriction sites *SnaB*I and *PpuM*I.
[c]Oligonucleotides TG13/10 (*b*) and TG14/12 (*b'*) were used to replace DNA between restriction sites *PpuM*I and *Xba*I.
[d]Oligonucleotides SC39/40 (*b*) and SC43/44 (*b'*) were used to replace DNA between restriction sites *Xba*I and *Sap*I.
[e]Oligonucleotides SC59/60 (*b*) and SC61/62 (*b'*) were used to remove an unwanted aspartic acid between the E39-to-D53 and L54-to-I86 regions.

Table 3-3. Growth properties and ATPase activity in cells expressing chimeric subunits

Strain/plamids	Gene products	Succinate growth[a]	ATP hydrolysis activity[b]	
			No LDAO[c]	0.5% LDAO
KM2/pTAM37/pTAM46	b_{his}/b_{V5}	+++	0.62 ± 0.04	1.21 ± 0.01
KM2/pBR322	Δb	–	0.13 ± 0.02	0.22 ± 0.01
KM2/pSBC56	$b_{C21S,\ E39\text{-}D53,\ his}$	+	0.58 ± 0.03	1.27 ± 0.07
KM2/pSBC57	$b'_{C21S,\ E39\text{-}D53,\ V5}$	–	0.20 ± 0.01	0.18 ± 0.04
KM2/pSBC56/pSBC57	$b_{C21S,\ E39\text{-}D53,\ his}/b'_{C21S,\ E39\text{-}D53,\ V5}$	+	0.61 ± 0.02	1.26 ± 0.06
KM2/pSBC58	$b_{C21S,\ L54\text{-}I86,\ his}$	–	0.42 ± 0.01	0.71 ± 0.02
KM2/pSBC76	$b'_{C21S,\ L54\text{-}I86,\ V5}$	+++	0.22 ± 0.01	0.31 ± 0.02
KM2/pSBC58/pSBC76	$b_{C21S,\ L54\text{-}I86,\ his}/b'_{C21S,\ L54\text{-}I86,\ V5}$	+++	0.47 ± 0.03	0.76 ± 0.06
KM2/pSBC97	$b_{C21S,\ E39\text{-}I86,\ his}$	+	0.50 ± 0.04	0.87 ± 0.08
KM2/pSBC98	$b'_{C21S,\ E39\text{-}I86,\ V5}$	++	0.19 ± 0.01	0.26 ± 0.01
KM2/pSBC97/pSBC98	$b_{C21S,\ E39\text{-}I86,\ his}/b'_{C21S,\ E39\text{-}I86,\ V5}$	++	0.49 ± 0.04	0.88 ± 0.02
KM2/pSBC94	$b_{C21S,\ L54\text{-}A107,\ his}$	–	0.22 ± 0.01	0.30 ± 0.01
KM2/pSBC79	$b'_{C21S,\ L54\text{-}A107,\ V5}$	–	0.15 ± 0.01	0.44 ± 0.03
KM2/pSBC94/pSBC79	$b_{C21S,\ L54\text{-}A107,\ his}/b'_{C21S,\ L54\text{-}A107,\ V5}$	–	0.23 ± 0.03	0.29 ± 0.03
KM2/pSBC95	$b_{C21S,\ E39\text{-}A107,\ his}$	–	0.12 ± 0.03	0.34 ± 0.01
KM2/pSBC96	$b'_{C21S,\ E39\text{-}A107,\ V5}$	–	0.12 ± 0.02	0.16 ± 0.03
KM2/pSBC95/pSBC96	$b_{C21S,\ E39\text{-}A107,\ his}/b'_{C21S,\ E39\text{-}A107,\ V5}$	–	0.14 ± 0.03	0.37 ± 0.02

[a]Symbols: +++, wild-type growth; ++, colonies smaller than wild-type; +, small colony formation; –, no growth.
[b]Reported in µmol of P_i/mg of membrane protein/min.
[c]Used to release F_1 from the inhibitory effect of F_O.

Table 3-4. Proton pumping rates of membranes prepared from cells expressing chimeric E39-I86 subunits

Strain/plasmids	Gene products	Final fluorescence value (percent)	Initial rate of decrease (percent/min)
KM2/pTAM37/pTAM46	b_{his}/b_{V5}	22.2 ± 0.1	66.9 ± 0.6
KM2/pBR322	Δb	91.7 ± 0.5	0.5 ± 0.2
KM2/pSBC97	$b_{C21S,\ E39\text{-}I86,\ his}$	34.5 ± 0.8	27 ± 2
KM2/pSBC98	$b'_{C21S,\ E39\text{-}I86,\ V5}$	76.0 ± 0.4	6.1 ± 1.1
KM2/pSBC97/pSBC98	$b_{C21S,\ E39\text{-}I86,\ his}/b'_{C21S,\ E39\text{-}I86,\ V5}$	28.0 ± 0.5	48 ± 3

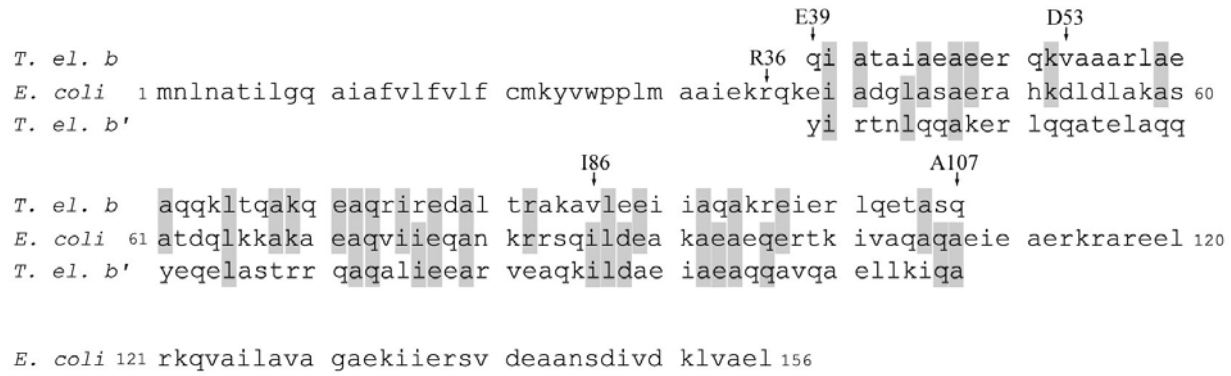

Figure 3-1. Alignment of *E. coli* and *T. elongatus* sequences. The full length *E. coli b* subunit is shown aligned to the region of the *T. elongatus b* and *b'* subunits corresponding to E39-A107. Identical amino acids are highlighted in grey and the positions mentioned in the text are labeled.

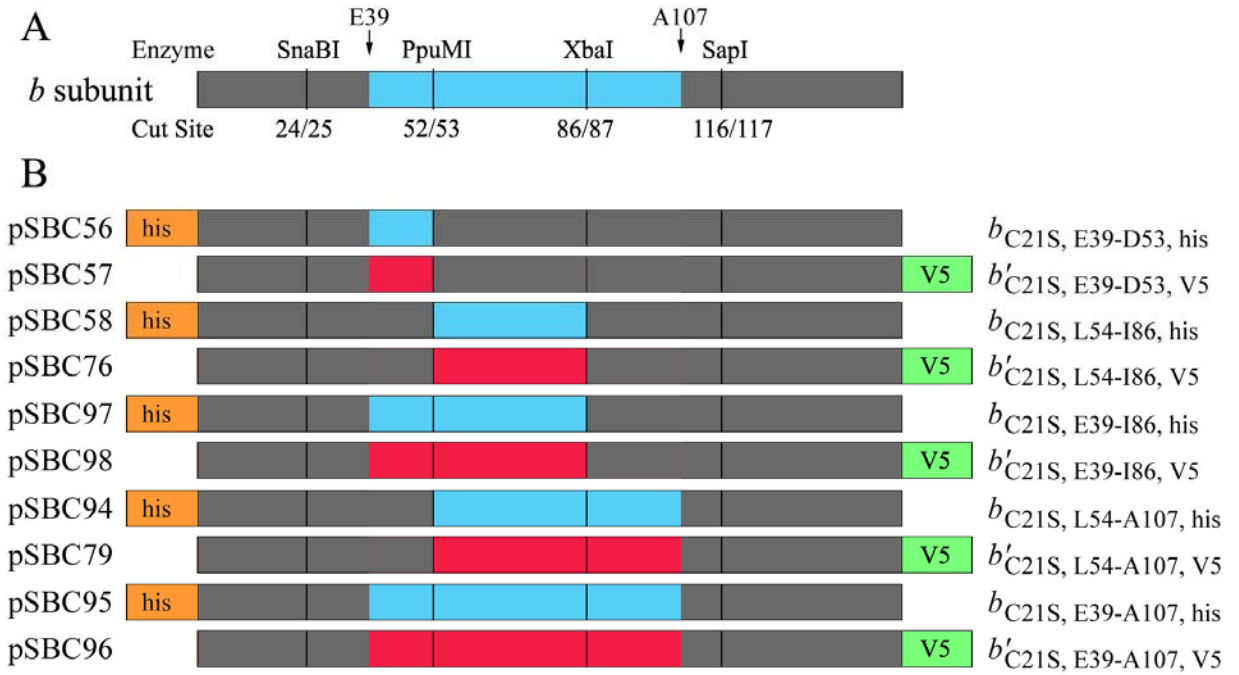

Figure 3-2. Plasmids used in this study. A) Map of the *b* subunit showing the relevant features used in plasmid construction. The wild-type *E. coli b* subunit sequence is colored gray and the region replaced by homologous sequence from *T. elongatus* is blue. The first and last amino acids of the replaced regions are indicated above the *b* subunit along with the restriction sites used for cassette mutagenesis. The amino acids where these enzymes cut are indicated below the b subunit. B) A graphical representation of the ten chimeric *b* subunits used in this study. The plasmid names are listed on the left and the expressed subunits on the right. Regions of the wild-type *b* subunit that were replaced with *T. elongatus b* subunit are colored blue and *b'* subunit colored red. A six histidine tag on the amino terminus is shown in orange and a V5 epitope tag on the carboxyl terminus with the sequence GKPIPNPLLGLDS is shown in green.

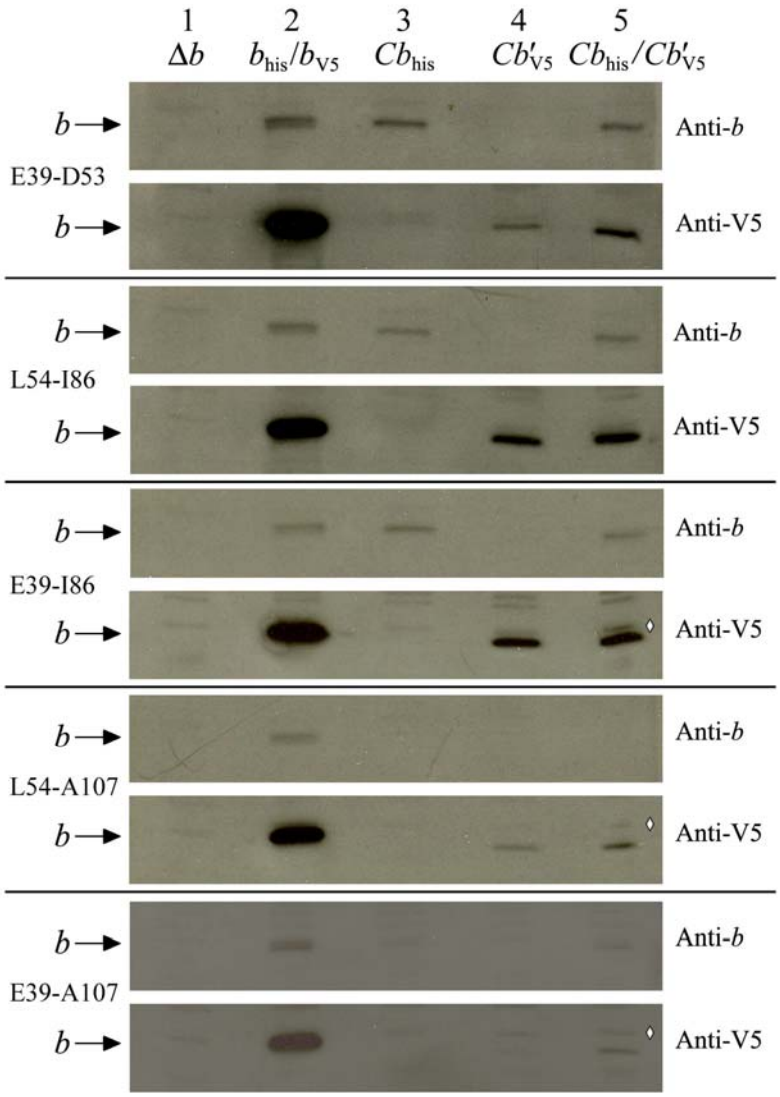

Figure 3-3. Immunoblot of membranes prepared from *E. coli* strain KM2 (Δ*b*) expressing chimeric *b* subunits. Aliquots of membrane proteins (1 μg) were separated on 15% SDS-PAGE gels and transferred to nitrocellulose membranes as previously described [349]. The presence of *b* subunit was detected using both a polyclonal antibody raised against the *b* subunit and an antibody against the V5 epitope tag appended to the carboxyl terminus of the chimeric *b'* subunits. The position of the *b* subunit band and the region that was replaced with *T. elongatus* sequence are indicated on the left side of the figure and the primary antibody on the right. Membrane samples were loaded as follows: Lane 1, negative control KM2/pBR322 (Δb); Lane 2, positive control KM2/pTAM37/pTAM46 (b_{his}/b_{V5}); Lane 3, chimeric b_{his} subunits; Lane 4, chimeric b'_{V5} subunits; Lane 5, coexpression of chimeric b_{his} and b'_{V5} subunits. The commercial anti-V5 antibody gave a much stronger signal than the polyclonal anti-*b* subunit antibody and also detected an extra band running near the level of the *b* subunit, indicated in Lane 5 with a white diamond (◊).

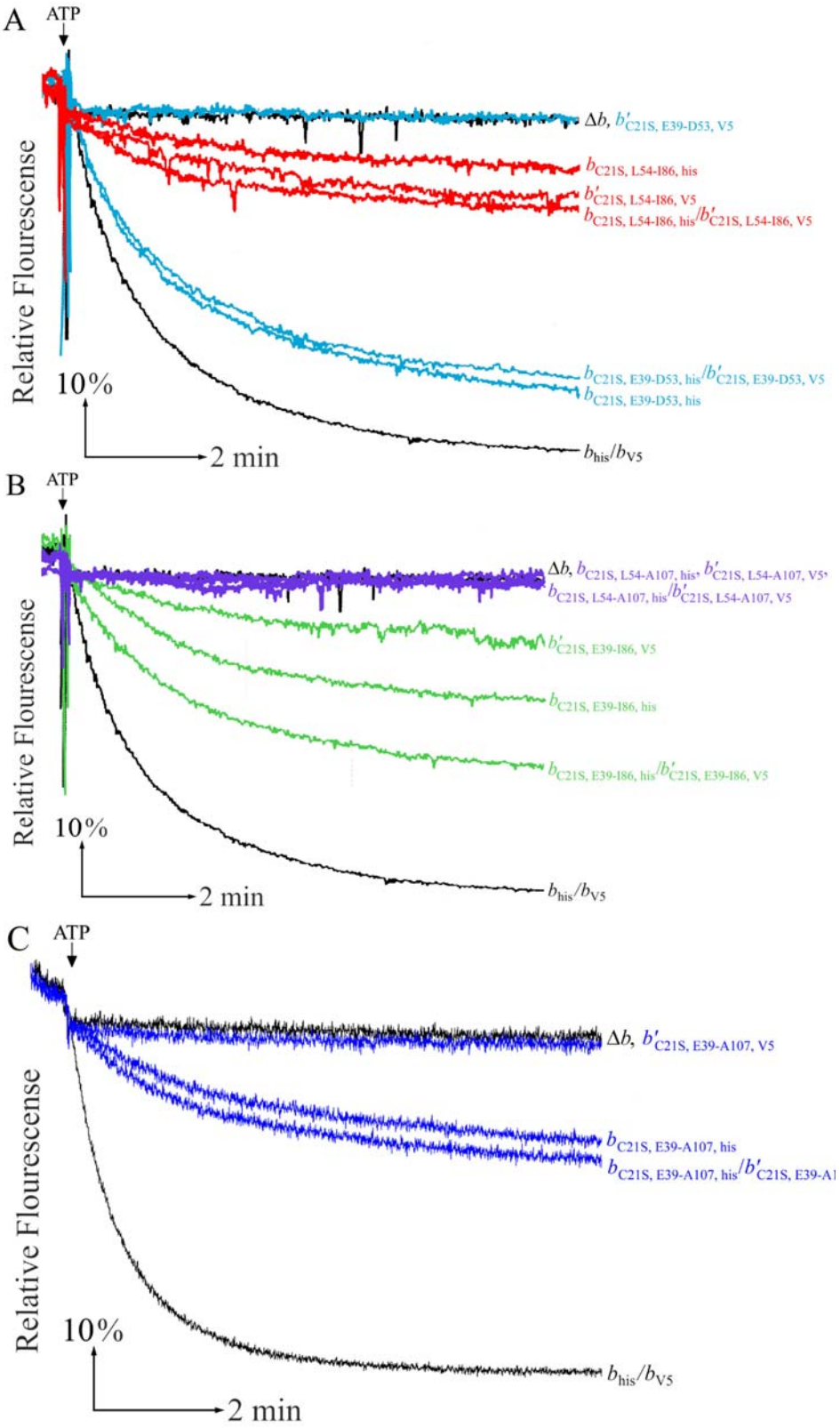

Figure 3-4. See next page for legend.

Figure 3-4. Proton pumping driven by ATP in membrane vesicles prepared from KM2 (Δb) cells expressing chimeric *b* subunits (see figure previous page). Aliquots of membrane proteins (500 μg) were suspended in 3.5 mL assay buffer (50 mM MOPS, pH 7.3, 10 mM $MgCl_2$) and fluorescence quenching of 9-amino-6-chloro-2-methoxyacridine (ACMA) was used to detect proton pumping in membrane vesicles after the addition of ATP as previously described [354]. The traces are plotted as relative fluorescence over time. The point where ATP was added is indicated above each graph and the chimeric subunits are indicated to the right of each trace. Each panel shows traces of membranes from the negative control KM2/pBR322 (Δb), positive control KM2/pTAM37/pTAM46 (b_{his}/b_{V5}), and the *b* and *b'* chimeric subunits expressed individually and together. A) Chimeric subunits containing *T. elongatus* sequence for the E39-D53 and L54-I86 regions. B) Chimeric subunits containing *T. elongatus* sequence for the E39-I86 and L54-A107 regions. C) Chimeric subunits containing *T. elongatus* sequence for the E39-A107 region. Assay for Panels A and B were obtained using a Perkin-Elmer LS-3B spectrofluorometer while Panel C was obtained using a Photon Technologies International QuantaMaster 4 spectrofluorometer.

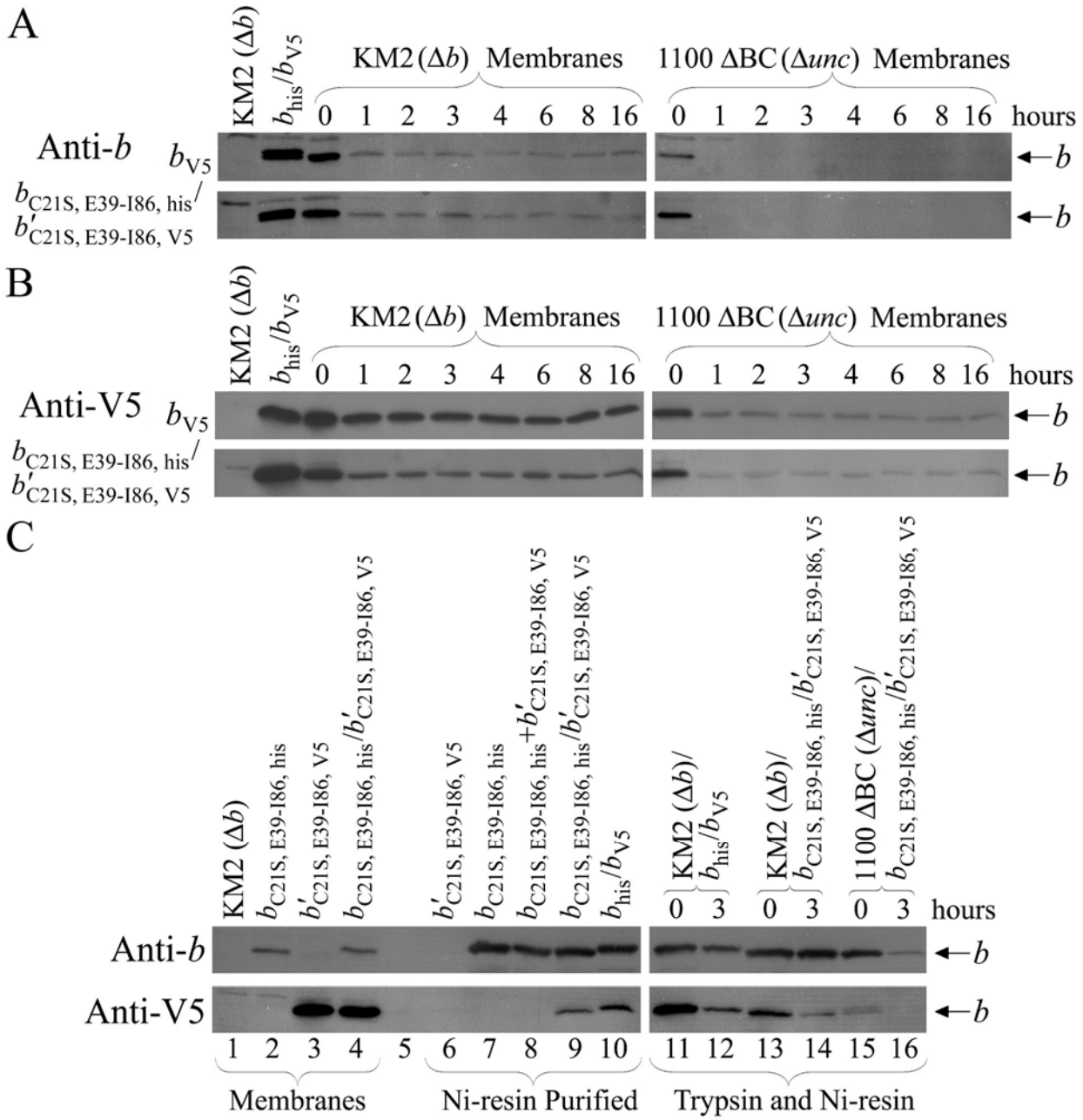

Figure 3-5. See next page for legend.

Figure 3-5. Incorporation of heterodimeric peripheral stalks into F_1F_O ATP synthase complexes (see figure previous page). Membranes samples were digested with trypsin and analyzed by Western blot as in Figure 3-3. Primary antibody against the *b* subunit is shown in Panel A and the V5 epitope tag is shown in Panel B. Membranes were prepared from strains KM2/pTAM46 (b_{V5}), 1100 ΔBC/pTAM46 (b_{V5}), KM2/pSBC97/pSBC98 ($b_{E39\text{-}I86,\ his}/b'_{E39\text{-}I86,\ V5}$) and 1100 ΔBC/pSBC97/pSBC98 ($b_{E39\text{-}I86,\ his}/b'_{E39\text{-}I86,\ V5}$). Proteolytic digestion and collection of aliquots were performed as described under experimental procedures. C) Aliquots of membrane samples were solubilized and purified over Ni-CAM as previously described [355]. A total of 10% of the total elutant from the Ni-resin purification was loaded in each lane of purified protein. Western blots were performed with antibodies against both the b subunit and the V5 epitope tag. Membranes were loaded into the lanes as follows: Lanes 1-4, 1 μg of nonpurified membranes from KM2/pBR322 (Δb), KM2/pSBC97 ($b_{E39\text{-}I86,\ his}$), KM2/pSBC98 ($b'_{E39\text{-}I86,\ V5}$) and KM2/pSBC97/pSBC98 ($b_{E39\text{-}I86,\ his}/b'_{E39\text{-}I86,\ V5}$); Lane 5, intentionally left empty; Lane 6, Ni-resin negative control KM2/pSBC98 ($b'_{E39\text{-}I86,\ V5}$); Lane 7, Ni-resin positive control KM2/pSBC97 ($b_{E39\text{-}I86,\ his}$); Lane 8, Ni-resin aggregation control KM2/pSBC97 ($b_{E39\text{-}I86,\ his}$) + KM2/pSBC98 ($b'_{E39\text{-}I86,\ V5}$); Lane 9, purification of KM2/pSBC97/pSBC98 ($b_{E39\text{-}I86,\ his}/b'_{E39\text{-}I86,\ V5}$); Lane 10, purification of heterodimer positive control KM2/pTAM37/pTAM46 (b_{his}/b_{V5}); Lanes 11 and 12, purification of trypsin digested KM2/pTAM37/pTAM46 (b_{his}/b_{V5}) at 0 and 3 hours; Lanes 13 and 14, purification of trypsin digested KM2/pSBC97/pSBC98 ($b_{E39\text{-}I86,\ his}/b'_{E39\text{-}I86,\ V5}$); Lanes 15 and 16, purification of trypsin digested 1100 ΔBC/pSBC97/pSBC98 ($b_{E39\text{-}I86,\ his}/b'_{E39\text{-}I86,\ V5}$, Δ*unc*).

CHAPTER 4
DISULFIDE CROSSLINK FORMATION WITHIN CHIMERIC PERIPHERAL STALKS OF *E. coli* F_1F_O ATP SYNTHASE

Introduction

In Chapter 3, I have shown that regions of the *Escherichia coli b* subunit tether and dimerization domains can be replaced with homologous sequence from the *b* and *b'* subunits of the photosynthetic organism *Thermosynechococcus elongatus* BP-1. These results were published in the *Journal of Bacteriology* [399]. The pair of chimeric subunits with *T. elongatus b* and *b'* sequence substituted in the region E39-I86 produced heterodimeric peripheral stalks and supported F_1F_O ATP synthase function. In the present chapter these chimeric subunits, $b_{E39\text{-}I86,\ his}$ and $b'_{E39\text{-}I86,\ V5}$, will be referred to as *Tb* and *Tb'* for simplicity.

Disulfide crosslinking results obtained from working with a soluble $b_{V25\text{-}L156}$ subunit which lacks the N-terminal membrane spanning domain have suggested that the *b* subunits may be arranged in a staggered conformation throughout the dimerization domain rather than in perfect register [326, 359]. This staggered model developed in the laboratory of our collaborator Dr. Stanley Dunn (University of Western Ontario) places residues b_{R83} and b_{A90} in close proximity.

To investigate this model in intact F_1F_O complexes, we have engineered cysteines into the *Tb* and *Tb'* subunits and analyzed the tendency for disulfide crosslinks to form between recombinant subunits under varying experimental conditions. Our results can be interpreted as support for a staggered model in intact F_1F_O containing a chimeric peripheral stalk. The evidence indicates residues Tb_{A83C} and Tb'_{A90C} are located in close spatial proximity. We also consider whether the activation of F_1F_O by ATP produced any detectable change in the efficiency of crosslink formation. An effect was observed at high concentrations of substrate, but it could not be attributed to catalytic activity.

Results

Functional Characterization of Cysteine Mutants

Four plasmids were constructed to express chimeric *b* subunits with individual cysteine substitutions at residues A83 and A90. Site-directed mutagenesis with the oligonucleotides listed in Table 4-1 was used to generate these four plasmids, listed in Table 4-2. Plasmids pSBC123 (Tb_{A83C}) and pSBC124 (Tb_{A90C}) were generated from the parent plasmid pSBC97 (*Tb*) while plasmids pSBC125 (Tb'_{A83C}) and pSBC126 (Tb'_{A90C}) were generated from pSBC98 (*Tb'*). All plasmids were confirmed by direct nucleotide sequencing. Growth on minimal A media supplemented with succinate was used as a test of F_1F_O ATP synthesis activity. None of the cysteine substitutions had any significant effect on the growth properties of mutants expressing homodimeric peripheral stalks as shown in Table 4-2 and Figure 4-1. All of the chimeric *b* subunits complemented deletion strain KM2 (Δ*b*) by supporting growth by oxidative phosphorylation. Likewise, all strains coexpressing both *Tb* and *Tb'* chimeric subunits with cysteine substitutions were capable of growth using succinate as the sole carbon source. Three of these strains, KM2/pSBC123/pSBC125 (Tb_{A83C}/Tb'_{A83C}), KM2/pSBC123/pSBC126 (Tb_{A83C}/Tb'_{A90C}) and KM2/pSBC124/pSBC126 (Tb_{A90C}/Tb'_{A90C}) grew in a manner comparable to the KM2/pSBC97/pSBC98 (*Tb*/*Tb'*) control. The fourth strain, KM2/pSBC124/pSBC125 (Tb_{A90C}/Tb'_{A83C}), exhibited smaller colony formation than the control but still retained biologically significant levels of enzyme function.

Membranes containing chimeric peripheral stalks with cysteine substitutions were assayed for ATP hydrolysis activity in both the absence and presence of 0.5% LDAO as listed in Table 4-2. The rate of ATP hydrolysis was used as an indirect measure of the amount of intact and assembled F_1F_O present. LDAO releases the F_1 subunit from the inhibitory effects of the ε

subunit [208, 215], producing information about the extent of coupling between F_1 and F_O. Membranes were prepared in the presence of 5 mM tris(2-carboxyethyl) phosphine (TCEP), a water-soluble reducing agent that maintains the cysteines in a reduced state (see below). An abundant amount of ATPase activity was observed for the strains KM2/pSBC123 (Tb_{A83C}) and KM2/pSBC124 (Tb_{A90C}). These strains exhibited ATP hydrolysis rate around 70% of the parent KM2/pSBC97 (*Tb*) strain that contained no cysteine substitutions. The addition of LDAO indicated proper coupling in the F_1F_O ATP synthases in these mutants. In contrast, membranes prepared from strains KM2/pSBC125 (Tb'_{A83C}) and KM2/pSBC126 (Tb'_{A90C}) exhibited little ATPase activity beyond that of the negative control, KM2/pBR322 (Δ*b*), even though they supported growth via oxidative phosphorylation *in vivo*. The parent plasmid pSBC98 (*Tb'*) displayed similar properties in Chapter 3 and was previously investigated in more detail. It was concluded that the chimeric peripheral stalk expressed by KM2/pSBC98 (*Tb'*) was capable of supporting growth *in vivo*, but these F_1F_O ATP synthases were not sufficiently stable to survive the membrane purification procedures. A similar effect appears to be occurring with strains KM2/pSBC125 (Tb'_{A83C}) and KM2/pSBC126 (Tb'_{A90C}), with the cysteine substitutions increasing the instability of the enzyme during purification. Finally, the strains KM2/pSBC123/pSBC125 (Tb_{A83C}/Tb'_{A83C}), KM2/pSBC123/pSBC126 (Tb_{A83C}/Tb'_{A90C}), KM2/pSBC124/pSBC125 (Tb_{A90C}/Tb'_{A83C}) and KM2/pSBC124/126 (Tb_{A90C}/Tb'_{A90C}) showed ATPase activity levels that were at least 75% of the KM2/pSBC97/pSBC98 (*Tb*/*Tb'*) control, indicating the presence of abundant assembled and intact enzyme.

The effects of the cysteine substitutions were further investigated by measuring ATP-driven proton pumping by fluorescence quenching of ACMA in inverted membrane vesicles (Figure 4-2). No significant effect was observed as a result of the cysteine substitutions.

All samples exhibited proton pumping activity indicative of functional coupling between F_1 and F_O. However, strains expressing homodimeric *Tb'* subunits showed significantly less proton pumping activity than strains expressing either homodimeric *Tb* subunits or both *Tb* and *Tb'* subunits, probably due to the instability of the *Tb'* samples during membrane preparation.

Development of the Crosslinking Assay

The crosslinking assay was optimized to determine conditions where disulfide crosslinks would form quickly and efficiently. Preliminary experiments indicated that crosslinks could easily be formed in the $(Tb'_{A83C})_2$ homodimeric peripheral stalk, so strain KM2/pSBC125 (Tb'_{A83C}) was used for optimization experiments. Initially, dithiothreitol (DTT) was used as a reducing agent. The addition of 1 mM DTT to the TM buffer prior to the purification of membranes was sufficient to maintain the majority of the chimeric subunits in the monomeric form, as shown in Figure 4-3A. DTT was later replaced by the less volatile compound TCEP, the effects of which are shown in Figure 4-3B. The addition of 1 mM TCEP was sufficient to prevent most chimeric subunits from spontaneously crosslinking. TCEP concentrations of both 1 and 5 mM were used in the experiments discussed below.

Disulfide crosslinking reactions can be stopped by adding reagents which react with free thiol groups in order to prevent further crosslink formation. The compound N-ethylmalemide (NEM) is often added to a final concentration of 10-20 mM for this purpose [118, 167, 168, 202, 242, 326, 337, 357, 359]. The amount of NEM required to quench free thiol groups was determined experimentally using membrane samples prepared from strain KM2/pSBC125 (Tb'_{A83C}) in the presence of 1 mM DTT. These membranes were diluted with TM buffer to a final concentration of 5 mg/mL. This concentration was chosen to accommodate purification over a nickel resin as described in Chapter 3. The oxidizing agent Cu^{2+} was added to a final concentration of 100 μM for 10 min and the samples analyzed by Western analysis. As shown in

Figure 4-4, final concentrations of 1-10 mM NEM were sufficient to prevent crosslink formation. The experiments discussed below will all use a final concentration of 5 mM NEM to prevent further crosslinking formation.

The amount of Cu^{2+} sufficient to induce rapid crosslink formation was determined experimentally. Previous crosslinking studies have generally used $CuCl_2$ in the 10-100 μM range for periods of time ranging from 1-48 hrs [154, 172, 180, 202, 242, 326, 331, 337, 357, 359, 378]. A much more rapid crosslink formation would be required to detect changes that occurs during enzyme activity because the inhibitory effects of the product ADP would become increasingly significant over time. Crosslinking time courses with a range of Cu^{2+} concentrations were analyzed by Western analysis (Figure 4-5). A final concentration of 500 μM Cu^{2+} was sufficient to bring the crosslinking reaction to near completion within 2 min.

Disulfide Crosslink Formation Between Chimeric Subunits

Crosslink formation in homodimeric peripheral stalks was investigated by oxidizing membranes prepared from the stains KM2/pSBC123 (Tb_{A83C}), KM2/pSBC124 (Tb_{A90C}), KM2/pSBC125 (Tb'_{A83C}) and KM2/pSBC126 (Tb'_{A90C}) with 500 μM Cu^{2+} and analyzing by Western blot (Figure 4-6). A small amount of crosslink formation was observed for KM2/pSBC123 (Tb_{A83C}), with around 20% of the total Tb_{A83C} subunit running as crosslinked dimer on the SDS-PAGE gel. In contrast, membranes prepared from the strains KM2/pSBC124 (Tb_{A90C}), KM2/pSBC125 (Tb'_{A83C}) and KM2/pSBC126 (Tb'_{A90C}) exhibited 50-70% disulfide formation upon Cu^{2+} treatment. The *Tb'* samples showed a high degree of spontaneous crosslink formation that raised their zero time point values significantly above those observed for the other samples (Figure 4-7). This increase in spontaneous crosslinking may be a result of the instability

of these F_1F_O complexes *in vitro*, affording the chimeric *b* subunits more flexibility than is normal in the presence of F_1.

The coexpression of a chimeric subunit containing a cysteine substitution along with the complementary cysteine-free subunit reduced homodimeric crosslink formation for all four chimeric *b* subunits (Figure 4-8). Between 20-40% crosslink formation was observed for strains KM2/pSBC123/pSBC98 (Tb_{A83C}/*Tb'*), KM2/pSBC124/pSBC98 (Tb_{A90C}/*Tb'*) and KM2/pSBC97/pSBC126 (*Tb*/Tb'_{A90C}), while about 15% dimer formation was seen for strain KM2/pSBC97/pSBC125 (*Tb*/Tb'_{A83C}). The decrease in both spontaneous and Cu^{2+} induced crosslink formation provides additional evidence of dimer formation between the complementary *Tb* and *Tb'* subunits beyond that presented in Chapter 3.

The formation of disulfide crosslinks in membranes prepared from cells expressing two different cysteine-containing chimeric subunits (Figure 4-9). Crosslink formation was detected for all four possible combinations with antibodies against both the *b* subunit and the V5 epitope tag. However, these crosslinked samples were actually a mixture of $(Tb)_2$ and $(Tb')_2$ homodimers along with (*Tb*/*Tb'*) heterodimers. In order to determine the extent of dimer formation in the heterodimeric peripheral stalks alone, a nickel resin purification procedure developed previously in our lab and described in Chapter 3 was employed [355]. As shown in Figure 4-10, a small amount of heterodimer crosslink formation was detected for strains KM2/pSBC123/pSBC125 (Tb_{A83C}/Tb'_{A83C}) and KM2/pSBC124/pSBC125 (Tb_{A90C}/Tb'_{A83C}) while strong heterodimer crosslinking was observed for strains KM2/pSBC123/pSBC126 (Tb_{A83C}/Tb'_{A90C}) and KM2/pSBC124/pSBC126 (Tb_{A90C}/Tb'_{A90C}).

Samples were crosslinked with a reduced amount of Cu^{2+} in order to investigate which crosslinks formed most efficiently, and hence may represent a more natural interaction between

the *b* subunits in the peripheral stalk. As shown in Figure 4-11, a disulfide crosslink could be formed in membranes prepared from the strain KM2/pSBC123/pSBC126 (Tb_{A83C}/Tb'_{A90C}) but not the other three *Tb*/*Tb'* combinations. The rate of crosslink formation in membranes prepared from strain KM2/pSBC123/pSBC126 (Tb_{A83C}/Tb'_{A90C}) was investigated with a crosslinking time course (Figure 4-12). Disulfide formation was essentially complete within 40 sec after addition of Cu^{2+} to a final concentration of 50 μM, demonstrating that this crosslink forms rapidly even at low Cu^{2+} concentrations. Finally, an ATP-driven proton pumping assay showed no functional effect as a result of forming this crosslink (Figure 4-13).

Effects of ATP on Crosslink Formation

The effects of ATP on disulfide crosslink formation between chimeric *b* subunits was investigated by crosslinking F_1F_O in the presence and absence of ATP. Preliminary results indicated a crosslinking change at the high ATP concentration of 45 mM in some constructs but not others. This effect was investigated further by crosslinking the homodimeric $(Tb)_2$ and $(Tb')_2$ subunits (Figure 4-14). Membranes prepared from the strain KM2/pSBC124 (Tb_{A90C}) showed identical crosslinking results both in the presence and absence of ATP, while crosslinking in membranes prepared from strains KM2/pSBC125 (Tb'_{A83C}) and KM2/pSBC126 (Tb'_{A90C}) was diminished in the presence of ATP. Likewise, crosslink formation between heterodimeric *Tb*/*Tb'* constructs was diminished in the presence of 45 mM ATP for membranes prepared from strains KM2/pSBC123/pSBC125 (Tb_{A83C}/Tb'_{A83C}), KM2/pSBC123/pSBC126 (Tb_{A83C}/Tb'_{A90C}), KM2/pSBC124/pSBC125 (Tb_{A90C}/Tb'_{A83C}) and KM2/pSBC124/pSBC126 (Tb_{A90C}/Tb'_{A90C}) (Figure 4-15).

The relevance of this effect on crosslink formation at 45 mM ATP to normal F_1F_O function was a concern, especially after evidence was obtained that a similar crosslinking change in the *E.*

coli b subunit occurred at 45 mM ATP but not 5 mM ATP (see Chapter 5). Even 5 mM ATP is sufficient to fully activate the enzyme [32], so the effect observed was unlikely to be a direct result of catalysis. The hypothesis that the excess ATP was chelating the 10 mM Mg^{2+} present in the TM buffer and having an indirect structural effect was considered. This hypothesis was tested by repeating the experiment in membranes prepared from the strain KM2/pSBC124/pSBC126 (Tb_{A90C}/Tb'_{A90C}) in the presence of increasing Mg^{2+} (Figure 4-16). A similar ATP-dependent reduction in crosslink formation was observed even in the presence of excess Mg^{2+}.

The effects of 45 mM ATP on enzyme activity were investigated by ATP-driven proton pumping analysis (Figure 4-17). It was discovered that 45 mM ATP caused a significant reduction in proton pumping activity compared to the 0.75 mM ATP normally used for this assay, even in the presence of 55 mM Mg^{2+}. Interestingly, this effect was not purely a chemical one produced by the presence of excess nucleotide. The addition of both 44.25 mM UTP and 0.75 mM ATP produced abundant ATP-driven proton pumping activity similar to that observed with 0.75 mM ATP alone. Furthermore, a direct relationship between ATP concentration and crosslink formation can be seen in membranes prepared from the stain KM2/pSBC125 (Tb'_{A83C}) (Figure 4-18). The ATP hydrolysis value for this strain indicated a low level of membrane-bound F_1 after sample preparation, meaning the effect of ATP concentration on disulfide formation also occurred in F_O alone.

Discussion

Disulfide crosslink formation was used to probe subunit-subunit interactions in *E. coli* F_1F_O ATP synthase containing a chimeric peripheral stalk. The chimeric *E. coli b* subunits, abbreviated *Tb* and *Tb'* for simplicity, contained sequence from the *b* and *b'* subunits of the photosynthetic organism *T. elongatus* for residues E39-I86. Cysteines were individually

substituted at residues A83 and A90, producing a total of four constructs – pSBC123 (Tb_{A83C}), pSBC124 (Tb_{A90C}), pSBC125 (Tb'_{A83C}) and pSBC126 (Tb'_{A90C}). No significant functional defect was observed as a result of any of the cysteine substitutions. All recombinant subunits were able to support growth by oxidative phosphorylation, readily formed intact F_1F_O, and exhibited coupled activity between F_1 and F_O. Crosslink formation was observed in heterodimeric peripheral stalks upon treatment with 500 μM Cu^{2+} for all four cysteine combinations, but especially in membranes prepared from strains KM2/pSBC123/pSBC126 (Tb_{A83C}/Tb'_{A90C}) and KM2/pSBC124/pSBC126 (Tb_{A90C}/Tb'_{A90C}). Crosslinking analysis using only 50 μM Cu^{2+} demonstrated that strain KM2/pSBC123/pSBC126 (Tb_{A83C}/Tb'_{A90C}) formed disulfide bonds rapidly and efficiently, whereas strain KM2/pSBC124/pSBC126 (Tb_{A90C}/Tb'_{A90C}) was unable to crosslink under these conditions. These results, shown in Figure 4-11, were not nickel resin purified and hence contained both $(Tb_{A83C})_2$ and $(Tb'_{A90C})_2$ homodimers in addition to the Tb_{A83C}/Tb'_{A90C} heterodimer. However, no crosslink formation is observed in either strain KM2/pSBC123/pSBC125 (Tb_{A83C}/Tb'_{A83C}) or KM2/pSBC124/pSBC126 (Tb_{A90C}/Tb'_{A90C}), both of which also contain $(Tb_{A83C})_2$ and $(Tb'_{A90C})_2$ homodimers. These results indicate that only the Tb_{A83C}/Tb'_{A90C} heterodimer is capable of crosslinking under the 50 μM Cu^{2+} conditions. Interestingly, the formation of this crosslink had no effect on ATP-driven proton pumping activity (Figure 4-13).

These crosslinking results are the first indication that the peripheral stalk may be in a staggered arrangement in the context of the entire F_1F_O ATP synthase. This staggered offset is approximately seven amino acids, or about two turns of an α-helix. It is also important to note that crosslink formation was not observed in membranes prepared from strain KM2/pSBC124/pSBC125 (Tb_{A90C}/Tb'_{A83C}) upon treatment with 50 μM Cu^{2+}. These results

imply that the chimeric *b* subunits have a predictable staggered arrangement, something that would not occur between the identical *b* subunit of the wild-type *E. coli* peripheral stalk. It is possible that the observed staggering effect is a result of the *T. elongatus* sequence rather than the normal *E. coli* structure. However, data that will be presented in Chapter 5 support the conclusion that the normal *E. coli* peripheral stalk forms disulfide crosslinks in a similar manner to the chimeric peripheral stalk. Moreover, data obtained previously using the soluble form of the *b* subunit also support a staggered model in the wild-type *b* subunit [326, 359].

An unexpected effect was observed when high levels of ATP were added to the crosslinking reaction. It was discovered that 45 mM ATP caused a reduction in crosslink formation for some homodimeric samples but not others. Disulfide crosslink formation in the heterodimeric peripheral stalks was reduced for all four cysteine combinations, but this effect of ATP could not be attributed to catalytic activity. Activity assays demonstrated that excess ATP actually caused a reduction in ATP-drive proton pumping. Interestingly, a comparable amount of UTP did not have such an effect, indicating that this is not a result caused by the presence of excess nucleotide.

Table 4-1. Oligonucleotides used in this chapter

Oligonucleotide pair[a, b] (mutation, restriction site)	Annealed oligonucleotides[c]
MP7/8 (Tb_{A83C}, +*Mlu*I)	MP7 – 5′ CGTGAAGATGCTCTGACGCGTTGCAAAGCTGTTCTAGACGAAGC 3′ MP8 – 3′ GCACTTCTACGAGACTGCGCAACGTTTCGACAAGATCTGCTTCG 5′
MP9/10 (Tb_{A90C}, +*Mlu*I)	MP9 – 5′ GATGCTCTGACGCGTGCTAAAGCTGTTCTAGACGAATGCAAAGCTGAGGC 3′ MP10 – 3′ CTACGAGACTGCGCACGATTTCGACAAGATCTGCTTACGTTTCGACTCCG 5′
MP11/12 (Tb'_{A83C}, +*Mlu*I)	MP11 – 5′ GGCTCAGGCTCTGATCGAAGAAGCACGCGTTGAATGTCAGAAAATTCTAGACG 3′ MP12 – 3′ CCGAGTCCGAGACTAGCTTCTTCGTGCGCAACTTACAGTCTTTTAAGATCTGC 5′
MP13/14 (Tb'_{A90C}, +*Mlu*I)	MP13 – 3′ CGAAGAAGCACGCGTTGAAGCTCAGAAAATTCTAGACGAATGTAAAGCTGAGGC 5′ MP14 – 5′ GCTTCTTCGTGCGCAACTTCGAGTCTTTTAAGATCTGCTTACATTTCGACTCCG 3′

[a] *Tb*, wild-type *E. coli b* subunit with sequence from the *b* subunit of *T. elongatus* substituted for amino acids E39-I86, a C21S mutation and a six histidine epitope tag at the amino terminus.

[b] *Tb'*, wild-type *E. coli b* subunit with sequence from the *b'* subunit of *T. elongatus* substituted for amino acids E39-I86, a C21S mutation and a V5 epitope tag (GKPIPNPLLGLDST) at the carboxyl terminus.

[c] Added restriction sites are underlined.

Table 4-2. Plasmids, growth on succinate and ATP hydrolysis

Strain/Plasmid(s)	Gene product	Antibiotic Resistance[b]	Growth on Succinate[c]	ATP Hydrolysis[d]		Source or reference
				Without LDAO	With 0.5% LDAO[e]	
KM2/pTAM37/pTAM46	b_{his}/b_{V5}[a]	Ap+Cm	+++	0.30 ± 0.02	1.21 ± 0.06	[355]
KM2/pBR322	Δ*b*	Ap	-	0.07 ± 0.01	0.16 ± 0.01	New England Biolabs
KM2/pSBC97	*Tb*	Cm	+	0.30 ± 0.02	1.03 ± 0.15	[399]
KM2/pSBC123	Tb_{A83C}	Cm	+	0.19 ± 0.03	0.71 ± 0.05	This study
KM2/pSBC124	Tb_{A90C}	Cm	+	0.20 ± 0.04	0.70 ± 0.06	This study
KM2/pSBC98	*Tb'*	Ap	++	0.17 ± 0.02	0.50 ± 0.06	[399]
KM2/pSBC125	Tb'_{A83C}	Ap	++	0.10 ± 0.01	0.22 ± 0.01	This study
KM2/pSBC126	Tb'_{A90C}	Ap	++	0.10 ± 0.01	0.23 ± 0.01	This study
KM2/pSBC97/pSBC98	*Tb/Tb'*	Ap+Cm	++	0.24 ± 0.02	0.88 ± 0.04	[399]
KM2/pSBC123/pSBC125	Tb_{A83C}/Tb'_{A83C}	Ap+Cm	++	0.19 ± 0.01	0.61 ± 0.01	This study
KM2/pSBC123/pSBC126	Tb_{A83C}/Tb'_{A90C}	Ap+Cm	++	0.23 ± 0.02	0.78 ± 0.02	This study
KM2/pSBC124/pSBC125	Tb_{A90C}/Tb'_{A83C}	Ap+Cm	+	0.19 ± 0.02	0.72 ± 0.05	This study
KM2/pSBC124/pSBC126	Tb_{A90C}/Tb'_{A90C}	Ap+Cm	++	0.21 ± 0.02	0.75 ± 0.07	This study

[a]his, six histidine epitope tag at the amino terminus; V5, epitope tag with the sequence GKPIPNPLLGLDST appended to the carboxyl terminus.
[b]Ap, ampicillin; Cm, chloramphenicol.
[c]Symbols: +++, wild-type growth; ++, colonies smaller than wild-type; +, small colony formation; -, no growth.
[d]Reported in units of μmol of P_i/mg membrane protein/min. Each sample was assayed in triplicate.
[e]Used to release F_1 from the inhibitory effect of F_O.

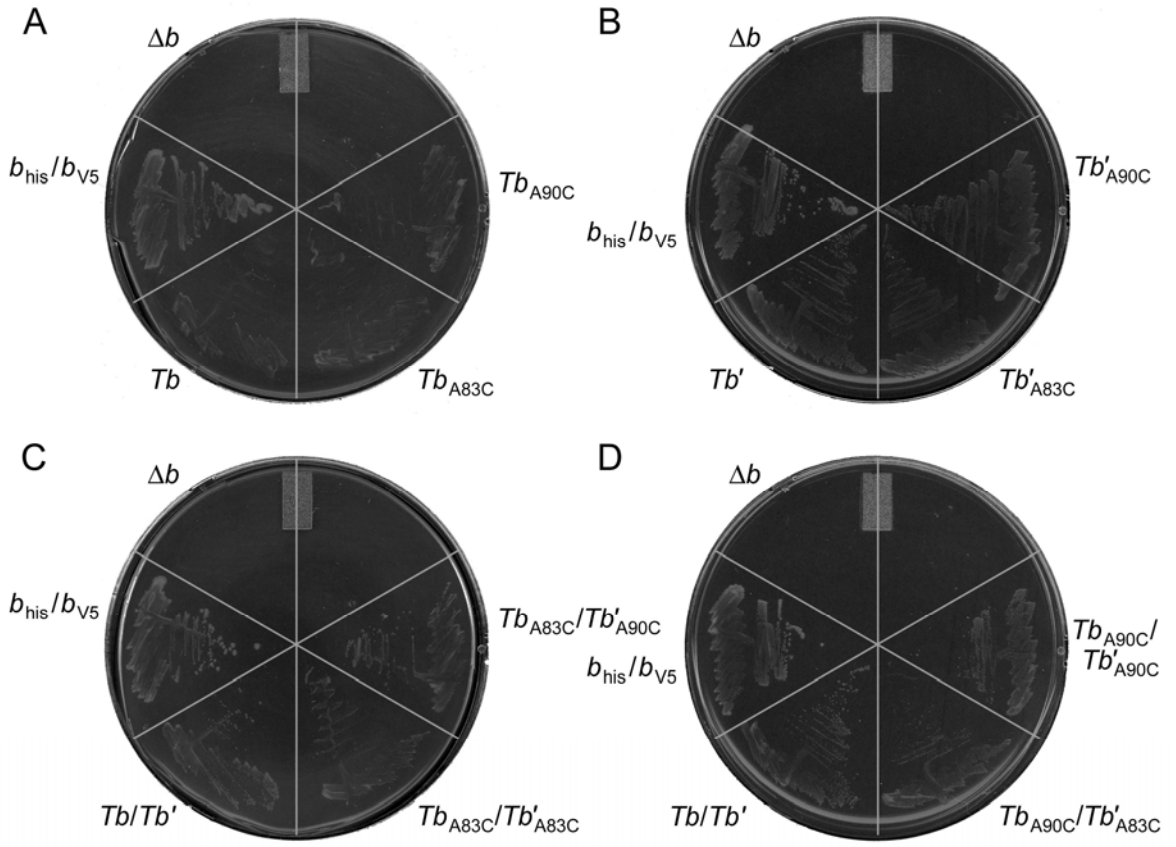

Figure 4-1. Effects of cysteine substitutions on enzyme viability. Growth on minimal A media with succinate as the sole carbon source was used to test the viability of F_1F_O ATP synthase complexes. All plates contain KM2/pTAM37/pTAM46 (b_{his}/b_{V5}) and KM2/pBR322 (Δ*b*) as positive and negative controls, respectively. A) The growth of KM2/pSBC97 (*Tb*) compared to KM2/pSBC123 (Tb_{A83C}) and KM2/pSBC124 (Tb_{A90C}). B) The growth of KM2/pSBC98 (*Tb'*) compared to KM2/pSBC125 (Tb'_{A83C}) and KM2/pSBC126 (Tb'_{A90C}). C) and D) The growth of KM2/pSBC97/pSBC98 (*Tb*/*Tb'*) compared to KM2/pSBC123/pSBC125 (Tb_{A83C}/Tb'_{A83C}), KM2/pSBC123/pSBC126 (Tb_{A83C}/Tb'_{A90C}), KM2/pSBC124/pSBC125 (Tb_{A90C}/Tb'_{A83C}) and KM2/pSBC124/pSBC126 (Tb_{A90C}/Tb'_{A90C}). Growth experiments were done in triplicate and the plates shown are representative of the results obtained.

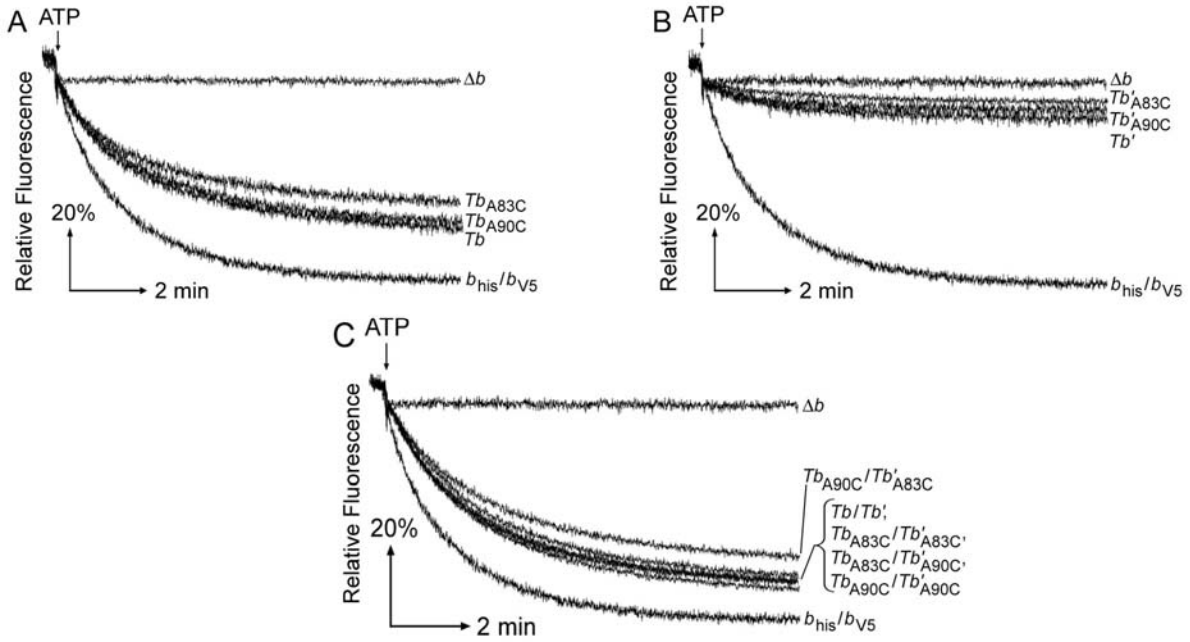

Figure 4-2. Effects of cysteine substitutions on ATP-driven proton pumping activity. The effects of the cysteine substitutions on ATP-driven proton pumping activity was measured by fluorescence quenching of ACMA. All panels contain KM2/pTAM37/pTAM46 (b_{his}/b_{V5}) and KM2/pBR322 (Δb) as positive and negative controls, respectively. A) Proton pumping of *Tb* constructs. Traces shown are KM2/pSBC97 (*Tb*), KM2/pSBC123 (Tb_{A83C}) and KM2/pSBC124 (Tb_{A90C}). B) Proton pumping of *Tb'* constructs. Traces shown are KM2/pSBC98 (*Tb'*), KM2/pSBC125 (Tb'_{A83C}) and KM2/pSBC126 (Tb'_{A90C}). (C) Proton pumping of coexpressed *Tb* and *Tb'* constructs. Traces shown are KM2/pSBC97/pSBC98 (*Tb*/*Tb'*), KM2/pSBC123/SBC125 (Tb_{A83C}/Tb'_{A83C}), KM2/pSBC123/pSBC126 (Tb_{A83C}/Tb'_{A90C}), KM2/pSBC124/pSBC125 (Tb_{A90C}/Tb'_{A83C}) and KM2/pSBC124/pSBC126 (Tb_{A90C}/Tb'_{A90C}). Experiments were done in quadruplicate and traces shown are representative of the results obtained.

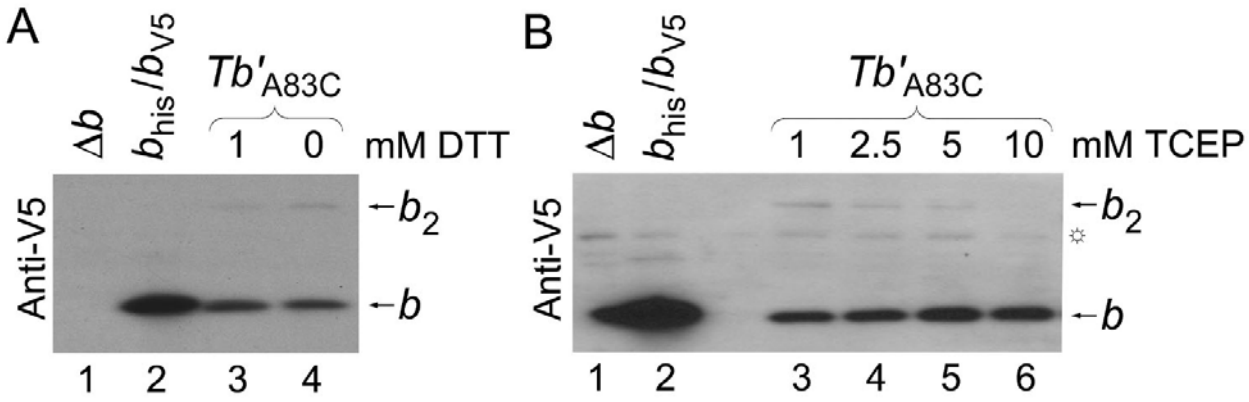

Figure 4-3. Effects of reducing agents on crosslink formation. Membranes from strain KM2/pSBC125 (*Tb'*$_{A83C}$) were prepared in TM buffer which contained either DTT or TCEP as a reducing agent. The extent of spontaneous crosslink formation was investigated by Western blot analysis in which 1 μg of untreated membrane protein was loaded per lane. A) DTT was added to the TM buffer to final concentrations of 0 and 1 mM. B) TCEP was added to the TM buffer to a final concentrations of 1, 2.5, 5 and 10 mM. The ☼ symbol indicates a nonspecific band.

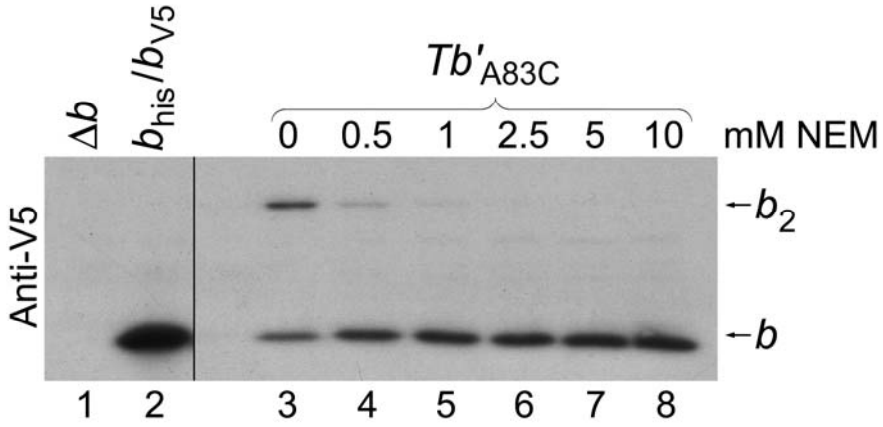

Figure 4-4. Determination of the amount of NEM required to prevent further disulfide formation. Membranes from the strain KM2/pSBC125 (Tb'_{A83C}) were prepared in the presence of 1 mM DTT and diluted to 5 mg/mL. Increasing amounts of NEM were added and the samples were vortexed briefly to mix. Crosslink formation was induced by the addition of 100 μM Cu^{2+} followed by a 10 min incubation in open tubes at room temperature with shaking. A total of 1 μg of each membrane sample was analyzed by Western blot. The vertical bar represents the removal of unwanted lanes *in silico*.

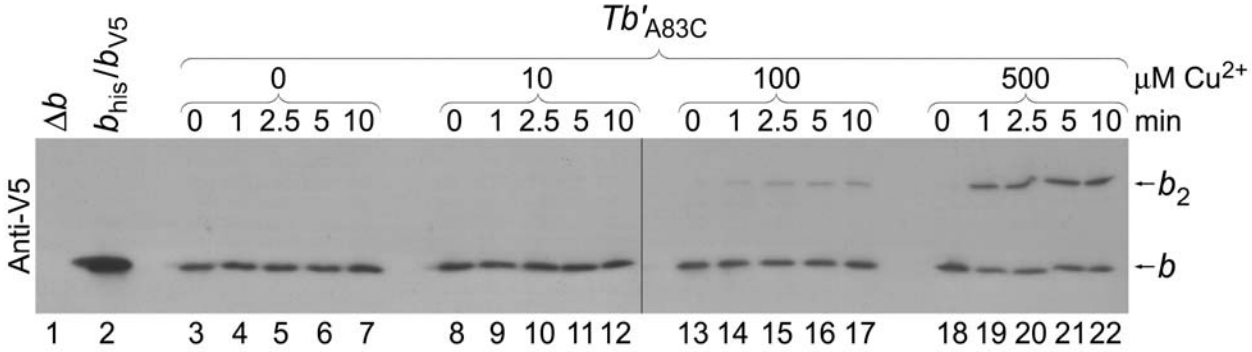

Figure 4-5. Crosslinking time course done in the presence of increasing concentrations of Cu^{2+}. Membrane were prepared from the strain KM2/pSBC125 (*Tb'*$_{A83C}$) in the presence of 1 mM DTT. Samples were diluted to 5 mg/mL and incubated with 0, 10, 100 or 500 μM Cu^{2+} for 10 min in open tubes at room temperature with shaking. Aliquots were removed at 0 (pre-Cu^{2+}), 1, 2.5, 5 and 10 min and stopped by the addition of NEM to a final concentration of 5 mM. Western analysis was done with 1 μg of membrane sample per lane. The vertical bar represents the joining of two separate gels *in silico*.

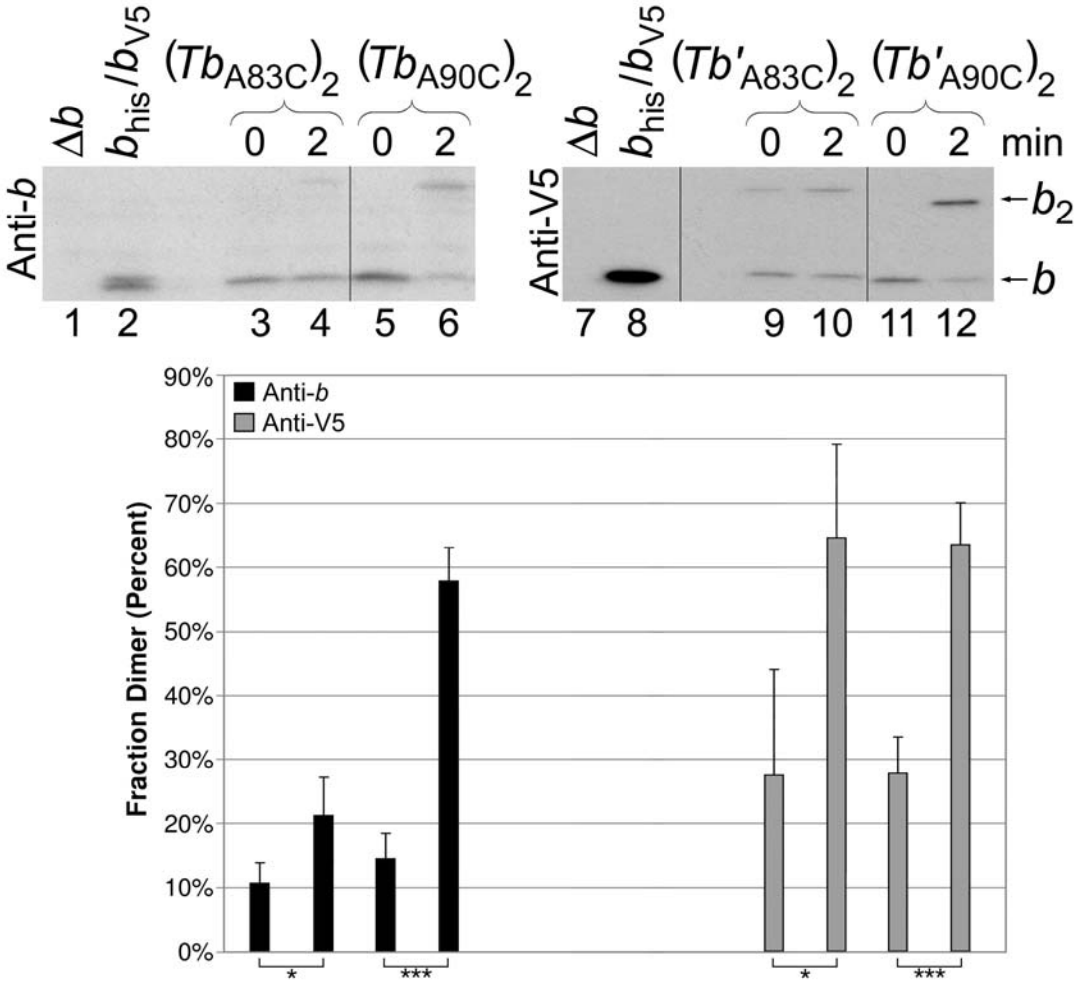

Figure 4-6. Crosslink formation in homodimeric $(Tb)_2$ and $(Tb')_2$ subunits. Membranes containing a single type of chimeric *b* subunit were prepared in the presence of 5 mM TCEP and crosslinked at 5 mg/mL for 2 min using 500 μM $CuCl_2$. The reactions were stopped by adding NEM to a final concentration of 5 mM. Zero time point samples had NEM added prior to Cu^{2+} to prevent crosslinking. Chimeric *b* subunits in membranes prepared from strains KM2/pSBC123 (Tb_{A83C}) and KM2/pSBC124 (Tb_{A90C}) were detected using an antibody against the *b* subunit while those from strains KM2/pSBC125 (Tb'_{A83C}) and KM2/pSBC126 (Tb'_{A90C}) were detected using an antibody against the V5 epitope tag. Total amounts of 1 μg and 10 μg membrane protein were loaded per lane for the anti-V5 and anti-*b* subunit Westerns, respectively. Vertical lines indicate the removal of unwanted lanes *in silico*. The average fraction dimer obtain from densitometry analysis of four experiments is charted below each blot. Samples with a low probability of being identical are indicated (*, $p < 0.05$; **, $p < 0.01$; ***, $p < 0.001$).

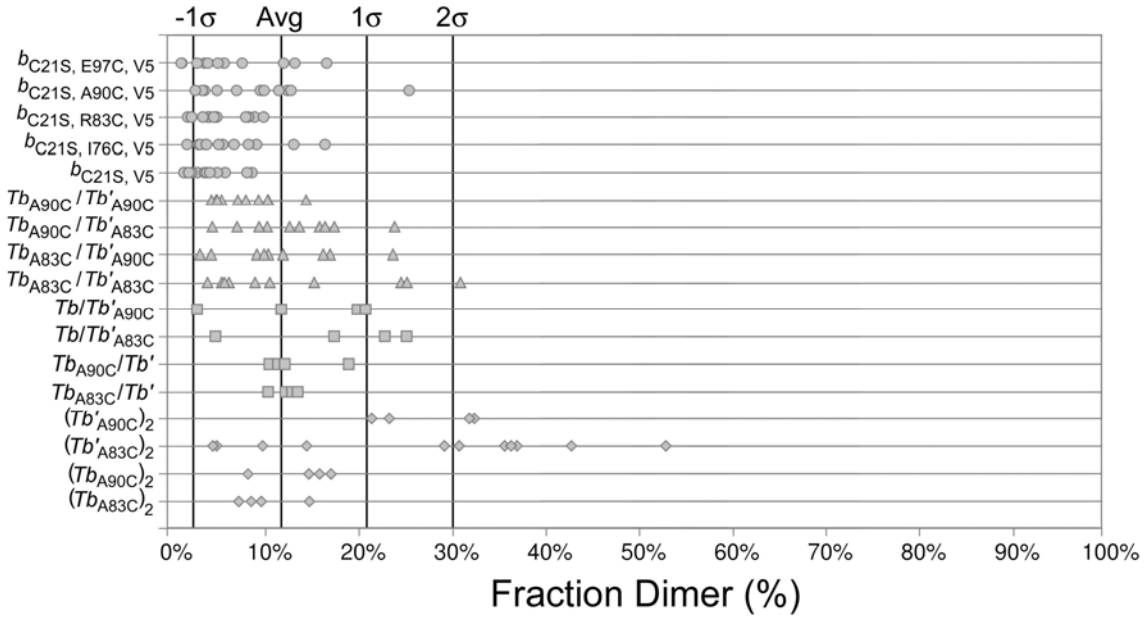

Figure 4-7. Extent of spontaneous crosslink formation. The fraction dimer of all zero second data points from Chapters 4 and 5 is plotted by sample. Vertical bars represent the average and standard deviations (σ).

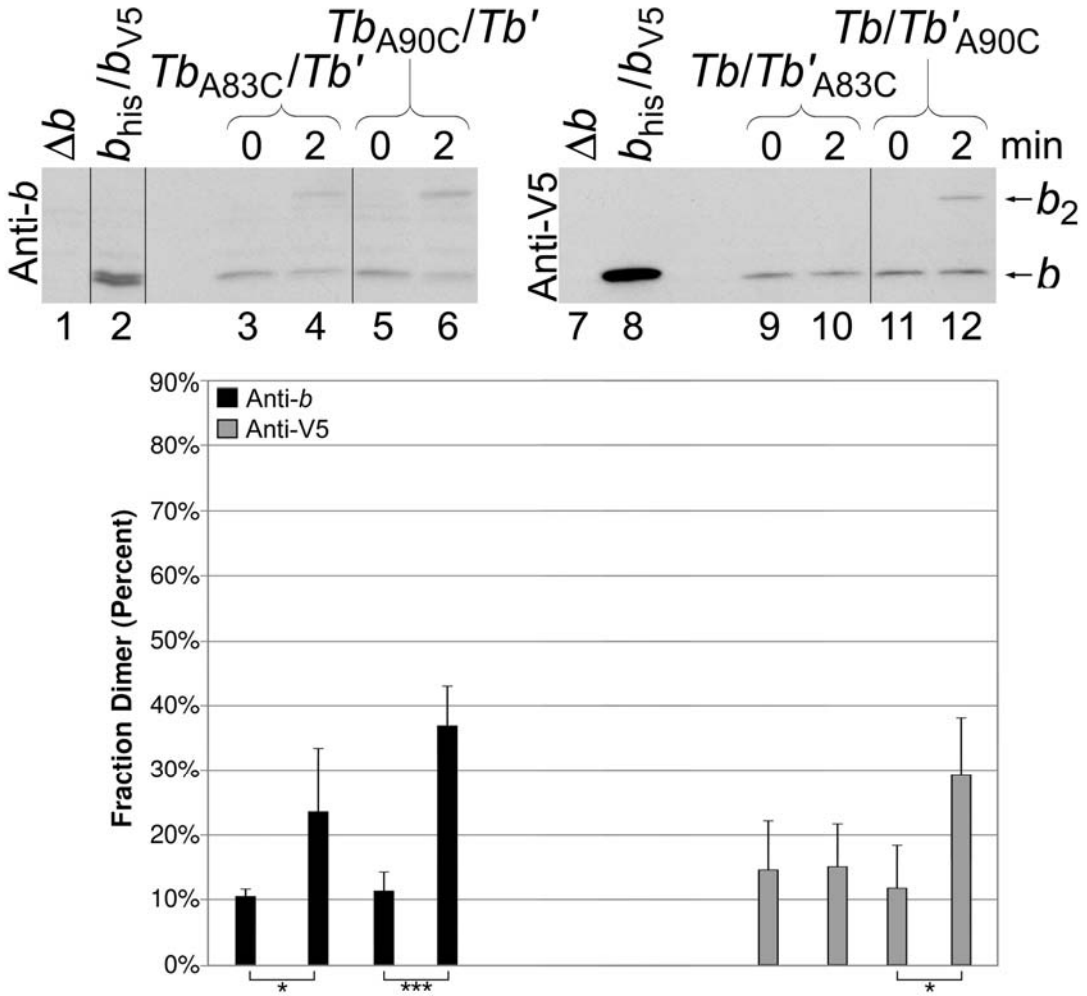

Figure 4-8. Effects of complementary subunits on homodimer crosslinking. Membranes expressing both a chimeric *Tb* or *Tb'* subunit with a substituted cysteine and the complementary cysteine-free subunit were crosslinked and analyzed as described in Figure 4-6. Membrane samples were prepared from strains KM2/pSBC123/pSBC98 (Tb_{A83C}/Tb'), KM2/pSBC124/pSBC98 (Tb_{A90C}/Tb'), KM2/pSBC97/pSBC125 (Tb/Tb'_{A83C}) and KM2/pSBC97/pSBC126 (Tb/Tb'_{A90C}). Vertical lines indicate the removal of unwanted lanes *in silico*. The average fraction dimer obtain from densitometry analysis of four experiments is charted below each blot. Samples with a low probability of being identical are indicated (*, $p < 0.05$; **, $p < 0.01$; ***, $p < 0.001$).

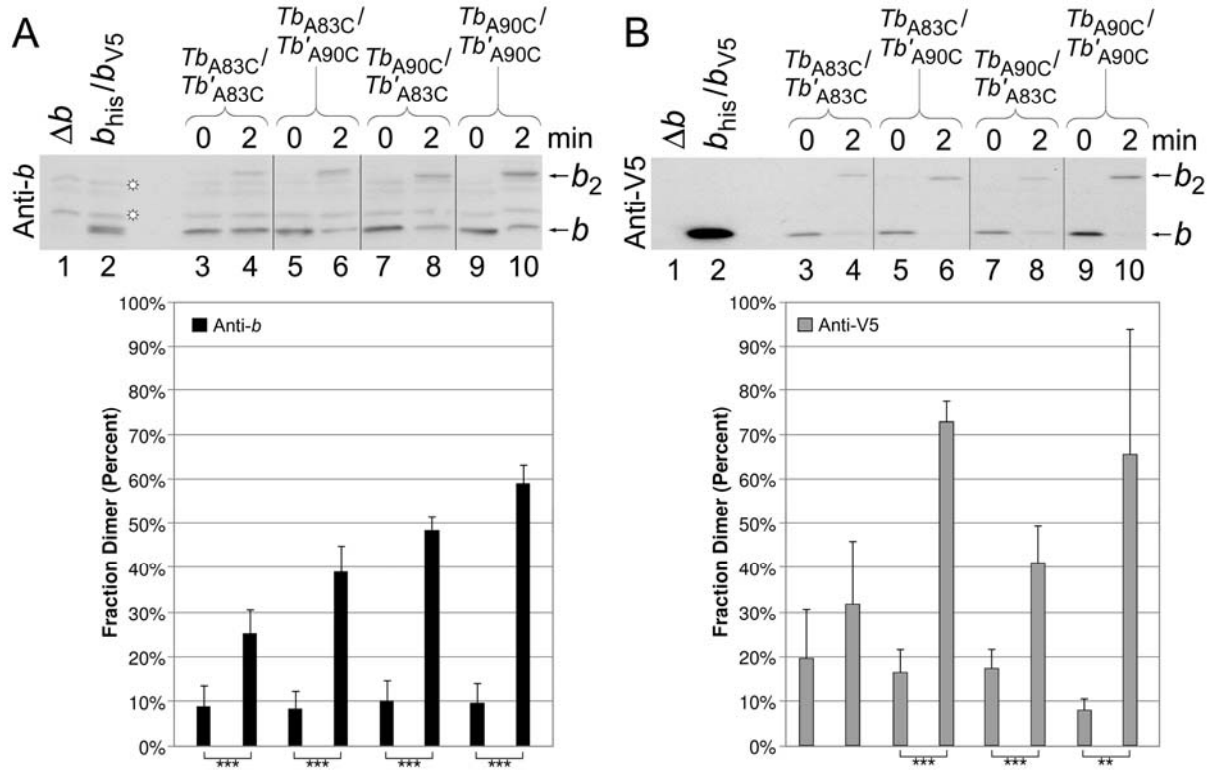

Figure 4-9. Crosslink formation in coexpressed *Tb* and *Tb'* subunits. Membranes expressing both chimeric *Tb* and *Tb'* subunits with substituted cysteines were crosslinked as described in Figure 4-6. Crosslinked membranes from KM2/pSBC123/pSBC125 (Tb_{A83C}/Tb'_{A83C}), KM2/pSBC123/pSBC126 (Tb_{A83C}/Tb'_{A90C}), KM2/pSBC124/pSBC125 (Tb_{A90C}/Tb'_{A83C}) and KM2/pSBC124/pSBC126 (Tb_{A90C}/Tb'_{A90C}) were analyzed by Western blots with antibodies against both the *b* subunit and the V5 epitope tag. A total amount of 1 μg and 10 μg membrane protein were loaded per lane for the anti-V5 and anti-*b* subunit Westerns, respectively. Vertical lines indicate the removal of unwanted lanes *in silico*, while ☼ indicates a nonspecific band detected by the anti-*b* subunit antibody. The average fraction dimer obtain from densitometry analysis of five experiments is charted below the blots. Samples with a low probability of being identical are indicated (*, $p < 0.05$; **, $p < 0.01$; ***, $p < 0.001$).

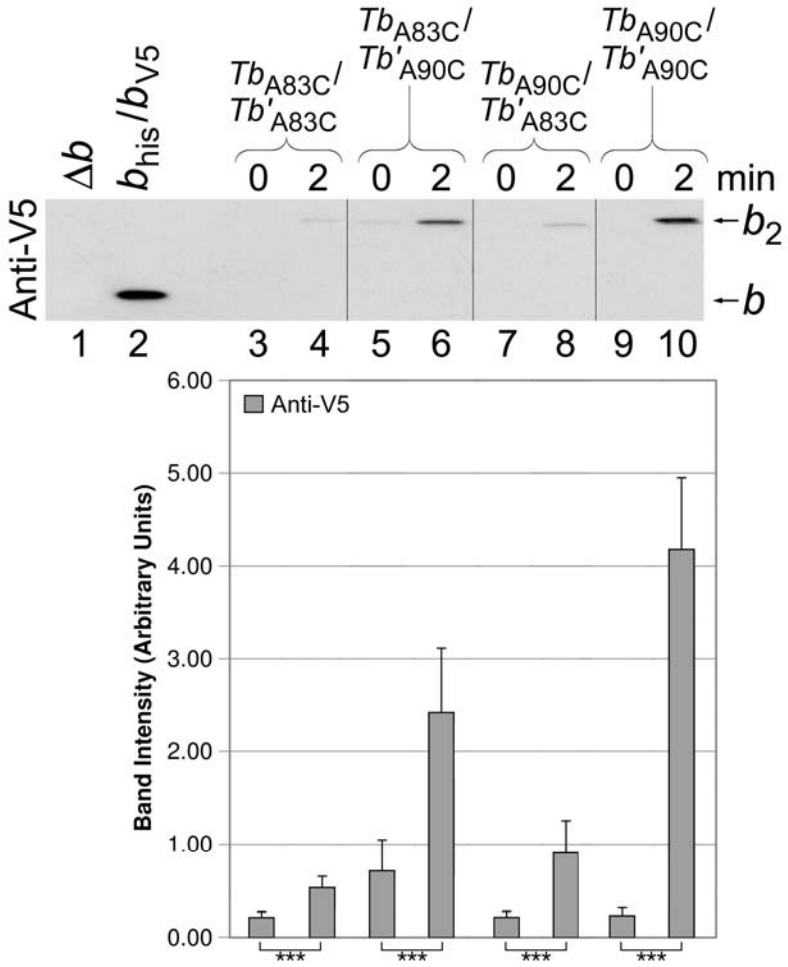

Figure 4-10. Crosslink formation in *Tb/Tb'* heterodimers. Membranes expressing both chimeric *Tb* and *Tb'* subunits with substituted cysteines were crosslinked as described in Figure 4-6. The crosslinked samples were purified over a nickel resin to retain only F_1F_O complexes containing a histidine tag and analyzed by Western blot using an antibody against the V5 epitope tag to detect enzymes containing heterodimeric peripheral stalks. Membrane samples were prepared from strains KM2/pSBC123/pSBC125 (Tb_{A83C}/Tb'_{A83C}), KM2/pSBC123/pSBC126 (Tb_{A83C}/Tb'_{A90C}), KM2/pSBC124/pSBC125 (Tb_{A90C}/Tb'_{A83C}) and KM2/pSBC124/pSBC126 (Tb_{A90C}/Tb'_{A90C}). A total of 10% of the elutant from the nickel resin was loaded per lane. Vertical lines indicate a removal of unwanted lanes *in silico*. The average band intensity in arbitrary units obtained from densitometry analysis of eight experiments is charted below. Samples with a low probability of being identical are indicated (*, $p < 0.05$; **, $p < 0.01$; ***, $p < 0.001$).

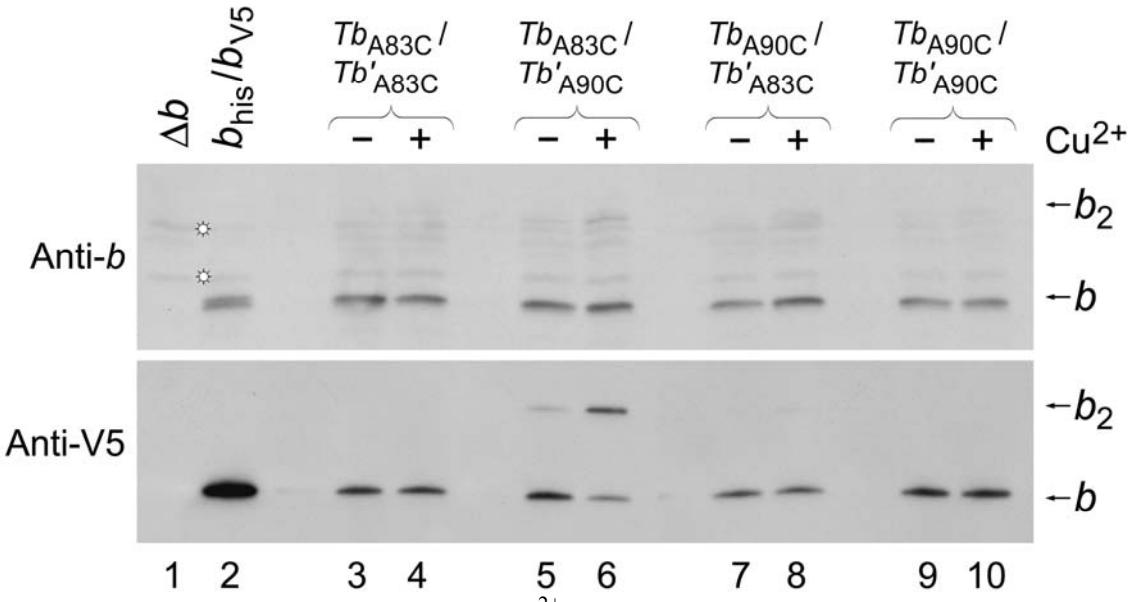

Figure 4-11. Crosslink formation with low Cu^{2+}. Membranes were prepared and crosslinked essentially as described in Figure 4-6 with the exception that Cu^{2+} was added to a final concentration of 50 μM and the crosslinking reaction was allowed to proceed for 10 min before quenching with NEM. Membrane samples prepared from strains KM2/pSBC123/pSBC125 (Tb_{A83C}/Tb'_{A83C}), KM2/pSBC123/pSBC126 (Tb_{A83C}/Tb'_{A90C}), KM2/pSBC124/pSBC125 (Tb_{A90C}/Tb'_{A83C}) and KM2/pSBC124/pSBC126 (Tb_{A90C}/Tb'_{A90C}) were crosslinked and analyzed by Western blot using antibodies against both the *b* subunit and the V5 epitope tag. A total amount of 1 μg and 10 μg membrane protein were loaded per lane for the anti-V5 and anti-*b* subunit Westerns, respectively. The symbol ☼ indicates a nonspecific band detected by the anti-*b* subunit antibody. The experiment was done in triplicate and the results shown are representative.

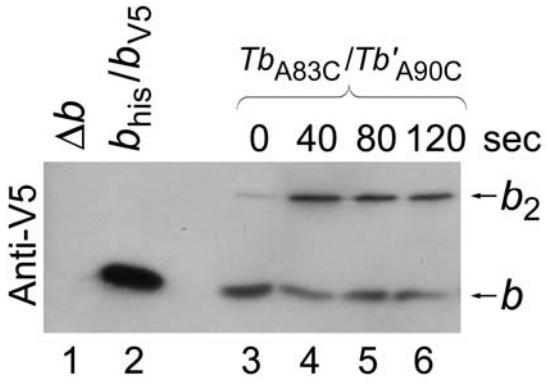

Figure 4-12. Crosslinking time course for membranes prepared from KM2/pSBC123/pSBC126 (Tb_{A83C}/Tb'_{A90C}). Membranes were prepared in the presence of 1 mM TCEP and diluted to 5 mg/mL for the crosslinking reaction. Crosslinking was induced by the addition of Cu^{2+} to a final concentration of 50 μM and the reactions were incubated at room temperature in open tubes with shaking. Aliquots were removed at 0 (pre-Cu^{2+}), 40, 80 and 120 sec and stopped by adding NEM to a final concentration of 5 mM. Membranes samples were analyzed by Western blot against the V5 epitope tag. A total of 1 μg of protein was loaded per lane.

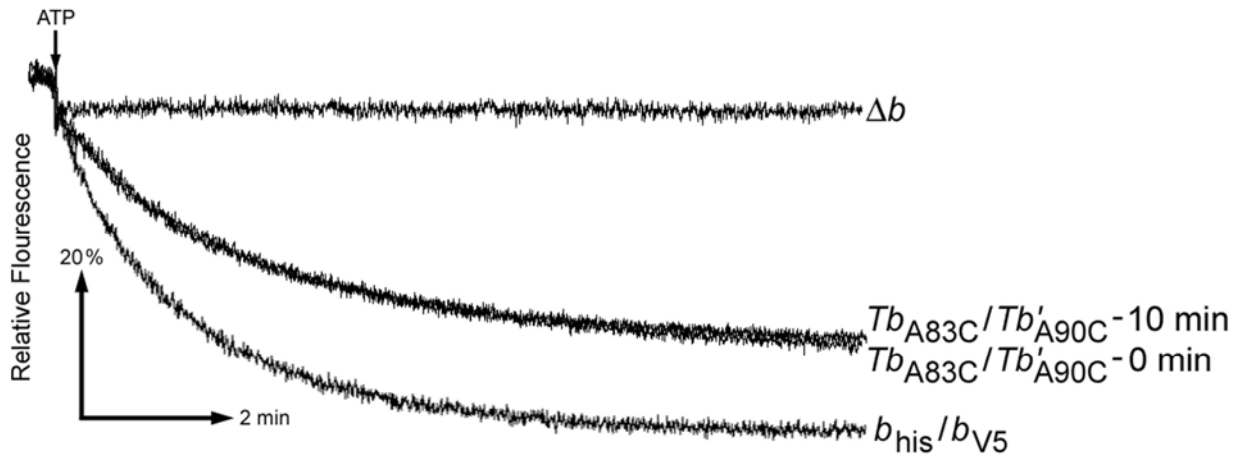

Figure 4-13. Effect of crosslink formation on ATP-driven proton pumping. Membranes from strain KM2/pSBC123/pSBC126 (Tb_{A83C}/Tb'_{A90C}) were prepared and crosslinked as described in Figure 4-11. A total of 0.5 mg of crosslinked membrane protein was assayed for ATP-driven proton pumping activity by the fluorescence quenching of ACMA. Membrane from KM2/pTAM37/pTAM46 (b_{his}/b_{V5}) and KM2/pBR322 (Δb) were assayed as positive and negative controls, respectively. The experiment was done in triplicate and results shown are representative.

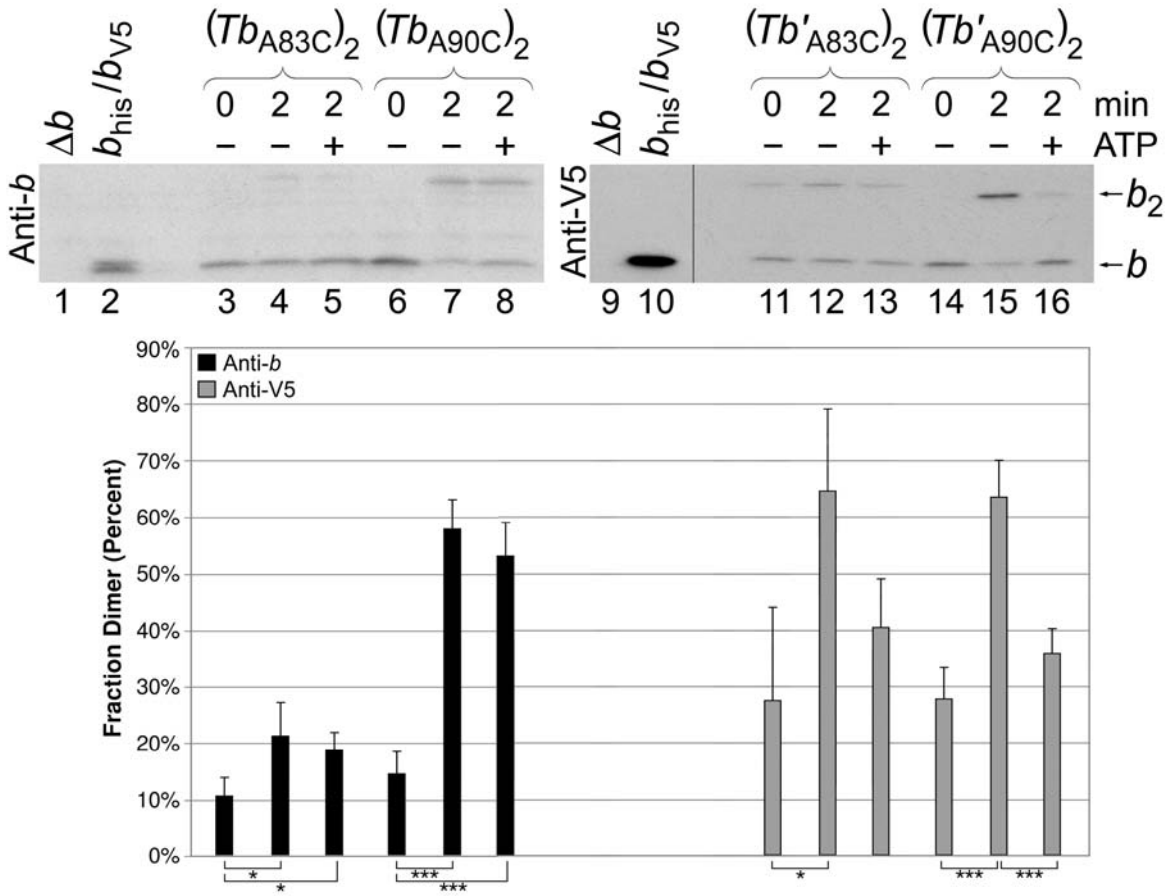

Figure 4-14. Effects of 45 mM ATP on crosslinking formation in homodimeric $(Tb)_2$ and $(Tb')_2$ subunits. The same crosslinking results shown in Figure 4-6 are shown above with additional samples crosslinked in the presence of 45 mM ATP. The membranes were prepared from strains KM2/pSBC123 (Tb_{A83C}), KM2/pSBC124 (Tb_{A90C}), KM2/pSBC125 (Tb'_{A83C}) and KM2/pSBC126 (Tb'_{A90C}) and analyzed by Western blot with antibodies against the *b* subunit and the V5 epitope tag. Total amounts of 1 μg and 10 μg membrane protein were loaded per lane for the anti-V5 and anti-*b* subunit Westerns, respectively. Vertical lines indicate the removal of unwanted lanes *in silico*. The average fraction dimer obtain from densitometry analysis of four experiments is charted below each blot. Samples with a low probability of being identical are indicated (*, $p < 0.05$; **, $p < 0.01$; ***, $p < 0.001$).

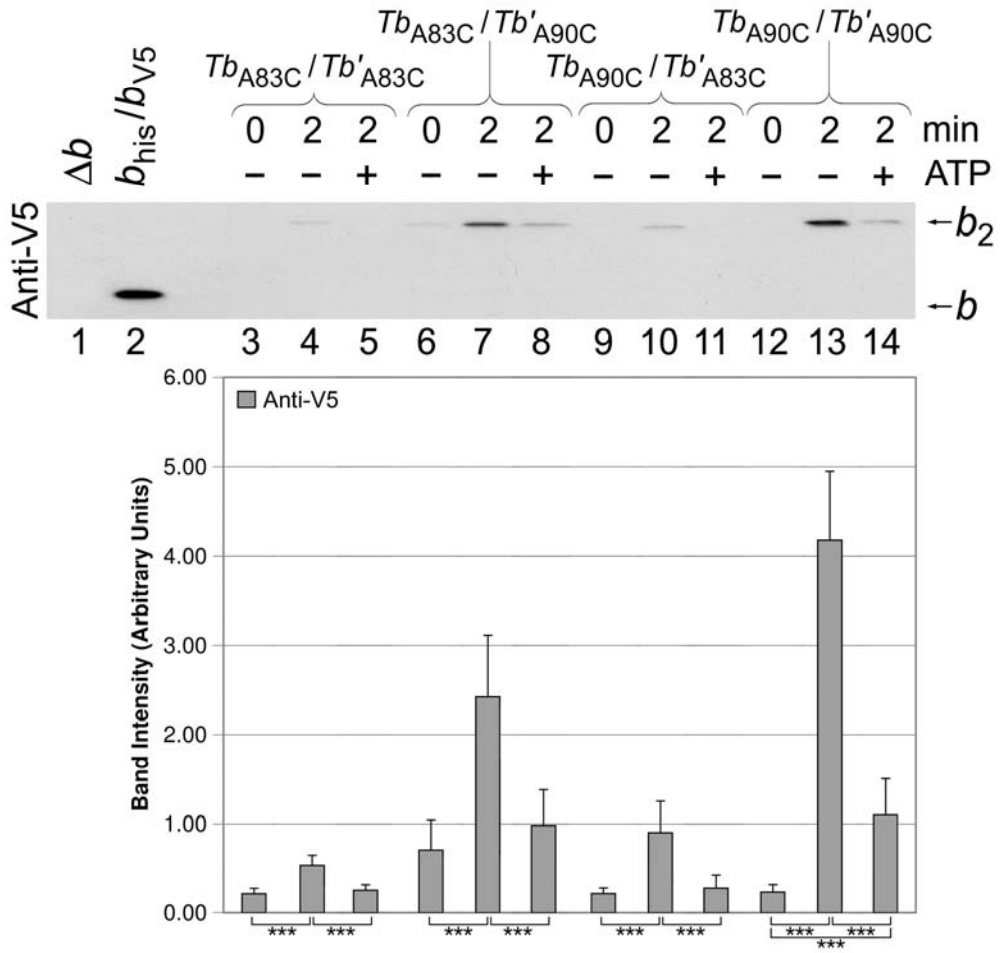

Figure 4-15. Effects of 45 mM ATP on crosslink formation in heterodimeric *Tb/Tb'* peripheral stalks. The same crosslinking results shown in Figure 4-10 are shown above with additional samples crosslinked in the presence of 45 mM ATP. The membranes were prepared from strains KM2/pSBC123/pSBC125 (Tb_{A83C}/Tb'_{A83C}), KM2/pSBC123/pSBC126 (Tb_{A83C}/Tb'_{A90C}), KM2/pSBC124/pSBC125 (Tb_{A90C}/Tb'_{A83C}) and KM2/pSBC124/pSBC126 (Tb_{A90C}/Tb'_{A90C}). Membranes were crosslinked and then purified over a nickel resin to retain only F_1F_O complexes containing a histidine tag. A total of 10% of the nickel resin elutant was analyzed by Western blot with a primary antibody against the V5 epitope tag to detect heterodimeric F_1F_O. The average band intensity in arbitrary units obtained from densitometry analysis of eight experiments is charted below. Samples with a low probability of being identical are indicated (*, $p < 0.05$; **, $p < 0.01$; ***, $p < 0.001$).

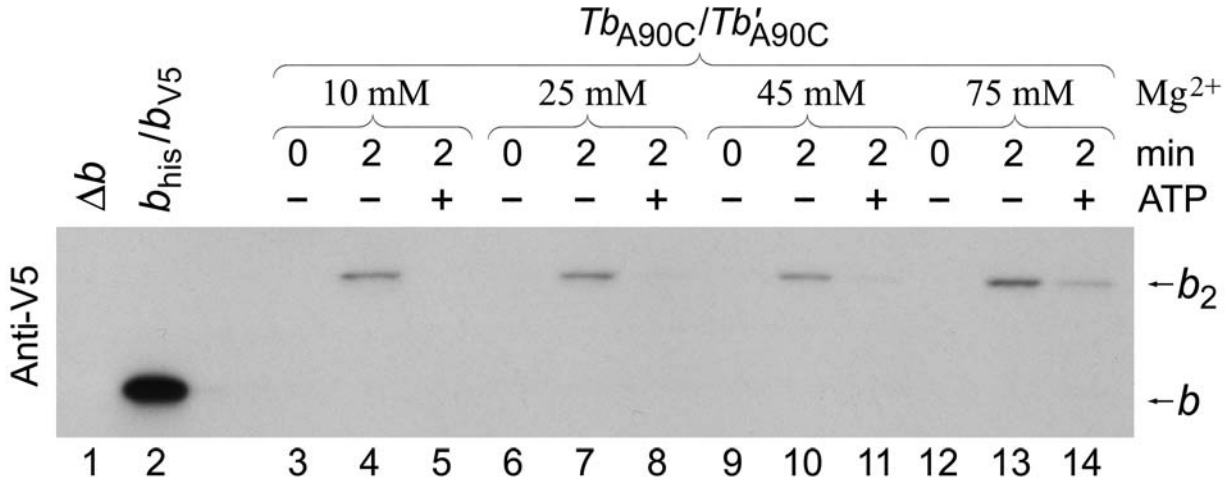

Figure 4-16. Effects of Mg^{2+} concentration on disulfide formation. Membranes from strain KM2/pSBC124/pSBC126 (Tb_{A90C}/Tb'_{A90C}) were prepared, crosslinked and purified over a nickel resin essentially as described in Figure 4-15. The only difference was the addition of $MgCl_2$ to the TM buffer to final concentrations of 10, 25, 45 and 75 mM. A total of 10% of the elutant from the nickel resin was analyzed by Western blot using a primary antibody against the V5 epitope tag.

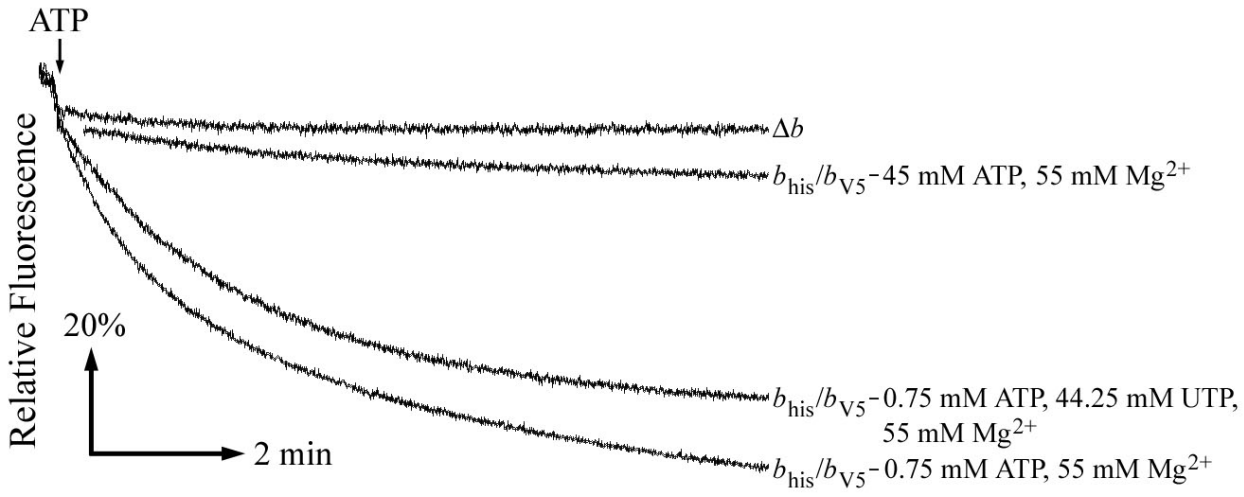

Figure 4-17. Effects of nucleotide concentration on ATP-driven proton pumping. Membranes from the strains KM2/pTAM37/pTAM46 (b_{his}/b_{V5}) and KM2/pBR322 (Δ*b*) were prepared in the presence of 1 mM TCEP. A total of 0.125 mg membrane protein was assay for ATP-driven proton pumping activity in the presence of varying nucleotide concentrations and 55 mM Mg^{2+}.

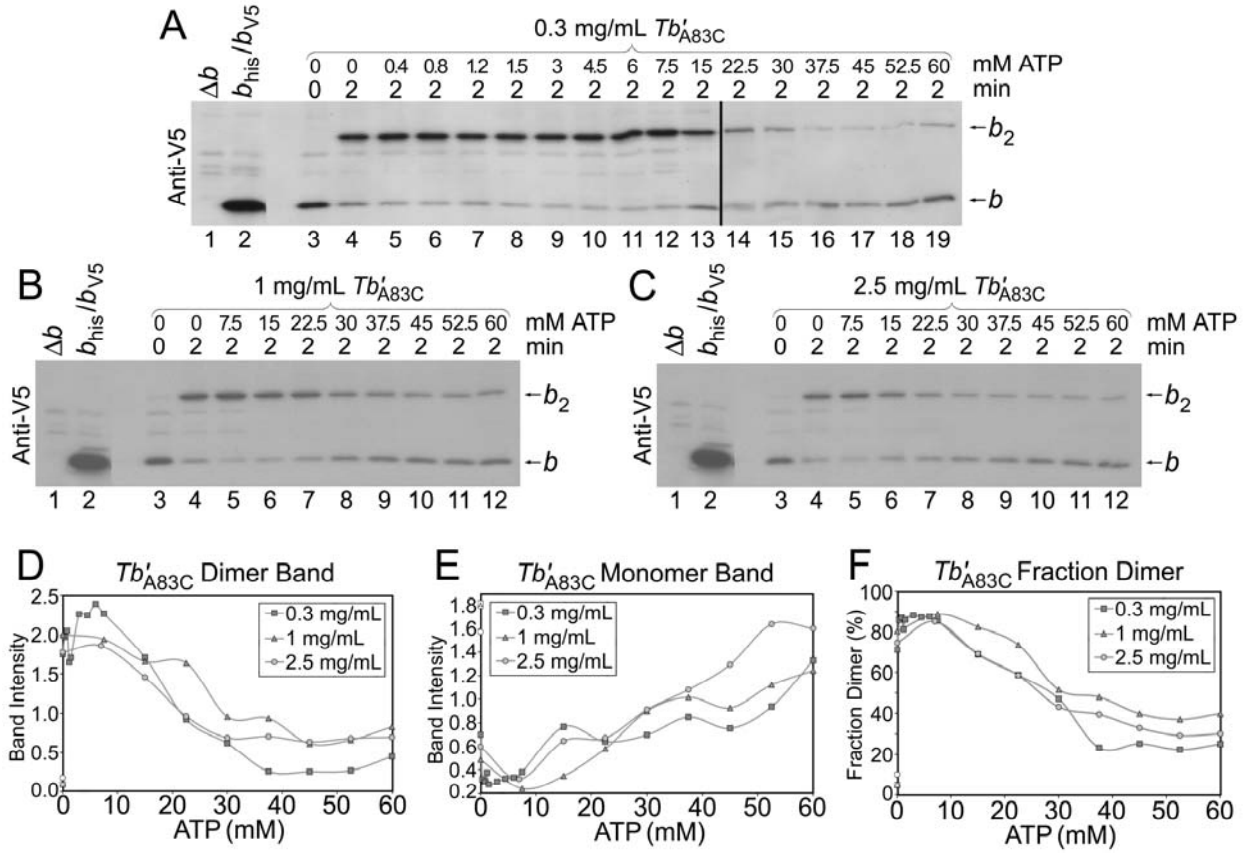

Figure 4-18. Crosslink formation in the presence of increasing ATP concentration. Membranes were prepared from the strain KM2/pSBC125 (*Tb'*$_{A83C}$) in the presence of 5 mM TCEP and diluted to A) 0.3 mg/mL, B) 1.0 mg/mL and C) 2.5 mg/mL. The diluted membranes were crosslinked with 500 μM Cu^{2+} in the presence of increasing concentrations of ATP at 37 °C for 2 min and quenched by adding NEM to a final concentration of 5 mM. A total of 1 μg of each sample was analyzed by Western blot using an antibody against the V5 epitope tag. The vertical bar indicates where two gels have been joined *in silico*. D) Intensity of the (*Tb'*$_{A83C}$)$_2$ dimer band as a function of ATP concentration. E) Intensity of the *Tb'*$_{A83C}$ monomer band as a function of ATP concentration. F) Fraction dimer as a function of ATP concentration.

CHAPTER 5
DISULFIDE CROSSLINK FORMATION WITHIN THE WILD-TYPE PERIPHERAL STALK OF *E. coli* F_1F_O ATP SYNTHASE

Introduction

Engineered *Escherichia coli* F_1F_O ATP synthases were generated that contained chimeric peripheral stalk where portions of the *b* subunit were replaced by homologous regions from the *b* and *b'* subunits of *Thermosynechococcus elongatus* (Chapter 3). Chimeric constructs containing *T. elongatus b* or *b'* sequence for the E39-I86 region, abbreviated *Tb* and *Tb'*, were modified by site-directed mutagenesis to individually substitute cysteines at residues A83 and A90. These residues were chosen to test the staggered model developed in the Dunn lab based on crosslinking analysis of the hydrophilic domain of wild-type *E. coli b* subunit [326, 359]. Disulfide crosslinking analysis of these constructs suggested that the heterodimeric *Tb*/*Tb'* peripheral stalk may adopt a staggered conformation in the context of the holoenzyme (Chapter 4). The strongest evidence for this staggered model is the rapid formation of a crosslink between Tb_{A83C}/Tb'_{A90C} at the low Cu^{2+} concentration of 50 μM. This result, along with the absence of crosslink formation between homodimeric $(Tb_{A83C})_2$ or $(Tb'_{A90C})_2$ at the same concentration of Cu^{2+}, indicate that the two chimeric subunits likely form a peripheral stalk where the offset conformation is favored over the parallel conformation.

The present chapter investigates crosslink formation in the wild-type *E. coli b* subunit to see if the results obtained in the chimeric peripheral stalk are applicable to the native peripheral stalk. Cysteines have been engineered into the wild-type *b* subunit at residues I76, R83, A90 and E97 and the tendency to form disulfide crosslinks in the homodimeric peripheral stalk was investigated. Crosslinking results obtained using the *E. coli b* subunit at both high and low concentrations of Cu^{2+} closely mirror those obtained in the chimeric peripheral stalks. These

results indicate that while a the wild-type peripheral stalk can be trapped in a parallel conformation, the possibility of a staggered arrangement cannot be ruled out.

Results

Functional Characterization of Mutants

The parent plasmid used for construction pSBC127 (b_{V5}), was generated by ligating a synthetic *b* subunit with a C-terminal V5 epitope tag (GenScript) into the *EcoR*I/*Kpn*I restriction sites of pUC19. The constructs pSBC128 ($b_{I76C, V5}$), pSBC129 ($b_{R83C, V5}$), pSBC130 ($b_{A90C, V5}$) and pSBC131 ($b_{E97C, V5}$) were made from pSBC127 (b_{V5}) by site directed mutagenesis using the oligonucleotides listed in Table 5-1. The primary sequence of all constructs was confirmed by direct nucleotide sequencing. Growth on minimal A media supplemented with succinate as the sole carbon source was used as a test of F_1F_O activity as shown in Table 5-2 and Figure 5-1. All engineered subunits were capable of supporting growth by oxidative phosphorylation. Strains KM2/pSBC127 (b_{V5}), KM2/pSBC128 ($b_{I76C, V5}$), KM2/pSBC129 ($b_{R83C, V5}$) and KM2/pSBC130 ($b_{A90C, V5}$) producing colonies slightly smaller than wild-type while KM2/pSBC131 ($b_{E97C, V5}$) formed small colonies. The addition of 0.2% casamino acids and IPTG to the minimal A media resulted in growth in all four strains identical to that of the wild-type.

The rate of ATP hydrolysis in membranes prepared from each strain was determined in both the presence and absence of 0.5% LDAO (Figure 5-2). The values obtained for ATP hydrolysis can be used as an indirect indication of F_1F_O assembly. All of the strains showed abundant intact and assembled F_1F_O as determined by their ATP hydrolysis rates. Membranes prepared from strains KM2/pSBC127 (b_{V5}), KM2/pSBC129 ($b_{R83C, V5}$), KM2/pSBC130 ($b_{A90C, V5}$) and KM2/pSBC131 ($b_{E97C, V5}$) showed ATPase activity comparable to wild type, while strain KM2/pSBC128 ($b_{I76C, V5}$) showed a slight decrease in ATPase activity to about 70% of wild-type. An ATP-driven proton pumping assay was used to measure coupling between F_1 and

F_O (Figure 5-2). Fully coupled enzyme activity was observed for strains KM2/pSBC127 (b_{V5}), KM2/pSBC129 ($b_{R83C, V5}$) and KM2/pSBC130 ($b_{A90C, V5}$), while reduced coupling was seen for KM2/pSBC128 ($b_{I76C, V5}$) and KM2/pSBC131 ($b_{E97C, V5}$). With the exception of strain KM2/pSBC128 ($b_{I76C, V5}$), the results indicate that the cysteine substitutions had no significant effect on assembly and activity of the engineered F_1F_O.

Crosslink Formation

The ability of the engineered *b* subunits to form disulfide crosslinks was investigated by diluting membrane vesicles to 5 mg/mL and adding 500 μM Cu^{2+} for 120 sec. The crosslinking reaction was stopped with 5 mM NEM and the results analyzed by Western blot (Figure 5-3). As expected, membranes prepared from strain KM2/pSBC127 (b_{V5}) showed no crosslink formation. Membranes prepared from strain KM2/pSBC129 ($b_{R83C, V5}$) produced about 20% dimer, comparable to the crosslink formation observed for strain KM2/pSBC123 (Tb_{A83C}) as shown in Chapter 4. Likewise, sample KM2/pSBC130 ($b_{A90C, V5}$) showed about 70% dimer formation, similar to the results obtained using strain KM2/pSBC124 (Tb_{A90C}). Strain KM2/pSBC131 ($b_{E97C, V5}$) only produced about 25% dimer, while KM2/pSBC128 ($b_{I76C, V5}$) remained essentially monomeric.

The efficiency of crosslink formation was investigated by reducing the Cu^{2+} concentration to 50 μM and allowing the reaction to occur for 10 min. None of the homodimeric subunits were capable of crosslink formation at the reduced Cu^{2+} concentration (Figure 5-4). The results presented in Chapter 4 are identical, with crosslink formation only observed in the heterodimeric peripheral stalks upon treatment with low concentrations of Cu^{2+}.

Effects of ATP on Crosslink Formation

The effects of catalysis on crosslink formation was investigated by crosslinking the engineered *b* subunits in the presence and absence of 5 mM ATP. As shown in Figure 5-5A, no significant effect on crosslinking was observed for any of the cysteine substitutions. Interestingly, the addition of ATP to the high concentration of 45 mM resulted in a decrease in crosslink formation (Figure 5-5B). This effect is most noticeable for strain KM2/pSBC130 ($b_{A90C, V5}$) due to the high level of crosslinking this sample exhibited upon oxidation. While the exact cause of this effect is uncertain, it is clear that enzyme catalysis is not responsible for the crosslinking effects because 5 mM ATP is sufficient to fully activity F_1F_O (Weber and Senior, 1997).

Discussion

The results obtained by oxidizing membranes prepared from strains KM2/pSBC129 ($b_{R83C, V5}$) and KM2/pSBC130 ($b_{A90C, V5}$) are consistent with those obtained with chimeric peripheral stalks described in Chapter 4. Upon treatment with the high Cu^{2+} concentration of 500 μM, only about 20% crosslink formation was observed in the $(b_{R83C})_2$ peripheral stalk (Figure 5-3). This result is identical to that observed in the $(Tb_{A83C})_2$ sample (Figure 4-6). Notice that although significantly higher crosslink formation was observed for the $(Tb'_{A83C})_2$ sample, this result is not directly comparable due to the loss of F_1 in the *Tb'* samples during membrane preparation. Around 70% crosslink formation was observed in the $(b_{A90C})_2$ peripheral stalk, comparable to what was observed in the $(Tb_{A90C})_2$ sample. Upon reduction of the Cu^{2+} concentration to 50 μM, no crosslink formation was observed in either the *E. coli* peripheral stalk or the homodimeric chimeric peripheral stalks (Figures 4-11 and 5-4). These results indicate that the wild-type peripheral stalk can be trapped in a parallel conformation. The existence of a staggered

arrangement in the wild-type peripheral stalk could not be tested directly and the possibility that this conformation exists could not be ruled out.

Cysteines were substituted in the additional positions b_{I76C} and b_{E97C} of the *E. coli b* subunit. Crosslinking with 500 μM Cu^{2+} resulted in approximately 25% crosslink formation for membranes prepared from strain KM2/pSBC128 ($b_{E97C, V5}$), while membranes from strain KM2/pSBC131 ($b_{I76C, V5}$) remained essentially monomeric. Reducing the Cu^{2+} concentration to 50 μM resulted in no crosslink formation in membranes prepared from these two strains. These results confirm previous crosslinking results done in the dimerization domain of the *b* subunit, but now extend these results to the context of the entire F_1F_O. Previous attempts to crosslink $b_{K52\text{-}k122, I76C}$, $b_{K52\text{-}k122, R83C}$, and $b_{K52\text{-}k122, A90C}$ by incubating with 10 μM Cu^{2+} for 24 hr resulted in no crosslink formation [359]. The work done here demonstrates that residue b_{E97C} also does not crosslink efficiently, a result that has never been reported in the literature.

Results reported here also show that the addition of 45 mM ATP inhibits crosslink formation in membranes prepared from strain KM2/pSBC130 ($b_{A90C, V5}$), while 5 mM ATP does not have any effect. These results are different from what was observed for the chimeric samples, where 45 mM ATP did not have any effect on crosslink formation from sample KM2/pSBC124 (Tb_{A90C}) (Figure 4-14). The reasons for this discrepancy are not apparent, but it is clear that the effects of ATP on crosslinking are not catalysis related, since 5 mM ATP is capable of fully activating the enzyme [32].

Table 5-1. Oligonucleotides used in this chapter

Oligonucleotide pair (mutation, restriction site)	Annealed Oligonucleotides[a]
SC69/70	SC69 – 5′ GCCCAGGTCATATGCGAGCAGGCGAACAAACGCCGC 3′
(b_{I76C}, +*Nde*I)	SC70 – 3′ CGGGTCCAGTATACGCTCGTCCGCTTGTTTGCGGCG 5′
SC71/72	SC71 – 5′ CATCGAGCAGGCGAACAAACGCTGCTCGCAGATCTTAGACGAAGCG 3′
(b_{R83C}, +*Bgl*II)	SC72 – 3′ GTAGCTCGTCCGCTTGTTTGCGACGAGCGTCTAGAATCTGCTTCGC 5′
SC73/74	SC73 – 5′ CGCCGCTCGCAGATCTTAGACGAATGCAAAGCTGAGGCAGAACAG 3′
(b_{A90C}, +*Bgl*II)	SC74 – 3′ GCGGCGAGCGTCTAGAATCTGCTTACGTTTCGACTCCGTCTTGTC 5′
SC75/76	SC75 – 5′ GCTGAGGCAGAGCAGTGCCGTACTAAAATCGTGGCCCAG 3′
(b_{E97C}, +*Bts*I)	SC76 – 3′ CGACTCCGTCTCGTCACGGCATGATTTTAGCACCGGGTC 5′

[a]Added restriction sites are underlined.

Table 5-2. Plasmids, growth of mutants on succinate and rates of ATP hydrolysis

Strain/Plasmid(s)	Gene product[a, b]	Antibiotic Resistance[c]	Growth on Succinate[d]		ATP Hydrolysis[f]		Source or reference
			No AA	AA + IPTG[e]	No LDAO	0.5% LDAO[g]	
KM2/pTAM37/pTAM46	b_{his}/b_{V5}[a]	Ap+Cm	+++	+++	0.30 ± 0.02	1.21 ± 0.06	[355]
KM2/pBR322	Δb	Ap	–	+	0.07 ± 0.01	0.16 ± 0.01	New England Biolabs
KM2/pSBC127	b_{V5}[b]	Ap	++	+++	0.29 ± 0.01	1.29 ± 0.08	This study
KM2/pSBC128	$b_{I76C, V5}$[b]	Ap	++	+++	0.19 ± 0.01	0.88 ± 0.03	This study
KM2/pSBC129	$b_{R83C, V5}$[b]	Ap	++	+++	0.28 ± 0.07	1.19 ± 0.07	This study
KM2/pSBC130	$b_{A90C, V5}$[b]	Ap	++	+++	0.29 ± 0.04	1.16 ± 0.11	This study
KM2/pSBC131	$b_{E97C, V5}$[b]	Ap	+	+++	0.33 ± 0.07	1.13 ± 0.07	This study

[a]his, six histidine epitope tag at the amino terminus; V5, epitope tag with the sequence GKPIPNPLLGLDST appended to the carboxyl terminus.
[b]The native cysteine at b_{21} has been mutated to serine for all pSBC plasmids.
[c]Ap, ampicillin; Cm, chloramphenicol.
[d]Symbols: +++, wild-type growth; ++, colonies smaller than wild-type; +, small colony formation.
[e]Succinate was supplemented with 0.2% case amino acids and IPTG.
[f]Reported in units of μmol of P_i/mg membrane protein/min. Each sample was assayed in triplicate.
[g]Used to release F_1 from the inhibitory effect of F_O.

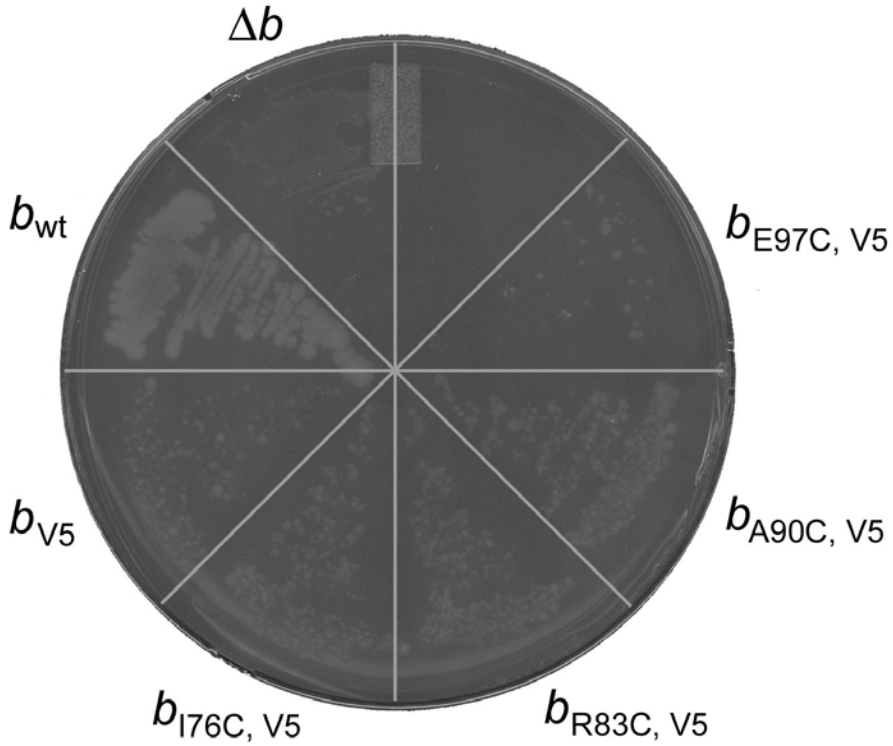

Figure 5-1. Effects of cysteine substitutions on enzyme viability. Growth on minimal A media with succinate as the main carbon source was used to test the viability of F_1F_O ATP synthase complexes. Case amino acids were added to 0.2% to encourage growth and IPTG was included to increase plasmid expression. Strains KM2/pKAM14 (b_{wt}) and KM2/pBR322 (Δ*b*) were used as positive and negative controls, respectively. Strains KM2/pSBC127 (b_{V5}), KM2/pSBC128 ($b_{I76C, V5}$), KM2/pSBC129 ($b_{R83C, V5}$), KM2/pSBC130 ($b_{A90C, V5}$) and KM2/pSBC131 ($b_{E97C, V5}$) were assayed in triplicate. The plate shown is representative of the results obtained.

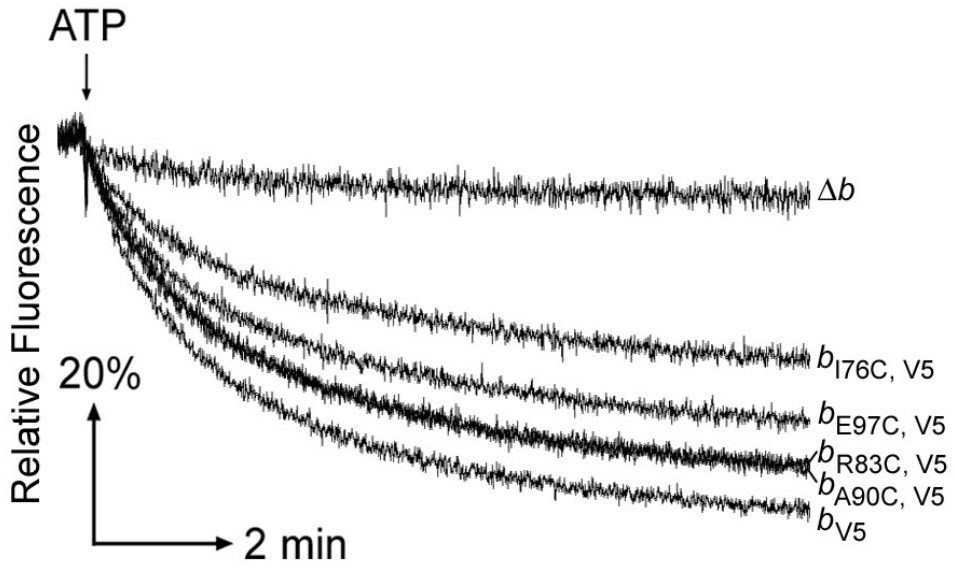

Figure 5-2. Effects of cysteine substitutions on ATP-driven proton pumping activity. The effects of the cysteine substitutions on ATP-driven proton pumping activity was measured by fluorescence quenching of ACMA. Membranes prepared from strains KM2/pSBC127 (b_{V5}) and KM2/pBR322 (Δ*b*) were used as positive and negative controls, respectively. Strains KM2/pSBC128 ($b_{I76C, V5}$), KM2/pSBC129 ($b_{R83C, V5}$), KM2/pSBC130 ($b_{A90C, V5}$) and KM2/pSBC131 ($b_{E97C, V5}$) were assayed in triplicate. Traces shown are representative of the results obtained.

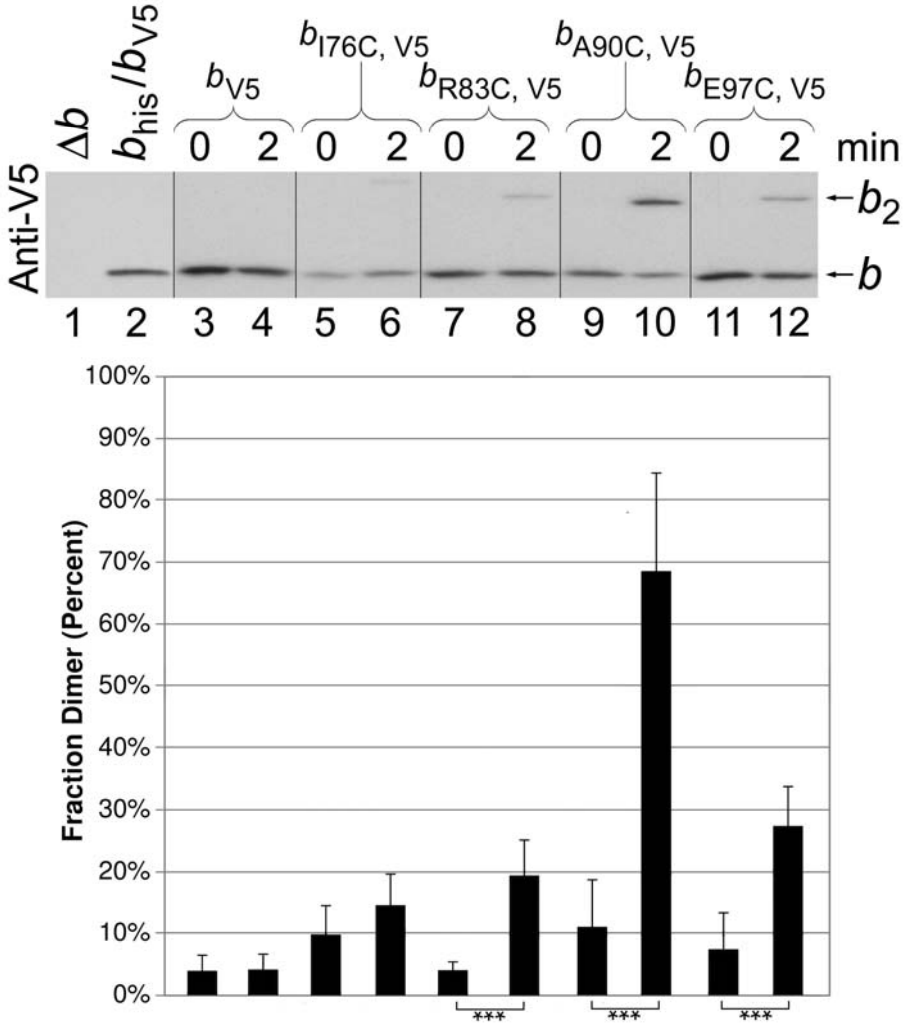

Figure 5-3. Crosslink formation in *E. coli* peripheral stalks containing cysteine substitutions. Membranes containing engineered *b* subunits were prepared in the presence of 5 mM TCEP and crosslinked at 5 mg/mL for 2 min using 500 μM $CuCl_2$. The reaction was quenched by adding NEM to a final concentration of 5 mM. Zero time point samples had NEM added prior to Cu^{2+} to prevent crosslinking. Membranes from strains KM2/pSBC127 (b_{V5}), KM2/pSBC128 (b_{I76C}), KM2/pSBC129 (b_{R83C}), KM2/pSBC130 (b_{A90C}) and KM2/pSBC131 (b_{E97C}) were analyzed by Western blot using a primary antibody against the V5 epitope tag. A total of 1 μg membrane protein was loaded per lane. Vertical lines indicate either the removal of unwanted lanes or the combining of two Westerns *in silico*. The average fraction dimer obtain from densitometry analysis of six experiments is charted below each blot. Samples with a low probability of being identical are indicated (*, $p < 0.05$; **, $p < 0.01$; ***, $p < 0.001$).

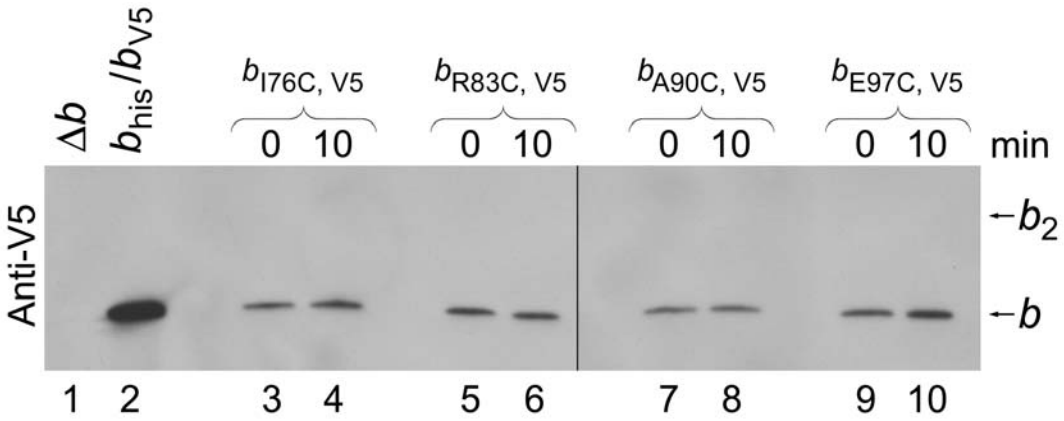

Figure 5-4. Crosslink formation with low Cu^{2+}. Membranes were prepared and crosslinked essentially as described in Figure 5-3 with the exception that Cu^{2+} was added to a final concentration of 50 μM and the crosslinking reaction was allowed to proceed for 10 min before the addition of NEM. Membrane samples prepared from strains KM2/pSBC128 (b_{I76C}), KM2/pSBC129 (b_{R83C}), KM2/pSBC130 (b_{A90C}) and KM2/pSBC131 (b_{E97C}) were crosslinked and analyzed by Western blot using a primary antibody against the V5 epitope tag. A total amount of 1 μg membrane protein was loaded per lane. Vertical lines indicate the combining of two Westerns *in silico*.

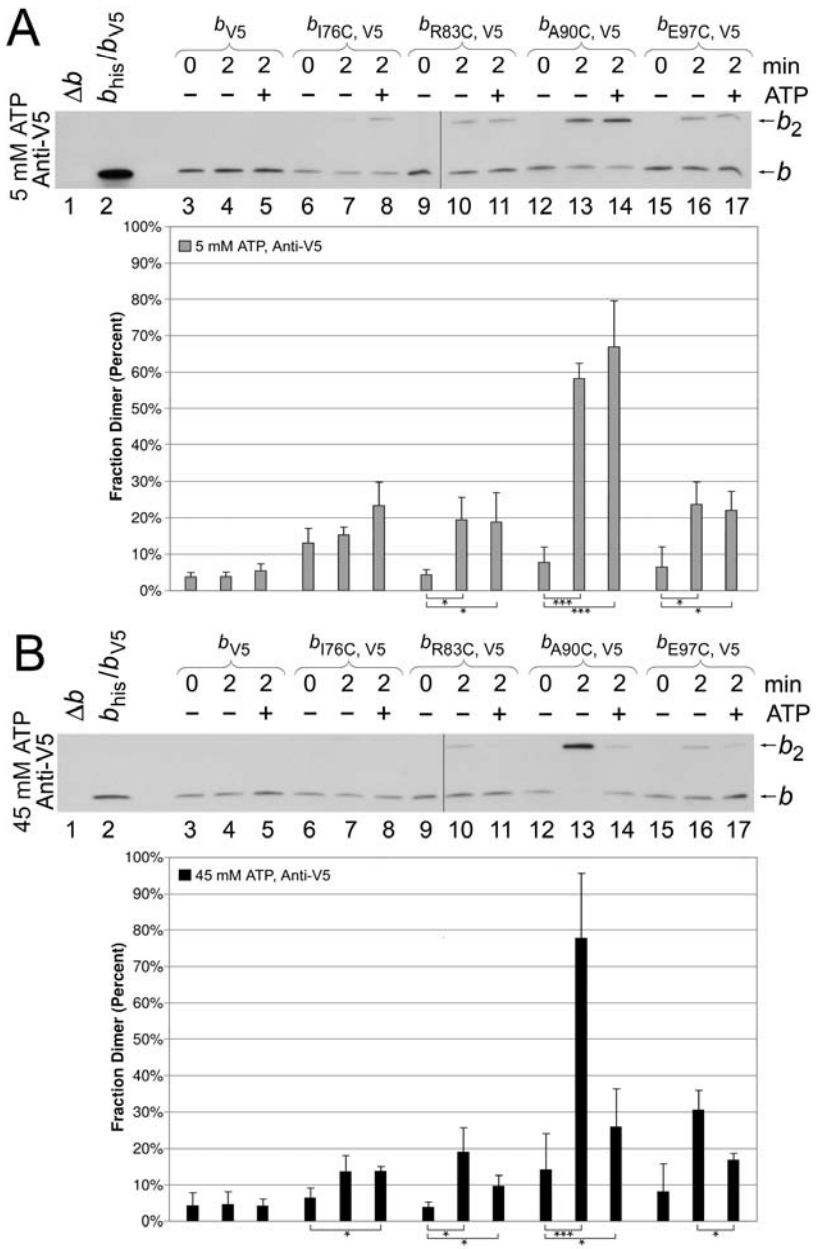

Figure 5-5. Effects of ATP on crosslinking formation in engineered *E. coli b* subunits. The same crosslinking results shown in Figure 5-3 are shown above with additional samples crosslinked in the presence of either A) 45 mM ATP or B) 5 mM ATP. The membranes were prepared from strains KM2/pSBC127 (b_{V5}), KM2/pSBC128 ($b_{I76C, V5}$), KM2/pSBC129 ($b_{R83C, V5}$), KM2/pSBC130 ($b_{A90C, V5}$) and KM2/pSBC131 ($b_{E97C, V5}$) and analyzed by Western blot with a primary antibody against the V5 epitope tag. A total amounts of 1 μg membrane protein was loaded per lane. Vertical lines indicate the joining of two Westerns *in silico*. The average fraction dimer obtain from densitometry analysis of four experiments is charted below each blot. Samples with a low probability of being identical are indicated (*, $p < 0.05$; **, $p < 0.01$; ***, $p < 0.001$).

CHAPTER 6
SPECIFIC INTERACTIONS BETWEEN δ AND THE INDIVIDUAL *b* SUBUNITS OF ATP SYNTHASE

Introduction

The F_1F_O ATP synthase of *E. coli* contains a dimer of identical *b* subunits that interact with a single δ subunit. The last four amino acids of the *b* subunit are critical for this interaction. The truncation of the C-terminal ends of both *b* subunit by four residues disrupts the *b*-δ interactions and prevents complex formation [324]. The C-terminal end of the *b* subunit is capable of forming a disulfide crosslink with the δ subunit. This crosslink is formed between the substitution δ_{M158C} and one member of the $(b_{+G157,+C158})_2$ peripheral stalk [325]. Additionally, experiments done using the soluble form of the peripheral stalk has produced evidence that the *b* subunits may be staggered relative to one another and that only a single full-length *b* subunit is required to bind F_1 [326]. In these experiments, a soluble full-length $b_{V25\text{-}L156}$ subunit and a truncated $b_{V25\text{-}L152}$ subunit were locked in both possible staggered arrangements with one subunit offset by two helical turns. It was found that truncating the N-terminally shifted $b_{V25\text{-}L152}$ subunit significantly affected binding to F_1, while deleting the same amino acids on the C-terminally shifted $b_{V25\text{-}L152}$ subunit had only a modest effect. These results suggested that only a single full-length $b_{V25\text{-}L156}$ subunit is required for the proper interactions with F_1, and the N-terminally shifted $b_{V25\text{-}L156}$ subunit forms these interactions.

Here I have investigated the interactions between the individual *b* subunits and the δ subunit in the context of the entire enzyme. The results demonstrate that a heterodimeric peripheral stalk containing a single full-length *b* subunit is capable of forming the required interactions with the δ subunit, confirming what has been observed in the Dunn lab using the soluble form of the *b* subunit. Sequence from the *b* and *b'* subunits of *T. elongatus* were then

substituted individually in the *E. coli b* subunit for residues E39-I86 in order to generate a peripheral stalk with a known staggered arrangement as shown in the previous chapters. The results obtained with these chimeric peripheral stalks indicate that the C-terminally shifted *b* subunit forms the critical interactions with the δ subunit, in contrast to the results obtained with the soluble *b* subunits [326]. The inclusion of the peripheral stalk in the entire enzyme adds additional conformational constraints which may account for the differing results.

Results

Functional Characterization of Mutants

A total of eight plasmids were constructed from the base plasmids pAES9 (*acb*δαγβε) and pKAM14 (*b*) using a combination of site-directed mutagenesis and ligation. Oligonucleotide primers used for site-directed mutagenesis are listed in Table 6-1, while the constructed plasmids are listed in Table 6-2. A more detailed description of the construction scheme can be found in Appendix B. Five of these plasmids are based on pAES9 and hence express the entire *unc* operon – pSBC99 (*acb*$\delta_{V5,\ M158C}$αγβε), pSBC100 (*acb*$_{+C158}\delta_{V5,\ M158C}$αγβε), pSBC101 (*acb*$_{+C158}\delta_{V5}$αγβε), pSBC140 (*acTb'*$_{+C158}\delta_{V5,\ M158C}$αγβε) and pSBC142 (*acTb*$_{+C158}\delta_{V5,\ M158C}$αγβε). The other three plasmids are based on pKAM14 and express only the *b* subunit – pSBC132 ($b_{his,\ \Delta153\text{-}156}$), pSBC141 (*Tb*$_{his,\ \Delta153\text{-}156}$) and pSBC143 (*Tb'*$_{his,\ \Delta153\text{-}156}$). The native cysteines at b_{C21}, δ_{C64} and δ_{C140} have been mutated to serine in all eight plasmids and all plasmids were confirmed by direct nucleotide sequencing.

The eight plasmids were expressed in six different combinations as listed in Table 6-2. All engineered F_1F_O were capable of supporting growth by oxidative phosphorylation as determined by growth on minimal A media with succinate as the main carbon source (Figure 6-1). Strains expressing chimeric subunits formed slightly smaller colonies that the engineered *E. coli*

subunits, but abundant enzyme activity was detected in all cases. ATP hydrolysis was determined for each strain in the presence and absence of LDAO as an indirect measure of enzyme assembly and coupling. Membranes prepared from strains expressing the modified *E. coli* subunits showed abundant levels of assembled F_1F_O as determined by ATP hydrolysis. Membranes from strain 1100 ΔBC/pSBC140/pSBC141 (*acTb'*$_{+C158}\delta_{V5,\ M158C}\alpha\gamma\beta\varepsilon$ + *Tb*$_{his,\ \Delta153\text{-}156}$) also produced ATP hydrolysis values that indicated a significant amount of enzyme assembly, while those from strain 1100 ΔBC/pSBC142/pSBC143 (*acTb*$_{+C158}\delta_{V5,\ M158C}\alpha\gamma\beta\varepsilon$ + *Tb'*$_{his,\ \Delta153\text{-}156}$) showed low levels of ATP hydrolysis. Both strains expressing chimeric peripheral stalks were capable of supporting growth by oxidative phosphorylation, indicating these constructs are active *in vivo*. The low levels of ATP hydrolysis observed *in vitro* may indicate that the chimeric peripheral stalks are not stable enough to survive the membrane purification procedure, an issue which has been seen in the previous chapters.

ATP-drive proton pumping was assayed by measuring the fluorescence quenching of ACMA. All membranes prepared from strains expressing modified *E. coli b* subunits showed a significant degree of coupling (Figure 6-2A). Strains which contained cysteine substitutions in both the *b* and δ subunit showed slightly lower levels of activity that those containing only a single cysteine, indicating that the cysteines produced some effect. Membranes prepared from strains expressing chimeric peripheral stalks showed low but detectable levels of coupling (Figure 6-2B), comparable to what has been observed in the previous chapters.

Development of Crosslinking Assay

Membranes were prepared in the presence of the reducing agent tris(2-carboxyethyl) phosphine (TCEP) to maintain the cysteines in a reduced state. The effects of TCEP were investigated by preparing membrane from the positive control 1100 ΔBC/pAES9 (*acb*δαγβε) in

the presence of 0, 1, 2.5 and 5 mM TCEP. These samples were assayed for ATP-driven proton pumping (Figure 6-3). The addition of 1 mM TCEP produced no detectable effect, while 2.5 mM TCEP reduced coupled activity and 5 mM completely eliminated detectable proton pumping. The caused of this effect is not clear, since 5 mM TCEP was used in the previous chapters without any detrimental result. The main difference is that the entire *unc* operon is being overexpressed in Figure 6-3, while in previous chapters the only subunit being overexpressed was the *b* subunit. All crosslinking experiments done in this chapter used membrane prepared in the presence of 1 mM TCEP.

The amount of Cu^{2+} required to crosslinking the *b* and δ subunits was determined experimentally. Membranes from strain 1100 ΔBC/pSBC100 ($acb_{+C158}\delta_{V5,\ M158C}\alpha\gamma\beta\varepsilon$) were prepared in the presence of 1, 2.5 and 5 mM TCEP. These membranes were diluted to 5 mg/mL and crosslinked in the presence of 0, 100, 200 or 300 μM Cu^{2+} for 30 minutes at room temperature with shaking. The reactions were quenched by adding NEM to a final concentration of 1 mM and the samples were analyzed by Western blot (Figure 6-4). A concentration of 100 μM Cu^{2+} was sufficient to crosslink membranes prepared in the presence of 1 mM TCEP, so this concentration of Cu^{2+} will be used in all subsequent crosslinking experiments. Interestingly, very little δ subunit was detected in membrane prepared in the presence of 5 mM TCEP, indicating a detrimental effect caused by the higher levels of reducing agent.

Crosslink Formation

All six strains listed in Table 6-2 were prepared in the presence of 1 mM TCEP and crosslinked with 100 μM Cu^{2+} for 30 min. The crosslinked samples were analyzed by Western blot (Figure 6-5). As expected, no crosslinked *b*-δ dimer was detected in membranes prepared from strains which contained only a single cysteine, 1100 ΔBC/pSBC99 ($acb\delta_{V5,\ M158C}\alpha\gamma\beta\varepsilon$) and

1100 ΔBC/pSBC101 (*acb*$_{+C158}$δ$_{V5}$αγβε) (lanes 3-6). The inclusion of both cysteines in strain 1100 ΔBC/pSBC100 (*acb*$_{+C158}$δ$_{V5,\ M158C}$αγβε) resulted in the formation of a crosslinked *b*-δ dimer that can be clearly seen in the Western blot against the V5 epitope tag (lanes 7-8). The coexpression of the truncated *b* subunit in strain 1100 ΔBC/pSBC100/pSBC132 (*acb*$_{+C158}$δ$_{V5,\ M158C}$αγβε + *b*$_{his,\ \Delta 153\text{-}156}$) also produced membranes which could be crosslinked to form the higher molecular weight *b*-δ dimer (lanes 9-10). Membranes prepared from strains 1100 ΔBC/pSBC140/pSBC141 (*acTb'*$_{+C158}$δ$_{V5,\ M158C}$αγβε + *Tb*$_{his,\ \Delta 153\text{-}156}$) and 1100 ΔBC/pSBC142/pSBC143 (*acTb*$_{+C158}$δ$_{V5,\ M158C}$αγβε + *Tb'*$_{his,\ \Delta 153\text{-}156}$) showed very little free δ subunit associated with the membranes (lanes 11-14). However, a small amount of *b*-δ crosslinked product was observed for the former and a significant amount for the latter (lanes 12 and 14, respectively). Note that the crosslinked product observed in lanes 10, 12 and 14 can contain both heterodimeric and homodimeric peripheral stalks crosslinked to the δ subunit.

A nickel resin purification procedure developed in the Cain lab was used to detect crosslink formation between heterodimeric peripheral stalks and the δ subunit. Figure 6-6A shows several important controls which demonstrate the specificity of the purification procedure. Lane 3 contains membranes prepared from strain KM2/pTAM46 (b_{V5}) and purified to confirm that samples lacking a histidine tag are not retained by the resin. Lane 4 contains membranes prepared from strain KM2/pTAM37 (b_{his}) and purified to demonstrate that the resin retains samples which contain a histidine tag and these samples are not detected by the antibody against the V5 epitope tag. Lane 5 contains an aggregation control which consists of membranes prepared from strains KM2/pTAM37 (b_{his}) and KM2/pTAM46 (b_{V5}) mixed together prior to purification to confirm that the F_1F_O complexes are not sticking together. Finally, lane 6 contains membranes prepared from strain KM2/pTAM37/pTAM46 (b_{his}/b_{V5}). A band is

observed in this lane with the antibody against the V5 epitope tag, indicating the presence of peripheral stalks containing both a histidine tag and a V5 epitope tag.

Membrane purified over a nickel resin and analyzed by Western blot are shown in Figure 6-6B. The positive control is lane 2 which contains membranes prepared from strain 1100 ΔBC/pSBC100 ($acb_{+C158}\delta_{V5,\ M158C}\alpha\gamma\beta\varepsilon$) that have been crosslinked to demonstrate the location of both the δ and *b*-δ bands. Membranes prepared from strain 1100 ΔBC/pSBC100/pSBC132 ($acb_{+C158}\delta_{V5,\ M158C}\alpha\gamma\beta\varepsilon + b_{his,\ \Delta153\text{-}156}$) were crosslinked as described above for Figure 6-5, purified over a nickel resin and analyzed by Western blot (lanes 3-4). The presence of a *b*-δ band in lane 4 clearly demonstrates that the heterodimeric $b_{+C158}/b_{his,\ \Delta153\text{-}156}$ peripheral stalk is capable of forming a crosslink with the $\delta_{V5,\ M158C}$ subunit. This result indicates that only a single full-length *b* subunit is required to form the essential interactions with the δ subunit. Likewise, membranes were prepared from strains 1100 ΔBC/pSBC140/pSBC141 ($acTb'_{+C158}\delta_{V5,\ M158C}\alpha\gamma\beta\varepsilon + Tb_{his,\ \Delta153\text{-}156}$) and 1100 ΔBC/pSBC142/pSBC143 ($acTb_{+C158}\delta_{V5,\ M158C}\alpha\gamma\beta\varepsilon + Tb'_{his,\ \Delta153\text{-}156}$) and crosslinked, purified and analyzed by Western blot (lanes 5-8). The band in lane 8 demonstrates that the heterodimeric peripheral stalk $Tb_{+C158}/Tb'_{his,\ \Delta153\text{-}156}$ was capable of crosslinking to the $\delta_{V5,\ M158C}$ subunit, while the lack of a band in lane 6 indicates that the $Tb_{his,\ \Delta153\text{-}156}/Tb'_{+C158}$ peripheral stalk was unable to form this crosslink. It can be determined from the previous chapters that the *Tb* subunit is extended C-terminally and the *Tb'* subunit N-terminally in the region of residues 83 and 90, clearly differentiating the two *b* subunits from one another. The crosslinking results indicate that a truncation on the N-terminally shifted *b* subunit still allowed complex formation and crosslinking of the C-terminally shifted *b* subunit to the δ subunit, but not in the alternate arrangement (see model Figure 6-8).

The low level of the δ subunit detected in membranes prepared from strains expressing chimeric peripheral stalks combined with the significant *in vivo* activity of these strains suggested that the F_1F_O complexes may be falling apart during membrane preparation. Samples 1100 ΔBC/pSBC140/pSBC141 (*acTb'*$_{+C158}\delta_{V5,\ M158C}\alpha\gamma\beta\varepsilon$ + *Tb*$_{his,\ \Delta153\text{-}156}$) and 1100 ΔBC/pSBC142/pSBC143 (*acTb*$_{+C158}\delta_{V5,\ M158C}\alpha\gamma\beta\varepsilon$ + *Tb'*$_{his,\ \Delta153\text{-}156}$) were prepared in the presence of 100 μM Cu^{2+} in an attempt to crosslink the *b* and δ subunits prior to complex disassociation. No significant increase in ATP hydrolysis was observed as a result of preparing membranes in the presence of Cu^{2+} (Figure 6-7A). A slight decrease in ATP-driven proton pumping was observed for both samples when prepared in the presence of Cu^{2+} as well as after crosslinking the membranes with 100 μM Cu^{2+} for 30 minutes (Figure 6-7B and 6-7C). Analysis of membranes prepared in the presence of Cu^{2+} by Western blot showed no significant change in crosslink formation (Figure 6-7D and 6-7E). These data show that preparing of membranes from these strains in the presence of Cu^{2+} did not enhance *b*-δ crosslink formation.

Discussion

The peripheral stalk of F_1F_O ATP synthase from *E. coli* consists of a dimer of identical *b* subunits which interact with the lone δ subunit. This interaction is abolished if the last four amino acids of both *b* subunits are truncated [324]. Here I have investigated if a single full-length *b* subunit is sufficient to form the necessary interactions with the δ subunit by utilizing a disulfide crosslink that can be formed between a cysteine extension appended to the *b* subunit and the δ_{M158C} substitution [325]. Membranes prepared from strain 1100 ΔBC/pSBC100/pSBC132 (*acb*$_{+C158}\delta_{V5,\ M158C}\alpha\gamma\beta\varepsilon$ + *b*$_{his,\ \Delta153\text{-}156}$) were crosslinked, purified over a nickel resin and analyzed by Western blot. The data demonstrated that F_1F_O containing heterodimeric *b*$_{+C158}$/*b*$_{his,\ \Delta153\text{-}156}$ peripheral stalks were capable of forming a disulfide crosslink to

the $\delta_{V5,\ M158C}$ subunit, indicating that a single full-length *b* subunit is sufficient to form the necessary interactions with the δ subunit in the context of the entire enzyme. These results correlate well with data obtained using a soluble form of the *b* subunit and F_1 [326].

Results presented in previous chapters showed that chimeric peripheral stalks created by substituting sequence from the *b* and *b'* subunit of *T. elongatus* for *E. coli* residues E39-I86 produced peripheral stalks that readily formed heterodimers with a staggered arrangement. These results correlate well with a previously proposed staggered model for the peripheral stalk based on work done with the soluble form of the *b* subunit [326, 359]. Here I have used the predicted staggering of the chimeric *Tb* and *Tb'* subunits to investigate which *b* subunit forms the essential interactions with the δ subunit. Crosslinking and nickel resin purification of membranes prepared from strains 1100 ΔBC/pSBC140/pSBC141 ($acTb'_{+C158}\delta_{V5,\ M158C}\alpha\gamma\beta\varepsilon$ + $Tb_{his,\ \Delta153\text{-}156}$) and 1100 ΔBC/pSBC142/pSBC143 ($acTb_{+C158}\delta_{V5,\ M158C}\alpha\gamma\beta\varepsilon$ + $Tb'_{his,\ \Delta153\text{-}156}$) clearly demonstrated that the $Tb_{his,\ \Delta153\text{-}156}/Tb'_{+C158}$ peripheral stalk was unable to crosslink while the $Tb_{+C158}/Tb'_{his,\ \Delta153\text{-}156}$ peripheral stalk formed a disulfide bond with the $\delta_{V5,\ M158C}$ subunit (see model Figure 6-8). These results indicate that F_1F_O complex formation can occur with a truncation to the N-terminally shifted *b* subunit as detected by formation of the *b*-δ crosslink. Crosslink formation was not detected for the alternate arrangement, indicating that either F_1F_O cannot form if the C-terminally shifted *b* subunit is truncated or that the *b*-δ disulfide crosslink cannot form with the N-terminally shifted *b* subunit. These data demonstrated an asymmetric interaction between the individual *b* subunits and the δ subunit. In contrast, work done using the soluble form of the *b* subunit and F_1 found the N-terminally shifted *b* subunit important for binding and crosslinking to the δ subunit [326]. The exact cause of this discrepancy is not clear,

but it may be due to additional forces exerted on the peripheral stalk by the other subunits of the intact enzyme.

Table 6-1. Oligonucleotides used in this chapter

Oligonucleotide pair (mutation, restriction site)	Annealed Oligonucleotides[a]
TB1/2 (b_{his}, +*Sph*I)	TB1 – 5′ CTAAATAGAAGCATGCTGCTGTGCACCACCACCACCACCACAATCTTAACGCAACAATCCTCGGC 3′ TB2 – 3′ GATTTATCTTCGTACGACGACACGTGGTGGTGGTGGTGGTGTTAGAATTGCGTTGTTAGGAGCCG 5′
TB10/11 (δ_{C140S}, +*Eco*RI, -*Cla*I)	TB10 – 5′ CGTCTGTCACGCAAAGTTAAGCTGAATTCGAAAATTGATAAGTCCGTAATGGCAGG 3′ TB11 – 3′ GCAGACAGTGCGTTTCAATTCGACTTAAGCTTTTAACTATTCAGGCATTACCGTCC 5′
TB12/13 (b_{C21S}, -*Sna*BI)	TB12 – 5′ CTGTTCGTTCTGTTCTCCATGAAGTACGTTTGGCCGCC 3′ TB13 – 3′ GACAAGCAAGACAAGAGGTACTTCATGCAAACCGGCGG 5′
TB40/41 ($b_{\Delta 153\text{-}156}$, +*Hind*III)	TB40 – 5′ CATCGTGGATAAGCTTTAAGGAGGGAGGGGCTG 3′ TB41 – 3′ GTAGCACCTATTCGAAATTCCTCCCTCCCCGAC 5′
SC4/5 ($b_{+G157,\,+C158}$, +*Sac*I)	SC4 – 5′ AACTTGTCGCTGAGCTCGGTTGTTAAGGAGGGAGGGG 3′ SC5 – 3′ TTGAACAGCGACTCGAGCCAACAATTCCTCCCTCCCC 5′
SC6/7 (δ_{M158C}, +*Cla*I)	SC6 – 5' CATCCGAGCGGGTGATTGCGTCATCGATGGCAGCGTAC 3' SC7 – 3' GTAGGCTCGCCCACTAACGCAGTAGCTACCGTCGCATG 5'
SC8/9 (δ_{C64S}, +*Pvu*II)	SC8 – 5' TTTATCGCAGTTTCTGGTGAGCAGCTGGACGAAAACGG 3' SC9 – 3' AAATAGCGTCAAAGACCACTCGTCGACCTGCTTTTGCC 5'
SC65/66[b] ($b_{\Delta(+C55)}$, +*Sna*BI)	SC65 – 5′ GCGTTTGTCCTGTTCGTTCTGTTCTCCATGAAGTACGTATGGCCGCCATTAATGG 3′ SC66 – 3′ CGCAAACAGGACAAGCAAGACAAGAGGTACTTCATGCATACCGGCGGTAATTACC 5′
CS3/4 (δ_{V5}, +*Xba*I)	CS3 – 5′ TGTAAGGAGGGAGGGGCTGATGGGTAAACCGATCCCGAACCCGCTGCTGGGTCTAGACTCTACTTCTGAATTTATTACGGTAGCTC 3′ CS4 – 3′ ACATTCCTCCCTCCCCGACTACCCATTTGGCTAGGGCTTGGGCGACGACCCAGATCTGAGATGAAGACTTAAATAATGCCATCGAG 5′

[a]Added restriction sites are underlined.
[b]SC65/66 were used to remove an unwanted insertion at b_{+C55}.

Table 6-2. Plasmids, growth of mutants on succinate and rates of ATP hydrolysis

Strain/Plasmid(s)	Modified Subunits[a, b]		Antibiotic	Growth on	ATP Hydrolysis[e]		Source
	b subunit	δ subunit	Resistance[c]	Succinate[d]	No LDAO	0.5% LDAO[f]	or Reference
1100 ΔBC/pAES9	b_{wt}	δ_{wt}	Cm	+++	0.80 ± 0.08	4.1 ± 0.2	[402]
1100 ΔBC/pACYC184	Δ*b*	Δδ	Cm	+	0.11 ± 0.01	0.37 ± 0.06	New England Biolabs
1100 ΔBC/pSBC99	b_{wt}	$\delta_{V5, M158C}$	Cm	+++	0.75 ± 0.04	3.4 ± 0.1	This study
1100 ΔBC/pSBC100	b_{+C158}	$\delta_{V5, M158C}$	Cm	+++	0.74 ± 0.01	2.9 ± 0.2	This study
1100 ΔBC/pSBC101	b_{+C158}	δ_{V5}	Cm	+++	0.57 ± 0.09	2.9 ± 0.2	This study
1100 ΔBC/pSBC100/pSBC132	b_{+C158} + $b_{his, \Delta 153-156}$	$\delta_{V5, M158C}$	Ap + Cm	+++	0.90 ± 0.04	4.2 ± 0.4	This study
1100 ΔBC/pSBC140/pSBC141	$Tb_{his, \Delta 153-156}$ + Tb'_{+158C}	$\delta_{V5, M158C}$	Ap + Cm	++	0.50 ± 0.07	1.5 ± 0.1	This study
1100 ΔBC/pSBC142/pSBC143	Tb_{+158C} + $Tb'_{his, \Delta 153-156}$	$\delta_{V5, M158C}$	Ap + Cm	++	0.20 ± 0.01	0.7 ± 0.1	This study

[a]his, six histidine epitope tag at the amino terminus of the *b* subunit; V5, epitope tag with the sequence GKPIPNPLLGLDST appended to the amino terminus of the δ subunit; +C158, glycine-cysteine extension appended to the *b* subunit C-terminus; *Tb* and *Tb'*, *E. coli b* subunits with residues E39-I86 replaced by *T. elogatus b* and *b'* subunit sequence, respectively.

[b]The native cysteines at b_{21}, δ_{64} and δ_{140} have been mutated to serine in all plasmids except pAES9.

[c]Ap, ampicillin; Cm, chloramphenicol.

[d]Symbols: +++, wild-type growth; ++, colonies smaller than wild-type; +, small colony formation. Succinate was supplemented with 0.2% case amino acids.

[e]Reported in units of μmol of P_i/mg membrane protein/min. Each sample was assayed in triplicate.

[f]Used to release F_1 from the inhibitory effect of F_O.

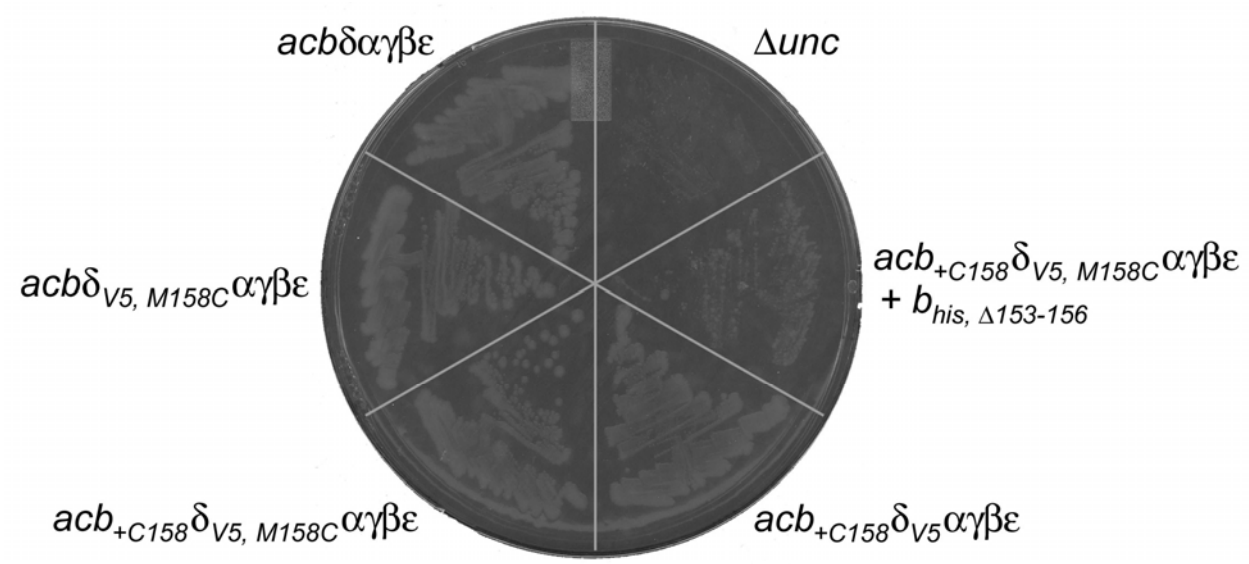

Figure 6-1. Effects of mutations on enzyme viability. Growth on minimal A media with succinate as the main carbon source was used to test the viability of F_1F_O ATP synthase complexes. Case amino acids were added to 0.2% to encourage growth. Strains 1100 ΔBC/pAES9 (*acb*δαγβε) and 1100 ΔBC/pACYC184 (Δ*unc*) were used as positive and negative controls, respectively. Strains 1100 ΔBC/pSBC99 ($acb\delta_{V5, M158C}\alpha\gamma\beta\varepsilon$),1100 ΔBC/pSBC100 ($acb_{+C158}\delta_{V5, M158C}\alpha\gamma\beta\varepsilon$),1100 ΔBC/pSBC101 ($acb_{+C158}\delta_{V5}\alpha\gamma\beta\varepsilon$) and 1100 ΔBC/pSBC100/pSBC132 ($acb_{+C158}\delta_{V5, M158C}\alpha\gamma\beta\varepsilon + b_{his, \Delta 153-156}$) were assayed in triplicate. The plate shown are representative of the results obtained.

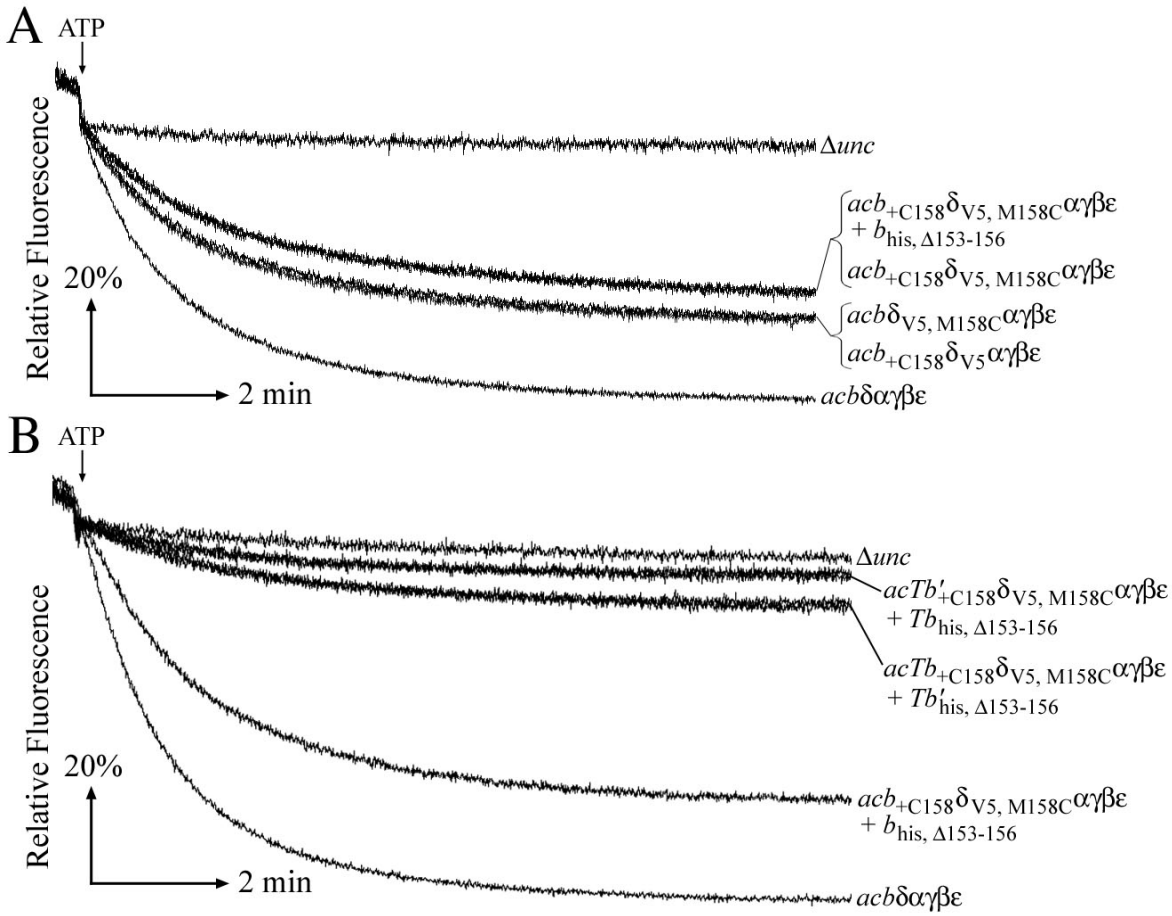

Figure 6-2. Effects of mutations on ATP-driven proton pumping activity. Coupled activity was measure by the fluorescence quenching of ACMA. Membrane prepared from strains 1100 ΔBC/pAES9 (*acb*δαγβε) and 1100 ΔBC/pACYC184 (Δ*unc*) were used as positive and negative controls, respectively. A) Assay of 125 μg membrane protein prepared from strains 1100 ΔBC/pSBC99 (*acb*$\delta_{V5,\ M158C}$αγβε), 1100 ΔBC/pSBC100 (*acb*$_{+C158}\delta_{V5,\ M158C}$αγβε), 1100 ΔBC/pSBC101 (*acb*$_{+C158}\delta_{V5}$αγβε) and 1100 ΔBC/pSBC100/pSBC132 (*acb*$_{+C158}\delta_{V5,\ M158C}$αγβε + *b*$_{his,\ \Delta153\text{-}156}$). B) Assay of 500 μg membrane protein prepared from strains 1100 ΔBC/pSBC100/pSBC132 (*acb*$_{+C158}\delta_{V5,\ M158C}$αγβε + *b*$_{his,\ \Delta153\text{-}156}$), 1100 ΔBC/pSBC140/pSBC141 (*acTb'*$_{+C158}\delta_{V5,\ M158C}$αγβε + *Tb*$_{his,\ \Delta153\text{-}156}$) and 1100 ΔBC/pSBC142/pSBC143 (*acTb*$_{+C158}\delta_{V5,\ M158C}$αγβε + *Tb'*$_{his,\ \Delta153\text{-}156}$). Each sample was assayed in triplicate and the results shown are representative.

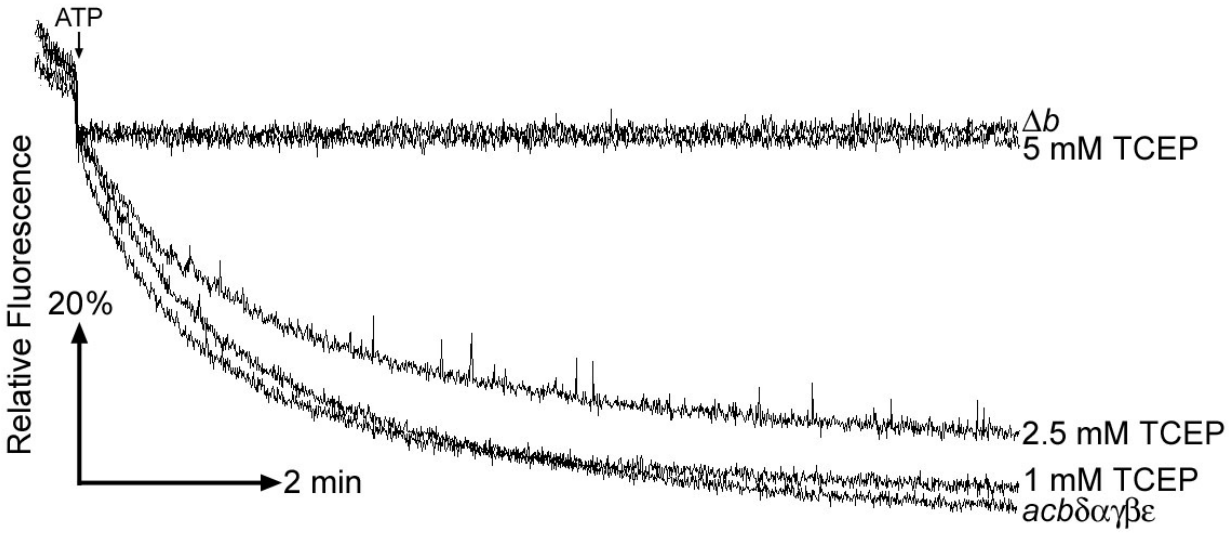

Figure 6-3. Effects of TCEP on ATP-driven proton pumping. Membranes from strain 1100 ΔBC/pAES9 (*acb*δαγβε) were prepared in the presence of 0, 1, 2.5 and 5 mM TCEP and assayed for coupled activity by the fluorescence quenching of ACMA. Each assay consisted of a total of 125 μg of membrane protein. Membranes prepared from strain 1100 ΔBC/pACYC184 (Δ*unc*) were used as a negative control.

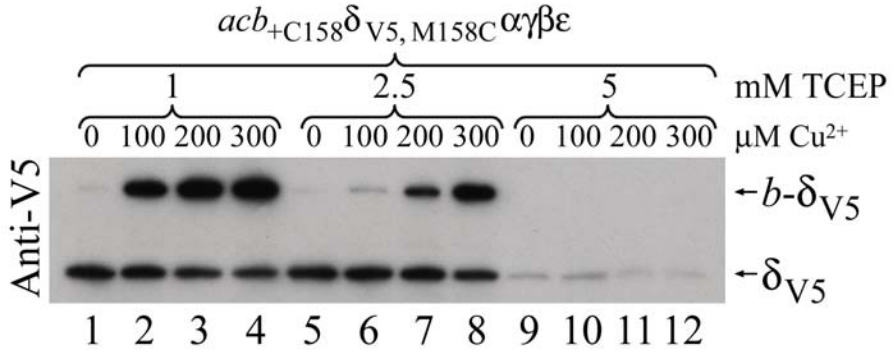

Figure 6-4. Crosslinking with increasing concentrations of Cu^{2+}. Membranes from strain 1100 ΔBC/pSBC100 ($acb_{+C158}\delta_{V5,\ M158C}\alpha\gamma\beta\varepsilon$) were prepared in the presence of 1, 2.5 and 5 mM TCEP. Membrane samples were diluted to 5 mg/mL and crosslinking for 30 minutes at room temperature in open tubes with shaking. $CuCl_2$ was added to a final concentration of 0, 100, 200 or 300 μM to start the crosslinking reaction. The reaction was quench by adding NEM to a final concentration of 1 mM. A total of 1 μg of each sample was analyzed by Western blot using a primary antibody against the V5 epitope tag.

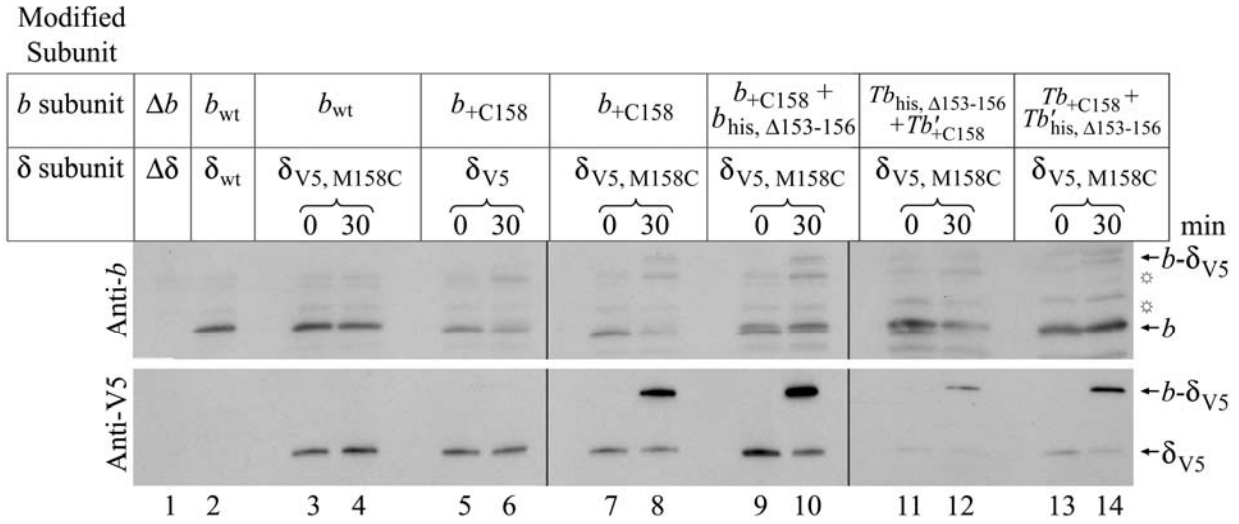

Figure 6-5. Disulfide crosslink formation of *b*-δ dimers. Membranes were prepared in the presence of 1 mM TCEP and diluted to 5 mg/mL. Samples were crosslinking at room temperature for 30 minutes with shaking using 100 μM Cu^{2+} and the reactions were quenched with 1 mM NEM. Zero time point samples had NEM added prior to Cu^{2+} to prevent crosslinking. A total of 10 μg and 1 μg of each sample were analyzed by Western blot using primary antibodies against the *b* subunit and the V5 epitope tag, respectively. Membranes prepared from strains 1100 ΔBC/pAES9 (*acb*δαγβε) and 1100 ΔBC/pACYC184 (Δ*unc*) were used as positive and negative controls, respectively. Membrane that were crosslinked and analyzed were prepared from strains 1100 ΔBC/pSBC99 ($acb\delta_{V5,\ M158C}\alpha\gamma\beta\varepsilon$), 1100 ΔBC/pSBC100 ($acb_{+C158}\delta_{V5,\ M158C}\alpha\gamma\beta\varepsilon$), 1100 ΔBC/pSBC101 ($acb_{+C158}\delta_{V5}\alpha\gamma\beta\varepsilon$), 1100 ΔBC/pSBC100/pSBC132 ($acb_{+C158}\delta_{V5,\ M158C}\alpha\gamma\beta\varepsilon + b_{his,\ \Delta153\text{-}156}$), 1100 ΔBC/pSBC140/pSBC141 ($acTb'_{+C158}\delta_{V5,\ M158C}\alpha\gamma\beta\varepsilon + Tb_{his,\ \Delta153\text{-}156}$) and 1100 ΔBC/pSBC142/pSBC143 ($acTb_{+C158}\delta_{V5,\ M158C}\alpha\gamma\beta\varepsilon + Tb'_{his,\ \Delta153\text{-}156}$). Vertical lines indicate the joining of multiple Western blots *in silico*. A nonspecific band detected by the antibody against the *b* subunit is indicated (☼). The experiment was repeated in triplicate and the results shown are representative.

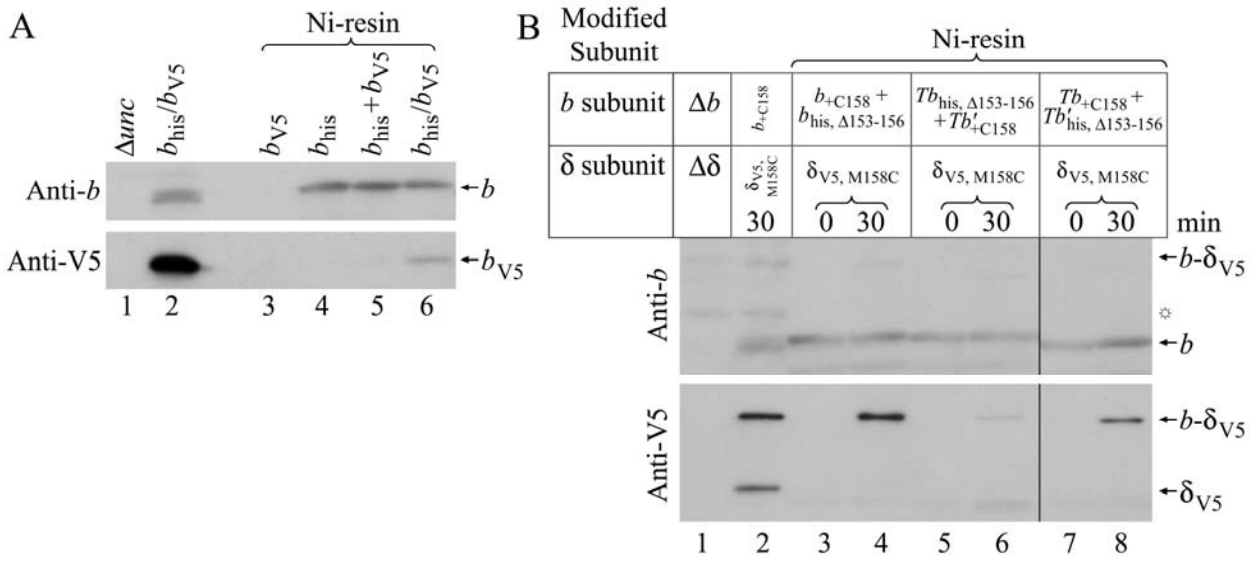

Figure 6-6. Disulfide crosslinking formation of *b*-δ dimers in F_1F_O containing heterodimeric peripheral stalks. A) Controls demonstrating the ability of the assay to detect heterodimeric peripheral stalks. Membranes were prepared, diluted to 5 mg/mL, purified over a nickel resin to retained only F_1F_O containing at least one histidine tag and analyzed by Western blot. Untreated membranes prepared from strains KM2/pBR322 (Δ*b*) and KM2/pTAM37/pTAM46 (b_{his}/b_{V5}) were used as negative and positive controls, respectively. The nickel resin controls: lane 3, KM2/pTAM46 (b_{V5}), control with no histidine tag; lane 4, KM2/TAM37 (b_{his}), control with histidine tag and no V5 epitope tag; lane 5, KM2/pTAM37 (b_{his}) + KM2/pTAM46 (b_{V5}), aggregation control; and lane 6, KM2/pTAM37/pTAM46 (b_{his}/b_{V5}), heterodimer positive control. B) Detection of *b*-δ crosslinked product in F_1F_O containing heterodimeric peripheral stalks. Untreated membranes prepared from strain 1100 ΔBC/pAES9 (*acb*δαγβε) were used as a negative control, while membranes prepared from strain 1100 ΔBC/pSBC100 ($acb_{+C158}\delta_{V5, M158C}\alpha\gamma\beta\varepsilon$) that were crosslinked but not purified were used as a positive control. Membrane samples were prepared from strains 1100 ΔBC/pSBC100/pSBC132 ($acb_{+C158}\delta_{V5, M158C}\alpha\gamma\beta\varepsilon + b_{his, \Delta153\text{-}156}$), 1100 ΔBC/pSBC140/pSBC141 ($acTb'_{+C158}\delta_{V5, M158C}\alpha\gamma\beta\varepsilon + Tb_{his, \Delta153\text{-}156}$) and 1100 ΔBC/pSBC142/pSBC143 ($acTb_{+C158}\delta_{V5, M158C}\alpha\gamma\beta\varepsilon + Tb'_{his, \Delta153\text{-}156}$) and crosslinked as described in Figure 6-5. These samples were purified over a nickel resin and analyzed by Western blot. All Western blots lanes contain a total of 10% of the elutant off the nickel resin or 10 μg and 1 μg of untreated membrane for antibodies against the *b* subunit and V5 epitope tag, respectively. A vertical line indicates the removal of unwanted lanes *in silico*. A nonspecific band detected by the antibody against the *b* subunit is indicated (☼). The experiment was repeated three times and results shown are representative.

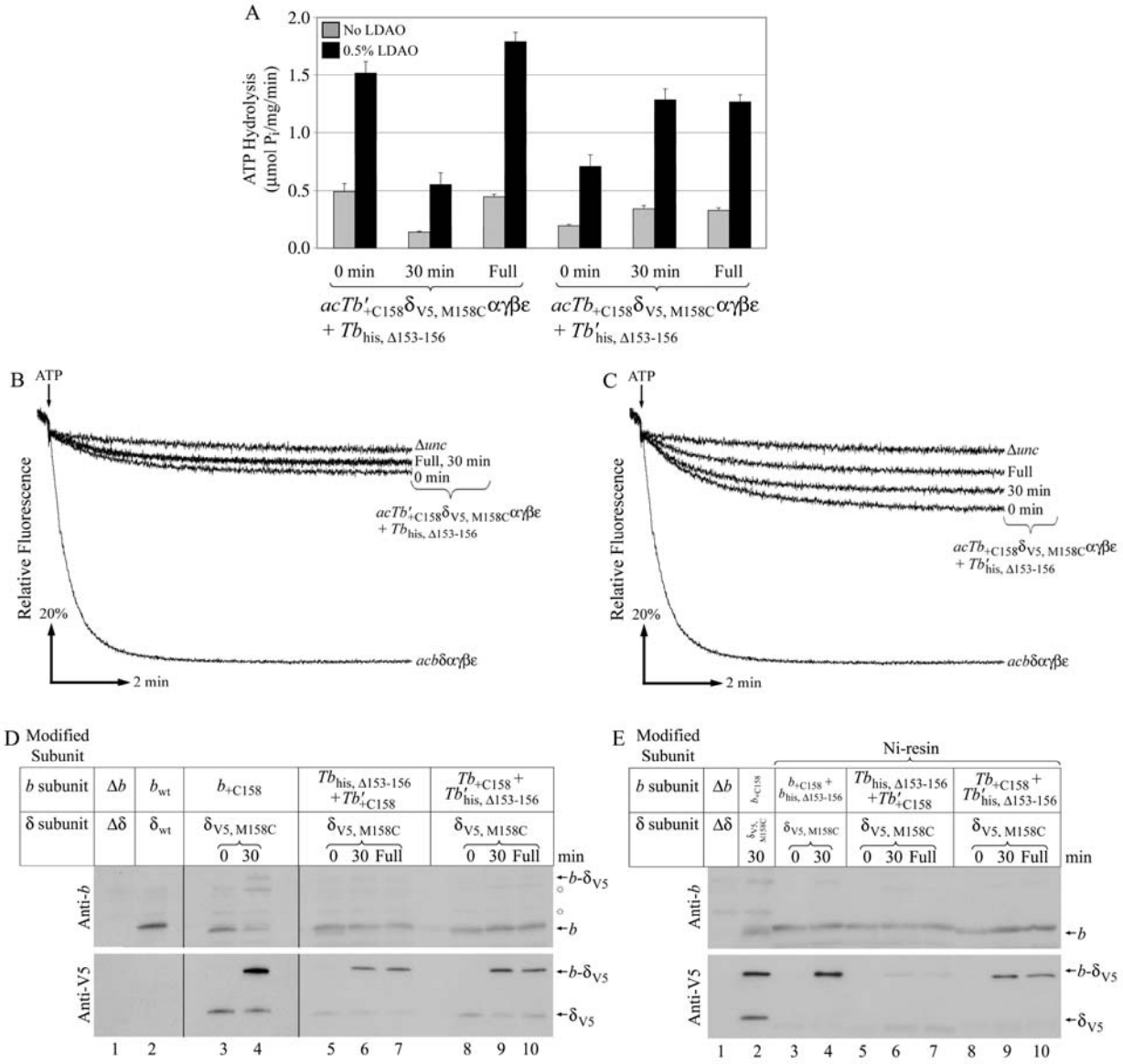

Figure 6-7. See figure legend next page.

Figure 6-7. Effects of 100 μM Cu^{2+} on ATP-driven proton pumping and crosslink formation (see figure previous page). Membranes from strains containing chimeric peripheral stalks were prepared in the presence or absence of 100 μM Cu^{2+}. Membranes that were prepared in the absence of Cu^{2+} were treated with 100 μM Cu^{2+} for 30 minutes. A) Effects of Cu^{2+} on the rate of ATP hydrolysis. Membranes prepared in the presence of 100 μM Cu^{2+} are labeled "Full", membranes treated with 100 μM Cu^{2+} for 30 minutes are labeled "30 min" and untreated membranes are labeled "0 min". B) and C) Effects of Cu^{2+} on ATP-driven proton pumping as detected by fluorescence quenching of ACMA. A total of 500 μg of membrane protein was assayed. Membrane prepared from strains 1100 ΔBC/pAES9 (*acb*δαγβε) and 1100 ΔBC/pACYC184 (Δ*unc*) were used as positive and negative controls, respectively. B) Assay of membranes prepared from strain 1100 ΔBC/pSBC140/pSBC141 ($acTb'_{+C158}\delta_{V5,\ M158C}\alpha\gamma\beta\varepsilon + Tb_{his,\ \Delta 153\text{-}156}$). C) Assay of membranes prepared from strain 1100 ΔBC/pSBC142/pSBC143 ($acTb_{+C158}\delta_{V5,\ M158C}\alpha\gamma\beta\varepsilon + Tb'_{his,\ \Delta 153\text{-}156}$). D) Disulfide crosslink formation of *b*-δ dimers. Membranes were prepared, treated and analyzed essentially as described Figure 6-5 with the addition of samples prepared in the presence of 100 μM Cu^{2+}. E) Disulfide crosslinking formation of *b*-δ dimers in F_1F_O containing heterodimeric peripheral stalks. Membranes were prepared, treated, purified and analyzed exactly as shown in Figure 6-6 with the addition of samples prepared in the presence of 100 μM Cu^{2+}.

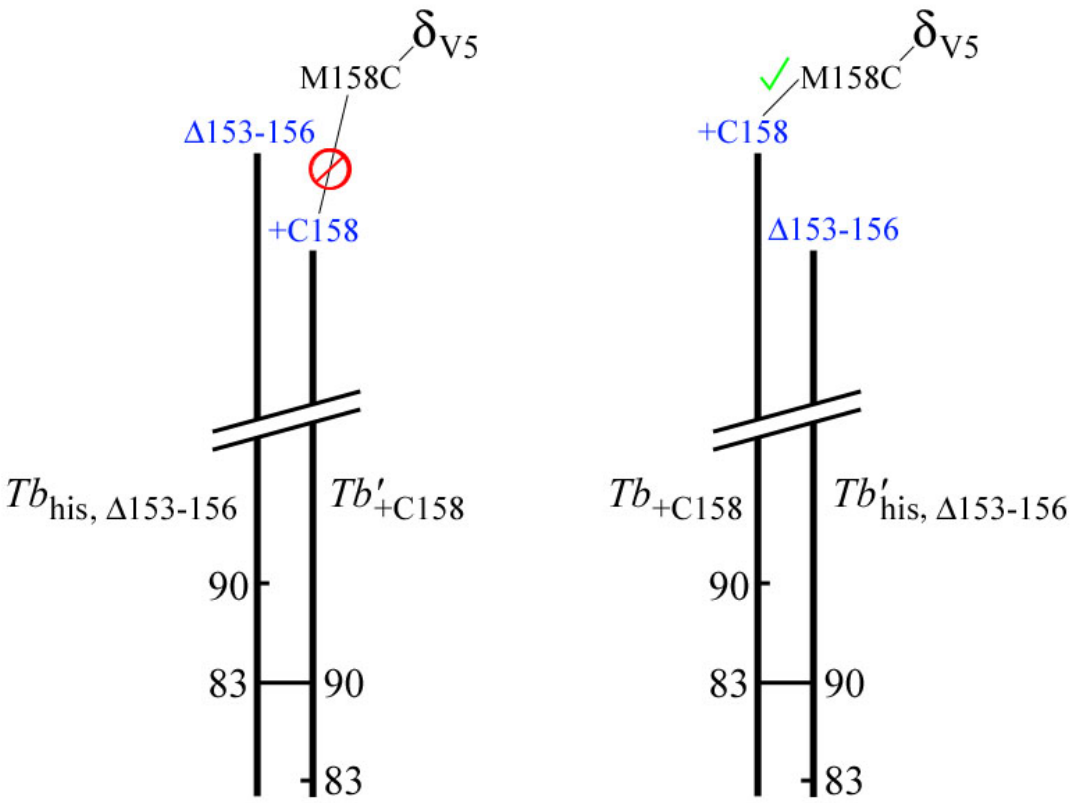

Figure 6-8. Proposed model to explain the *b*-δ crosslinking data obtained for F_1F_O containing chimeric peripheral stalks. The *b*-δ crosslink formation in heterodimeric peripheral stalks only occurs efficiently in the membrane prepared from strain 1100 ΔBC/pSBC142/pSBC143 ($acTb_{+C158}\delta_{V5,\ M158C}\alpha\gamma\beta\varepsilon$ + $Tb'_{his,\ \Delta153\text{-}156}$), while membranes prepared from strain 1100 ΔBC/pSBC140/pSBC141 ($acTb'_{+C158}\delta_{V5,\ M158C}\alpha\gamma\beta\varepsilon$ + $Tb_{his,\ \Delta153\text{-}156}$) show little *b*-δ dimer formation. Models showing both chimeric constructs demonstrate the staggered arrangement described in the previous chapters. Crosslink formation occurs efficiently if the cysteine extension is on the C-terminally shifted *b* subunit and the deletion is on the N-terminally shifted *b* subunit, but not in the alternate arrangement. Note that the N- and C-terminal shifts are known in the region of residues 83 and 90, but the propagation of these shifts to the extreme C-terminal ends is speculative.

CHAPTER 7
CONCLUSIONS AND FUTURE DIRECTIONS

Conclusions

Data presented in this study demonstrate that functional *Escherichia coli* F_1F_O ATP synthase complexes can be formed that contain heterodimeric peripheral stalks in which the region $b_{E39\text{-}I86}$ has been replaced by the homologous sequence from the *b* and *b'* subunits of *Thermosynechococcus elongatus* BP-1, abbreviated *Tb* and *Tb'*. Cysteines were subtituted individually at residues A83 and A90 in both *Tb* and *Tb'* subunits and disulfide crosslink formation was used as a probe for molecular structure. Strong evidence for a staggered arrangement in the peripheral stalk was obtain with the observation that rapid crosslink formation occurs in F_1F_O complexes with Tb_{A83C}/Tb'_{A90C} peripheral stalk. Disulfide crosslink formation was used to investigate interactions between the individual wild-type *b* subunits and the δ subunit of F_1. The results obtained demonstrated that a single *b* subunit is sufficient to form the critical interactions with the δ subunit. Finally, an investigation of the interactions between the chimeric peripheral stalk and the δ subunit found that the subunits in the peripheral stalk play distinct functional roles.

Figure 7-1 shows a model of the peripheral stalk generated from biochemical data. The only portion of the peripheral stalk in this model that has been solved as a high-resolution structure is the membrane spanning domain. The monomeric membrane spanning domain was solved using NMR [149], but the dimerized form shown in the model is speculation based on crosslinking data. The lack of evidence of an interaction between the *b* subunits in the tether domain along with EPR measurements [356] indicate that the two subunits of the peripheral stalk are probably separated in this region. The dimerization domain of the b subunit was crystallized as a linear α-helix, but the weight of the data indicate a coiled coil arrangement in this region.

The model shown was generated using a standard left-handed coiled coil for the dimerization domain. Crosslinking data presented in Chapter 4 strongly suggests a staggered arrangement in the $b_{R83\text{-}A90}$ region. The propogation of this staggered arrangement to the extreme C-terminal ends is spectulative. Although no high-resolution structure exists for the C-terminal end of the peripheral stalk, it is likely that this region is compact and globular in nature.

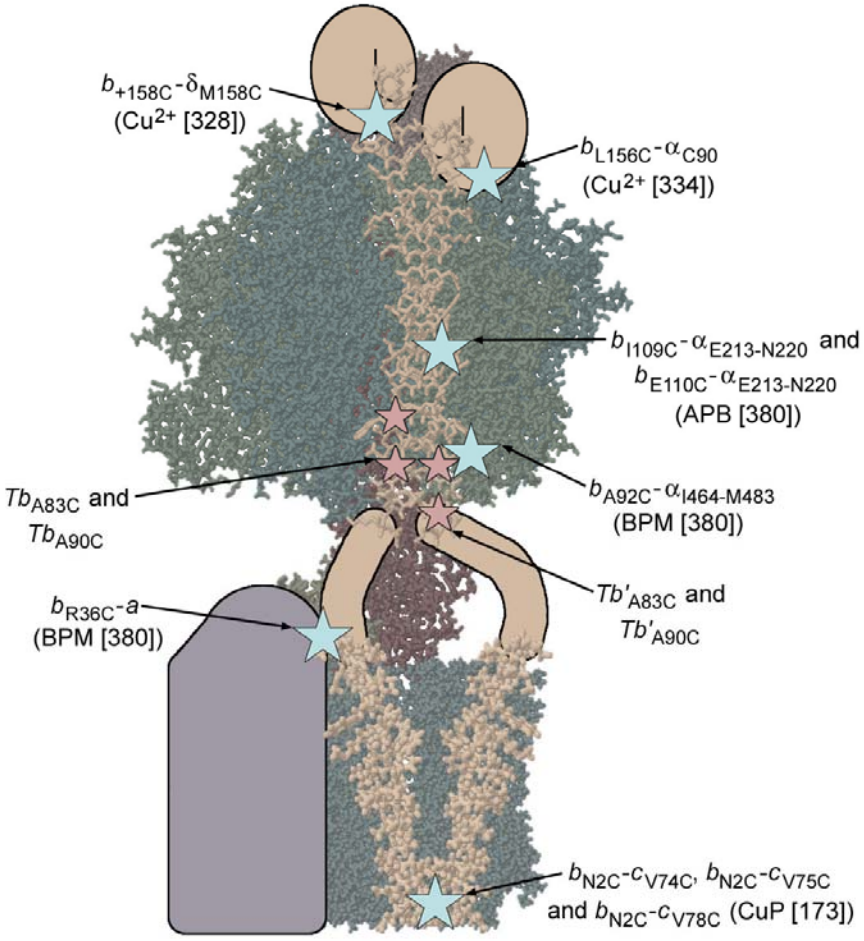

Figure 7-1. Model of the peripheral stalk based on the available biochemical data. The specific crosslinks are labeled along with the crosslinked reagent and the reference where the crosslink was reported.

The peripheral stalk field of the F_1F_O ATP synthase from *E. coli* currently has three main areas of controversy. First, are the *b* subunits arranged in a parallel, in-register conformation, or are they staggered relative to one another in an offset conformation? Second, is the expected coiled coil arrangement of the dimerization domain of the peripheral stalk a standard left handed

coiled coil or a novel right handed coiled coil? And third, does the peripheral stalk function as a flexible, rope-like tether or as a rigid, rod-like structure? All three of these questions are a reflection of our limited structural information regarding the peripheral stalk. Of these three, my data addresses the first controversy but sheds no light on the others.

The crosslinking data presented in Chapter 4 provide strong evidence that the chimeric peripheral stalk adopts a staggered conformation. The main result supporting this conclusion is the very rapid formation of a crosslink in the Tb_{A83C}/Tb'_{A90C} peripheral stalk at relatively low concentrations of oxidizing agent. This reaction is only possible if both cysteines are in a close spatial proximity to one another and in the appropriate orientation. However, other data in Chapter 4 indicates that while the Tb_{A83C}/Tb'_{A90C} crosslink may form most efficiently, there also exists the ability to form a disulfide bridge in the Tb_{A90C}/Tb'_{A90C} peripheral stalk (Figure 7-2A). If we assume that the dimerization domain of the peripheral stalk is in a coiled coil conformation, we must conclude that there is no way for residue Tb'_{A90C} to be in a position to react with both Tb_{A83C} and Tb_{A90C}. This becomes obvious if we consider that seven residues compose two turns of an α-helix and are located about 10.5 Å apart. An average disulfide bond is only 2.0 Å and will not form if the sulfur atoms are beyond 2.2 Å apart [4]. Hence I proposed that the F_1F_O complexes containing chimeric peripheral stalks are capable of adopting two different conformations, one staggered (Figure 7-2B) and one in parallel (Figure 7-2C). The efficiency of crosslink formation in the staggered orientation implies that it is likely to be the favored orientation in F_1F_O containing chimeric peripheral stalks. It is unclear if two distinct and static subpopulations exist or if these two conformations interconvert and exist togther in equilibrium.

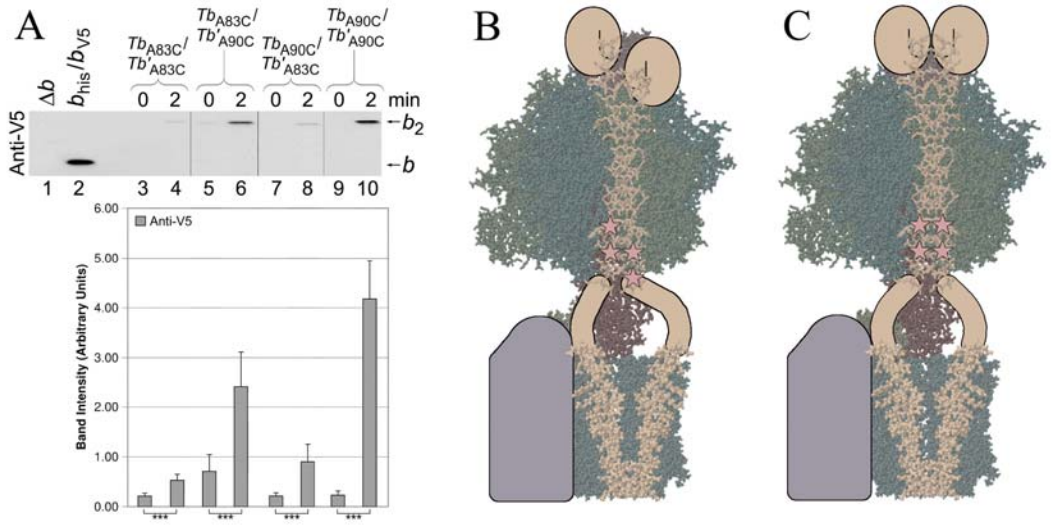

Figure 7-2. Existence of two distinct conformations in the chimeric peripheral stalks of F_1F_O ATP synthase. A) Crosslink formation in heterodimeric *Tb*/*Tb'* peripheral stalks. See the legend for Figure 4-10 for experimental details. Two conformations inferred from the crosslinking results in Panel A: B) staggered and C) in parallel.

Although the chimeric crosslinking data presented in Chapter 4 can be viewed as support for either the staggered and parallel models, it is unclear if these results are directly applicable to the wild-type peripheral stalk. Crosslinking data presented in Chapter 5 on wild-type *E. coli b* subunits supports the in-register model where a disulfide crosslink can form in the $(b_{A90C})_2$ peripheral stalk. The formation of a staggered crosslink could not be easily interpretable in the wild-type peripheral stalk and was not attempted in this study. The question of staggered versus parallel for the wild-type peripheral stalk still remains unresolved but the weight of the data presented here favors existence of the staggered conformation.

The data presented in Chapter 6 provides some of the strongest evidence to date that the *b* subunits in the peripheral stalk are functionally distinct. Crosslinking and affinity-purification experiments showed that a single full-length *b* subunit is sufficient to form the required interactions with the δ subunit. A similar experiment done in the soluble $b_{V25\text{-}L156}$ subunit also found a single full-length *b* subunit sufficient for binding to F_1 [326]. The data presented here

now verifies this conclusion to the context of the entire enzyme. However, a more striking result was obtained by repeating the *b*-δ crosslinking experiment in F_1F_O complexes containing a chimeric peripheral stalk. It was found that a peripheral stalk in which the *Tb'* subunit was truncated by four amino acids was still able to crosslink to the δ subunit, while truncating the *Tb* subunit prevented crosslink formation (Figure 7-3). These data indicate that the two *b* subunits are functionally distinct. When the subunits are clearly distinguishing in the dimerization domain by the insertion of *T. elongatus* sequence this results in a positional effect propogated all the way at the C-terminal ends. Interestingly, the results obtained here contradict a similar experiment done using the soluble form of the $b_{V25\text{-}L156}$ subunit. In a previous study a full-length $b_{V25\text{-}L156}$ subunit was locked in an offset conformation with a truncated $b_{V25\text{-}L152}$ subunit and the binding interactions with F_1 were investigated by crosslink formation [326]. Here the authors found that the N-terminally shifted *b* subunit was essential for the proper interactions with F_1, while my data implies the opposite. This contradiction highlights the limitations of working with the soluble form of the peripheral stalk and the importance of considering the influence of the entire enzyme complex.

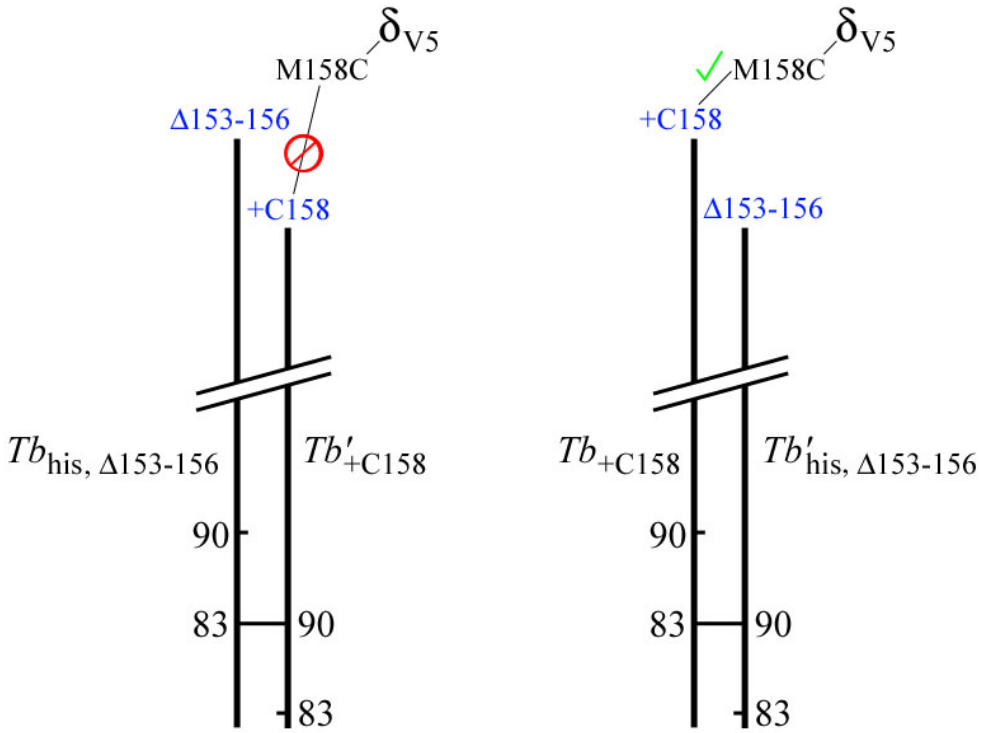

Figure 7-3. Model explaining the crosslinking results between the chimeric peripheral stalk and the δ subunit as presented in Chapter 6. The results demonstrate distinct functional roles for the individual *b* subunits. Note that the propagation of the offset in the dimerization domain to the extreme C-terminal ends is speculative.

Future Directions

Much structural and functional information is available for the F_1F_O ATP synthase from *E. coli*, but the picture is still not complete. The main areas where further study is needed is on the *a*, *b* and δ subunits and their interactions with one another. The most desirable accomplishment would be a high resolution structure of the entire F_1F_O complex, but this has proven to be difficult to obtain. Multiple membrane protein crystallography laboratories have been trying for at least two decades. In lieu of a full structure, I feel that the most informative approach would be the development of high-throughput biochemical assays. Making individual mutations by site-directed mutagenesis and analyzing their effects on enzyme viability is a slow process. An ideal technique would involve the creation of random amino acid substitutions in a predefined region via custom oligonucleotide synthesis, for example in the membrane spanning domain of

the *b* subunit. A high-throughput screen could then be employed to determine which of these substitutions allows growth on nonfermentable media and which did not. A technique such as this would provide information about residues which were critical for interactions between the *b* and *a* subunits as well as between adjacent *b* subunits. A similar technique could then be used to probe for second site suppressors located in an individual helix of the *a* subunit. A similar high-throughput technique could be used to screen for disulfide crosslinks. One way to do this would be to engineer a cysteine substitution into a particular amino acid of the *b* subunit and then randomly engineer cysteines into an individual helix of the *a* subunit. A batch of strains expressing these random mutations in the *a* subunit would be grown up and their membranes prepared. These membranes could be crosslinked and analyzed by Western blot. Any *b*-*a* crosslinked product that formed could be analyzed further to determine the location of the cysteine residue in subunit *a*. Although there are certainly complications surrounding these proposed experiments, they would ultimately yield more information about the interactions under investigation due to their high-throughput nature.

I also feel that the time has come to move away from using just the soluble region of the *b* subunit and focus on the entire enzyme. Discrepancies have been found between experiments done in $b_{V25\text{-}L156}$ and those done in the holoenzyme, implying that the soluble form of the $b_{V25\text{-}L156}$ subunit is not exactly the same as the full *b* subunit integrated into an F_1F_O complex.

It is also possible that the *E. coli* system is no longer the best system in which to experiment. A large amount of structural information is available from the bovine mitochondrial enzyme, while many of the mutational studies done in bacteria have not been repeated in the mitochondrial ATP synthase. There exist a number of mutational and crosslinking studies that can be used to test the structure of the mitochondrial enzyme, in particular the recently

crystallized peripheral stalk. This work can be done using yeast as a host organism. Although not as simple to work with as *E. coli*, changes to the ATP synthase genes can be made in yeast and their effects studied in a reasonable time span. Although our knowledge of ATP synthase has grown greatly over the past decades, there are still enough unanswered questions to keep researchers busy for many more years.

APPENDIX A
PLASMID CONSTRUCTION

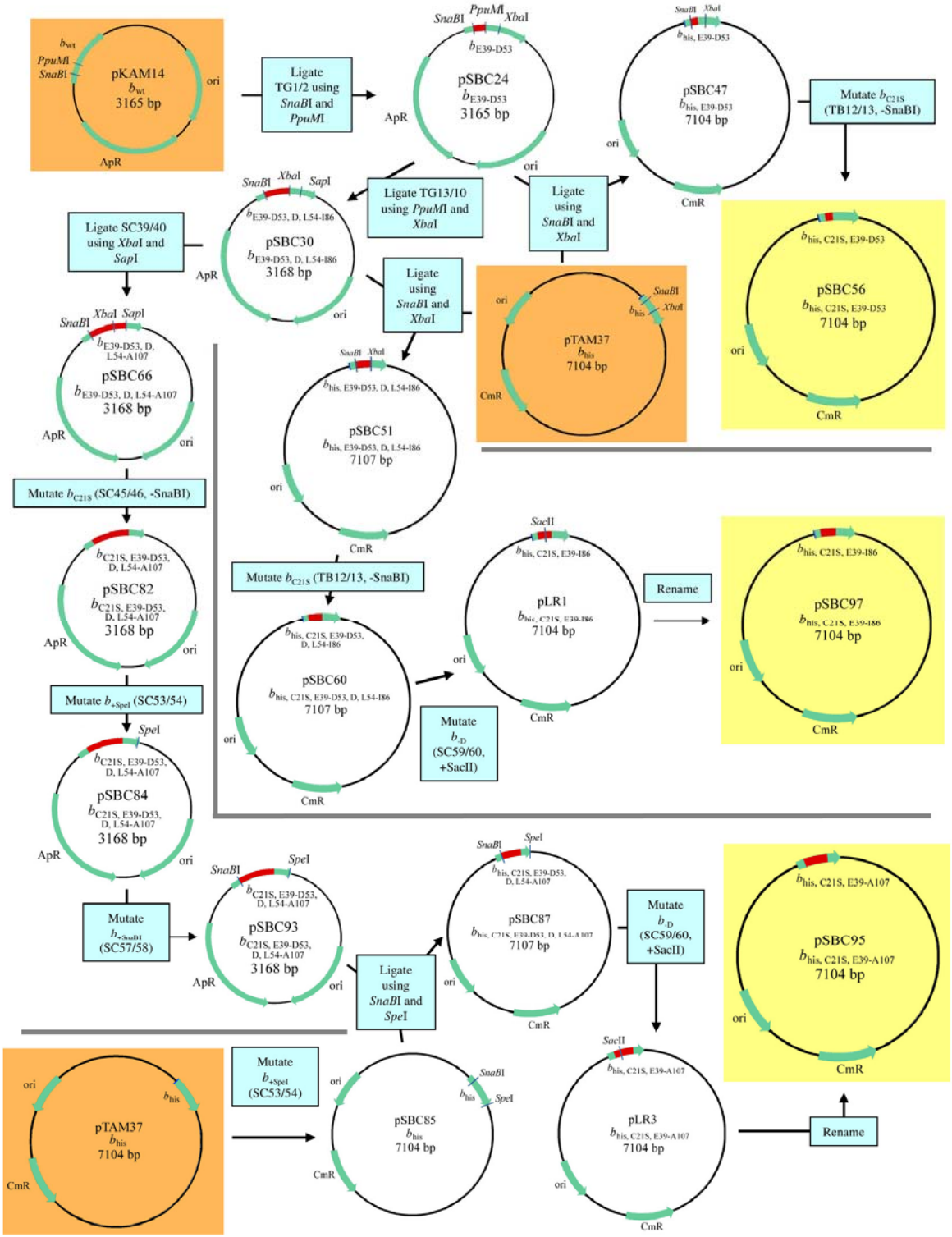

Figure A-1. Construction of plasmids for Chapter 3 (Part 1/3)

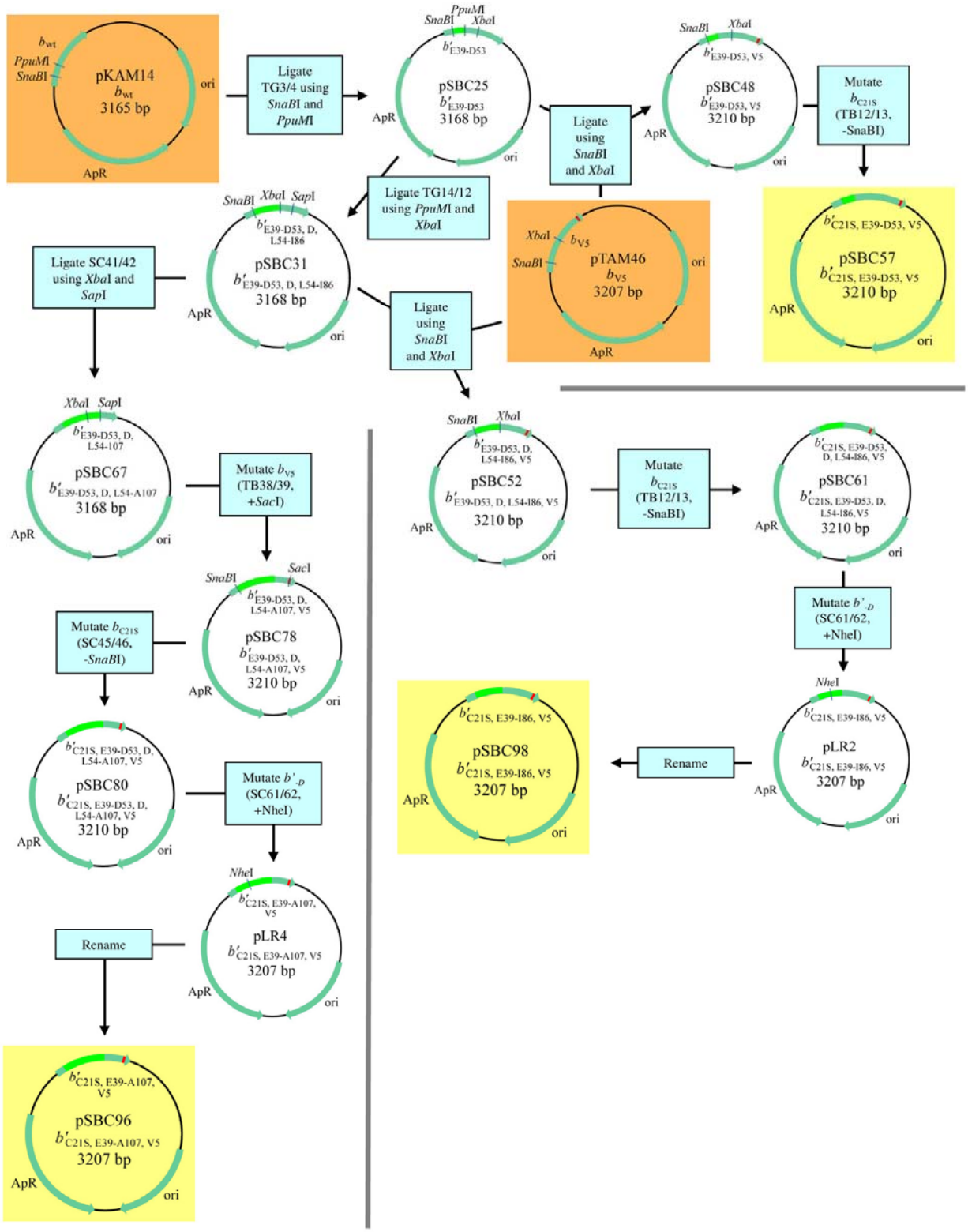

Figure A-2. Construction of plasmids for Chapter 3 (Part 2/3)

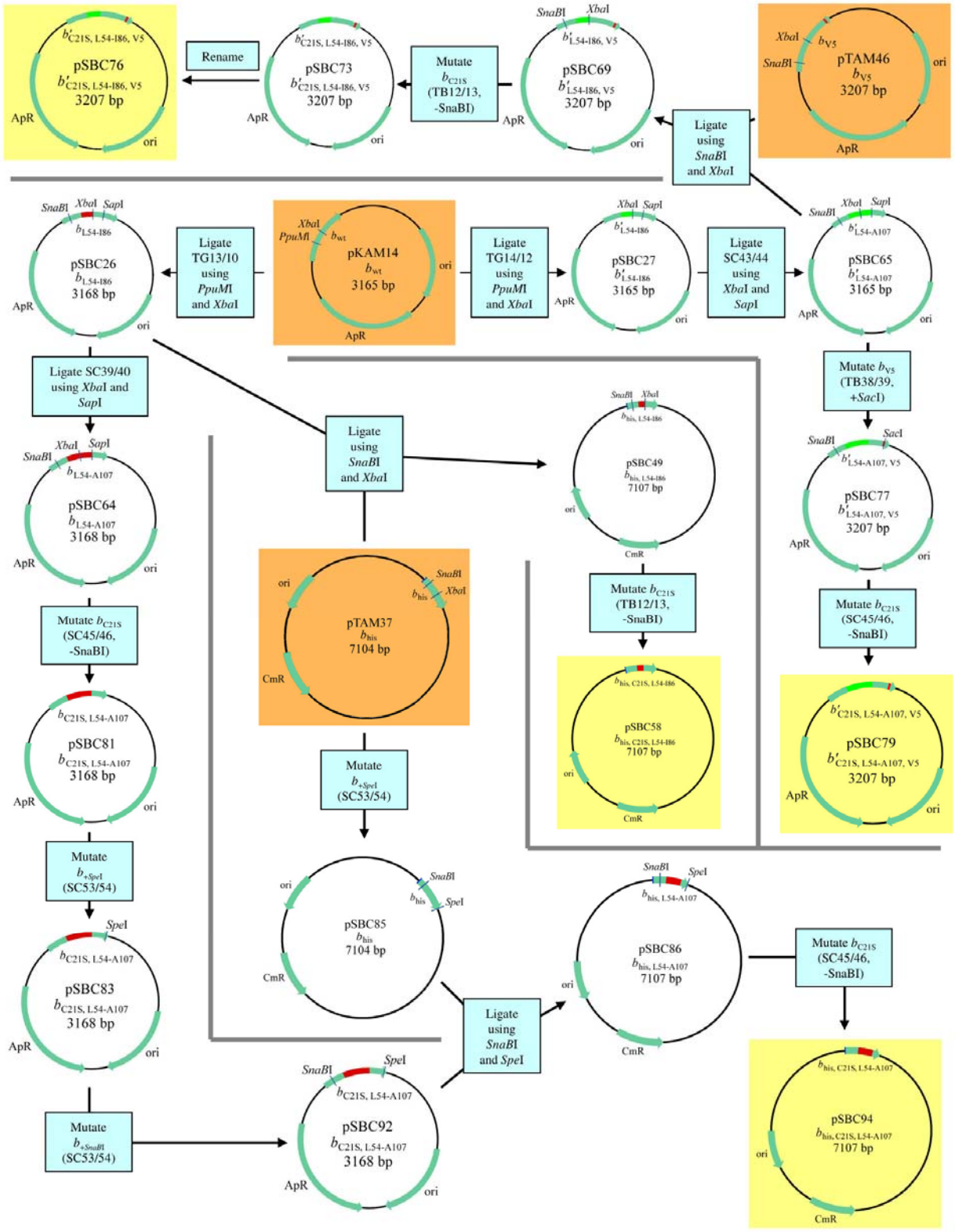

Figure A-3. Construction of plasmids for Chapter 3 (Part 3/3)

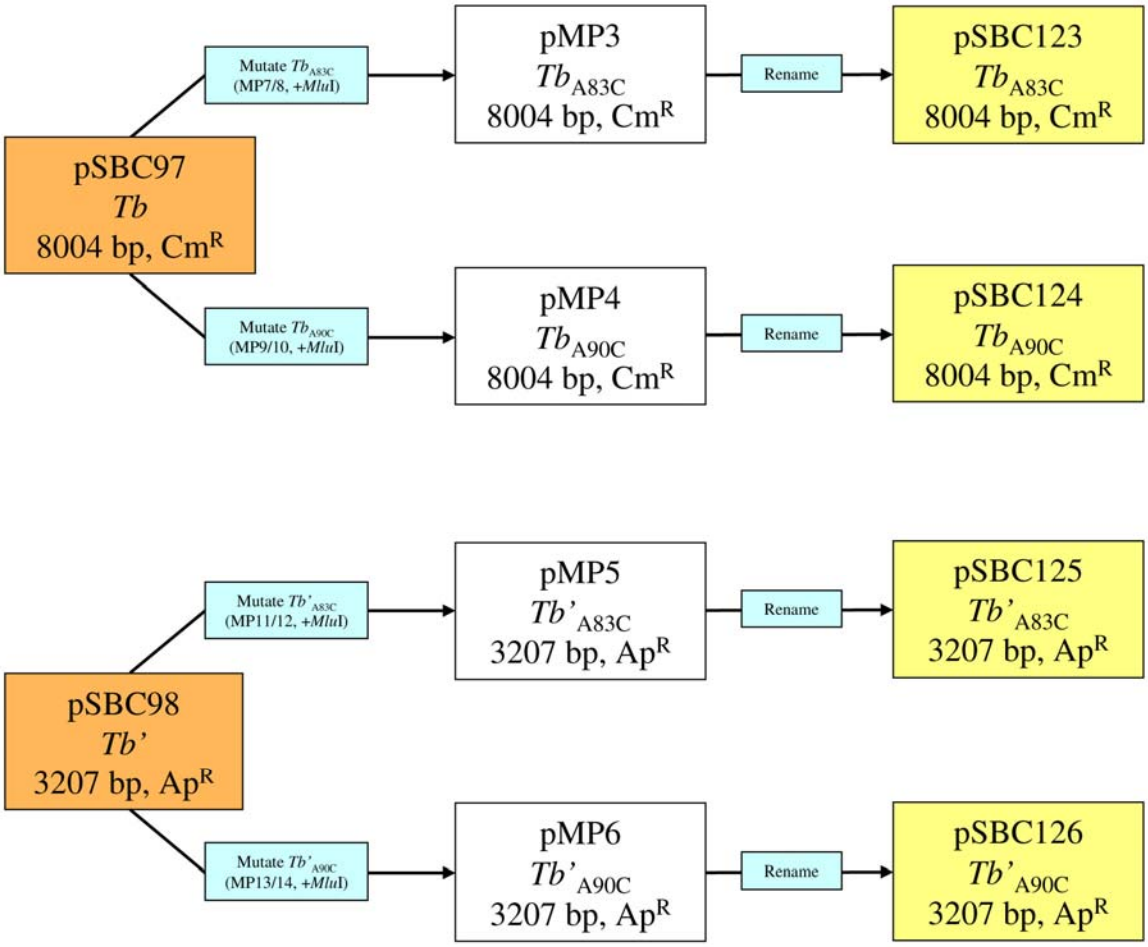

Figure A-4. Construction of plasmids for Chapter 4

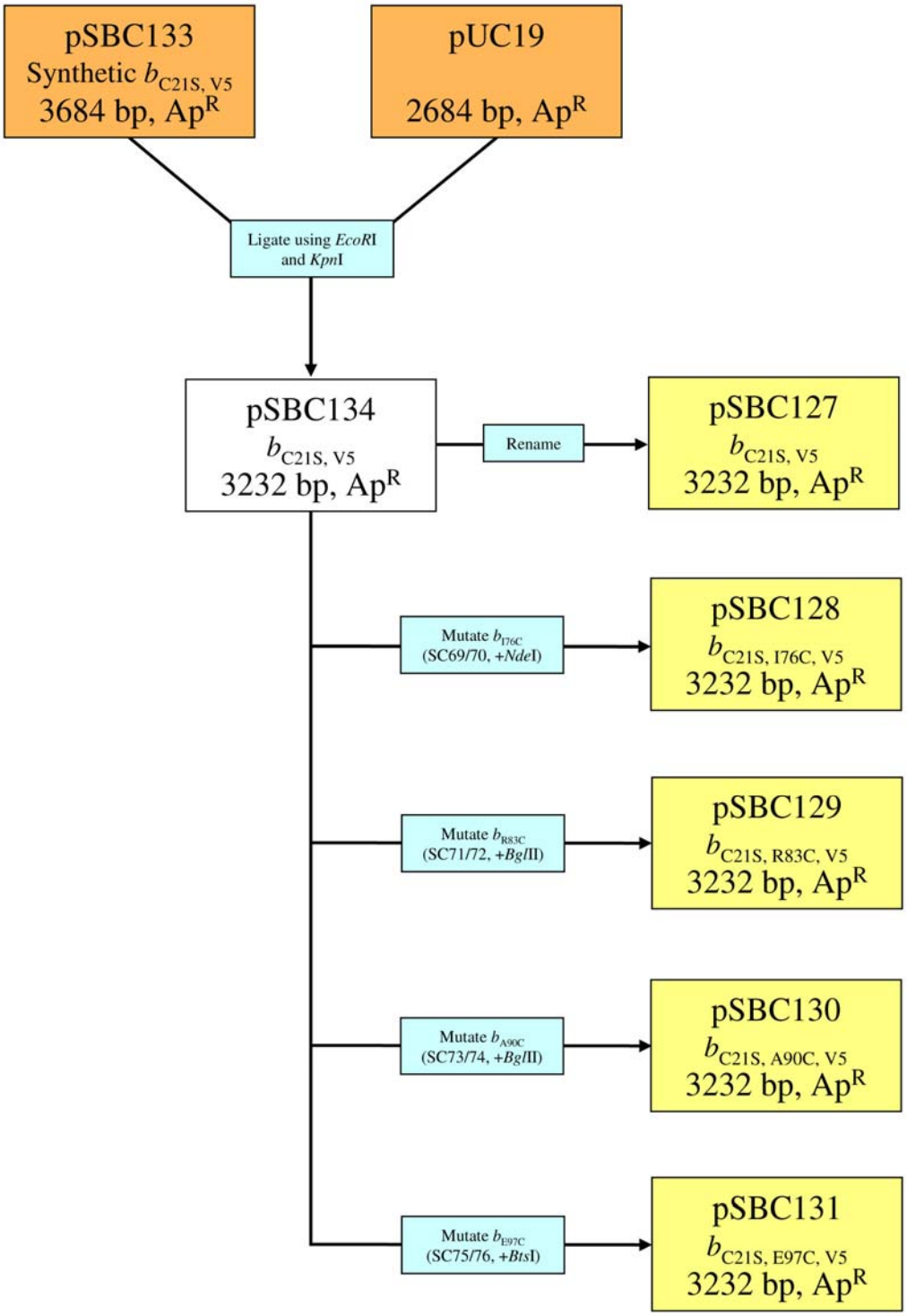

Figure A-5. Construction of plasmids for Chapter 5

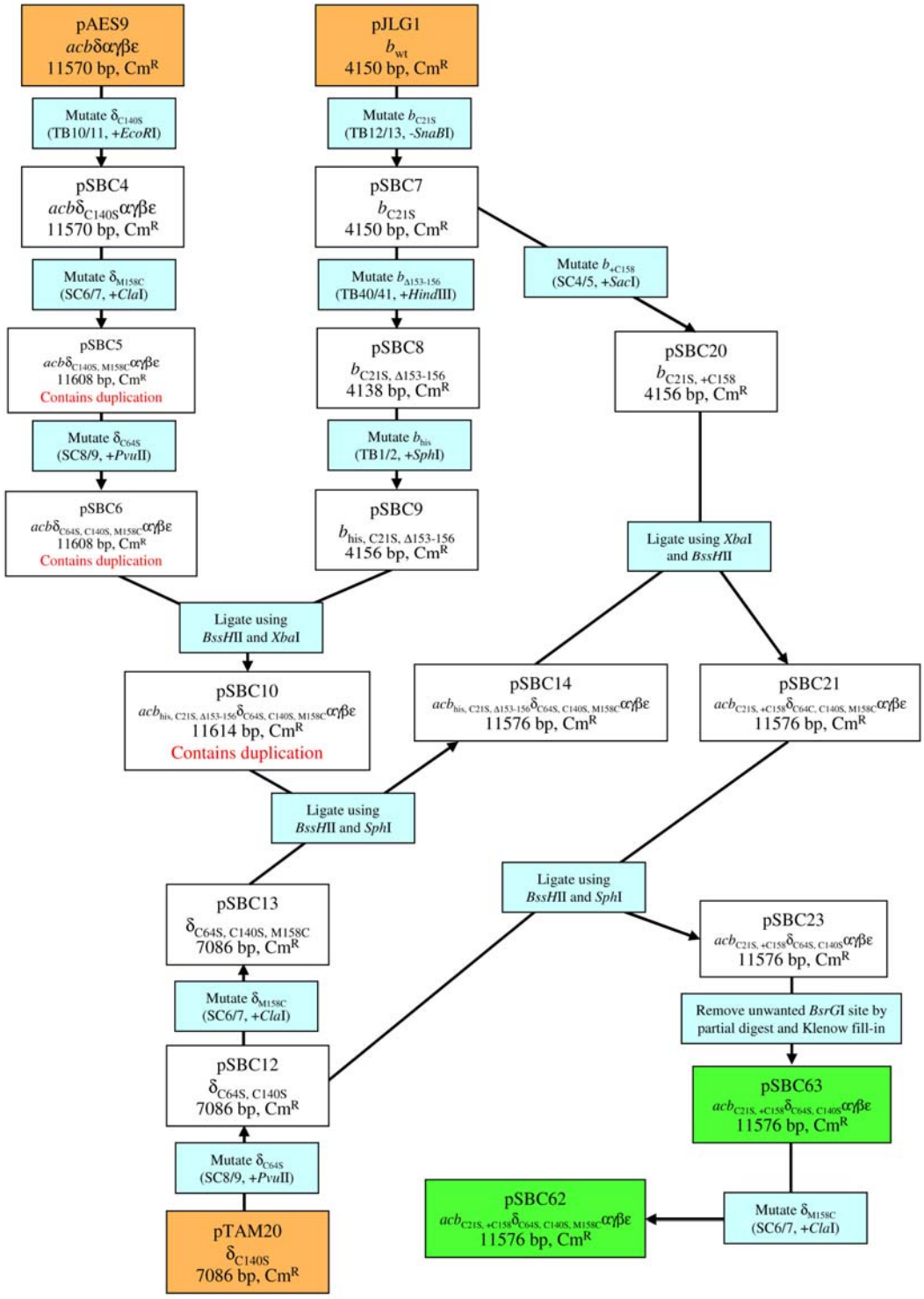

Figure A-6. Construction of plasmids for Chapter 6 (Part 1/2)

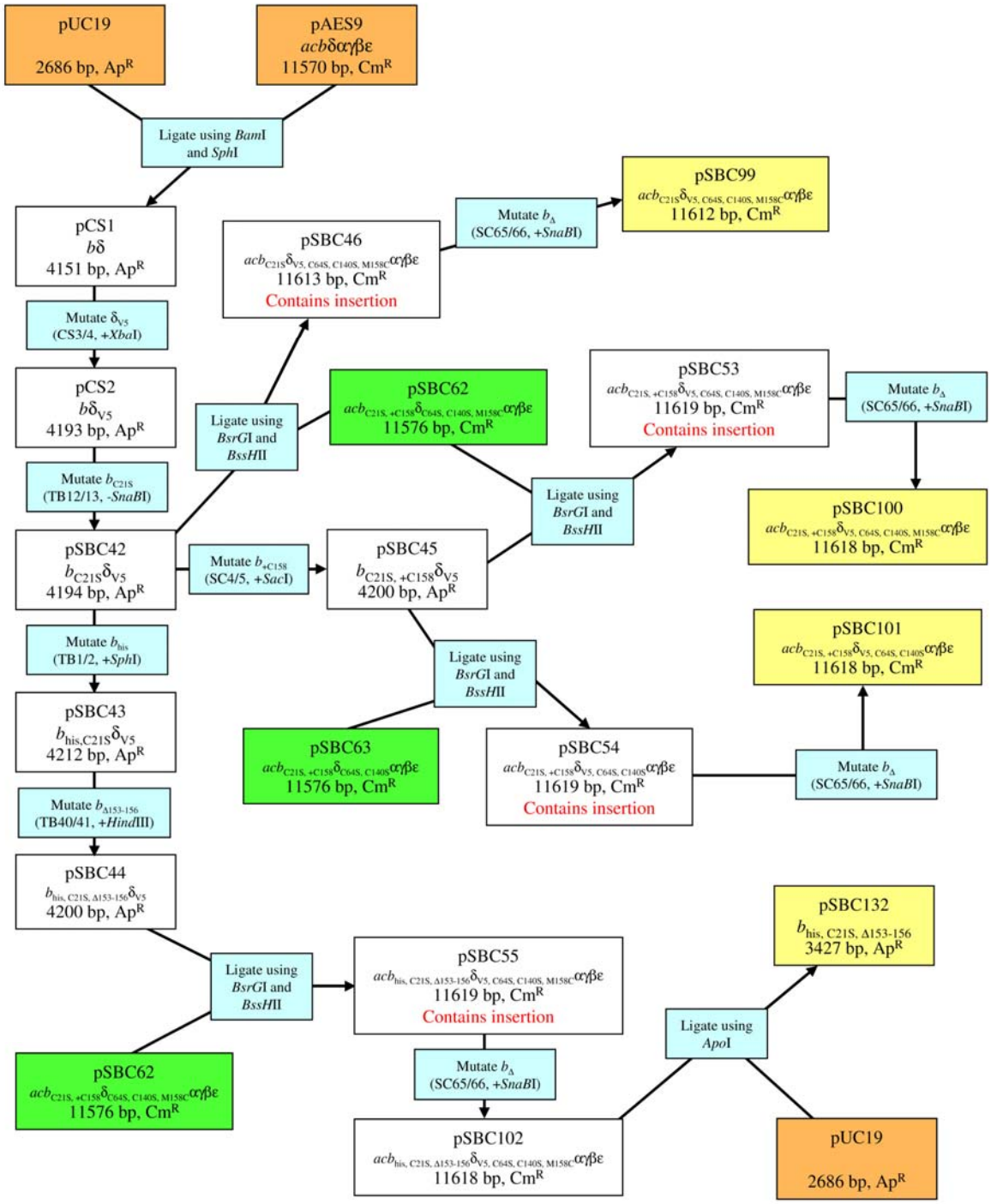

Figure A-7. Construction of plasmids for Chapter 6 (Part 2/2)

LIST OF REFERENCES

1. **Deckers-Hebestreit, G. and K. Altendorf.** 1996. The F_0F_1-type ATP synthases of bacteria: structure and function of the F_0 complex. Annu. Rev. Microbiol. **50:**791-824.

2. **Dimroth, P., C.v. Ballmoos, and T. Meier.** 2006. Catalytic and mechanical cycles in F-ATP synthases. Fourth in the Cycles Review Series. EMBO Rep. **7:**276-82.

3. **Capaldi, R.A. and R. Aggeler.** 2002. Mechanism of the F_1F_0-type ATP synthase, a biological rotary motor. Trends Biochem. Sci. **27:**154-60.

4. **Takemoto, L.J.** 1997. Disulfide bond formation of cysteine-37 and cysteine-66 of beta B2 crystallin during cataractogenesis of the human lens. Exp. Eye. Res. **64:**609-14.

5. **Bass, R.B. and J.J. Falke.** 1999. The aspartate receptor cytoplasmic domain: *in situ* chemical analysis of structure, mechanism and dynamics. Structure. **7:**829-40.

6. **Lynch, B.A. and D.E. Koshland.** 1991. Disulfide cross-linking studies of the transmembrane regions of the aspartate sensory receptor of *Escherichia coli*. Proc. Natl. Acad. Sci. USA. **88:**10402-6.

7. **Karlin, A., E. Holtzman, N. Yodh, P. Lobel, J. Wall, and J. Hainfeld.** 1983. The arrangement of the subunits of the acetylcholine receptor of Torpedo californica. J. Biol. Chem. **258:**6678-81.

8. **Kurtenbach, E., C.A. Curtis, E.K. Pedder, A. Aitken, A.C. Harris, and E.C. Hulme.** 1990. Muscarinic acetylcholine receptors. Peptide sequencing identifies residues involved in antagonist binding and disulfide bond formation. J. Biol. Chem. **265:**13702-8.

9. **Hamdan, F.F., S.D. Ward, N.A. Siddiqui, L.M. Bloodworth, and J. Wess.** 2002. Use of an *in situ* disulfide cross-linking strategy to map proximities between amino acid residues in transmembrane domains I and VII of the M3 muscarinic acetylcholine receptor. Biochemistry. **41:**7647-58.

10. **Pakula, A.A. and M.I. Simon.** 1992. Determination of transmembrane protein structure by disulfide cross-linking: the *Escherichia coli* Tar receptor. Proc. Natl. Acad. Sci. USA. **89:**4144-8.

11. **Punginelli, C., B. Maldonado, S. Grahl, R. Jack, M. Alami, J. Schröder, B.C. Berks, and T. Palmer.** 2007. Cysteine scanning mutagenesis and topological mapping of the *Escherichia coli* twin-arginine translocase TatC Component. J. Bacteriol. **189:**5482-94.

12. **Lobo, I.A., R.A. Harris, and J.R. Trudell.** 2008. Cross-linking of sites involved with alcohol action between transmembrane segments 1 and 3 of the glycine receptor following activation. J. Neurochem. **104:**1649-62.

13. **Ren, X., D.A. Nicoll, G. Galang, and K.D. Philipson.** 2008. Intermolecular cross-linking of Na^+-Ca^{2+} exchanger proteins: evidence for dimer formation. Biochemistry. **47:**6081-7.

14. **Rimon, A., T. Tzubery, L. Galili, and E. Padan.** 2002. Proximity of cytoplasmic and periplasmic loops in NhaA Na^+/H^+ antiporter of *Escherichia coli* as determined by site-directed thiol cross-linking. Biochemistry. **41:**14897-905.

15. **Or, E., R. Goldshleger, and S.J. Karlish.** 1999. Characterization of disulfide cross-links between fragments of proteolyzed Na,K-ATPase. Implications for spatial organization of trans-membrane helices. J. Biol. Chem. **274:**2802-9.

16. **Karnik, S.S. and H.G. Khorana.** 1990. Assembly of functional rhodopsin requires a disulfide bond between cysteine residues 110 and 187. J. Biol. Chem. **265:**17520-4.

17. **Bubis, J. and H.G. Khorana.** 1990. Sites of interaction in the complex between β and γ subunits of transducin. J. Biol. Chem. **265:**12995-9.

18. **First, E.A. and S.S. Taylor.** 1984. Induced interchain disulfide bonding in cAMP-dependent protein kinase II. J. Biol. Chem. **259:**Apr 10.

19. **Luo, Y., B. Li, G. Yang, J. Gergely, and T. Tao.** 2002. Cross-linking between the regulatory regions of troponin-I and troponin-C abolishes the inhibitory function of troponin. Biochemistry. **41:**12891-8.

20. **Hughes, R.E., P.A. Rice, T.A. Steitz, and N.D. Grindley.** 1993. Protein-protein interactions directing resolvase site-specific recombination: a structure-function analysis. EMBO J. **12:**1447-58.

21. **Grantcharova, V.P., D.S. Riddle, and D. Baker.** 2000. Long-range order in the src SH3 folding transition state. Proc. Natl. Acad. Sci. USA. **97:**7084-9.

22. **Clarke, J. and A.R. Fersht.** 1993. Engineered disulfide bonds as probes of the folding pathway of barnase: increasing the stability of proteins against the rate of denaturation. Biochemistry. **32:**4322-9.

23. **Mason, J.M., N. Gibbs, R.B. Sessions, and A.R. Clarke.** 2002. The influence of intramolecular bridges on the dynamics of a protein folding reaction. Biochemistry. **41:**12093-9.

24. **Shandiz, A.T., B.R. Capraro, and T.R. Sosnick.** 2007. Intramolecular cross-linking evaluated as a structural probe of the protein folding transition state. Biochemistry. **46:**13711-9.

25. **Betz, S.F.** 1993. Disulfide bonds and the stability of globular proteins. Protein Sci. **2:**1551-8.

26. **Boyer, P.D.** 1975. A model for conformational coupling of membrane potential and proton translocation to ATP synthesis and to active transport. FEBS Lett. **58:**1-6.

27. **Boyer, P.D.** 1989. A perspective of the binding change mechanism for ATP synthesis. FASEB J. **3:**2164-78.

28. **Kayalar, C., J. Rosing, and P.D. Boyer.** 1977. An alternating site sequence for oxidative phosphorylation suggested by measurement of substrate binding patterns and exchange reaction inhibitions. J. Biol. Chem. **252:**2486-91.

29. **Adolfsen, R. and E.N. Moudrianakis.** 1976. Binding of adenine nucleotides to the purified 13S coupling factor of bacterial oxidative phosphorylation. Arch. Biochem. Biophys. **172:**425-33.

30. **Noji, H., R. Yasuda, M. Yoshida, and K.K. Jr.** 1997. Direct observation of the rotation of F_1-ATPase. Nature. **386:**299-302.

31. **Cross, R.L., C. Grubmeyer, and H.S. Penefsky.** 1982. Mechanism of ATP hydrolysis by beef heart mitochondrial ATPase. Rate enhancements resulting from cooperative interactions between multiple catalytic sites. J. Biol. Chem. **257:**12101-5.

32. **Weber, J. and A.E. Senior.** 1997. Catalytic mechanism of F_1-ATPase. Biochim. Biophys. Acta. **1319:**19-58.

33. **Ren, H. and W.S. Allison.** 2000. Substitution of β_{E201} in the $\alpha_3\beta_3\gamma$ subcomplex of the F_1-ATPase from the thermophilic Bacillus PS3 increases the affinity of catalytic sites for nucleotides. J. Biol. Chem. **275:**10057-63.

34. **Löbau, S., J. Weber, and A.E. Senior.** 1998. Catalytic site nucleotide binding and hydrolysis in F_1F_O-ATP synthase. Biochemistry. **37:**10846-53.

35. **Bianchet, M.A., P.L. Pedersen, and L.M. Amzel.** 2000. Notes on the mechanism of ATP synthesis. J. Bioenerg. Biomembr. **32:**517-21.

36. **Weber, J. and A.E. Senior.** 2001. Bi-site catalysis in F_1-ATPase: does it exist? J. Biol. Chem. **276:**35422-8.

37. **Senior, A.E., S. Nadanaciva, and J. Weber.** 2002. The molecular mechanism of ATP synthesis by F_1F_O-ATP synthase. Biochim. Biophys. Acta. **1553:**188-211.

38. **Duncan, T.M. and A.E. Senior.** 1985. The defective proton-ATPase of uncD mutants of *Escherichia coli*. Two mutations which affect the catalytic mechanism. J. Biol. Chem. **260:**4901-7.

39. **Senior, A.E.** 1990. The proton-translocating ATPase of *Escherichia coli*. Annu. Rev. Biophys. Biophys. Chem. **19:**7-41.

40. **Penefsky, H.S. and R.L. Cross.** 1991. Structure and mechanism of F_OF_1-type ATP synthases and ATPases. Adv. Enzymol. Relat. Areas. Mol. Biol. **64:**173-214.

41. **Senior, A.E.** 1988. ATP synthesis by oxidative phosphorylation. Physiol. Rev. **68:**177-231.

42. **Senior, A.E.** 1992. Catalytic sites of *Escherichia coli* F_1-ATPase. J. Bioenerg. Biomembr. **24:**479-84.

43. **Turina, P. and R.A. Capaldi.** 1994. ATP hydrolysis-driven structural changes in the γ subunit of *Escherichia coli* ATPase monitored by fluorescence from probes bound at introduced cysteine residues. J. Biol. Chem. **269:**13465-71.

44. **Xiao, R. and H.S. Penefsky.** 1994. Unisite catalysis and the δ subunit of F_1-ATPase in *Escherichia coli*. J. Biol. Chem. **269:**19232-7.

45. **Dunn, S.D. and R.G. Tozer.** 1987. Activation and inhibition of the *Escherichia coli* F_1-ATPase by monoclonal antibodies which recognize the ε subunit. Arch. Biochem. Biophys. **253:**73-80.

46. **Park, M.Y., H. Omote, M. Maeda, and M. Futai.** 1994. Conserved Glu-181 and Arg-182 residues of *Escherichia coli* H^+-ATPase (ATP synthase) β subunit are essential for catalysis: properties of 33 mutants between β_{E161} and β_{K201} residues. J. Biochem. **116:**1139-45.

47. **Penefsky, H.S.** 1985. Reaction mechanism of the membrane-bound ATPase of submitochondrial particles from beef heart. J. Biol. Chem. **260:**13728-34.

48. **Weber, J., S. Wilke-Mounts, R.S. Lee, E. Grell, and A.E. Senior.** 1993. Specific placement of tryptophan in the catalytic sites of *Escherichia coli* F_1-ATPase provides a direct probe of nucleotide binding: maximal ATP hydrolysis occurs with three sites occupied. J. Biol. Chem. **268:**20126-33.

49. **Fischer, S., C. Etzold, P. Turina, G. Deckers-Hebestreit, K. Altendorf, and P. Gräber.** 1994. ATP synthesis catalyzed by the ATP synthase of *Escherichia coli* reconstituted into liposomes. Eur. J. Biochem. **225:**167-72.

50. **Dou, C., P.A. Fortes, and W.S. Allison.** 1998. The $\alpha_3(\beta_{Y341W})_3\gamma$ subcomplex of the F_1-ATPase from the thermophilic Bacillus PS3 fails to dissociate ADP when MgATP is hydrolyzed at a single catalytic site and attains maximal velocity when three catalytic sites are saturated with MgATP. Biochemistry. **37:**16757-64.

51. **Adachi, K., K. Oiwa, T. Nishizaka, S. Furuike, H. Noji, H. Itoh, M. Yoshida, and K. Kinosita.** 2007. Coupling of rotation and catalysis in F_1-ATPase revealed by single-molecule imaging and manipulation. Cell. **130:**309-21.

52. **Adachi, K., R. Yasuda, H. Noji, H. Itoh, Y. Harada, M. Yoshida, and K. Kinosita.** 2000. Stepping rotation of F_1-ATPase visualized through angle-resolved single-fluorophore imaging. Proc. Natl. Acad. Sci. USA. **97:**7243-7.

53. **Yasuda, R., H. Noji, K. Kinosita, and M. Yoshida.** 1998. F_1-ATPase is a highly efficient molecular motor that rotates with discrete 120 degree steps. Cell. **93:**1117-24.

54. **Börsch, M., M. Diez, B. Zimmermann, R. Reuter, and P. Gräber.** 2002. Stepwise rotation of the γ subunit of EF_0F_1-ATP synthase observed by intramolecular single-molecule fluorescence resonance energy transfer. FEBS Lett. **527:**147-52.

55. **Yasuda, R., H. Noji, M. Yoshida, K. Kinosita, and H. Itoh.** 2001. Resolution of distinct rotational substeps by submillisecond kinetic analysis of F_1-ATPase. Nature. **410:**898-904.

56. **Hirono-Hara, Y., H. Noji, M. Nishiura, E. Muneyuki, K.Y. Hara, R. Yasuda, K. Kinosita, and M. Yoshida.** 2001. Pause and rotation of F_1-ATPase during catalysis. Proc. Natl. Acad. Sci. USA. **98:**13649-54.

57. **Nishizaka, T., K. Oiwa, H. Noji, S. Kimura, E. Muneyuki, M. Yoshida, and K. Kinosita.** 2004. Chemomechanical coupling in F_1-ATPase revealed by simultaneous observation of nucleotide kinetics and rotation. Nat. Struct. Mol. Biol. **11:**142-8.

58. **Shimabukuro, K., R. Yasuda, E. Muneyuki, K.Y. Hara, K. Kinosita, and M. Yoshida.** 2003. Catalysis and rotation of F_1 motor: cleavage of ATP at the catalytic site occurs in 1 ms before 40 degree substep rotation. Proc. Natl. Acad. Sci. USA. **100:**14731-6.

59. **Kinosita, K., K. Adachi, and H. Itoh.** 2004. Rotation of F_1-ATPase: how an ATP-driven molecular machine may work. Annu. Rev. Biophys. Biomol. Struct. **33:**245-68.

60. **Oiwa, K., D.M. Jameson, J.C. Croney, C.T. Davis, J.F. Eccleston, and M. Anson.** 2003. The 2'-O- and 3'-O-Cy3-EDA-ATP(ADP) complexes with myosin subfragment-1 are spectroscopically distinct. Biophys. J. **84:**634-42.

61. **Wood, J.M., J.G. Wise, A.E. Senior, M. Futai, and P.D. Boyer.** 1987. Catalytic properties of the F_1-adenosine triphosphatase from *Escherichia coli* K-12 and its genetic variants as revealed by ^{18}O exchanges. J. Biol. Chem. **262:**2180-6.

62. **O'Neal, C.C. and P.D. Boyer.** 1984. Assessment of the rate of bound substrate interconversion and of ATP acceleration of product release during catalysis by mitochondrial adenosine triphosphatase. J. Biol. Chem. **259:**5761-7.

63. **Al-Shawi, M.K., D. Parsonage, and A.E. Senior.** 1990. Thermodynamic analyses of the catalytic pathway of F_1-ATPase from *Escherichia coli*. Implications regarding the nature of energy coupling by F_1-ATPases. J. Biol. Chem. **265:**4402-10.

64. **Senior, A.E. and M.K. Al-Shawi.** 1992. Further examination of seventeen mutations in *Escherichia coli* F_1-ATPase β subunit. J. Biol. Chem. **267:**21471-8.

65. **Pänke, O., D.A. Cherepanov, K. Gumbiowski, S. Engelbrecht, and W. Junge.** 2001. Viscoelastic dynamics of actin filaments coupled to rotary F-ATPase: angular torque profile of the enzyme. Biophys. J. **81:**1220-33.

66. **Wang, H. and G. Oster.** 1998. Energy transduction in the F_1 motor of ATP synthase. Nature. **396:**279-82.

67. **Junge, W.** 1999. ATP synthase and other motor proteins. Proc. Natl. Acad. Sci. USA. **96:**4735-7.

68. **Cherepanov, D.A., A.Y. Mulkidjanian, and W. Junge.** 1999. Transient accumulation of elastic energy in proton translocating ATP synthase. FEBS Lett. **449:**1-6.

69. **Kinosita, K., R. Yasuda, H. Noji, and K. Adachi.** 2000. A rotary molecular motor that can work at near 100% efficiency. Philos. Trans. R. Soc. Lond. B. Biol. Sci. **355:**473-89.

70. **Walker, J.E., M. Saraste, and N.J. Gay.** 1984. The *unc* operon. Nucleotide sequence, regulation and structure of ATP-synthase. Biochim. Biophys. Acta. **768:**164-200.

71. **Schneider, E. and K. Altendorf.** 1985. All three subunits are required for the reconstitution of an active proton channel (F_O) of *Escherichia coli* ATP synthase (F_1F_O). EMBO J. **4:**515-8.

72. **Meyenburg, K.v., B.B. Jørgensen, O. Michelsen, L. Sørensen, and J.E. McCarthy.** 1985. Proton conduction by subunit *a* of the membrane-bound ATP synthase of *Escherichia coli* revealed after induced overproduction. EMBO J. **4:**2357-63.

73. **Eya, S., M. Maeda, K. Tomochika, Y. Kanemasa, and M. Futai.** 1989. Overproduction of truncated subunit *a* of H^+-ATPase causes growth inhibition of *Escherichia coli*. J. Bacteriol. **171:**6853-8.

74. **Hermolin, J. and R.H. Fillingame.** 1995. Assembly of F_O sector of *Escherichia coli* H^+ ATP synthase. Interdependence of subunit insertion into the membrane. J. Biol. Chem. **270:**2815-7.

75. **Akiyama, Y., A. Kihara, and K. Ito.** 1996. Subunit *a* of proton ATPase F_0 sector is a substrate of the FtsH protease in *Escherichia coli*. FEBS Lett. **399:**26-8.

76. **Long, J.C., S. Wang, and S.B. Vik.** 1998. Membrane topology of subunit *a* of the F_1F_O ATP synthase as determined by labeling of unique cysteine residues. J. Biol. Chem. **273:**16235-40.

77. **Wada, T., J.C. Long, D. Zhang, and S.B. Vik.** 1999. A novel labeling approach supports the five-transmembrane model of subunit *a* of the *Escherichia coli* ATP synthase. J. Biol. Chem. **274:**17353-7.

78. **Hartzog, P.E. and B.D. Cain.** 1994. Second-site suppressor mutations at glycine 218 and histidine 245 in the α subunit of F_1F_O ATP synthase in *Escherichia coli*. J. Biol. Chem. **269:**32313-7.

79. **Cain, B.D. and R.D. Simoni.** 1986. Impaired proton conductivity resulting from mutations in the *a* subunit of F_1F_0 ATPase in *Escherichia coli*. J. Biol. Chem. **261:**10043-50.

80. **Cain, B.D.** 2000. Mutagenic analysis of the F_0 stator subunits. J. Bioenerg. Biomembr. **32:**365-71.

81. **Vik, S.B. and B.J. Antonio.** 1994. A mechanism of proton translocation by F_1F_O ATP synthases suggested by double mutants of the *a* subunit. J. Biol. Chem. **269:**30364-9.

82. **Vik, S.B., A.R. Patterson, and B.J. Antonio.** 1998. Insertion scanning mutagenesis of subunit *a* of the F_1F_O ATP synthase near His245 and implications on gating of the proton channel. J. Biol. Chem. **273:**16229-34.

83. **Aksimentiev, A., I.A. Balabin, R.H. Fillingame, and K. Schulten.** 2004. Insights into the molecular mechanism of rotation in the F_O sector of ATP synthase. Biophys. J. **86:**1332-44.

84. **Elston, T., H. Wang, and G. Oster.** 1998. Energy transduction in ATP synthase. Nature. **391:**510-3.

85. **Junge, W., H. Lill, and S. Engelbrecht.** 1997. ATP synthase: an electrochemical transducer with rotatory mechanics. Trends Biochem. Sci. **22:**420-3.

86. **Valiyaveetil, F.I. and R.H. Fillingame.** 1998. Transmembrane topography of subunit *a* in the *Escherichia coli* F_1F_O ATP synthase. J. Biol. Chem. **273:**16241-7.

87. **Vik, S.B., J.C. Long, T. Wada, and D. Zhang.** 2000. A model for the structure of subunit *a* of the *Escherichia coli* ATP synthase and its role in proton translocation. Biochim. Biophys. Acta. **1458:**457-66.

88. **Long, J.C., J. DeLeon-Rangel, and S.B. Vik.** 2002. Characterization of the first cytoplasmic loop of subunit *a* of the *Escherichia coli* ATP synthase by surface labeling, cross-linking, and mutagenesis. J. Biol. Chem. **277:**27288-93.

89. **Zhang, D. and S.B. Vik.** 2003. Helix packing in subunit *a* of the *Escherichia coli* ATP synthase as determined by chemical labeling and proteolysis of the cysteine-substituted protein. Biochemistry. **42:**331-7.

90. **Vik, S.B., D. Lee, C.E. Curtis, and L.T. Nguyen.** 1990. Mutagenesis of the *a* subunit of the F_1F_O-ATP synthase from *Escherichia coli* in the region of Asn-192. Arch. Biochem. Biophys. **282:**125-31.

91. **Vik, S.B., D. Lee, and P.A. Marshall.** 1991. Temperature-sensitive mutations at the carboxy terminus of the α subunit of the *Escherichia coli* F_1F_O ATP synthase. J. Bacteriol. **173:**4544-8.

92. **Patterson, A.R., T. Wada, and S.B. Vik.** 1999. His(15) of subunit *a* of the *Escherichia coli* ATP synthase is important for the structure or assembly of the membrane sector F_O. Arch. Biochem. Biophys. **368:**193-7.

93. **Yamada, H., Y. Moriyama, M. Maeda, and M. Futai.** 1996. Transmembrane topology of *Escherichia coli* H^+-ATPase (ATP synthase) subunit *a*. FEBS Lett. **390:**34-8.

94. **Jäger, H., R. Birkenhäger, W.D. Stalz, K. Altendorf, and G. Deckers-Hebestreit.** 1998. Topology of subunit *a* of the *Escherichia coli* ATP synthase. Eur. J. Biochem. **251:**122-32.

95. **Rastogi, V.K. and M.E. Girvin.** 1999. Structural changes linked to proton translocation by subunit *c* of the ATP synthase. Nature. **402:**263-8.

96. **Cain, B.D. and R.D. Simoni.** 1989. Proton translocation by the F_1F_0 ATPase of *Escherichia coli*. Mutagenic analysis of the *a* subunit. J. Biol. Chem. **264:**3292-300.

97. **Hatch, L.P., G.B. Cox, and S.M. Howitt.** 1995. The essential arginine residue at position 210 in the *a* subunit of the *Escherichia coli* ATP synthase can be transferred to position 252 with partial retention of activity. J. Biol. Chem. **270:**29407-12.

98. **Lightowlers, R.N., S.M. Howitt, L. Hatch, F. Gibson, and G.B. Cox.** 1987. The proton pore in the *Escherichia coli* F_OF_1-ATPase: a requirement for arginine at position 210 of the *a* subunit. Biochim. Biophys. Acta. **894:**399-406.

99. **Valiyaveetil, F.I. and R.H. Fillingame.** 1997. On the role of Arg-210 and Glu-219 of subunit *a* in proton translocation by the *Escherichia coli* F_OF_1-ATP synthase. J. Biol. Chem. **272:**32635-41.

100. **Eya, S., M. Maeda, and M. Futai.** 1991. Role of the carboxyl terminal region of H^+-ATPase (F_0F_1) *a* subunit from *Escherichia coli*. Arch. Biochem. Biophys. **284:**71-7.

101. **Gardner, J.L. and B.D. Cain.** 1999. Amino acid substitutions in the *a* subunit affect the ε subunit of F_1F_O ATP synthase from *Escherichia coli*. Arch. Biochem. Biophys. **361:**302-8.

102. **Langemeyer, L. and S. Engelbrecht.** 2007. Essential arginine in subunit *a* and aspartate in subunit *c* of F_OF_1 ATP synthase: effect of repositioning within helix 4 of subunit *a* and helix 2 of subunit *c*. Biochim. Biophys. Acta. **1767:**998-1005.

103. **Ishmukhametov, R.R., J.B. Pond, A. Al-Huqail, M.A. Galkin, and S.B. Vik.** 2008. ATP synthesis without R210 of subunit *a* in the *Escherichia coli* ATP synthase. Biochim. Biophys. Acta. **1777:**32-8.

104. **Vik, S.B., B.D. Cain, K.T. Chun, and R.D. Simoni.** 1988. Mutagenesis of the α subunit of the F_1F_O-ATPase from *Escherichia coli*. Mutations at Glu-196, Pro-190, and Ser-199. J. Biol. Chem. **263:**6599-605.

105. **Lightowlers, R.N., S.M. Howitt, L. Hatch, F. Gibson, and G. Cox.** 1988. The proton pore in the *Escherichia coli* F_OF_1-ATPase: substitution of glutamate by glutamine at position 219 of the α subunit prevents F_O-mediated proton permeability. Biochim. Biophys. Acta. **933:**241-8.

106. **Hatch, L.P., G.B. Cox, and S.M. Howitt.** 1998. Glutamate residues at positions 219 and 252 in the *a* subunit of the *Escherichia coli* ATP synthase are not functionally equivalent. Biochim. Biophys. Acta. **1363:**217-23.

107. **Cain, B.D. and R.D. Simoni.** 1988. Interaction between Glu-219 and His-245 within the *a* subunit of F_1F_0-ATPase in *Escherichia coli*. J. Biol. Chem. **263:**6606-12.

108. **Gardner, J.L. and B.D. Cain.** 2000. The *a* subunit A217R substitution affects catalytic activity of F_1F_O ATP synthase. Arch. Biochem. Biophys. **380:**201-7.

109. **Howitt, S.M., R.N. Lightowlers, F. Gibson, and G.B. Cox.** 1990. Mutational analysis of the function of the *a* subunit of the F_OF_1-APPase of *Escherichia coli*. Biochim. Biophys. Acta. **1015:**264-8.

110. **Hartzog, P.E. and B.D. Cain.** 1993. Mutagenic analysis of the *a* subunit of the F_1F_O ATP synthase in *Escherichia coli*: Gln-252 through Tyr-263. J. Bacteriol. **175:**1337-43.

111. **Lewis, M.J. and R.D. Simoni.** 1992. Deletions in hydrophilic domains of subunit *a* from the *Escherichia coli* F_1F_O-ATP synthase interfere with membrane insertion or F_O assembly. J. Biol. Chem. **267:**3482-9.

112. **Sondek, J. and D. Shortle.** 1990. Accommodation of single amino acid insertions by the native state of staphylococcal nuclease. Proteins. **7:**299-305.

113. **Heinz, D.W., W.A. Baase, F.W. Dahlquist, and B.W. Matthews.** 1993. How amino-acid insertions are allowed in an α-helix of T4 lysozyme. Nature. **361:**561-4.

114. **Wang, S. and S.B. Vik.** 1994. Single amino acid insertions probe the *a* subunit of the *Escherichia coli* F_1F_O-ATP synthase. J. Biol. Chem. **269:**3095-9.

115. **Schwem, B.E. and R.H. Fillingame.** 2006. Cross-linking between helices within subunit *a* of *Escherichia coli* ATP synthase defines the transmembrane packing of a four-helix bundle. J. Biol. Chem. **281:**37861-7.

116. **Angevine, C.M., K.A. Herold, O.D. Vincent, and R.H. Fillingame.** 2007. Aqueous access pathways in ATP synthase subunit *a*. Reactivity of cysteine substituted into transmembrane helices 1, 3, and 5. J. Biol. Chem. **282:**9001-7.

117. **Moore, K.J., C.M. Angevine, O.D. Vincent, B.E. Schwem, and R.H. Fillingame.** 2008. The Cytoplasmic Loops of Subunit *a* of *Escherichia coli* ATP Synthase May Participate in the Proton Translocating Mechanism. J. Biol. Chem. **283:**13044-52.

118. **Jiang, W. and R.H. Fillingame.** 1998. Interacting helical faces of subunits *a* and *c* in the F_1F_O ATP synthase of *Escherichia coli* defined by disulfide cross-linking. Proc. Natl. Acad. Sci. USA. **95:**6607-12.

119. **Girvin, M.E., V.K. Rastogi, F. Abildgaard, J.L. Markley, and R.H. Fillingame.** 1998. Solution structure of the transmembrane H^+-transporting subunit *c* of the F_1F_O ATP synthase. Biochemistry. **37:**8817-24.

120. **Dmitriev, O.Y. and R.H. Fillingame.** 2007. The rigid connecting loop stabilizes hairpin folding of the two helices of the ATP synthase subunit *c*. Protein Sci. **16:**2118-22.

121. **Deckers-Hebestreit, G., R. Schmid, H.H. Kiltz, and K. Altendorf.** 1987. F_0 portion of *Escherichia coli* ATP synthase: orientation of subunit *c* in the membrane. Biochemistry. **26:**5486-92.

122. **Hoppe, J., J. Brunner, and B.B. Jørgensen.** 1984. Structure of the membrane-embedded F_O part of F_1F_O ATP synthase from *Escherichia coli* as inferred from labeling with 3-(Trifluoromethyl)-3-(m-[125I]iodophenyl)diazirine. Biochemistry. **23:**5610-6.

123. **Girvin, M.E. and R.H. Fillingame.** 1993. Helical structure and folding of subunit *c* of F_1F_O ATP synthase: ^{1}H NMR resonance assignments and NOE analysis. Biochemistry. **32:**12167-77.

124. **Girvin, M.E. and R.H. Fillingame.** 1994. Hairpin folding of subunit *c* of F_1F_O ATP synthase: ^{1}H distance measurements to nitroxide-derivatized aspartyl-61. Biochemistry. **33:**665-74.

125. **Girvin, M.E. and R.H. Fillingame.** 1995. Determination of local protein structure by spin label difference 2D NMR: the region neighboring Asp61 of subunit *c* of the F_1F_O ATP synthase. Biochemistry. **34:**1635-45.

126. **Schneider, E. and K. Altendorf.** 1987. Bacterial adenosine 5'-triphosphate synthase (F_1F_O): purification and reconstitution of F_O complexes and biochemical and functional characterization of their subunits. Microbiol. Rev. **51:**477-97.

127. **Miller, M.J., M. Oldenburg, and R.H. Fillingame.** 1990. The essential carboxyl group in subunit *c* of the F_1F_O ATP synthase can be moved and H^+-translocating function retained. Proc. Natl. Acad. Sci. USA. **87:**4900-4.

128. **Fraga, D., J. Hermolin, and R.H. Fillingame.** 1994. Transmembrane helix-helix interactions in F_0 suggested by suppressor mutations to A24D/D61G mutant of ATP synthase subunit. J. Biol. Chem. **269:**2562-7.

129. **Girvin, M.E., J. Hermolin, R. Pottorf, and R.H. Fillingame.** 1989. Organization of the F_O sector of *Escherichia coli* H^+-ATPase: the polar loop region of subunit *c* extends from the cytoplasmic face of the membrane. Biochemistry. **28:**4340-3.

130. **Hensel, M., G. Deckers-Hebestreit, R. Schmid, and K. Altendorf.** 1990. Orientation of subunit *c* of the ATP synthase of *Escherichia coli*--a study with peptide-specific antibodies. Biochim. Biophys. Acta. **1016:**63-70.

131. **Fraga, D. and R.H. Fillingame.** 1991. Essential residues in the polar loop region of subunit *c* of *Escherichia coli* F_1F_0 ATP synthase defined by random oligonucleotide-primed mutagenesis. J. Bacteriol. **173:**2639-43.

132. **Fraga, D., J. Hermolin, M. Oldenburg, M.J. Miller, and R.H. Fillingame.** 1994. Arginine 41 of subunit *c* of *Escherichia coli* H^+-ATP synthase is essential in binding and coupling of F_1 to F_0. J. Biol. Chem. **269:**7532-7.

133. **Laan, M.v.d., P. Bechtluft, S. Kol, N. Nouwen, and A.J. Driessen.** 2004. F_1F_O ATP synthase subunit *c* is a substrate of the novel YidC pathway for membrane protein biogenesis. J. Cell Biol. **165:**213-22.

134. **Kol, S., N. Nouwen, and A.J. Driessen.** 2008. The charge distribution in the cytoplasmic loop of subunit *c* of the F_1F_O ATPase is a determinant for YidC targeting. J. Biol. Chem. **283:**9871-7.

135. **Kol, S., B.R. Turrell, J.d. Keyzer, M.v.d. Laan, N. Nouwen, and A.J. Driessen.** 2006. YidC-mediated membrane insertion of assembly mutants of subunit *c* of the F_1F_O ATPase. J. Biol. Chem. **281:**29762-8.

136. **Birkenhäger, R., M. Hoppert, G. Deckers-Hebestreit, F. Mayer, and K. Altendorf.** 1995. The F_0 complex of the *Escherichia coli* ATP synthase. Investigation by electron spectroscopic imaging and immunoelectron microscopy. Eur. J. Biochem. **230:**58-67.

137. **Singh, S., P. Turina, C.J. Bustamante, D.J. Keller, and R. Capaldi.** 1996. Topographical structure of membrane-bound *Escherichia coli* F_1F_O ATP synthase in aqueous buffer. FEBS Lett. **397:**30-4.

138. **Takeyasu, K., H. Omote, S. Nettikadan, F. Tokumasu, A. Iwamoto-Kihara, and M. Futai.** 1996. Molecular imaging of *Escherichia coli* F_OF_1-ATPase in reconstituted membranes using atomic force microscopy. FEBS Lett. **392:**110-3.

139. **Jiang, W., J. Hermolin, and R.H. Fillingame.** 2001. The preferred stoichiometry of *c* subunits in the rotary motor sector of *Escherichia coli* ATP synthase is 10. Proc. Natl. Acad. Sci. USA. **98:**4966-71.

140. **Stahlberg, H., D.J. Müller, K. Suda, D. Fotiadis, A. Engel, T. Meier, U. Matthey, and P. Dimroth.** 2001. Bacterial Na^+-ATP synthase has an undecameric rotor. EMBO Rep. **2:**229-33.

141. **Meier, T., U. Matthey, C.v. Ballmoos, J. Vonck, T.K.v. Nidda, W. Kühlbrandt, and P. Dimroth.** 2003. Evidence for structural integrity in the undecameric *c* rings isolated from sodium ATP synthases. J. Mol. Biol. **325:**389-97.

142. **Seelert, H., A. Poetsch, N.A. Dencher, A. Engel, H. Stahlberg, and D.J. Müller.** 2000. Structural biology. Proton-powered turbine of a plant motor. Nature. **405:**418-9.

143. **Pogoryelov, D., J. Yu, T. Meier, J. Vonck, P. Dimroth, and D.J. Muller.** 2005. The c_{15} ring of the *Spirulina platensis* F-ATP synthase: F_1/F_O symmetry mismatch is not obligatory. EMBO Rep. **6:**1040-4.

144. **Jones, P.C., W. Jiang, and R.H. Fillingame.** 1998. Arrangement of the multicopy H^+-translocating subunit *c* in the membrane sector of the *Escherichia coli* F_1F_O ATP synthase. J. Biol. Chem. **273:**17178-85.

145. **Vincent, O.D., B.E. Schwem, P.R. Steed, W. Jiang, and R.H. Fillingame.** 2007. Fluidity of structure and swiveling of helices in the subunit *c* ring of *Escherichia coli* ATP synthase as revealed by cysteine-cysteine cross-linking. J. Biol. Chem. **282:**33788-94.

146. **Stock, D., A.G. Leslie, and J.E. Walker.** 1999. Molecular architecture of the rotary motor in ATP synthase. Science. **286:**1700-5.

147. **Meier, T., P. Polzer, K. Diederichs, W. Welte, and P. Dimroth.** 2005. Structure of the rotor ring of F-Type Na^+-ATPase from *Ilyobacter tartaricus*. Science. **308:**659-62.

148. **Murata, T., I. Yamato, Y. Kakinuma, A.G. Leslie, and J.E. Walker.** 2005. Structure of the rotor of the V-Type Na^+-ATPase from *Enterococcus hirae*. Science. **308:**654-9.

149. **Dmitriev, O., P.C. Jones, W. Jiang, and R.H. Fillingame.** 1999. Structure of the membrane domain of subunit *b* of the *Escherichia coli* F_0F_1 ATP synthase. J. Biol. Chem. **274:**15598-604.

150. **Sambongi, Y., Y. Iko, M. Tanabe, H. Omote, A. Iwamoto-Kihara, I. Ueda, T. Yanagida, Y. Wada, and M. Futai.** 1999. Mechanical rotation of the *c* subunit oligomer in ATP synthase (F_OF_1): direct observation. Science. **286:**1722-4.

151. **Kato-Yamada, Y., H. Noji, R. Yasuda, K.K. Jr, and M. Yoshida.** 1998. Direct observation of the rotation of ε subunit in F_1-ATPase. J. Biol. Chem. **273:**19375-7.

152. **Pänke, O., K. Gumbiowski, W. Junge, and S. Engelbrecht.** 2000. F-ATPase: specific observation of the rotating *c* subunit oligomer of EF_OEF_1. FEBS Lett. **472:**34-8.

153. **Tsunoda, S.P., R. Aggeler, H. Noji, K.K. Jr, M. Yoshida, and R.A. Capaldi.** 2000. Observations of rotation within the F_OF_1-ATP synthase: deciding between rotation of the F_Oc subunit ring and artifact. FEBS Lett. **470:**244-8.

154. **Tsunoda, S.P., R. Aggeler, M. Yoshida, and R.A. Capaldi.** 2001. Rotation of the *c* subunit oligomer in fully functional F_1F_O ATP synthase. Proc. Natl. Acad. Sci. USA. **98:**898-902.

155. **Ueno, H., T. Suzuki, K.K. Jr, and M. Yoshida.** 2005. ATP-driven stepwise rotation of F_OF_1-ATP synthase. Proc. Natl. Acad. Sci. USA. **102:**1333-8.

156. **Junge, W., O. Pänke, D.A. Cherepanov, K. Gumbiowski, M. Müller, and S. Engelbrecht.** 2001. Inter-subunit rotation and elastic power transmission in F_OF_1-ATPase. FEBS Lett. **504:**152-60.

157. **Steed, P.R. and R.H. Fillingame.** 2008. Subunit *a* facilitates aqueous access to a membrane-embedded region of subunit *c* in *Escherichia coli* F_1F_O ATP synthase. J. Biol. Chem. **283:**12365-72.

158. **Dmitriev, O.Y., K. Altendorf, and R.H. Fillingame.** 1995. Reconstitution of the F_O complex of *Escherichia coli* ATP synthase from isolated subunits. Varying the number of essential carboxylates by co-incorporation of wild-type and mutant subunit *c* after purification in organic solvent. Eur. J. Biochem. **233:**478-83.

159. **Hermolin, J. and R.H. Fillingame.** 1989. H^+-ATPase activity of *Escherichia coli* F_1F_O is blocked after reaction of dicyclohexylcarbodiimide with a single proteolipid (subunit *c*) of the F_O complex. J. Biol. Chem. **264:**3896-903.

160. **Fraga, D. and R.H. Fillingame.** 1989. Conserved polar loop region of *Escherichia coli* subunit *c* of the F_1F_0 H^+-ATPase. Glutamine 42 is not absolutely essential, but substitutions alter binding and coupling of F_1 to F_0. J. Biol. Chem. **264:**6797-803.

161. **Hatch, L., A.L. Fimmel, and F. Gibson.** 1993. The role of arginine in the conserved polar loop of the *c*-subunit of the *Escherichia coli* H^+-ATPase. Biochim. Biophys. Acta. **1141:**183-9.

162. **Miller, M.J., D. Fraga, C.R. Paule, and R.H. Fillingame.** 1989. Mutations in the conserved proline 43 residue of the uncE protein (subunit *c*) of *Escherichia coli* F_1F_O-ATPase alter the coupling of F_1 to F_O. J. Biol. Chem. **264:**305-11.

163. **Mosher, M.E., L.K. White, J. Hermolin, and R.H. Fillingame.** 1985. H^+-ATPase of *Escherichia coli*. An uncE mutation impairing coupling between F_1 and F_O but not F_O-mediated H^+ translocation. J. Biol. Chem. **260:**4807-14.

164. **Zhang, Y., M. Oldenburg, and R.H. Fillingame.** 1994. Suppressor mutations in F_1 subunit ε recouple ATP-driven H^+ translocation in uncoupled c_{Q42E} mutant of *Escherichia coli* F_1F_O ATP synthase. J. Biol. Chem. **269:**10221-4.

165. **Watts, S.D. and R.A. Capaldi.** 1997. Interactions between the F_1 and F_O parts in the *Escherichia coli* ATP synthase. Associations involving the loop region of *c* subunits. J. Biol. Chem. **272:**15065-8.

166. **Zhang, D. and S.B. Vik.** 2003. Close proximity of a cytoplasmic loop of subunit *a* with *c* subunits of the ATP synthase from *Escherichia coli*. J. Biol. Chem. **278:**12319-24.

167. **Jones, P.C., J. Hermolin, W. Jiang, and R.H. Fillingame.** 2000. Insights into the rotary catalytic mechanism of F_OF_1 ATP synthase from the cross-linking of subunits *b* and *c* in the *Escherichia coli* enzyme. J. Biol. Chem. **275:**31340-6.

168. **Zhang, Y. and R.H. Fillingame.** 1995. Subunits coupling H^+ transport and ATP synthesis in the *Escherichia coli* ATP synthase. Cys-Cys cross-linking of F_1 subunit ε to the polar loop of F_O subunit *c*. J. Biol. Chem. **270:**24609-14.

169. **Schulenberg, B., R. Aggeler, J. Murray, and R.A. Capaldi.** 1999. The γε-*c* subunit interface in the ATP synthase of *Escherichia coli*. cross-linking of the ε subunit to the *c* subunit ring does not impair enzyme function, that of γ to *c* subunits leads to uncoupling. J. Biol. Chem. **274:**34233-7.

170. **Hermolin, J., O.Y. Dmitriev, Y. Zhang, and R.H. Fillingame.** 1999. Defining the domain of binding of F_1 subunit ε with the polar loop of F_O subunit *c* in the *Escherichia coli* ATP synthase. J. Biol. Chem. **274:**17011-6.

171. **Watts, S.D., Y. Zhang, R.H. Fillingame, and R.A. Capaldi.** 1995. The γ subunit in the *Escherichia coli* ATP synthase complex (ECF_1F_O) extends through the stalk and contacts the $_c$ subunits of the F_O part. FEBS Lett. **368:**235-8.

172. **Watts, S.D., C. Tang, and R.A. Capaldi.** 1996. The stalk region of the *Escherichia coli* ATP synthase. Tyrosine 205 of the γ subunit is in the interface between the F_1 and F_O parts and can interact with both the ε and *c* oligomer. J. Biol. Chem. **271:**28341-7.

173. **Oberfeld, B., J. Brunner, and P. Dimroth.** 2006. Phospholipids occupy the internal lumen of the *c* ring of the ATP synthase of *Escherichia coli*. Biochemistry. **45:**1841-51.

174. **Yoshida, M., H. Okamoto, N. Sone, H. Hirata, and Y. Kagawa.** 1977. Reconstitution of thermostable ATPase capable of energy coupling from its purified subunits. Proc. Natl. Acad. Sci. USA. **74:**936-40.

175. **Sternweis, P.C.** 1978. The ε subunit of *Escherichia coli* coupling factor 1 is required for its binding to the cytoplasmic membrane. J. Biol. Chem. **253:**3123-8.

176. **Klionsky, D.J., W.S. Brusilow, and R.D. Simoni.** 1984. *In vivo* evidence for the role of the ε subunit as an inhibitor of the proton-translocating ATPase of *Escherichia coli*. J. Bacteriol. **160:**1055-60.

177. **Kuki, M., T. Noumi, M. Maeda, A. Amemura, and M. Futai.** 1988. Functional domains of ε subunit of *Escherichia coli* H^+-ATPase (F_OF_1). J. Biol. Chem. **263:**17437-42.

178. **Lötscher, H.R., C. deJong, and R.A. Capaldi.** 1984. Inhibition of the adenosinetriphosphatase activity of *Escherichia coli* F_1 by the water-soluble carbodiimide 1-ethyl-3-[3-(dimethylamino)propyl]carbodiimide is due to modification of several carboxyls in the β subunit. Biochemistry. **23:**4134-40.

179. **Dallmann, H.G., T.G. Flynn, and S.D. Dunn.** 1992. Determination of the 1-ethyl-3-[(3-dimethylamino)propyl]-carbodiimide- induced cross-link between the β and ε subunits of *Escherichia coli* F_1-ATPase. J. Biol. Chem. **267:**18953-60.

180. **Aggeler, R., M.A. Haughton, and R.A. Capaldi.** 1995. Disulfide bond formation between the COOH-terminal domain of the β subunits and the γ and ε subunits of the *Escherichia coli* F_1-ATPase. Structural implications and functional consequences. J. Biol. Chem. **270:**9185-91.

181. **Wilkens, S., F.W. Dahlquist, L.P. McIntosh, L.W. Donaldson, and R.A. Capaldi.** 1995. Structural features of the ε subunit of the *Escherichia coli* ATP synthase determined by NMR spectroscopy. Nat. Struct. Biol. **2:**961-7.

182. **Rodgers, A.J. and M.C. Wilce.** 2000. Structure of the γ-ε complex of ATP synthase. Nat. Struct. Biol. **7:**1051-4.

183. **Skakoon, E.N. and S.D. Dunn.** 1993. Orientation of the ε subunit in *Escherichia coli* ATP synthase. Arch. Biochem. Biophys. **302:**279-84.

184. **Jounouchi, M., M. Takeyama, T. Noumi, Y. Moriyama, M. Maeda, and M. Futai.** 1992. Role of the amino terminal region of the ε subunit of *Escherichia coli* H^+-ATPase (F_OF_1). Arch. Biochem. Biophys. **292`:**87-94.

185. **Tang, C. and R.A. Capaldi.** 1996. Characterization of the interface between γ and ε subunits of *Escherichia coli* F_1-ATPase`. J. Biol. Chem. **271:**3018-24.

186. **Schulenberg, B., F. Wellmer, H. Lill, W. Junge, and S. Engelbrecht.** 1997. Cross-linking of chloroplast F_OF_1-ATPase subunit ε to γ without effect on activity. ε and γ are parts of the rotor. Eur. J. Biochem. **249:**134-41.

187. **Cruz, J.A., C.A. Radkowski, and R.E. McCarty.** 1997. Functional Consequences of Deletions of the N Terminus of the ε Subunit of the Chloroplast ATP Synthase. Plant Physiol. **113:**1185-1192.

188. **Xiong, H., D. Zhang, and S.B. Vik.** 1998. Subunit ε of the *Escherichia coli* ATP synthase: novel insights into structure and function by analysis of thirteen mutant forms. Biochemistry. **37:**16423-9.

189. **Nowak, K.F., V. Tabidze, and R.E. McCarty.** 2002. The C-terminal domain of the ε subunit of the chloroplast ATP synthase is not required for ATP synthesis. Biochemistry. **41:**15130-4.

190. **Cipriano, D.J. and S.D. Dunn.** 2006. The role of the ε subunit in the *Escherichia coli* ATP synthase. The C-terminal domain is required for efficient energy coupling. J. Biol. Chem. **281:**501-7.

191. **Cipriano, D.J., Y. Bi, and S.D. Dunn.** 2002. Genetic fusions of globular proteins to the ε subunit of the *Escherichia coli* ATP synthase: Implications for *in vivo* rotational catalysis and ε subunit function. J. Biol. Chem. **277:**16782-90.

192. **Wilkens, S. and R.A. Capaldi.** 1998. Solution structure of the ε subunit of the F_1-ATPase from *Escherichia coli* and interactions of this subunit with β subunits in the complex. J. Biol. Chem. **273:**26645-51.

193. **Uhlin, U., G.B. Cox, and J.M. Guss.** 1997. Crystal structure of the ε subunit of the proton-translocating ATP synthase from *Escherichia coli*. Structure. **5:**1219-30.

194. **Capaldi, R.A. and B. Schulenberg.** 2000. The ε subunit of bacterial and chloroplast F_1F_0 ATPases. Structure, arrangement, and role of the ε subunit in energy coupling within the complex. Biochim. Biophys. Acta. **1458:**263-9.

195. **Mendel-Hartvig, J. and R.A. Capaldi.** 1991. Catalytic site nucleotide and inorganic phosphate dependence of the conformation of the ε subunit in *Escherichia coli* adenosinetriphosphatase. Biochemistry. **30:**1278-84.

196. **Hausrath, A.C., G. Grüber, B.W. Matthews, and R.A. Capaldi.** 1999. Structural features of the γ subunit of the *Escherichia coli* F_1 ATPase revealed by a 4.4-A resolution map obtained by x-ray crystallography. Proc. Natl. Acad. Sci. USA. **96:**13697-702.

197. **Hausrath, A.C., R.A. Capaldi, and B.W. Matthews.** 2001. The conformation of the ε and γ subunits within the *Escherichia coli* F_1 ATPase. J. Biol. Chem. **276:**47227-32.

198. **Wilkens, S. and R.A. Capaldi.** 1994. Asymmetry and structural changes in ECF_1 examined by cryoelectronmicroscopy. Biol. Chem. Hoppe Seyler. **375:**43-51.

199. **Aggeler, R. and R.A. Capaldi.** 1996. Nucleotide-dependent movement of the ε subunit between α and β subunits in the *Escherichia coli* F_1F_0-type ATPase. J. Biol. Chem. **271:**13888-91.

200. **Tsunoda, S.P., A.J. Rodgers, R. Aggeler, M.C. Wilce, M. Yoshida, and R.A. Capaldi.** 2001. Large conformational changes of the ε subunit in the bacterial F_1F_O ATP synthase provide a ratchet action to regulate this rotary motor enzyme. Proc. Natl. Acad. Sci. USA. **98:**6560-4.

201. **Ganti, S. and S.B. Vik.** 2007. Chemical modification of mono-cysteine mutants allows a more global look at conformations of the ε subunit of the ATP synthase from *Escherichia coli*. J. Bioenerg. Biomembr. **39:**99-107.

202. **Schulenberg, B. and R.A. Capaldi.** 1999. The ε subunit of the F_1F_O complex of *Escherichia coli*. cross-linking studies show the same structure *in situ* as when isolated. J. Biol. Chem. **274:**28351-5.

203. **Suzuki, T., T. Murakami, R. Iino, J. Suzuki, S. Ono, Y. Shirakihara, and M. Yoshida.** 2003. F_OF_1-ATPase/synthase is geared to the synthesis mode by conformational rearrangement of ε subunit in response to proton motive force and ADP/ATP balance. J. Biol. Chem. **278:**46840-6.

204. **Yagi, H., N. Kajiwara, H. Tanaka, T. Tsukihara, Y. Kato-Yamada, M. Yoshida, and H. Akutsu.** 2007. Structures of the thermophilic F_1-ATPase ε subunit suggesting ATP-regulated arm motion of its C-terminal domain in F_1. Proc. Natl. Acad. Sci. USA. **104:**11233-8.

205. **Smith, J.B., P.C. Sternweis, and L.A. Heppel.** 1975. Partial purification of active δ and ε subunits of the membrane ATPase from *Escherichia coli*. J. Supramol. Struct. **3:**248-55.

206. **Smith, J.B. and P.C. Sternweis.** 1977. Purification of membrane attachment and inhibitory subunits of the proton translocating adenosine triphosphatase from *Escherichia coli*. Biochemistry. **16:**306-11.

207. **Laget, P.P. and J.B. Smith.** 1979. Inhibitory properties of endogenous subunit *e* in the *Escherichia coli* F_1 ATPase. Arch. Biochem. Biophys. **197:**83-9.

208. **Lötscher, H.R., C. deJong, and R.A. Capaldi.** 1984. Interconversion of high and low adenosinetriphosphatase activity forms of *Escherichia coli* F_1 by the detergent lauryldimethylamine oxide. Biochemistry. **23:**4140-3.

209. **Patrie, W.J. and R.E. McCarty.** 1984. Specific binding of coupling factor 1 lacking the δ and ε subunits to thylakoids. J. Biol. Chem. **259:**11121-8.

210. **Nelson, N., H. Nelson, and E. Racker.** 1972. Partial resolution of the enzymes catalyzing photophosphorylation. XII. Purification and properties of an inhibitor isolated from chloroplast coupling factor 1. J. Biol. Chem. **247:**7657-62.

211. **Sakurai, H., K. Shinohara, T. Hisabori, and K. Shinohara.** 1981. Enhancement of adenosine triphosphatase activity of purified chloroplast coupling factor 1 in aqueous organic solvent. J. Biochem. **90:**95-102.

212. **Richter, M.L., W.J. Patrie, and R.E. McCarty.** 1984. Preparation of the ε subunit and ε subunit-deficient chloroplast coupling factor 1 in reconstitutively active forms. J. Biol. Chem. **259:**7371-3.

213. **Pick, U. and S. Bassilian.** 1982. Activation of magnesium ion specific adenosinetriphosphatase in chloroplast coupling factor 1 by octyl glucoside. Biochemistry. **21:**6144-52.

214. **Yu, F. and R.E. McCarty.** 1985. Detergent activation of the ATPase activity of chloroplast coupling factor 1. Arch. Biochem. Biophys. **238:**61-8.

215. **Dunn, S.D., R.G. Tozer, and V.D. Zadorozny.** 1990. Activation of *Escherichia coli* F_1-ATPase by lauryldimethylamine oxide and ethylene glycol: relationship of ATPase activity to the interaction of the ε and β subunits. Biochemistry. **29:**4335-40.

216. **Peskova, Y.B. and R.K. Nakamoto.** 2000. Catalytic control and coupling efficiency of the *Escherichia coli* F_OF_1 ATP synthase: influence of the F_O sector and ε subunit on the catalytic transition state. Biochemistry. **39:**11830-6.

217. **Gavilanes-Ruiz, M., M. Tommasino, and R.A. Capaldi.** 1988. Structure-function relationships of the *Escherichia coli* ATP synthase probed by trypsin digestion. Biochemistry. **27:**603-9.

218. **Mendel-Hartvig, J. and R.A. Capaldi.** 1991. Nucleotide-dependent and dicyclohexylcarbodiimide-sensitive conformational changes in the ε subunit of *Escherichia coli* ATP synthase. Biochemistry. **30:**10987-91.

219. **Aggeler, R., K. Chicas-Cruz, S.X. Cai, J.F. Keana, and R.A. Capaldi.** 1992. Introduction of reactive cysteine residues in the ε subunit of *Escherichia coli* F_1 ATPase, modification of these sites with tetrafluorophenyl azide-maleimides, and examination of changes in the binding of the ε subunit when different nucleotides are in catalytic sites. Biochemistry. **31:**2956-61.

220. **Hara, K.Y., Y. Kato-Yamada, Y. Kikuchi, T. Hisabori, and M. Yoshida.** 2001. The role of the $\beta_{DELSEED}$ motif of F_1-ATPase: propagation of the inhibitory effect of the ε subunit. J. Biol. Chem. **276:**23969-73.

221. **García, J.J. and R.A. Capaldi.** 1998. Unisite catalysis without rotation of the γ-ε domain in *Escherichia coli* F_1-ATPase. J. Biol. Chem. **273:**15940-5.

222. **Bulygin, V.V., T.M. Duncan, and R.L. Cross.** 1998. Rotation of the ε subunit during catalysis by *Escherichia coli* F_OF_1-ATP synthase. J. Biol. Chem. **273:**31765-9.

223. **Dunn, S.D. and M. Futai.** 1980. Reconstitution of a functional coupling factor from the isolated subunits of *Escherichia coli* F_1 ATPase. J. Biol. Chem. **255:**113-8.

224. **Futai, M.** 1977. Reconstitution of ATPase activity from the isolated α, β, and γ subunits of the coupling factor, F_1, of *Escherichia coli*. Biochem. Biophys. Res. Commun. **79:**1231-7.

225. **Abrahams, J.P., A.G. Leslie, R. Lutter, and J.E. Walker.** 1994. Structure at 2.8 A resolution of F_1-ATPase from bovine heart mitochondria. Nature. **370:**621-8.

226. **Duncan, T.M., V.V. Bulygin, Y. Zhou, M.L. Hutcheon, and R.L. Cross.** 1995. Rotation of subunits during catalysis by Escherichia coli F_1-ATPase. Proc. Natl. Acad. Sci. USA. **92:**10964-8.

227. **Sabbert, D., S. Engelbrecht, and W. Junge.** 1996. Intersubunit rotation in active F-ATPase. Nature. **381:**623-5.

228. **Häsler, K., S. Engelbrecht, and W. Junge.** 1998. Three-stepped rotation of subunits γ and ε in single molecules of F-ATPase as revealed by polarized, confocal fluorometry. FEBS Lett. **426:**301-4.

229. **Diez, M., B. Zimmermann, M. Börsch, M. König, E. Schweinberger, S. Steigmiller, R. Reuter, S. Felekyan, V. Kudryavtsev, C.A. Seidel, and P. Gräber.** 2004. Proton-powered subunit rotation in single membrane-bound F_0F_1-ATP synthase. Nat. Struct. Mol. Biol. **11:**135-41.

230. **Steigmiller, S., B. Zimmermann, M. Diez, M. Börsch, and P. Gräber.** 2004. Binding of single nucleotides to H^+-ATP synthases observed by fluorescence resonance energy transfer. Bioelectrochemistry. **63:**79-85.

231. **Bragg, P.D. and C. Hou.** 1987. Ligand-induced conformational changes in the *Escherichia coli* F_1 adenosine triphosphatase probed by trypsin digestion. Biochim. Biophys. Acta. **894:**127-37.

232. **Zhou, Y., T.M. Duncan, V.V. Bulygin, M.L. Hutcheon, and R.L. Cross.** 1996. ATP hydrolysis by membrane-bound Escherichia coli F_OF_1 causes rotation of the γ subunit relative to the β subunits. Biochim. Biophys. Acta. **1275:**96-100.

233. **Shin, K., R.K. Nakamoto, M. Maeda, and M. Futai.** 1992. F_OF_1-ATPase γ subunit mutations perturb the coupling between catalysis and transport. J. Biol. Chem. **267:**20835-9.

234. **Nakamoto, R.K., M. Maeda, and M. Futai.** 1993. The γ subunit of the *Escherichia coli* ATP synthase. Mutations in the carboxyl-terminal region restore energy coupling to the amino-terminal mutant γ_{M23K}. J. Biol. Chem. **268:**867-72.

235. **Ketchum, C.J., M.K. Al-Shawi, and R.K. Nakamoto.** 1998. Intergenic suppression of the γ_{M23K} uncoupling mutation in F_OF_1 ATP synthase by β_{E381} substitutions: the role of the $\beta_{DELSEED}$ segment in energy coupling. Biochem. J. **330:**707-12.

236. **Iwamoto, A., J. Miki, M. Maeda, and M. Futai.** 1990. H^+-ATPase γ subunit of *Escherichia coli*. Role of the conserved carboxyl-terminal region. J. Biol. Chem. **265:**5043-8.

237. **Müller, M., O. Pänke, W. Junge, and S. Engelbrecht.** 2002. F_1-ATPase, the C-terminal end of subunit γ is not required for ATP hydrolysis-driven rotation. J. Biol. Chem. **277:**23308-13.

238. **Greene, M.D. and W.D. Frasch.** 2003. Interactions among γ_{R268}, γ_{Q269}, and the β subunit catch loop of *Escherichia coli* F_1-ATPase are important for catalytic activity. J. Biol. Chem. **278:**51594-8.

239. **Nakamoto, R.K., M.K. Al-Shawi, and M. Futai.** 1995. The ATP synthase γ subunit. Suppressor mutagenesis reveals three helical regions involved in energy coupling. J. Biol. Chem. **270:**14042-6.

240. **Zhou, Y., T.M. Duncan, and R.L. Cross.** 1997. Subunit rotation in *Escherichia coli* F_OF_1-ATP synthase during oxidative phosphorylation. Proc. Natl. Acad. Sci. USA. **94:**10583-7.

241. **Aggeler, R. and R.A. Capaldi.** 1993. ATP hydrolysis-linked structural changes in the N-terminal part of the γ subunit of *Escherichia coli* F_1-ATPase examined by cross-linking studies. J. Biol. Chem. **268:**14576-8.

242. **Gumbiowski, K., D. Cherepanov, M. Muller, O. Panke, P. Promto, S. Winkler, W. Junge, and S. Engelbrecht.** 2001. F-ATPase: forced full rotation of the rotor despite covalent cross-link with the stator. J. Biol. Chem. **276:**42287-92.

243. **Müller, M., K. Gumbiowski, D.A. Cherepanov, S. Winkler, W. Junge, S. Engelbrecht, and O. Pänke.** 2004. Rotary F_1-ATPase. Is the C-terminus of subunit γ fixed or mobile? Eur. J. Biochem. **271:**3914-22.

244. **Nakamoto, R.K., C.J. Ketchum, and M.K. al-Shawi.** 1999. Rotational coupling in the F_OF_1 ATP synthase. Annu. Rev. Biophys. Biomol. Struct. **28:**205-34.

245. **Al-Shawi, M.K., D. Parsonage, and A.E. Senior.** 1990. Adenosine triphosphatase and nucleotide binding activity of isolated β-subunit preparations from *Escherichia coli* F_1F_0-ATP synthase. J. Biol. Chem. **265:**5595-601.

246. **Abrahams, J.P., S.K. Buchanan, M.J.V. Raaij, I.M. Fearnley, A.G. Leslie, and J.E. Walker.** 1996. The structure of bovine F_1-ATPase complexed with the peptide antibiotic efrapeptin. Proc. Natl. Acad. Sci. USA. **93:**9420-4.

247. **Raaij, M.J.v., J.P. Abrahams, A.G. Leslie, and J.E. Walker.** 1996. The structure of bovine F_1-ATPase complexed with the antibiotic inhibitor aurovertin B. Proc. Natl. Acad. Sci. USA. **93:**6913-7.

248. **Orriss, G.L., A.G. Leslie, K. Braig, and J.E. Walker.** 1998. Bovine F_1-ATPase covalently inhibited with 4-chloro-7-nitrobenzofurazan: the structure provides further support for a rotary catalytic mechanism. Structure. **6:**831-7.

249. **Gibbons, C., M.G. Montgomery, A.G. Leslie, and J.E. Walker.** 2000. The structure of the central stalk in bovine F_1-ATPase at 2.4 A resolution. Nat. Struct. Biol. **7:**1055-61.

250. **Gledhill, J.R., M.G. Montgomery, A.G. Leslie, and J.E. Walker.** 2007. How the regulatory protein, IF1, inhibits F_1-ATPase from bovine mitochondria. Proc. Natl. Acad. Sci. USA. **104:**15671-6.

251. **Cabezón, E., M.G. Montgomery, A.G. Leslie, and J.E. Walker.** 2003. The structure of bovine F_1-ATPase in complex with its regulatory protein IF1. Nat. Struct. Biol. **10:**744-50.

252. **Gledhill, J.R., M.G. Montgomery, A.G. Leslie, and J.E. Walker.** 2007. Mechanism of inhibition of bovine F_1-ATPase by resveratrol and related polyphenols. Proc. Natl. Acad. Sci. USA. **104:**13632-7.

253. **Bowler, M.W., M.G. Montgomery, A.G. Leslie, and J.E. Walker.** 2007. Ground state structure of F_1-ATPase from bovine heart mitochondria at 1.9 A resolution. J. Biol. Chem. **282:**14238-42.

254. **Menz, R.I., A.G. Leslie, and J.E. Walker.** 2001. The structure and nucleotide occupancy of bovine mitochondrial F_1-ATPase are not influenced by crystallisation at high concentrations of nucleotide. FEBS Lett. **494:**11-4.

255. **Braig, K., R.I. Menz, M.G. Montgomery, A.G. Leslie, and J.E. Walker.** 2000. Structure of bovine mitochondrial F_1-ATPase inhibited by Mg^{2+} ADP and aluminium fluoride. Structure. **8:**567-73.

256. **Menz, R.I., J.E. Walker, and A.G. Leslie.** 2001. Structure of bovine mitochondrial F_1-ATPase with nucleotide bound to all three catalytic sites: implications for the mechanism of rotary catalysis. Cell. **106:**331-41.

257. **Kagawa, R., M.G. Montgomery, K. Braig, A.G. Leslie, and J.E. Walker.** 2004. The structure of bovine F_1-ATPase inhibited by ADP and beryllium fluoride. EMBO J. **23:**2734-44.

258. **Shirakihara, Y., A.G. Leslie, J.P. Abrahams, J.E. Walker, T. Ueda, Y. Sekimoto, M. Kambara, K. Saika, Y. Kagawa, and M. Yoshida.** 1997. The crystal structure of the nucleotide-free $\alpha_3\beta_3$ subcomplex of F_1-ATPase from the thermophilic Bacillus PS3 is a symmetric trimer. Structure. **5:**825-36.

259. **Stocker, A., S. Keis, J. Vonck, G.M. Cook, and P. Dimroth.** 2007. The structural basis for unidirectional rotation of thermoalkaliphilic F_1-ATPase. Structure. **15:**904-14.

260. **Groth, G. and E. Pohl.** 2001. The structure of the chloroplast F_1-ATPase at 3.2 A resolution. J. Biol. Chem. **276:**1345-52.

261. **Groth, G.** 2002. Structure of spinach chloroplast F_1-ATPase complexed with the phytopathogenic inhibitor tentoxin. Proc. Natl. Acad. Sci. USA. **99:**3464-8.

262. **Bianchet, M.A., J. Hullihen, P.L. Pedersen, and L.M. Amzel.** 1998. The 2.8-A structure of rat liver F_1-ATPase: configuration of a critical intermediate in ATP synthesis/hydrolysis. Proc. Natl. Acad. Sci. USA. **95:**11065-70.

263. **Chen, C., A.K. Saxena, W.N. Simcoke, D.N. Garboczi, P.L. Pedersen, and Y.H. Ko.** 2006. Mitochondrial ATP synthase. Crystal structure of the catalytic F_1 unit in a vanadate-induced transition-like state and implications for mechanism. J. Biol. Chem. **281:**13777-83.

264. **Walker, J.E., M. Saraste, M.J. Runswick, and N.J. Gay.** 1982. Distantly related sequences in the α and β subunits of ATP synthase, myosin, kinases and other ATP-requiring enzymes and a common nucleotide binding fold. EMBO J. **1:**945-51.

265. **Rao, R., J. Pagan, and A.E. Senior.** 1988. Directed mutagenesis of the strongly conserved lysine 175 in the proposed nucleotide-binding domain of α subunit from *Escherichia coli* F_1-ATPase. J. Biol. Chem. **263:**15957-63.

266. **Weber, J., C. Bowman, S. Wilke-Mounts, and A.E. Senior.** 1995. α_{D261} is a key residue in noncatalytic sites of *Escherichia coli* F_1-ATPase. J. Biol. Chem. **270:**21045-9.

267. **Rao, R., D. Cunningham, R.L. Cross, and A.E. Senior.** 1988. Pyridoxal 5'-diphospho-5'-adenosine binds at a single site on isolated α subunit from *Escherichia coli* F_1-ATPase and specifically reacts with lysine 201. J. Biol. Chem. **263:**5640-5.

268. **Ohta, S., M. Tsubo, T. Oshima, M. Yoshida, and Y. Kagawa.** 1980. Nucleotide binding to isolated α and β subunits of proton translocating adenosine triphosphatase studied with circular dichroism. J. Biochem. **87:**1609-17.

269. **Dunn, S.D.** 1980. ATP causes a large change in the conformation of the isolated α subunit of *Escherichia coli* F_1 ATPase. J. Biol. Chem. **255:**11857-60.

270. **Pagan, J. and A.E. Senior.** 1990. Tight ATP and ADP binding in the noncatalytic sites of *Escherichia coli* F_1-ATPase is not affected by mutation of bulky residues in the 'glycine-rich loop'. FEBS Lett. **273:**147-9.

271. **Weber, J., R.S. Lee, E. Grell, J.G. Wise, and A.E. Senior.** 1992. On the location and function of β_{Y331} in the catalytic site of *Escherichia coli* F_1-ATPase. J. Biol. Chem. **267:**1712-8.

272. **Wise, J.G.** 1990. Site-directed mutagenesis of the conserved β_{Y331} of *Escherichia coli* ATP synthase yields catalytically active enzymes. J. Biol. Chem. **265:**10403-9.

273. **Odaka, M., C. Kaibara, T. Amano, T. Matsui, E. Muneyuki, K. Ogasahara, K. Yutani, and M. Yoshida.** 1994. Tyr-341 of the β subunit is a major K_m-determining residue of TF_1-ATPase: parallel effect of its mutations on K_d(ATP) of the β subunit and on K_m(ATP) of the $\alpha_3\beta_3\gamma$ complex. J. Biochem. **115:**789-96.

274. **Omote, H., N.P. Le, M.Y. Park, M. Maeda, and M. Futai.** 1995. β subunit Glu-185 of *Escherichia coli* H^+-ATPase (ATP synthase) is an essential residue for cooperative catalysis. J. Biol. Chem. **270:**25656-60.

275. **Amano, T., K. Tozawa, M. Yoshida, and H. Murakami.** 1994. Spatial precision of a catalytic carboxylate of F_1-ATPase beta subunit probed by introducing different carboxylate-containing side chains. FEBS Lett. **348:**93-8.

276. **Takeyama, M., K. Ihara, Y. Moriyama, T. Noumi, K. Ida, N. Tomioka, A. Itai, M. Maeda, and M. Futai.** 1990. The glycine-rich sequence of the β subunit of *Escherichia coli* H^+-ATPase is important for activity. J. Biol. Chem. **265:**21279-84.

277. **Tagaya, M., T. Noumi, K. Nakano, M. Futai, and T. Fukui.** 1988. Identification of α subunit Lys201 and β subunit Lys155 at the ATP-binding sites in *Escherichia coli* F_1-ATPase. FEBS Lett. **233:**347-51.

278. **Ida, K., T. Noumi, M. Maeda, T. Fukui, and M. Futai.** 1991. Catalytic site of F_1-ATPase of *Escherichia coli*. Lys-155 and Lys-201 of the β subunit are located near the γ-phosphate group of ATP in the presence of Mg^{2+}. J. Biol. Chem. **266:**5424-9.

279. **Omote, H., M. Maeda, and M. Futai.** 1992. Effects of mutations of conserved Lys-155 and Thr-156 residues in the phosphate-binding glycine-rich sequence of the F_1-ATPase β subunit of *Escherichia coli*. J. Biol. Chem. **267:**20571-6.

280. **Shen, H., B.Y. Yao, and D.M. Mueller.** 1994. Primary structural constraints of P-loop of mitochondrial F_1-ATPase from yeast. J. Biol. Chem. **269:**9424-8.

281. **Jounouchi, M., M. Maeda, and M. Futai.** 1993. The α subunit of ATP synthase (F_OF_1): the Lys-175 and Thr-176 residues in the conserved sequence (Gly-X-X-X-X-Gly-Lys-Thr/Ser) are located in the domain required for stable subunit-subunit interaction. J. Biochem. **114:**171-6.

282. **Kanazawa, H., Y. Horiuchi, M. Takagi, Y. Ishino, and M. Futai.** 1980. Coupling factor F_1 ATPase with defective β subunit from a mutant of *Escherichia coli*. J. Biochem. **88:**695-703.

283. **Miki, J., K. Fujiwara, M. Tsuda, T. Tsuchiya, and H. Kanazawa.** 1990. Suppression mutations in the defective β subunit of F_1-ATPase from *Escherichia coli*. J. Biol. Chem. **265:**21567-72.

284. **Iwamoto, A., H. Omote, H. Hanada, N. Tomioka, A. Itai, M. Maeda, and M. Futai.** 1991. Mutations in Ser174 and the glycine-rich sequence (Gly149, Gly150, and Thr156) in the β subunit of *Escherichia coli* H^+-ATPase. J. Biol. Chem. **266:**16350-5.

285. **Omote, H., M.Y. Park, M. Maeda, and M. Futai.** 1994. The α/β subunit interaction in H^+-ATPase (ATP synthase). An *Escherichia coli* α subunit mutation (α_{R296C}) restores

coupling efficiency to the deleterious β subunit mutant (β_{S174F}). J. Biol. Chem. **269:**10265-9.

286. **Nakanishi-Matsui, M., S. Kashiwagi, T. Ubukata, A. Iwamoto-Kihara, Y. Wada, and M. Futai.** 2007. Rotational catalysis of *Escherichia coli* ATP synthase F_1 sector. Stochastic fluctuation and a key domain of the β subunit. J. Biol. Chem. **282:**20698-704.

287. **Kashiwagi, S., A. Iwamoto-Kihara, M. Kojima, T. Nonaka, M. Futai, and M. Nakanishi-Matsui.** 2008. Effects of mutations in the β subunit hinge domain on ATP synthase F_1 sector rotation: interaction between Ser 174 and Ile 163. Biochem. Biophys. Res. Commun. **365:**227-31.

288. **Turina, P., R. Aggeler, R.S. Lee, A.E. Senior, and R.A. Capaldi.** 1993. The cysteine introduced into the α subunit of the *Escherichia coli* F1-ATPase by the mutation α_{R376C} is near the α-β subunit interface and close to a noncatalytic nucleotide binding site. J. Biol. Chem. **268:**6978-84.

289. **Noumi, T., M. Futai, and H. Kanazawa.** 1984. Replacement of serine 373 by phenylalanine in the α subunit of *Escherichia coli* F_1-ATPase results in loss of steady-state catalysis by the enzyme. J. Biol. Chem. **259:**10076-9.

290. **Maggio, M.B., J. Pagan, D. Parsonage, L. Hatch, and A.E. Senior.** 1987. The defective proton-ATPase of uncA mutants of *Escherichia coli*. Identification by DNA sequencing of residues in the α subunit which are essential for catalysis or normal assembly. J. Biol. Chem. **262:**8981-4.

291. **Soga, S., T. Noumi, M. Takeyama, M. Maeda, and M. Futai.** 1989. Mutational replacements of conserved amino acid residues in the α subunit change the catalytic properties of *Escherichia coli* F_1-ATPase. Arch. Biochem. Biophys. **268:**643-8.

292. **Maggio, M.B., D. Parsonage, and A.E. Senior.** 1988. A mutation in the α subunit of F_1-ATPase from *Escherichia coli* affects the binding of F_1 to the membrane. J. Biol. Chem. **263:**4619-23.

293. **Lee, R.S., S. Wilke-Mounts, and A.E. Senior.** 1992. F_1-ATPase with cysteine instead of serine at residue 373 of the α subunit. Arch. Biochem. Biophys. **297:**334-9.

294. **Hsu, S.Y., T. Noumi, M. Takeyama, M. Maeda, S. Ishibashi, and M. Futai.** 1987. β subunit of *Escherichia coli* F_1-ATPase. An amino acid replacement within a conserved sequence (G-X-X-X-X-G-K-T/S) of nucleotide-binding proteins. FEBS Lett. **218:**222-6.

295. **Weber, J., S. Wilke-Mounts, and A.E. Senior.** 1994. Cooperativity and stoichiometry of substrate binding to the catalytic sites of *Escherichia coli* F_1-ATPase. Effects of magnesium, inhibitors, and mutation. J. Biol. Chem. **269:**20462-7.

296. **Tommasino, M. and R.A. Capaldi.** 1985. Effect of dicyclohexylcarbodiimide on unisite and multisite catalytic activities of the adenosinetriphosphatase of *Escherichia coli*. Biochemistry. **24:**3972-6.

297. **Nadanaciva, S., J. Weber, and A.E. Senior.** 1999. Binding of the transition state analog MgADP-fluoroaluminate to F_1-ATPase. J. Biol. Chem. **274:**7052-8.

298. **Boltz, K.W. and W.D. Frasch.** 2006. Hydrogen bonds between the α and β subunits of the F_1-ATPase allow communication between the catalytic site and the interface of the β catch loop and the γ subunit. Biochemistry. **45:**11190-9.

299. **Schäfer, H.J., G. Rathgeber, and Y. Kagawa.** 1995. 2,8-Diazido-ATP--a short-length bifunctional photoaffinity label for photoaffinity cross-linking of a stable F_1 in ATP synthase (from thermophilic bacteria PS3). FEBS Lett. **377:**408-12.

300. **Tsunoda, S.P., E. Muneyuki, T. Amano, M. Yoshida, and H. Noji.** 1999. Cross-linking of two β subunits in the closed conformation in F_1-ATPase. J. Biol. Chem. **274:**5701-6.

301. **Lill, H., F. Hensel, W. Junge, and S. Engelbrecht.** 1996. Cross-linking of engineered subunit δ to $(\alpha\beta)_3$ in chloroplast F-ATPase. J. Biol. Chem. **271:**32737-42.

302. **Ogilvie, I., R. Aggeler, and R.A. Capaldi.** 1997. Cross-linking of the δ subunit to one of the three α subunits has no effect on functioning, as expected if δ is a part of the stator that links the F_1 and F_O parts of the *Escherichia coli* ATP synthase. J. Biol. Chem. **272:**16652-6.

303. **Wilkens, S., J. Zhou, R. Nakayama, S.D. Dunn, and R.A. Capaldi.** 2000. Localization of the δ subunit in the *Escherichia coli* F_1F_O-ATPsynthase by immuno electron microscopy: the δ subunit binds on top of the F_1. J. Mol. Biol. **295:**387-91.

304. **Wilkens, S., S.D. Dunn, J. Chandler, F.W. Dahlquist, and R.A. Capaldi.** 1997. Solution structure of the N-terminal domain of the δ subunit of the *E. coli* ATPsynthase. Nat. Struct. Biol. **4:**198-201.

305. **Wilkens, S., D. Borchardt, J. Weber, and A.E. Senior.** 2005. Structural characterization of the interaction of the δ and α subunits of the *Escherichia coli* F_1F_O-ATP synthase by NMR spectroscopy. Biochemistry. **44:**11786-94.

306. **Mendel-Hartvig, J. and R.A. Capaldi.** 1991. Structure-function relationships of domains of the δ subunit in *Escherichia coli* adenosine triphosphatase. Biochim. Biophys. Acta. **1060:**115-24.

307. **Hundal, T., B. Norling, and L. Ernster.** 1983. Lack of ability of trypsin-treated mitochondrial F_1-ATPase to bind the oligomycin-sensitivity conferring protein (OSCP). FEBS Lett. **162:**5-10.

308. **Weber, J., A. Muharemagic, S. Wilke-Mounts, and A.E. Senior.** 2003. F_1F_O-ATP synthase. Binding of δ subunit to a 22-residue peptide mimicking the N-terminal region of α subunit. J. Biol. Chem. **278:**13623-6.

309. **Weber, J., S. Wilke-Mounts, and A.E. Senior.** 2003. Identification of the F_1-binding surface on the δ subunit of ATP synthase. J. Biol. Chem. **278:**13409-16.

310. **Weber, J., A. Muharemagic, S. Wilke-Mounts, and A.E. Senior.** 2004. Analysis of sequence determinants of F_1F_O-ATP synthase in the N-terminal region of α subunit for binding of δ subunit. J. Biol. Chem. **279:**25673-9.

311. **Senior, A.E., A. Muharemagic, and S. Wilke-Mounts.** 2006. Assembly of the stator in *Escherichia coli* ATP synthase. Complexation of α subunit with other F_1 subunits is prerequisite for δ subunit binding to the N-terminal region of α. Biochemistry. **45:**15893-902.

312. **Häsler, K., O. Pänke, and W. Junge.** 1999. On the stator of rotary ATP synthase: the binding strength of subunit δ to $(\alpha\beta)_3$ as determined by fluorescence correlation spectroscopy. Biochemistry. **38:**13759-65.

313. **Weber, J., S. Wilke-Mounts, and A.E. Senior.** 2002. Quantitative determination of binding affinity of δ subunit in *Escherichia coli* F_1-ATPase: effects of mutation, Mg^{2+}, and pH on K_d. J. Biol. Chem. **277:**18390-6.

314. **Jounouchi, M., M. Takeyama, P. Chaiprasert, T. Noumi, Y. Moriyama, M. Maeda, and M. Futai.** 1992. Escherichia coli H^+-ATPase: role of the δ subunit in binding F_1 to the F_O sector. Arch. Biochem. Biophys. **292:**376-81.

315. **Collinson, I.R., M.J. vanRaaij, M.J. Runswick, I.M. Fearnley, J.M. Skehel, G.L. Orriss, B. Miroux, and J.E. Walker.** 1994. ATP synthase from bovine heart mitochondria. *In vitro* assembly of a stalk complex in the presence of F_1-ATPase and in its absence. J. Mol. Biol. **242:**408-21.

316. **Dunn, S.D. and J. Chandler.** 1998. Characterization of a $b_2\delta$ complex from *Escherichia coli* ATP synthase. J. Biol. Chem. **273:**8646-51.

317. **Sawada, K., N. Kuroda, H. Watanabe, C. Moritani-Otsuka, and H. Kanazawa.** 1997. Interaction of the δ and *b* subunits contributes to F_1 and F_O interaction in the *Escherichia coli* F_1F_O-ATPase. J. Biol. Chem. **272:**30047-53.

318. **Rodgers, A.J., S. Wilkens, R. Aggeler, M.B. Morris, S.M. Howitt, and R.A. Capaldi.** 1997. The subunit *b*-δ domain of the *Escherichia coli* F_1F_O ATPase. The *b* subunits interact with F_1 as a dimer and through the δ subunit. J. Biol. Chem. **272:**31058-64.

319. **Hazard, A.L. and A.E. Senior.** 1994. Mutagenesis of subunit δ from *Escherichia coli* F_1F_O-ATP synthase. J. Biol. Chem. **269:**418-26.

320. **Ogilvie, I., S. Wilkens, A.J. Rodgers, R. Aggeler, and R.A. Capaldi.** 1998. The second stalk: the δ-*b* subunit connection in ECF_1F_O. Acta. Physiol. Scand. Suppl. **643:**169-75.

321. **Tozer, R.G. and S.D. Dunn.** 1986. Column centrifugation generates an intersubunit disulfide bridge in *Escherichia coli* F_1-ATPase. Eur. J. Biochem. **161:**513-8.

322. **Bragg, P.D. and C. Hou.** 1986. Effect of disulfide cross-linking between α and δ subunits on the properties of the F_1 adenosine triphosphatase of *Escherichia coli*. Biochim. Biophys. Acta. **851:**385-94.

323. **Beckers, G., R.J. Berzborn, and H. Strotmann.** 1992. Zero-length crosslinking between subunits δ and I of the H^+-translocating ATPase of chloroplasts. Biochim. Biophys. Acta. **1101:**97-104.

324. **McLachlin, D.T., J.A. Bestard, and S.D. Dunn.** 1998. The *b* and δ subunits of the *Escherichia coli* ATP synthase interact via residues in their C-terminal regions. J. Biol. Chem. **273:**15162-8.

325. **McLachlin, D.T. and S.D. Dunn.** 2000. Disulfide linkage of the *b* and δ subunits does not affect the function of the *Escherichia coli* ATP synthase. Biochemistry. **39:**3486-90.

326. **Wood, K.S. and S.D. Dunn.** 2007. Role of the asymmetry of the homodimeric b_2 stator stalk in the interaction with the F_1 sector of *Escherichia coli* ATP synthase. J. Biol. Chem. **282:**31920-7.

327. **Kanazawa, H. and M. Futai.** 1982. Structure and function of H^+-ATPase: what we have learned from *Escherichia coli* H^+-ATPase. Ann. NY Acad. Sci. **402:**45-64.

328. **Senior, A.E.** 1984. Disposition of polar and nonpolar residues on outer surfaces of transmembrane helical segments of proteins involved in proton translocation. Arch. Biochem. Biophys. **234:**138-43.

329. **Walker, J.E., M. Saraste, and N.J. Gay.** 1982. *E. coli* F_1-ATPase interacts with a membrane protein component of a proton channel. Nature. **298:**867-9.

330. **Bhatt, D., S.P. Cole, T.B. Grabar, S.B. Claggett, and B.D. Cain.** 2005. Manipulating the length of the *b* subunit F_1 binding domain in F_1F_0 ATP synthase from *Escherichia coli*. J. Bioenerg. Biomembr. **37:**67-74.

331. **Rodgers, A.J. and R.A. Capaldi.** 1998. The second stalk composed of the *b* and δ subunits connects F_O to F_1 via an α subunit in the *Escherichia coli* ATP synthase. J. Biol. Chem. **273:**29406-10.

332. **Sorgen, P.L., M.R. Bubb, K.A. McCormick, A.S. Edison, and B.D. Cain.** 1998. Formation of the *b* subunit dimer is necessary for interaction with F_1-ATPase. Biochemistry. **37:**923-32.

333. **Dunn, S.D.** 1992. The polar domain of the *b* subunit of *Escherichia coli* F_1F_0-ATPase forms an elongated dimer that interacts with the F_1 sector. J. Biol. Chem. **267:**7630-6.

334. **Greie, J.C., G. Deckers-Hebestreit, and K. Altendorf.** 2000. Secondary structure composition of reconstituted subunit *b* of the *Escherichia coli* ATP synthase. Eur. J. Biochem. **267:**3040-8.

335. **Weber, J.** 2006. ATP synthase: subunit-subunit interactions in the stator stalk. Biochim. Biophys. Acta. **1757:**1162-70.

336. **Revington, M., S.D. Dunn, and G.S. Shaw.** 2002. Folding and stability of the *b* subunit of the F_1F_O ATP synthase. Protein Sci. **11:**1227-38.

337. **Revington, M., D.T. McLachlin, G.S. Shaw, and S.D. Dunn.** 1999. The dimerization domain of the *b* subunit of the *Escherichia coli* F_1F_O-ATPase. J. Biol. Chem. **274:**31094-101.

338. **Dunn, S.D., D.T. McLachlin, and M. Revington.** 2000. The second stalk of *Escherichia coli* ATP synthase. Biochim. Biophys. Acta. **1458:**356-63.

339. **Takeyama, M., T. Noumi, M. Maeda, and M. Futai.** 1988. F_O portion of *Escherichia coli* H^+-ATPase. Carboxyl-terminal region of the *b* subunit is essential for assembly of functional F_O. J. Biol. Chem. **263:**16106-12.

340. **Greie, J.C., T. Heitkamp, and K. Altendorf.** 2004. The transmembrane domain of subunit *b* of the *Escherichia coli* F_1F_O ATP synthase is sufficient for H^+-translocating activity together with subunits *a* and *c*. Eur. J. Biochem. **271:**3036-42.

341. **Stalz, W.D., J.C. Greie, G. Deckers-Hebestreit, and K. Altendorf.** 2003. Direct interaction of subunits *a* and *b* of the F_O complex of *Escherichia coli* ATP synthase by forming an ab_2 subcomplex. J. Biol. Chem. **278:**27068-71.

342. **Kumamoto, C.A. and R.D. Simoni.** 1986. Genetic evidence for interaction between the *a* and *b* subunits of the F_O portion of the *Escherichia coli* proton translocating ATPase. J. Biol. Chem. **261:**10037-42.

343. **DeLeon-Rangel, J., D. Zhang, and S.B. Vik.** 2003. The role of transmembrane span 2 in the structure and function of subunit *a* of the ATP synthase from *Escherichia coli*. Arch. Biochem. Biophys. **418:**55-62.

344. **Schneider, E. and K. Altendorf.** 1984. Subunit *b* of the membrane moiety (F_O) of ATP synthase (F_1F_O) from *Escherichia coli* is indispensable for H^+ translocation and binding of the water-soluble F_1 moiety. Proc. Natl. Acad. Sci. USA. **81:**7279-83.

345. **Altendorf, K., W. Stalz, J. Greie, and G. Deckers-Hebestreit.** 2000. Structure and function of the F_O complex of the ATP synthase from *Escherichia coli*. J. Exp. Biol. **203:**19-28.

346. **Deckers-Hebestreit, G., J. Greie, W. Stalz, and K. Altendorf.** 2000. The ATP synthase of *Escherichia coli*: structure and function of F_0 subunits. Biochim. Biophys. Acta. **1458:**364-73.

347. **McCormick, K.A., G. Deckers-Hebestreit, K. Altendorf, and B.D. Cain.** 1993. Characterization of mutations in the *b* subunit of F_1F_O ATP synthase in *Escherichia coli*. J. Biol. Chem. **268:**24683-91.

348. **Caviston, T.L., C.J. Ketchum, P.L. Sorgen, R.K. Nakamoto, and B.D. Cain.** 1998. Identification of an uncoupling mutation affecting the *b* subunit of F_1F_0 ATP synthase in *Escherichia coli*. FEBS Lett. **429:**201-6.

349. **Grabar, T.B. and B.D. Cain.** 2004. Genetic complementation between mutant *b* subunits in F_1F_O ATP synthase. J. Biol. Chem. **279:**31205-11.

350. **Welch, A.K., S.B. Claggett, and B.D. Cain.** 2008. The b_{R36} contributes to efficient coupling in F_1F_O ATP synthase in *Escherichia coli*. J. Bioenerg. Biomembr. **40:**1-8.

351. **Blair, A., L. Ngo, J. Park, I.T. Paulsen, and M.H. Saier.** 1996. Phylogenetic analyses of the homologous transmembrane channel-forming proteins of the F_0F_1-ATPases of bacteria, chloroplasts and mitochondria. Microbiology. **142:**17-32.

352. **Tiburzy, H.J. and R.J. Berzborn.** 1997. Subunit II (*b'*) and not subunit I (*b*) of photosynthetic ATP synthases is equivalent to subunit *b* of the ATP synthases from nonphotosynthetic eubacteria. Evidence for a new assignment of *b*-type F_O subunits. Z. Naturforsch. **52:**789-98.

353. **Sorgen, P.L., T.L. Caviston, R.C. Perry, and B.D. Cain.** 1998. Deletions in the second stalk of F_1F_O-ATP synthase in *Escherichia coli*. J. Biol. Chem. **273:**27873-8.

354. **Sorgen, P.L., M.R. Bubb, and B.D. Cain.** 1999. Lengthening the second stalk of F_1F_O ATP synthase in *Escherichia coli*. J. Biol. Chem. **274:**36261-6.

355. **Grabar, T.B. and B.D. Cain.** 2003. Integration of *b* subunits of unequal lengths into F_1F_O-ATP synthase. J. Biol. Chem. **278:**34751-6.

356. **Steigmiller, S., M. Börsch, P. Gräber, and M. Huber.** 2005. Distances between the *b* subunits in the tether domain of F_OF_1-ATP synthase from *E. coli*. Biochim. Biophys. Acta. **1708:**143-53.

357. **McLachlin, D.T. and S.D. Dunn.** 1997. Dimerization interactions of the *b* subunit of the *Escherichia coli* F_1F_O-ATPase. J. Biol. Chem. **272:**21233-9.

358. **DelRizzo, P.A., Y. Bi, S.D. Dunn, and B.H. Shilton.** 2002. The "second stalk" of *Escherichia coli* ATP synthase: structure of the isolated dimerization domain. Biochemistry. **41:**6875-84.

359. **DelRizzo, P.A., Y. Bi, and S.D. Dunn.** 2006. ATP synthase *b* subunit dimerization domain: a right-handed coiled coil with offset helices. J. Mol. Biol. **364:**735-46.

360. **Bi, Y., J.C. Watts, P.K. Bamford, L.A. Briere, and S.D. Dunn.** 2008. Probing the functional tolerance of the *b* subunit of *Escherichia coli* ATP synthase for sequence manipulation through a chimera approach. Biochim. Biophys. Acta. **[Epub ahead of print]:**

361. **Wise, J.G. and P.D. Vogel.** 2008. Subunit *b* dimer of the *Escherichia coli* ATP synthase can form left-handed coiled coils. Biophys. J. **[Epub ahead of print]:**

362. **Hornung, T., O.A. Volkov, T.M. Zaida, S. Delannoy, J.G. Wise, and P.D. Vogel.** 2008. Structure of the Cytosolic Part of the Subunit *b*-Dimer of *Escherichia coli* F_OF_1-ATP Synthase. Biophys. J. **[Epub ahead of print]:**

363. **Cipriano, D.J., K.S. Wood, Y. Bi, and S.D. Dunn.** 2006. Mutations in the dimerization domain of the *b* subunit from the *Escherichia coli* ATP synthase. Deletions disrupt function but not enzyme assembly. J. Biol. Chem. **281:**12408-13.

364. **Senior, A.E.** 1983. Secondary and tertiary structure of membrane proteins involved in proton translocation. Biochim. Biophys. Acta. **726:**81-95.

365. **McCormick, K.A. and B.D. Cain.** 1991. Targeted mutagenesis of the *b* subunit of F_1F_O ATP synthase in *Escherichia coli*: Glu-77 through Gln-85. J. Bacteriol. **173:**7240-8.

366. **Kersten, M.V., S.D. Dunn, J.G. Wise, and P.D. Vogel.** 2000. Site-directed spin-labeling of the catalytic sites yields insight into structural changes within the F_OF_1-ATP synthase of *Escherichia coli*. Biochemistry. **39:**3856-60.

367. **Motz, C., T. Hornung, M. Kersten, D.T. McLachlin, S.D. Dunn, J.G. Wise, and P.D. Vogel.** 2004. The subunit *b* dimer of the F_OF_1-ATP synthase: interaction with F_1-ATPase as deduced by site-specific spin-labeling. J. Biol. Chem. **279:**49074-81.

368. **Wilkens, S., S.D. Dunn, and R.A. Capaldi.** 1994. A cryoelectron microscopy study of the interaction of the *Escherichia coli* F_1-ATPase with subunit *b* dimer. FEBS Lett. **354:**37-40.

369. **Wilkens, S. and R.A. Capaldi.** 1998. ATP synthase's second stalk comes into focus. Nature. **393:**29.

370. **Wilkens, S. and R.A. Capaldi.** 1998. Electron microscopic evidence of two stalks linking the F_1 and F_O parts of the *Escherichia coli* ATP synthase. Biochim. Biophys. Acta. **1365:**93-7.

371. **Steffens, K., E. Schneider, G. Deckers-Hebestreit, and K. Altendorf.** 1987. F_O portion of *Escherichia coli* ATP synthase. Further resolution of trypsin-generated fragments from subunit *b*. J. Biol. Chem. **262:**5866-9.

372. **Howitt, S.M., A.J. Rodgers, P.D. Jeffrey, and G.B. Cox.** 1996. A mutation in which alanine 128 Is replaced by aspartic acid abolishes dimerization of the *b* subunit of the F_OF_1-ATPase from *Escherichia coli*. J. Biol. Chem. **271:**7038-42.

373. **Diez, M., M. Börsch, B. Zimmermann, P. Turina, S.D. Dunn, and P. Gräber.** 2004. Binding of the *b*-subunit in the ATP synthase from *Escherichia coli*. Biochemistry. **43:**1054-64.

374. **Krebstakies, T., B. Zimmermann, P. Gräber, K. Altendorf, M. Börsch, and J.C. Greie.** 2005. Both rotor and stator subunits are necessary for efficient binding of F_1 to F_O in functionally assembled *Escherichia coli* ATP synthase. J. Biol. Chem. **280:**33338-45.

375. **Weber, J., S. Wilke-Mounts, S. Nadanaciva, and A.E. Senior.** 2004. Quantitative determination of direct binding of *b* subunit to F_1 in *Escherichia coli* F_1F_O-ATP synthase. J. Biol. Chem. **279:**11253-8.

376. **Aris, J.P. and R.D. Simoni.** 1983. Cross-linking and labeling of the *Escherichia coli* F_1F_0-ATP synthase reveal a compact hydrophilic portion of F_0 close to an F_1 catalytic subunit. J. Biol. Chem. **258:**14599-609.

377. **Hermolin, J., J. Gallant, and R.H. Fillingame.** 1983. Topology, organization, and function of the psi subunit in the F_O sector of the H^+-ATPase of *Escherichia coli*. J. Biol. Chem. **258:**14550-5.

378. **McLachlin, D.M., A.M. Coveny, S.M. Clark, and S.D. Dunn.** 2000. Site-directed cross-linking of *b* to the α, β, and *a* subunits of the *Escherichia coli* ATP synthase. J. Biol. Chem. **275:**17571-7.

379. **Greie, J.C., G. Deckers-Hebestreit, and K. Altendorf.** 2000. Subunit organization of the stator part of the F_O complex from *Escherichia coli* ATP synthase. J. Bioenerg. Biomembr. **32:**357-64.

380. **Herrmann, R.G., J. Steppuhn, G.S. Herrmann, and N. Nelson.** 1993. The nuclear-encoded polypeptide Cfo-II from spinach is a real, ninth subunit of chloroplast ATP synthase. FEBS Lett. **326:**192-8.

381. **Bird, C.R., B. Koller, A.D. Auffret, A.K. Huttly, C.J. Howe, T.A. Dyer, and J.C. Gray.** 1985. The wheat chloroplast gene for CF_0 subunit I of ATP synthase contains a large intron. EMBO J. **4:**1381-1388.

382. **Richter, M.L., R. Hein, and B. Huchzermeyer.** 2000. Important subunit interactions in the chloroplast ATP synthase. Biochim. Biophys. Acta. **1458:**326-42.

383. **Richter, M.L., H.S. Samra, F. He, A.J. Giessel, and K.K. Kuczera.** 2005. Coupling proton movement to ATP synthesis in the chloroplast ATP synthase. J. Bioenerg. Biomembr. **37:**467-73.

384. **Falk, G. and J.E. Walker.** 1988. DNA sequence of a gene cluster coding for subunits of the F_0 membrane sector of ATP synthase in *Rhodospirillum rubrum*. Support for modular evolution of the F_1 and F_0 sectors. Biochem. J. **254:**109-22.

385. **Cozens, A.L. and J.E. Walker.** 1987. The organization and sequence of the genes for ATP synthase subunits in the cyanobacterium *Synechococcus* 6301. Support for an endosymbiotic origin of chloroplasts. J. Mol. Biol. **194:**359-83.

386. **Dunn, S.D., E. Kellner, and H. Lill.** 2001. Specific heterodimer formation by the cytoplasmic domains of the *b* and *b'* subunits of cyanobacterial ATP synthase. Biochemistry. **40:**187-92.

387. **Peng, G., M. Bostina, M. Radermacher, I. Rais, M. Karas, and H. Michel.** 2006. Biochemical and electron microscopic characterization of the F_1F_O ATP synthase from the hyperthermophilic eubacterium *Aquifex aeolicus*. FEBS Lett. **580:**5934-40.

388. **Nakamura, Y., T. Kaneko, S. Sato, M. Ikeuchi, H. Katoh, S. Sasamoto, A. Watanabe, M. Iriguchi, K. Kawashima, T. Kimura, Y. Kishida, C. Kiyokawa, M. Kohara, M. Matsumoto, A. Matsuno, N. Nakazaki, S. Shimpo, M. Sugimoto, C. Takeuchi, M. Yamada, and S. Tabata.** 2002. Complete genome structure of the thermophilic cyanobacterium *Thermosynechococcus elongatus* BP-1. DNA Res. **9:**123-30.

389. **Okajima, K., S. Yoshihara, Y. Fukushima, X. Geng, M. Katayama, S. Higashi, M. Watanabe, S. Sato, S. Tabata, Y. Shibata, S. Itoh, and M. Ikeuchi.** 2005. Biochemical and functional characterization of BLUF-type flavin-binding proteins of two species of cyanobacteria. J. Biochem. **137:**741-50.

390. **Pattanayek, R., D.R. Williams, S. Pattanayek, Y. Xu, T. Mori, C.H. Johnson, P.L. Stewart, and M. Egli.** 2006. Analysis of KaiA-KaiC protein interactions in the cyano-bacterial circadian clock using hybrid structural methods. EMBO J. **25:**2017-28.

391. **Collinson, I.R., J.M. Skehel, I.M. Fearnley, M.J. Runswick, and J.E. Walker.** 1996. The F_1F_0-ATPase complex from bovine heart mitochondria: the molar ratio of the subunits in the stalk region linking the F_1 and F_0 domains. Biochemistry. **35:**12640-6.

392. **Walker, J.E., M.J. Runswick, and L. Poulter.** 1987. ATP synthase from bovine mitochondria. The characterization and sequence analysis of two membrane-associated sub-units and of the corresponding cDNAs. J. Mol. Biol. **197:**89-100.

393. **Walker, J.E. and V.K. Dickson.** 2006. The peripheral stalk of the mitochondrial ATP synthase. Biochim. Biophys. Acta. **1757:**286-96.

394. **Dickson, V.K., J.A. Silvester, I.M. Fearnley, A.G. Leslie, and J.E. Walker.** 2006. On the structure of the stator of the mitochondrial ATP synthase. EMBO J. **25:**2911-8.

395. **Carbajo, R.J., F.A. Kellas, M.J. Runswick, M.G. Montgomery, J.E. Walker, and D. Neuhaus.** 2005. Structure of the F_1-binding domain of the stator of bovine F_1F_O-ATPase and how it binds an α subunit. J. Mol. Biol. **351:**824-38.

396. **Vik, S.B. and R.R. Ishmukhametov.** 2005. Structure and function of subunit *a* of the ATP synthase of *Escherichia coli*. J. Bioenerg. Biomembr. **37:**445-9.

397. **Smith, P.K., R.I. Krohn, G.T. Hermanson, A.K. Mallia, F.H. Gartner, M.D. Provenzano, E.K. Fujimoto, N.M. Goeke, B.J. Olson, and D.C. Klenk.** 1985. Measurement of Protein Using Bicinchoninic Acid. Analytical Biochemistry. **150:**76-85.

398. **Webb, M.R.** 1992. A continuous spectrophotometric assay for inorganic phosphate and for measuring phosphate release kinetics in biological systems. Proc. Natl. Acad. Sci. USA. **89:**4884-7.

399. **Claggett, S.B., T.B. Grabar, S.D. Dunn, and B.D. Cain.** 2007. Functional incorporation of chimeric *b* subunits into F_1F_O ATP synthase. J. Bacteriol. **189:**5463-71.

400. **Galkin, M.A., R.R. Ishmukhametov, and S.B. Vik.** 2006. A functionally inactive, cold-stabilized form of the Escherichia coli F_1F_O ATP synthase. Biochim. Biophys. Acta. **1757:**206-14.

401. **Stack, A.E. and C.B. D.** 1994. Mutations in the δ subunit influence the assembly of F_1F_O ATP synthase in *Escherichia coli*. J. Bacteriol. **176:**540-2.

BIOGRAPHICAL SKETCH

Shane B. Claggett was born in 1979 to James R. Claggett and Sue Ellen Claggett. He attended grade school in both Florida and Connecticut during which time he taught himself computer programming and basic electronics. Shane attended the University of Florida from 1997-2000 and obtained a bachelor's degree in chemistry. He worked in Dr. Jim Winefordner's analytical chemistry lab during his undergraduate studies where he wrote custom software for the instruments and assays under development. From 2000-2003 Shane was employed as a software developer at Medical Manager in Alachua, Florida. Shane entered graduate school at the University of Florida in 2003 to pursue a graduate degree in biochemistry and was fortunate to marry Dawn Yang on August 6th, 2006. A major focus of Shane's life has been the study of martial arts and meditation, including Tae Kwon Do, Aikido, Shaolin Kung Fu, Tai Chi Chuan and Chi Gung.